

Original article

Development of an experimentally useful model of acute myocardial infarction: 2/3 nephrectomized triple nitric oxide synthases-deficient mouse



Taro Uchida^{a,1}, Yumi Furuno^{b,1}, Akihito Tanimoto^c, Yumiko Toyohira^d, Kumiko Arakaki^e, Mika Kina-Tanada^a, Haruaki Kubota^a, Mayuko Sakanashi^a, Toshihiro Matsuzaki^a, Katsuhiko Noguchi^a, Junko Nakasone^a, Tomonori Igarashi^f, Susumu Ueno^f, Masayuki Matsushita^g, Shogo Ishiuchi^h, Hiroaki Masuzakiⁱ, Yusuke Ohya^e, Nobuyuki Yanagihara^d, Hiroaki Shimokawa^j, Yutaka Otsuji^b, Masahito Tamura^b, Masato Tsutsui^{a,*}

^a Department of Pharmacology, Graduate School of Medicine, University of the Ryukyus, Okinawa, Japan

^b Second Department of Internal Medicine, School of Medicine, Institute of Industrial Ecological Sciences, University of Occupational and Environmental Health, Kitakyushu, Japan

^c Department of Pathology, Kagoshima University Graduate School of Medical and Dental Sciences, Kagoshima, Japan

^d Department of Pharmacology, School of Medicine, Institute of Industrial Ecological Sciences, University of Occupational and Environmental Health, Kitakyushu, Japan

^e Third Department of Internal Medicine, Graduate School of Medicine, University of the Ryukyus, Okinawa, Japan

^f Department of Occupational Toxicology, Institute of Industrial Ecological Sciences, University of Occupational and Environmental Health, Kitakyushu, Japan

^g Department of Physiology, Graduate School of Medicine, University of the Ryukyus, Okinawa, Japan

^h Department of Neurosurgery, Graduate School of Medicine, University of the Ryukyus, Okinawa, Japan

ⁱ Second Department of Internal Medicine, Graduate School of Medicine, University of the Ryukyus, Okinawa, Japan

^j Department of Cardiovascular Medicine, Tohoku University Graduate School of Medicine, Sendai, Japan

ARTICLE INFO

Article history:

Received 23 July 2014

Received in revised form 9 September 2014

Accepted 17 September 2014

Available online 28 September 2014

Keywords:

Arteriosclerosis

Acute myocardial infarction

Nitric oxide synthase

Sudden cardiac death

ABSTRACT

We investigated the effect of subtotal nephrectomy on the incidence of acute myocardial infarction (AMI) in mice deficient in all three nitric oxide synthases (NOSs). Two-thirds nephrectomy (NX) was performed on male triple NOSs^{-/-} mice. The 2/3NX caused sudden cardiac death due to AMI in the triple NOSs^{-/-} mice as early as 4 months after the surgery. The 2/3NX triple NOSs^{-/-} mice exhibited electrocardiographic ST-segment elevation, reduced heart rate variability, echocardiographic regional wall motion abnormality, and accelerated coronary arteriosclerotic lesion formation. Cardiovascular risk factors (hypertension, hypercholesterolemia, and hyperglycemia), an increased number of circulating bone marrow-derived vascular smooth muscle cell (VSMC) progenitor cells (a pro-arteriosclerotic factor), and cardiac up-regulation of stromal cell-derived factor (SDF)-1 α (a chemotactic factor of the progenitor cells) were noted in the 2/3NX triple NOSs^{-/-} mice and were associated with significant increases in plasma angiotensin II levels (a marker of renin-angiotensin system activation) and urinary 8-isoprostane levels (a marker of oxidative stress). Importantly, combined treatment with a clinical dosage of an angiotensin II type 1 receptor blocker, irbesartan, and a calcium channel antagonist, amlodipine, markedly prevented coronary arteriosclerotic lesion formation and the incidence of AMI and improved the prognosis of those mice, along with ameliorating all those pro-arteriosclerotic parameters. The 2/3NX triple NOSs^{-/-} mouse is a new experimentally useful model of AMI. Renin-angiotensin system activation, oxidative stress, cardiovascular risk factors, and SDF-1 α -induced recruitment of bone marrow-derived VSMC progenitor cells appear to be involved in the pathogenesis of AMI in this model.

© 2014 Elsevier Ltd. All rights reserved.

Abbreviations: ACE, angiotensin-converting enzyme; ADMA, asymmetric dimethyl-arginine; AMI, acute myocardial infarction; APC, activated protein C; apo E, apolipoprotein E; AT, angiotensin II type 1; CKD, chronic kidney disease; ECG, electrocardiography; FITC, fluorescein isothiocyanate; GAPDH, glyceraldehyde-3-phosphate dehydrogenase; HDL, high-density lipoprotein; mAb, monoclonal antibody; NO, nitric oxide; NOS, NO synthase; NX, nephrectomy; Sca-1⁺, stem cell antigen-1⁺; SDF-1 α , stromal cell-derived factor-1 α ; VSMC, vascular smooth muscle cell; WHHL, Watanabe heritable hyperlipidemic; WT, wild-type.

* Corresponding author at: Department of Pharmacology, Graduate School of Medicine, University of the Ryukyus, 207 Uehara, Nishihara, Okinawa 903-0215, Japan. Tel.: +81 98 895 1133; fax: +81 98 895 1411.

E-mail address: tsutsui@med.u-ryukyu.ac.jp (M. Tsutsui).

¹ These authors contributed equally to this work.

1. Introduction

Acute myocardial infarction is a disorder in which cardiac myocytes undergo necrosis as a consequence of interrupted coronary blood flow [1]. Acute myocardial infarction is a major cause of morbidity and mortality worldwide, with more than 7 million people in the world suffering from acute myocardial infarction each year [1]. Over the past two decades, the in-hospital mortality rate after admission for acute myocardial infarction has substantially declined to less than 10%, owing to

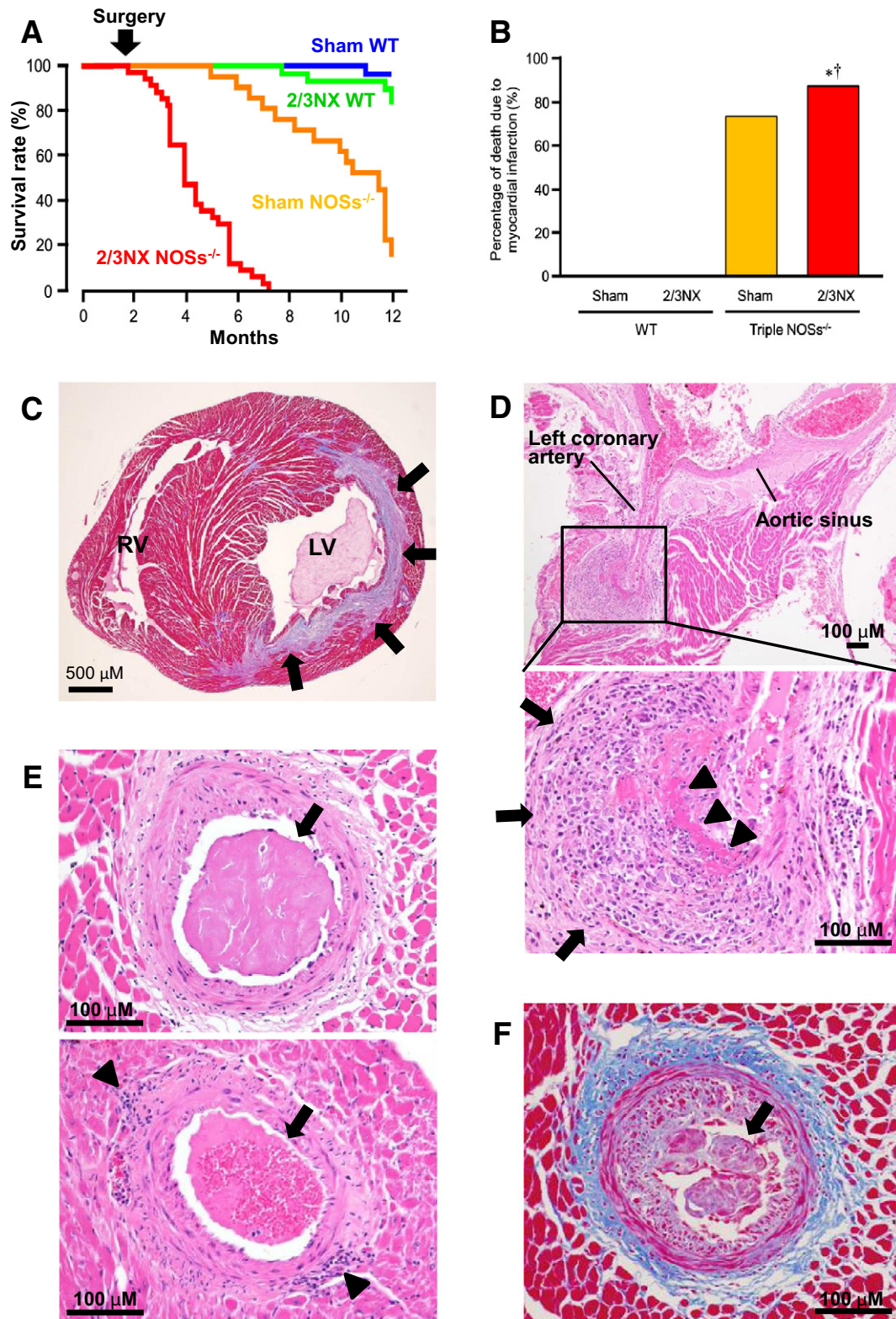


Fig. 1. Sudden cardiac death due to spontaneous myocardial infarction in 2/3 nephrectomized (NX) male triple nitric oxide synthases (NOSs)-deficient mice. (A) Survival rate ($n = 28-49$). NOSs^{-/-}, triple NOSs^{-/-} mice; WT, wild-type mice; sham, sham-operated. (B) Percentage of death due to myocardial infarction in the total causes of death ($n = 2-32$). Sham, sham operation. (C) Lateral wall myocardial infarction (arrows) (Azan staining). LV, left ventricle; RV, right ventricle. (D) Marked infiltration of inflammatory cells (arrows) and fibrinoid necrosis (triangles) at the adventitia of the left coronary artery (hematoxylin-eosin staining). (E) Intracoronary thrombi (arrows) and adventitial infiltration of inflammatory cells (triangles) (hematoxylin-eosin staining). (F) Intimal thickening, perivascular fibrosis (blue color), and intracoronary thrombus (arrow) (Azan staining).

recent therapeutic advances such as coronary reperfusion therapy [2]. However, the overall mortality rate, including out-of-hospital deaths, is very high (approximately 30%) even at present [3]. This is because the majority of these deaths occur before stricken individuals reach the hospital [3]. Outside the hospital, once the individuals develop severe complications, such as malignant cardiac arrhythmia, cardiogenic shock, or cardiac rupture, it is extremely difficult to save their lives [3]. Thus, in order to suppress this fatal cardiovascular disorder, research and development of therapeutic strategies for preventing acute myocardial infarction are of critical importance. However, due to lack of an experimentally useful animal model that develops acute myocardial infarction, the research and development of such strategies have made little progress.

Nitric oxide (NO) plays an essential role in maintaining cardiovascular homeostasis. NO is synthesized by three distinct NO synthase (NOS) isoforms, including neuronal, inducible, and endothelial NOSs, and exerts a variety of biological actions under both physiological and

pathological conditions [4–9]. We previously generated mice in which all three NOS genes are completely disrupted [10] and reported that triple NOS^{-/-} mice, but not single endothelial NOS^{-/-} mice, spontaneously emerge acute myocardial infarction [11]. However, our model was not useful for experiments because it took a very long time (approximately 1 year) for them to develop acute myocardial infarction [11].

Chronic kidney disease (CKD) is a condition characterized by progressive and irreversible loss of renal function. It is estimated that over 10% of the adult population in developed countries suffer some degree of CKD [12,13]. Previous epidemiological studies have indicated that the presence of CKD significantly increases the risk of acute myocardial infarction in men, and that the impact of CKD on the risk of cardiovascular disease is as strong as that of diabetes mellitus and pre-existing ischemic heart disease [14–16]. In the clinical course of the progression of CKD, the number of nephrons decreases regardless of etiology, and this pathological renal remodeling is thought to be the final common

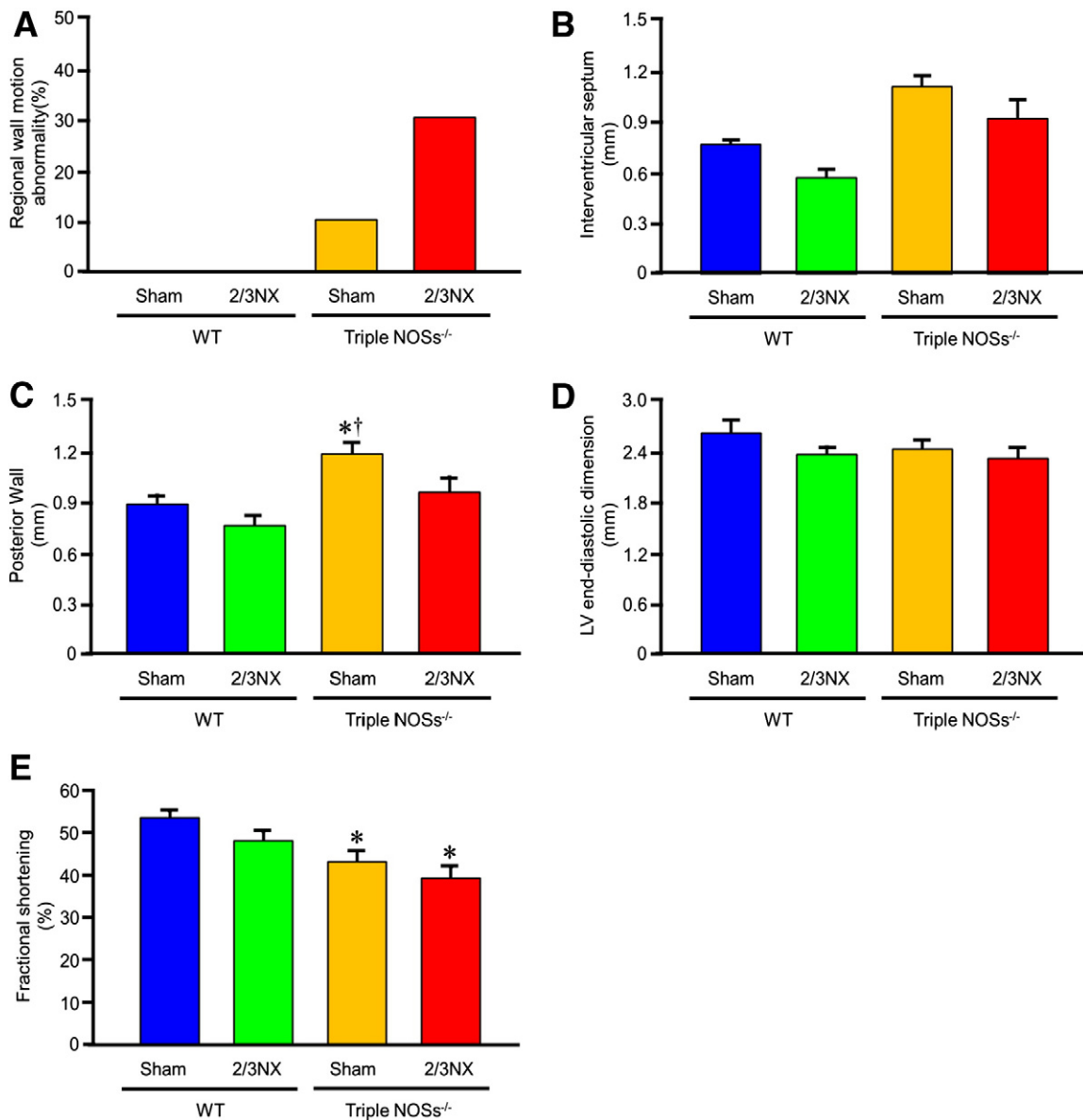


Fig. 2. Echocardiographic abnormalities in 2/3NX triple NOSs^{-/-} mice at 2 months after the surgery. (A) Regional wall motion abnormality ($n = 10$). NOSs^{-/-}, triple NOSs^{-/-} mice; WT, wild-type mice; sham, sham-operated. (B) Wall thickness of interventricular septum ($n = 10$). (C) Wall thickness of posterior wall ($n = 10$). (D) Left ventricular (LV) end-diastolic dimension ($n = 10$). (E) Fractional shortening ($n = 10$).

pathway in the pathogenesis of CKD. Such a disease state is modeled in experimental animals by surgically dissecting a large part of the renal mass [17,18].

In the present study, based on these backgrounds, we investigated the effect of subtotal nephrectomy on the incidence of acute myocardial infarction in our male triple NOSs^{-/-} mice in order to establish an experimentally useful model of acute myocardial infarction.

2. Materials and methods

Materials and methods are described in the online Supplementary Methods and Results.

3. Results

3.1. Subtotal 2/3 nephrectomy (NX) caused an early onset of acute myocardial infarction in male triple NOSs^{-/-} mice

Because animals with 5/6NX are widely used as an experimental model of CKD, we first studied the effect of 5/6NX on survival rate in male triple NOSs^{-/-} mice. However, almost all the triple NOSs^{-/-} mice died shortly after the 5/6NX (data not shown). Thus, we next examined the effect of 2/3NX. In male wild-type (WT) mice, the 2/3NX did not significantly affect the survival rate as compared with sham operation, and more than 80% of the 2/3NX WT mice lived during the 10 months of follow-up (Fig. 1A). In contrast,

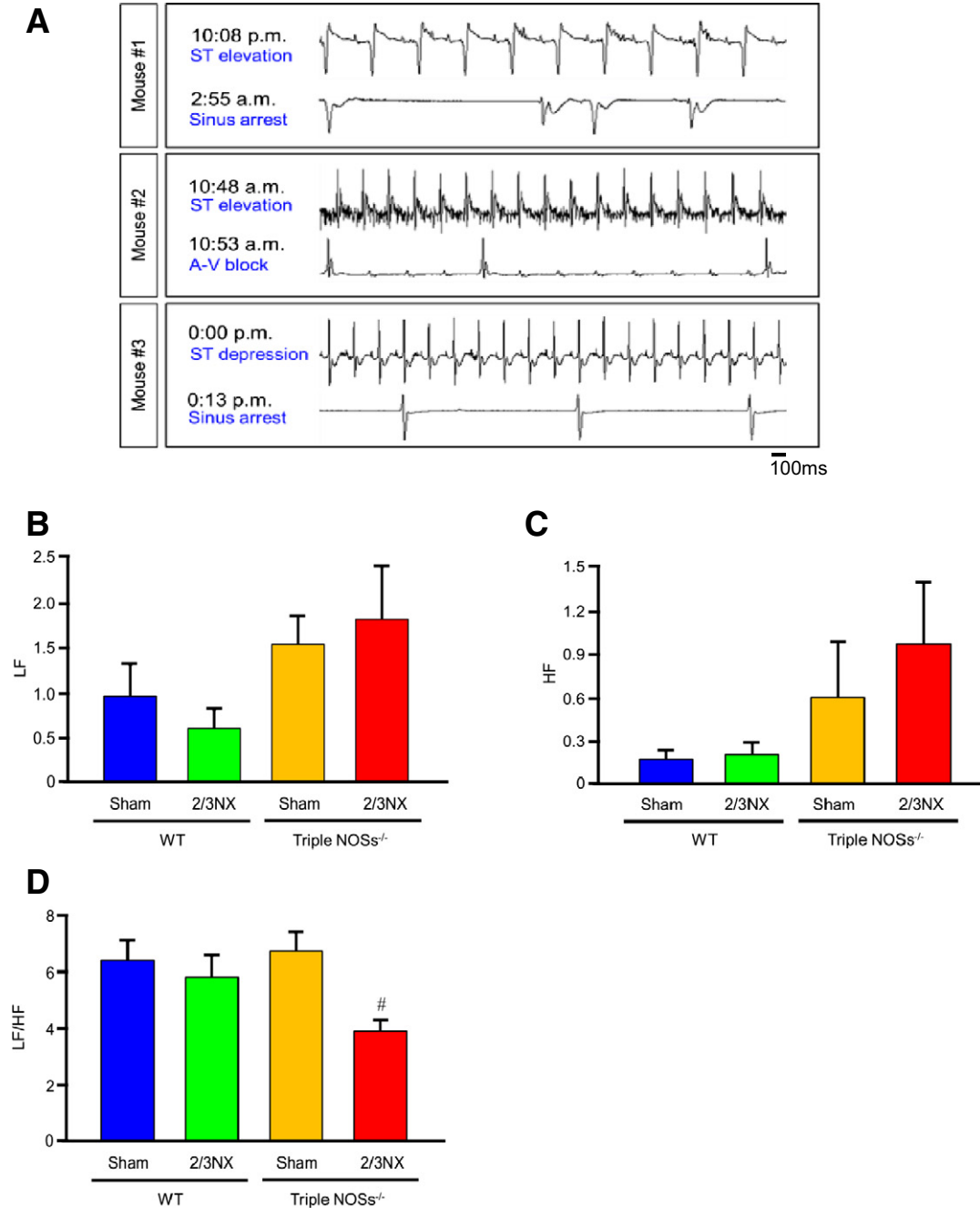


Fig. 3. Telemetry electrocardiographic abnormalities in 2/3NX triple NOSs^{-/-} mice at 2 months after the surgery. (A) Electrocardiographic (ECG) abnormalities in 3 2/3NX triple NOSs^{-/-} mice that died during ECG recording (died within 24 hours after subcutaneous implantation of telemetry transmitters). A-V, atrioventricular. (B) Low-frequency (LF) power ($n = 10-12$). (C) High-frequency (HF) power ($n = 10-12$). (D) LF/HF ratio ($n = 10-12$). * $P < 0.05$ vs. sham-operated WT mice; [#] $P < 0.05$ vs. sham-operated triple NOSs^{-/-} mice.

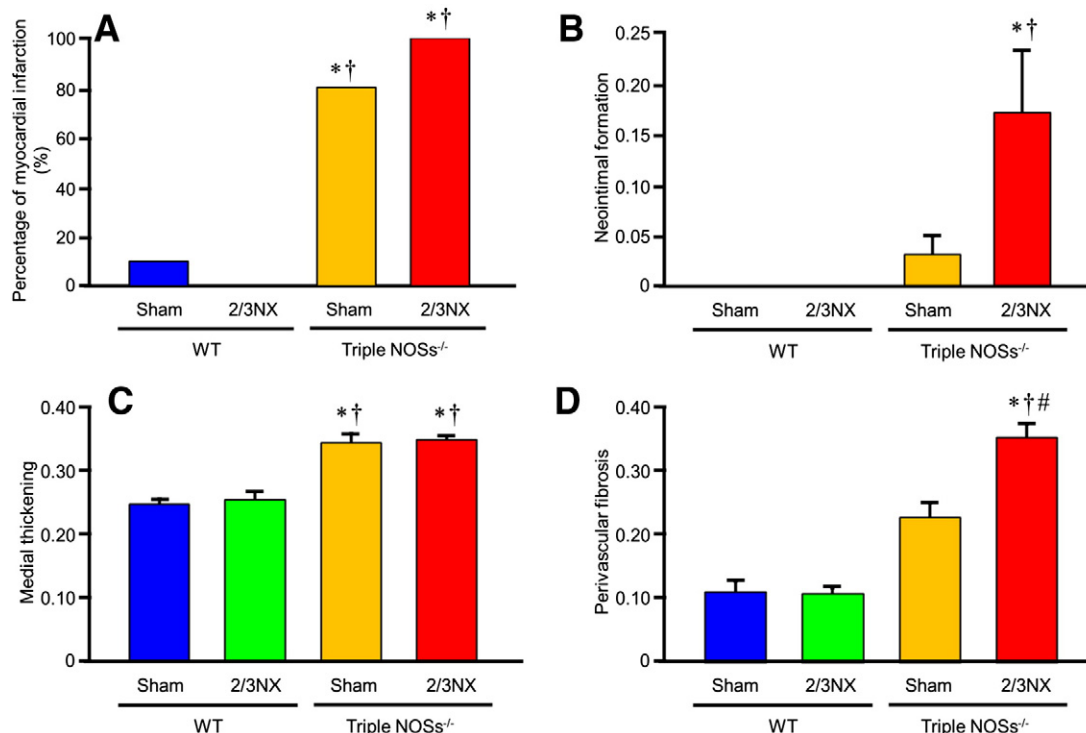


Fig. 4. Coronary arteriosclerotic lesion formation in 2/3NX triple NOSs^{-/-} mice at 2 months after the surgery. After the echocardiography and telemetry ECG, pathological examination of the heart was performed. Four 2/3NX triple NOSs^{-/-} mice that died before 2 months after the surgery and 3 2/3NX triple NOSs^{-/-} mice that died during telemetry ECG were included in the analysis. The heart was cut into 5 equal-thick parts in a short-axis direction, and respective 5 sections were examined. (A) Percentage of acute and/or old myocardial infarction ($n = 10-16$). NOSs^{-/-}, triple NOSs^{-/-} mice; WT, wild-type mice; sham, sham-operated. (B) Neointimal formation (the ratio of intima area to media area) ($n = 10-16$). (C) Medial thickening (the ratio of media area to total vascular area) ($n = 10-16$). (D) Perivascular fibrosis (the ratio of perivascular area to total vascular area) ($n = 10-16$). * $P < 0.05$ vs. sham-operated WT mice; † $P < 0.05$ vs. 2/3NX WT mice; # $P < 0.05$ vs. sham-operated triple NOSs^{-/-} mice.

in the triple NOSs^{-/-} mice, the 2/3NX significantly and markedly reduced the survival rate compared with sham operation, and, importantly, approximately 90% of the 2/3NX triple NOSs^{-/-} mice suddenly died as early as 4 months after the surgery (Fig. 1A).

We next explored the effect of 2/3NX on the incidence of acute myocardial infarction in the triple NOSs^{-/-} mice by a postmortem examination, which revealed a marked increase in the incidence of myocardial infarction (the percentage of death due to myocardial infarction in the total causes of death) compared with sham operation. Noticeably, 87.8% (43/49) of the 2/3NX triple NOSs^{-/-} mice died due to acute and/or old myocardial infarction (Fig. 1B). It was conceivable that the 2/3NX triple NOSs^{-/-} mice would die mainly due to myocardial infarction-complicated arrhythmias or heart failure (including cardiogenic shock). It is difficult to distinguish between death due to arrhythmias and heart failure since heart failure is often accompanied by arrhythmias and since arrhythmias are always seen prior to any death. Thus, we categorized those causes of death as death due to myocardial infarction. No cerebrovascular disease was observed in any of the dead 2/3NX triple NOSs^{-/-} mice. Fig. 1C represents the lateral wall myocardial infarction seen in the dead 2/3NX triple NOSs^{-/-} mice. The coronary arteries of the dead 2/3NX triple NOSs^{-/-} mice exhibited severe coronary arteriosclerotic lesion formation, including infiltration of inflammatory cells (Fig. 1D), neointimal formation (Fig. 1F), medial thickening (Fig. 1F), perivascular fibrosis (Fig. 1F), and fibrinoid necrosis (Fig. 1D), as well as coronary thrombus formation (Figs. 1E, F). On the other hand, coronary atherosclerotic lesions, such as extracellular lipid accumulation, atheromatous plaque formation, or infiltration of foamy macrophages in the coronary artery, were rarely observed.

3.2. 2/3NX caused echocardiographic and electrocardiographic abnormalities and accelerated coronary arteriosclerotic lesion formation in triple NOSs^{-/-} mice at 2 months after the surgery

We then examined cardiac functional abnormalities and the extent of coronary arteriosclerotic lesion formation in the 2/3NX triple NOSs^{-/-} mice at 2 months post-surgery via echocardiography, telemetry electrocardiography (ECG), and pathological examination. Of the 16 2/3NX triple NOSs^{-/-} mice, 4 died before 2 months after the surgery. Echocardiography showed regional wall motion abnormality in 30% (3/10) of the 2/3NX triple NOSs^{-/-} mice and 10% (1/10) of the sham triple NOSs^{-/-} mice (Fig. 2A). Wall thickness of interventricular septum and posterior wall tended to be thinner and fractional shortening tended to be more reduced in the 2/3NX triple NOSs^{-/-} mice as compared with the sham triple NOSs^{-/-} mice, and fractional shortening was significantly decreased in the 2/3NX triple NOSs^{-/-} mice when compared with the sham WT mice (Figs. 2B, C, E). There was no significant difference in left ventricular end-diastolic dimension between the 2/3NX triple NOSs^{-/-} mice and other mice (Fig. 2D).

Of the 12 2/3NX triple NOSs^{-/-} mice that received subcutaneous implantation of telemetry transmitters, 3 died during ECG recording (within 24 hours after the implantation), and ECG revealed ST-segment elevation followed by sinus arrest, ST-segment elevation followed by advanced atrioventricular block, and ST-segment depression followed by sinus arrest (Fig. 3A). Transient ST-segment depression was detected in other 2 2/3NX triple NOSs^{-/-} mice and 1 sham triple NOSs^{-/-} mice. No ischemic ECG change was seen in sham or 2/3NX WT mice. We evaluated heart rate variability parameters, such as low-frequency (LF) power, high-frequency (HF) power, and LF/HF ratio.

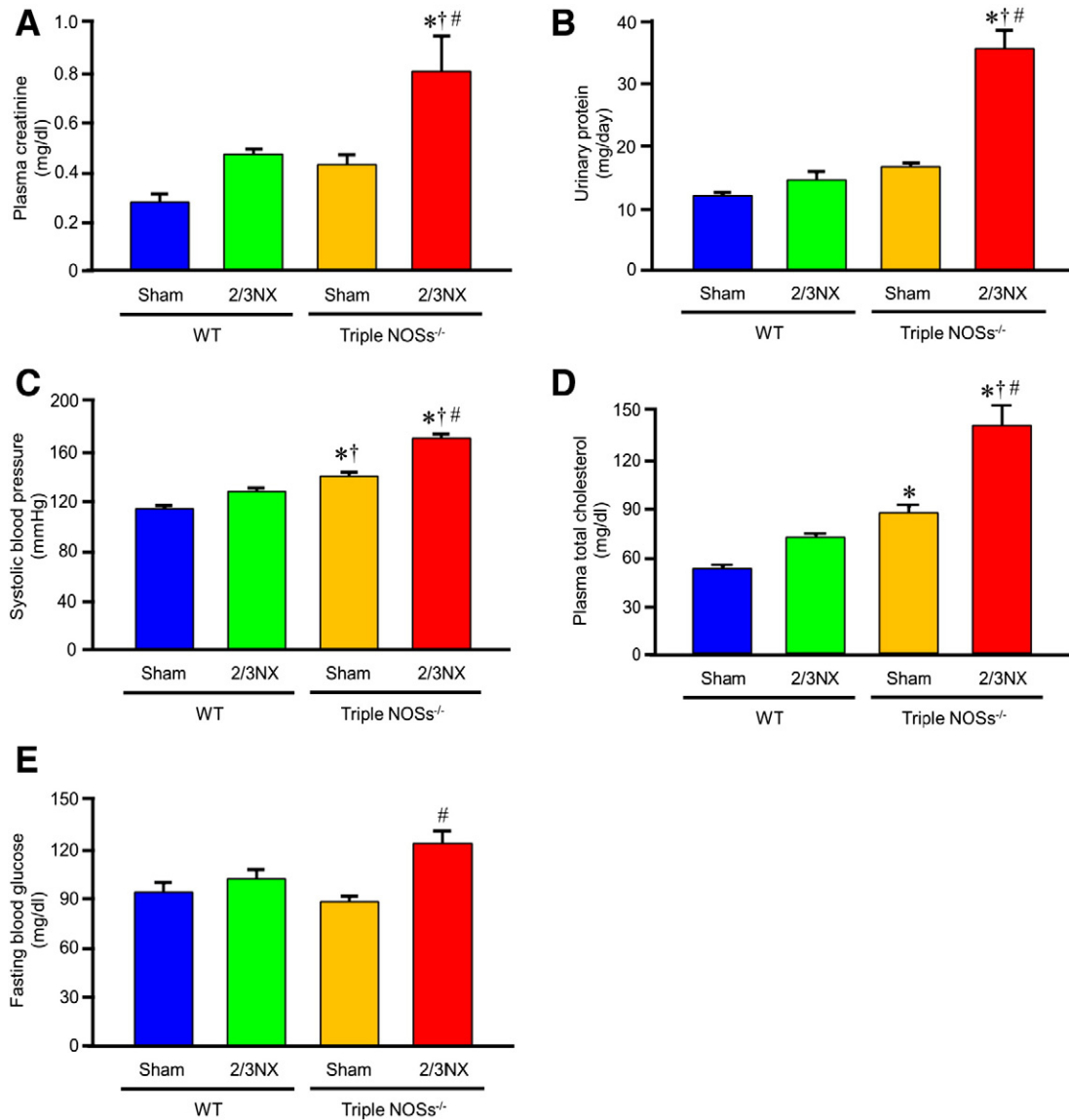


Fig. 5. Renal dysfunction and cardiovascular risk factors in the 2/3NX triple NOSs^{-/-} mice. These parameters were assessed at 2 months after the surgery. (A) Plasma creatinine levels ($n = 10$). (B) Urinary protein levels ($n = 12$). (C) Systolic blood pressure ($n = 12$). (D) Plasma total cholesterol levels ($n = 10$). (E) Fasting blood glucose levels ($n = 10$). * $P < 0.05$ vs. sham-operated WT mice; † $P < 0.05$ vs. 2/3NX WT mice; # $P < 0.05$ vs. sham-operated triple NOSs^{-/-} mice.

The LF power and the HF power tended to be increased in the 2/3NX triple NOSs^{-/-} mice, and the LF/HF ratio was significantly decreased in the 2/3NX triple NOSs^{-/-} mice as compared with the sham NOSs^{-/-} mice (Figs. 3B–D).

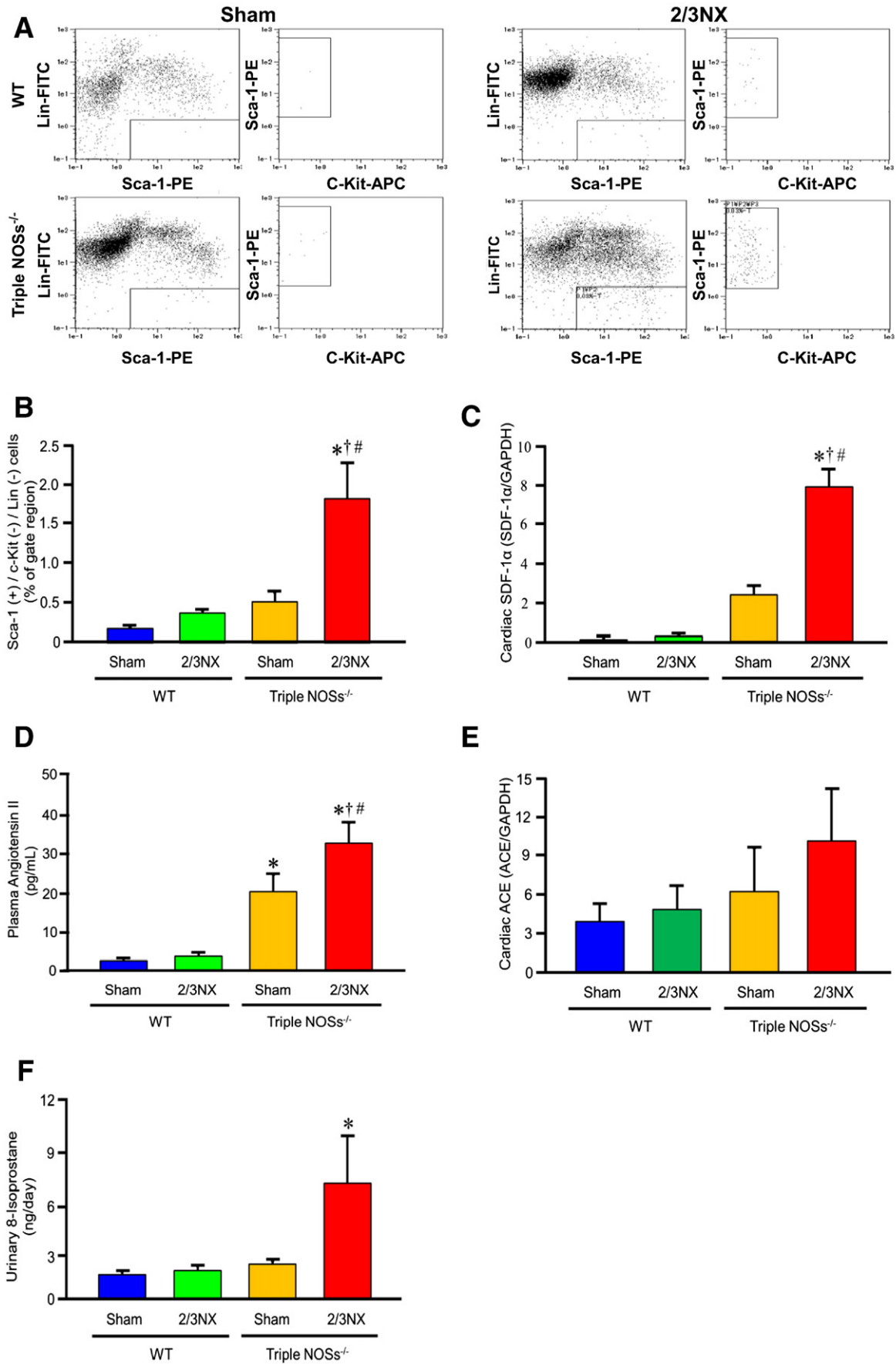
After echocardiography and telemetry ECG, we quantitated the extent of coronary arteriosclerosis. Four 2/3NX triple NOSs^{-/-} mice that died before 2 months after the surgery and 3 2/3NX triple NOSs^{-/-} mice that died during telemetry ECG were included in the analysis. The heart was cut into 5 equal-thick parts in a short-axis direction, and respective 5 sections were examined. Acute and/or old myocardial infarction was recognized in 100% (16/16) of the 2/3NX triple NOSs^{-/-} mice and 80% (8/10) of the sham triple NOSs^{-/-} mice

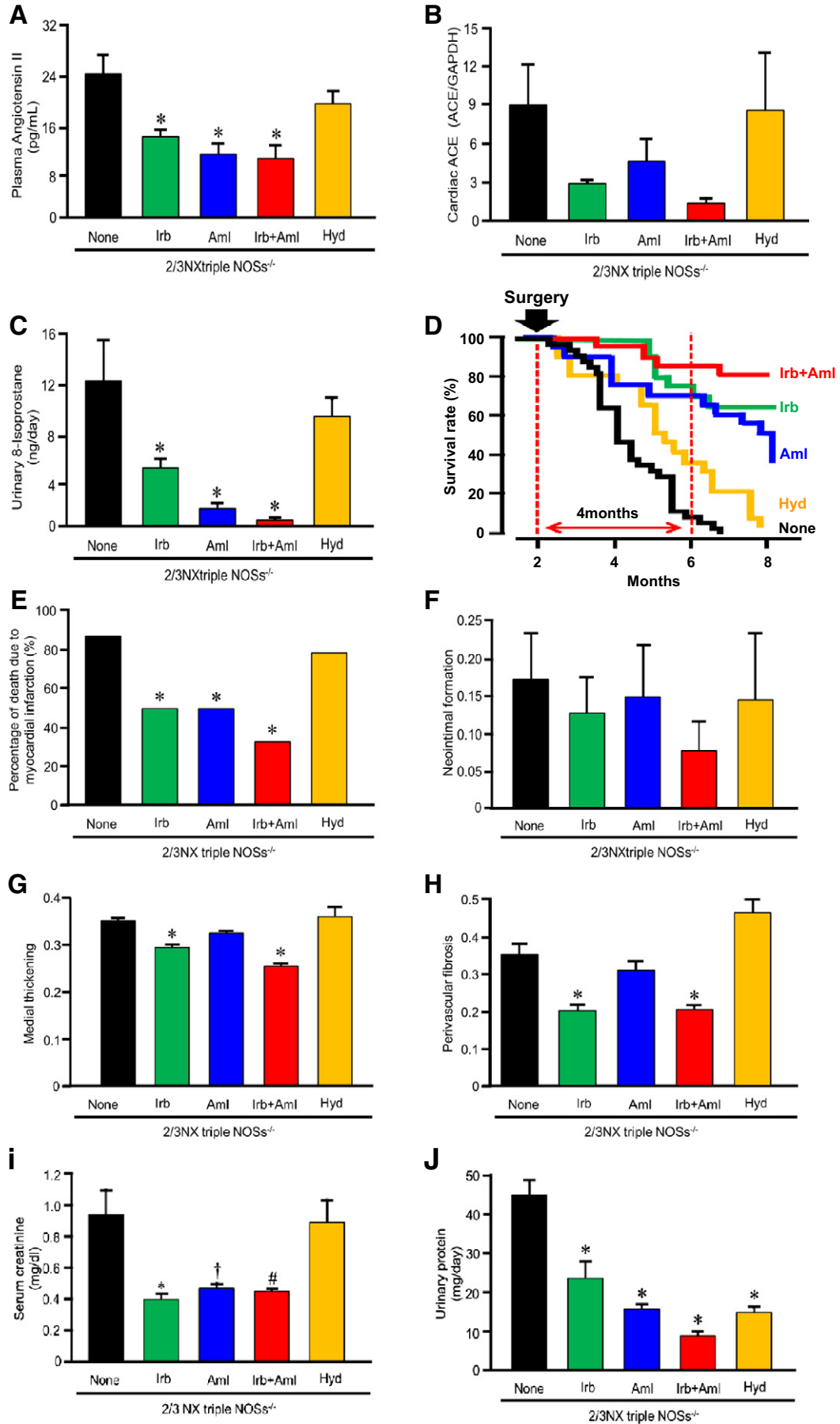
(Fig. 4A). The extents of neointimal formation, medial thickening, and perivascular fibrosis were all markedly accelerated in the 2/3NX triple NOSs^{-/-} mice as compared with the sham WT mice (Figs. 4B–D). Coronary thrombus formation was also noted in 1 2/3NX triple NOSs^{-/-} mice.

3.3. 2/3NX reduced renal function in triple NOSs^{-/-} mice

There were significant increases in plasma creatinine and urinary protein levels, markers of renal function, after the 2/3NX (assessed at 2 months after the surgery) in the triple NOSs^{-/-} mice compared with sham operation (Figs. 5A, B).

Fig. 6. Stromal cell-derived factor (SDF)-1 α -induced recruitment of circulating bone marrow-derived vascular smooth muscle cell (VSMC) progenitor cells, renin-angiotensin system activation, and oxidative stress in the 2/3NX triple NOS^{-/-} mice. (A and B) The number of circulating stem cell antigen-1⁺ (Sca-1⁺)/c-Kit⁻/Lin⁻ cells (interpreted as bone marrow-derived VSMC progenitor cells) analyzed at 1 week after the surgery ($n = 7$). (C) Cardiac SDF-1 α protein levels assayed at 1 week after the surgery ($n = 4-6$). (D) Plasma angiotensin II levels measured at 2 months after the surgery ($n = 8$). (E) Cardiac angiotensin-converting enzyme (ACE) protein expression levels evaluated at 2 months after the surgery ($n = 7$). (F) Urinary 8-isoprostane levels assessed at 2 months after the surgery ($n = 8$). * $P < 0.05$ vs. sham-operated WT mice; † $P < 0.05$ vs. 2/3NX WT mice; # $P < 0.05$ vs. sham-operated triple NOSs^{-/-} mice.





3.4. 2/3NX exacerbated cardiovascular risk factors in triple NOSs^{-/-} mice

Because severe coronary arteriosclerotic lesions were detected in the 2/3NX triple NOSs^{-/-} mice, we then examined the presence or absence of cardiovascular risk factors. The 2/3NX caused significant increases in systolic blood pressure (measured at 1 month after the surgery), plasma total cholesterol levels, and fasting blood glucose levels (evaluated at 2 months after the surgery) in the triple NOSs^{-/-} mice compared with sham operation (Figs. 5C–E).

3.5. 2/3NX caused mobilization of circulating bone marrow-derived vascular smooth muscle cell (VSMC) progenitor cells and up-regulation of cardiac stromal cell-derived factor 1 α (SDF-1 α) levels in triple NOSs^{-/-} mice

It has been reported that bone marrow-derived VSMC progenitor cells contribute to arteriosclerotic lesion formation after vascular injury and that SDF-1 α recruits the VSMC progenitor cells to vascular lesions [19]. We thus analyzed the effects of 2/3NX on the number of circulating bone marrow-derived VSMC progenitor cells and cardiac SDF-1 α protein levels in the triple NOSs^{-/-} mice. The 2/3NX significantly and markedly augmented the number of circulating stem cell antigen-1⁺ (Sca-1⁺)/c-Kit⁻/Lin⁻ cells, which are interpreted as bone marrow-derived VSMC progenitor cells (evaluated at 1 week after the surgery), and the cardiac SDF-1 α protein levels (assayed at 1 week after the surgery) in the triple NOSs^{-/-} mice compared with sham operation (Figs. 6A–C and Online Supplementary Fig. 1).

3.6. 2/3NX caused renin–angiotensin system activation and oxidative stress in triple NOSs^{-/-} mice

We next investigated the molecular mechanisms for acute myocardial infarction caused by the 2/3NX in the triple NOSs^{-/-} mice. The 2/3NX evoked prominent increases in plasma angiotensin II levels and cardiac angiotensin-converting enzyme (ACE) protein levels, markers of renin–angiotensin system activation (assessed at 2 months after the surgery) in the triple NOSs^{-/-} mice compared with sham operation (Figs. 6D and E, and Online Supplementary Fig. 2), although the values of the cardiac ACE protein levels did not reach a statistically significant level because of variations in the data. The 2/3NX also elicited a marked rise in urinary 8-isoprostane levels, a marker of oxidative stress (measured at 2 months after the surgery), in the triple NOSs^{-/-} mice (Fig. 6F).

3.7. Combined treatment with an angiotensin II type 1 (AT₁) receptor blocker, irbesartan, and an antioxidant calcium channel antagonist, amlodipine, markedly prevented coronary arteriosclerotic lesion formation and the occurrence of myocardial infarction and improved the prognosis of 2/3NX triple NOSs^{-/-} mice

Finally, in order to examine the involvement of renin–angiotensin system activation and oxidative stress in the pathogenesis of acute myocardial infarction in the 2/3NX triple NOSs^{-/-} mice, and also in order to validate the experimental usefulness of this acute myocardial infarction model, we investigated the effects on the cardiovascular abnormalities in this model of treatment with a selective and potent AT₁ receptor blocker, irbesartan; an antioxidant dihydropyridine calcium channel antagonist, amlodipine; a combination of both; or an

anti-hypertensive agent, hydralazine. We used the clinical therapeutic dosage of irbesartan and amlodipine. Single treatment with irbesartan or amlodipine markedly reduced the plasma angiotensin II levels, the cardiac ACE protein levels, and the urinary 8-isoprostane levels in the 2/3NX triple NOSs^{-/-} mice, while the combined treatment with irbesartan and amlodipine more potently decreased those values (Figs. 7A–C and Online Supplementary Fig. 3), although the data of the cardiac ACE protein levels again did not reach a statistically significant level owing to dispersion of the data (Fig. 7B and Online Supplementary Fig. 3). Mono-treatment with irbesartan or amlodipine significantly improved the survival rate in the 2/3NX triple NOSs^{-/-} mice, while the irbesartan/amlodipine co-treatment more powerfully ameliorated it. More importantly, these significant effects were noted within the short time of 4 months after the drug treatment, indicating the usefulness of this model for pharmacological studies (Fig. 7D). The sole treatment with irbesartan or amlodipine inhibited the incidence of myocardial infarction (the percentage of death due to myocardial infarction in the total causes of death) and coronary arteriosclerotic lesion formation (neointimal formation, medial thickening, and perivascular fibrosis) in the 2/3NX triple NOSs^{-/-} mice, while the simultaneous treatment with irbesartan and amlodipine more intensely prevented both the incidence of myocardial infarction (Fig. 7E) and coronary lesion formation (Figs. 7F–H). On the other hand, although the treatment with hydralazine significantly lowered systolic blood pressure in the 2/3NX triple NOSs^{-/-} mice to the same extent as the treatment with irbesartan plus amlodipine (Fig. 8A), it did not significantly affect the plasma angiotensin II levels, the cardiac ACE protein levels, the urinary 8-isoprostane levels, the survival rate, the incidence of myocardial infarction, or coronary lesion formation (Figs. 7A–H).

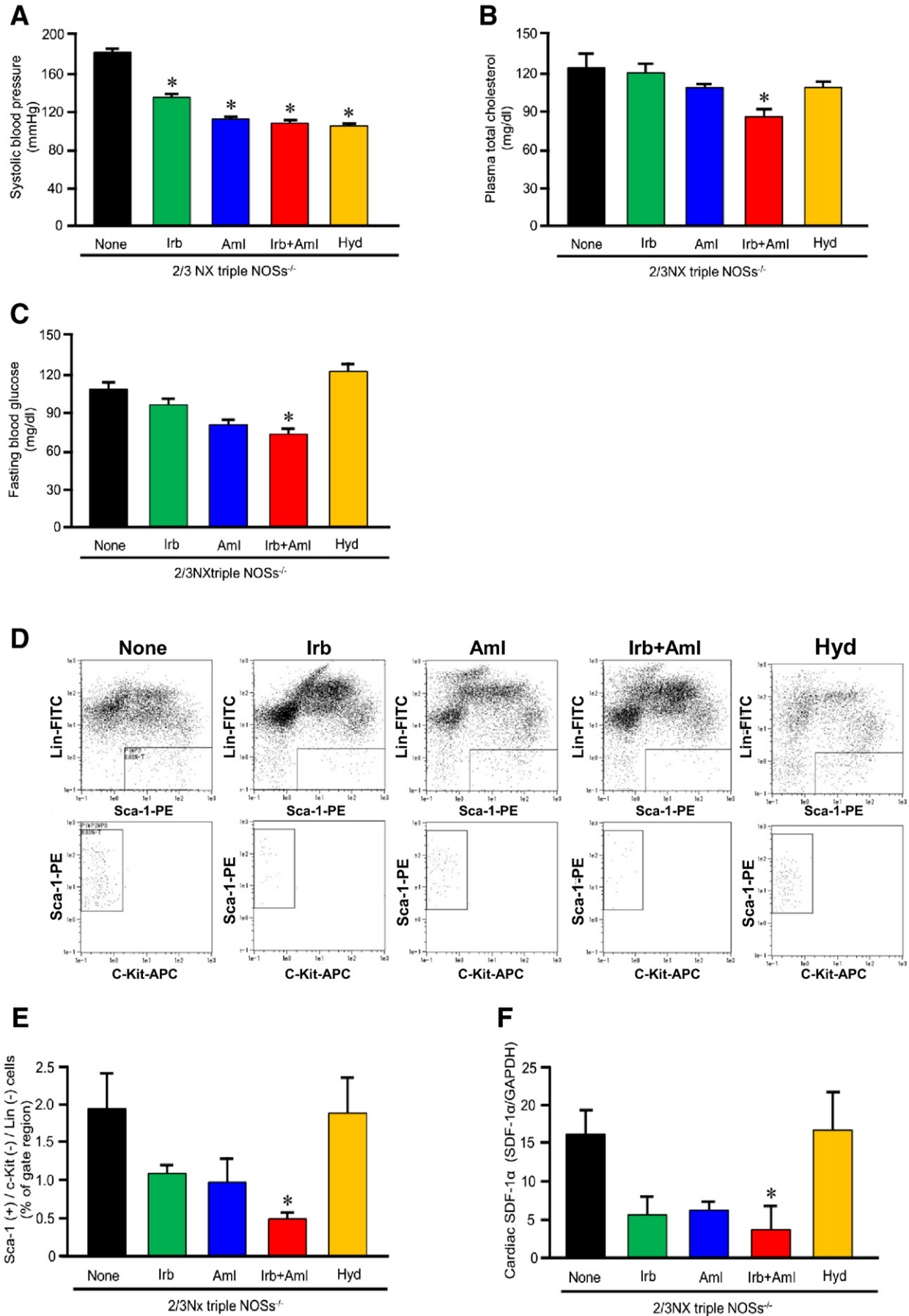
The treatments with irbesartan, amlodipine, and their combination significantly diminished the plasma creatinine levels and the urinary protein levels in the 2/3NX triple NOSs^{-/-} mice (Figs. 7I, J). The treatment with hydralazine also significantly attenuated the urinary protein levels, whereas it had no effect on the plasma creatinine levels (Figs. 7I, J). These results suggest that the decrease in the plasma creatinine levels might have been related to the renal protective actions of the pharmacological agents, while the reduction in the urinary protein levels might have been associated with the lowering of renal intraglomerular pressure induced by these anti-hypertensives.

The plasma total cholesterol levels and the fasting blood glucose levels in the 2/3NX triple NOSs^{-/-} mice tended to be lessened by the treatment with irbesartan or amlodipine, while statistically significant effects were noted only by the combined irbesartan/amlodipine treatment (Figs. 8B, C). Similarly, while the number of circulating Sca-1⁺/c-Kit⁻/Lin⁻ cells and the cardiac SDF-1 α protein levels in the 2/3NX triple NOSs^{-/-} mice tended to be suppressed by the irbesartan or amlodipine treatment, statistically significant effects were recognized exclusively by the simultaneous treatment with the two agents (Figs. 8D–F and Online Supplementary Fig. 4).

4. Discussion

The major novel findings of the present study are as follows: (i) 2/3NX caused sudden cardiac death due to acute myocardial infarction in male triple NOSs^{-/-} mice as early as 4 months after the surgery. (ii) The 2/3NX triple NOSs^{-/-} mice exhibited electrocardiographic ST-segment elevation, reduced heart rate variability, echocardiographic regional wall motion abnormality, and accelerated coronary

Fig. 7. Effects of treatment with an angiotensin II type 1 (AT₁) receptor blocker, irbesartan; an antioxidant calcium channel antagonist, amlodipine; a combination of irbesartan and amlodipine; or an anti-hypertensive agent, hydralazine, on renin–angiotensin system activation, oxidative stress, survival rate, incidence of myocardial infarction, coronary arteriosclerotic lesion formation, and renal function in the 2/3NX triple NOSs^{-/-} mice. Irb, irbesartan (50 mg/kg/day in chow); Aml, amlodipine (3.2 mg/kg/day in drinking water); Hyd, hydralazine (250 mg/mL in drinking water). The effects of the drugs on coronary lesion formation were assessed in the 2/3NX triple NOSs^{-/-} mice at 2 months after the surgery. (A) Plasma angiotensin II levels ($n = 10$). (B) Cardiac ACE protein expression levels ($n = 7$). (C) Urinary 8-isoprostane levels ($n = 8$). (D) Survival rate ($n = 20$ –49). (E) Percentage of death due to myocardial infarction in the total causes of death ($n = 6$ –49). (F) Neointimal formation (the ratio of intima area to media area) ($n = 6$ –16). (G) Medial thickening (the ratio of media area to total vascular area) ($n = 6$ –16). (H) Perivascular fibrosis (the ratio of perivascular area to total vascular area) ($n = 6$ –16). (I) Serum creatinine levels ($n = 10$). (J) Urinary protein levels ($n = 10$). * $P < 0.05$ vs. none (untreated control).



arteriosclerotic lesion formation. (iii) Cardiovascular risk factors (hypertension, hypercholesterolemia, and hyperglycemia), an increased number of circulating bone marrow-derived VSMC progenitor cells, and cardiac up-regulation of SDF-1 α were noted in the 2/3NX triple NOSs^{-/-} mice and were associated with significant increases in plasma angiotensin II levels and urinary 8-isoprostane levels. (iv) Simultaneous treatment with a clinical dosage of an angiotensin II type 1 receptor blocker, irbesartan, and an antioxidant calcium channel antagonist, amlodipine, markedly prevented coronary arteriosclerotic lesion formation and the incidence of myocardial infarction and improved the prognosis of those mice, along with ameliorating all those pro-arteriosclerotic parameters. Here we report the establishment of a new experimentally useful model of acute myocardial infarction.

4.1. Animal models that develops acute myocardial infarction

Five animal models that emerge acute myocardial infarction have thus far been reported. The first reported acute myocardial infarction model is a rat treated with a non-selective NOS inhibitor, such as N^ω-nitro-L-arginine methyl ester (L-NAME) or N^ω-nitro-L-arginine (L-NNA), chronically [20–23]. However, we clarified that arteriosclerotic vascular lesion formation caused by long-term treatment with L-NAME or L-NNA is not mediated by simple inhibition of NOSs activities [24]. While L-NAME- or L-NNA-treated rat shows multiple small infarcts without sudden death, those findings are quite different from human pathologies. The L-NAME- or L-NNA-treated rat has not been used at all as an acute myocardial infarction model. The second generated acute myocardial infarction model is the mouse with homozygous null mutations in the genes for both the high-density lipoprotein (HDL) receptor SR-B1 and apolipoprotein (apo) E [25]. The SR-B1^{-/-}/apoE^{-/-} mouse dies of acute myocardial infarction before 2 months of age (in childhood) even when fed a standard chow diet [25]. This short-term occurrence of acute myocardial infarction would be useful for experiments. However, the clinical course in human patients with acute myocardial infarction, which usually occurs in adulthood, is different from the natural course in the SR-B1^{-/-}/apoE^{-/-} mouse. The third produced model is the myocardial infarction-prone Watanabe heritable hyperlipidemic (WHHLMI) rabbit. The WHHLMI rabbit is not useful for experiments either because it takes a very long time (1 to 3 years) to develop acute myocardial infarction. The fourth created model is the SR-B1^{-/-}/hypomorphic apo ER61 (apoER^{h/h}) mouse, which shows high-fat diet-induced acute myocardial infarction [26]. Although the SR-B1^{-/-}/apoER^{h/h} mouse may be a good model, it has not been used at all in experiments in which the effects of drugs or therapies are examined since its generation was published 9 years ago, and only one article with this mouse has been published after the generation [27]. We reported a fifth model, the triple NOSs^{-/-} mouse, that spontaneously develops acute myocardial infarction. Unfortunately, however, it takes a very long time (approximately 1 year) for acute myocardial infarction to occur in our mouse. In the present study, the majority of the 2/3NX triple NOSs^{-/-} mice exhibited sudden cardiac death due to acute myocardial infarction within as little as 4 months after the surgery, and the experimental usefulness of this model was validated by demonstrating the preventive effects of the combined treatment with irbesartan and amlodipine on the occurrence of acute myocardial infarction. Therefore, our 2/3NX triple NOSs^{-/-} mouse is a new experimentally useful model of acute myocardial infarction.

Severe coronary arteriosclerosis, including infiltration of inflammatory cells, neointimal formation, medial thickening, and perivascular fibrosis, as well as coronary thrombus formation, was noted in the 2/3NX triple NOSs^{-/-} mice. These findings closely resemble the human pathology seen in the infarct-related coronary arteries in patients with myocardial infarction. We previously indicated that endothelium-dependent relaxations to acetylcholine are completely lacking in the triple NOSs^{-/-} mice and that contractions to phenylephrine are markedly enhanced, suggesting the presence of vascular dysfunction in the triple NOSs^{-/-} mice [11]. Thus, it is likely that acute myocardial infarction in the 2/3NX triple NOSs^{-/-} mice resulted from coronary arteriosclerosis, coronary thrombosis, and coronary vasospasm.

Heart rate variability is considered a noninvasive marker to evaluate autonomic nervous system function. It has been reported that low heart rate variability has prognostic value in patients with myocardial infarction and is associated with a higher risk of death in patients with coronary artery disease [28,29]. Consistent with the findings, significantly lower LF/HF ratio was noted in the 2/3NX triple NOSs^{-/-} mice.

4.2. Clinical implications

Several lines of evidence imply the clinical significance of the 2/3NX triple NOSs^{-/-} model. First, the natural course in which acute myocardial infarction occurs in the triple NOSs^{-/-} mice with partial nephrectomy closely resembles the clinical course in which patients with CKD develop acute myocardial infarction. Second, it has been suggested that the defective NOSs system is present in patients with CKD [30], as evidenced by the facts that in such patients urinary NOx excretion, a marker of systemic NO production derived from all three types of NOSs, are reduced [31], that whole body NO production (assessed by giving an intravenous infusion of [¹⁵N₂]-arginine and measuring isotopic plasma enrichment of [¹⁵N]-citrulline) is decreased [32], and that plasma levels of asymmetric dimethylarginine (ADMA), an endogenous NOS inhibitor, are elevated [33]. Finally, it has been reported that the defective NOSs system also exists in patients with coronary arteriosclerosis and myocardial infarction, as demonstrated by the findings that plasma and/or urinary NOx levels are reduced in such patients [34], that plasma ADMA concentrations are elevated in patients with arteriosclerosis and risk of myocardial infarction [35], and that the NOS gene polymorphisms are associated with arteriosclerosis, risk of myocardial infarction, and low plasma NOx levels in humans [36]. Thus, our acute myocardial infarction model may have clinical implications. However, since pathological conditions of the 2/3NX triple NOSs^{-/-} mice may be different from those of the patients with CKD, results obtained from our model must be interpreted with caution.

4.3. Mechanisms for acute myocardial infarction in the 2/3NX triple NOSs^{-/-} mice

Because significant increases in systolic blood pressure, plasma total cholesterol levels, and fasting blood glucose levels were noted in the 2/3NX triple NOSs^{-/-} mice, a clustering of cardiovascular risk factors seems to be involved in the pathogenesis of their acute myocardial infarction. In agreement with this evidence, it has been shown that patients with CKD have a high prevalence of those cardiovascular risk factors, and that those factors are associated with increased risks of acute myocardial infarction and sudden cardiac death [37].

It has recently been reported that bone marrow-derived mononuclear cells differentiate into VSMC progenitor cells, which circulate in

Fig. 8. Effects of treatment with an AT1 receptor blocker, irbesartan; a calcium channel antagonist, amlodipine; a combination of irbesartan and amlodipine; or an anti-hypertensive agent, hydralazine, on cardiovascular risk factors and SDF-1 α -induced recruitment of circulating bone marrow-derived VSMC progenitor cells in the 2/3NX triple NOSs^{-/-} mice. (A) Systolic blood pressure ($n = 10$ –12). (B) Plasma total cholesterol levels ($n = 10$ –12). (C) Fasting blood glucose levels ($n = 10$ –12). (D and E) The number of circulating Sca-1⁺/c-Kit⁻/Lin⁻ cells ($n = 7$). (F) Cardiac SDF-1 α protein levels ($n = 7$). * $P < 0.05$ vs. none (untreated control).

the blood, accumulate in vascular wall, and contribute to vascular lesion formation [38,39]. It has also been shown that the CXC chemokine SDF-1 α is a pivotal chemotactic factor of bone marrow-derived VSMC progenitor cells [40]. In the present study, the number of circulating Sca-1⁺/c-Kit⁻/Lin⁻ cells (interpreted as bone marrow-derived VSMC progenitor cells) [41] and the cardiac SDF-1 α protein levels were markedly increased in the 2/3NX triple NOSs^{-/-} mice. Thus, it is possible that SDF-1 α -induced recruitment of the circulating bone marrow-derived VSMC progenitor cells was also involved in the occurrence of acute myocardial infarction in the 2/3NX triple NOSs^{-/-} mice.

Renin-angiotensin system activation (as evidenced by increases in plasma angiotensin II levels and cardiac ACE expression levels) and oxidative stress (as indicated by elevation in urinary 8-isoprostane levels) were noted in the 2/3NX triple NOSs^{-/-} mice. Based on these findings, we used the selective and potent AT1 receptor blocker, irbesartan, and the antioxidant calcium channel antagonist, amlodipine, to further examine the involvement of renin-angiotensin system activation and oxidative stress in the pathogenesis of acute myocardial infarction. It has been indicated that amlodipine is a charged molecule, is highly lipophilic, and has a much higher affinity for lipid-laden cellular membranes than do other calcium channel antagonists, exerting a powerful antioxidant activity, independent of its calcium channel antagonistic action [42]. In the present study, the simultaneous treatment with irbesartan and amlodipine potently suppressed renin-angiotensin system activation and oxidative stress, and markedly prevented coronary arteriosclerotic lesion formation and the incidence of myocardial infarction, and improved the prognosis of the 2/3NX triple NOSs^{-/-} mice. Furthermore, the simultaneous irbesartan/amlodipine treatment significantly ameliorated the cardiovascular risk factors, the increased number of circulating Sca-1⁺/c-Kit⁻/Lin⁻ cells, and the enhanced cardiac SDF-1 α expression levels in those mice. Therefore, it is conceivable that renin-angiotensin system activation and oxidative stress are involved in the pathogenesis of acute myocardial infarction in the 2/3NX triple NOSs^{-/-} mice. Consistent with these results, it has been reported that renin-angiotensin system activation and oxidative stress are recognized in patients with CKD, and that both factors accelerate arteriosclerotic lesion formation [13].

The treatment with hydralazine exerted an anti-hypertensive action to the same extent as the combined treatment with irbesartan and amlodipine. However, the hydralazine treatment did not show any beneficial effects on the incidence of myocardial infarction, the prognosis, or the pro-arteriosclerotic parameters in the 2/3NX triple NOSs^{-/-} mice. Thus, it is suggested that the beneficial effects of the irbesartan/amlodipine treatment are not caused by changes of blood pressure.

4.4. Clinical perspectives

The mechanism(s) by which CKD is complicated by acute myocardial infarction is not fully understood. Our findings provide novel evidence that the NO/NOS system plays a pivotal role in the pathogenesis of this reno-cardiac connection. The AT1 receptor blockers and calcium channel antagonists are widely used to treat hypertension in patients with CKD, and the former are also employed to retard the progression of CKD. In the present study, the clinical dosage of irbesartan and amlodipine exhibited cardiovascular and renal protective actions in the 2/3NX triple NOSs^{-/-} mice. These results suggest the therapeutic importance of the AT1 receptor blockers and calcium channel antagonists in preventing complications of acute myocardial infarction in CKD as well as the progression of CKD.

4.5. Conclusions

We have succeeded in developing a novel experimentally useful model of acute myocardial infarction. Renin-angiotensin system activation, oxidative stress, cardiovascular risk factors, and SDF-1 α -induced

recruitment of circulating bone marrow-derived VSMC progenitor cells appear to be involved in the pathogenesis of acute myocardial infarction in the 2/3NX triple NOSs^{-/-} mice. This model may contribute to the elucidation of the pathogenesis of acute myocardial infarction, and to the research and development of novel therapeutic strategies for preventing this fatal cardiovascular disorder.

Sources of funding

This work was supported in part by a Grant-in-Aid for Scientific Research from the Japan Society for the Promotion of Science (23590305), Special Account Budgets for Education and Research granted by the Japan Ministry of Education, Grants from the Promotion Project of Medical Clustering of Okinawa prefecture and the University of the Ryukyus, and a Grant and Donation from the Sumitomo Dainippon Pharma Co, Japan. These funding sources had no involvement regarding the conduct of the research or preparation of the article.

Conflict of interest

We obtained irbesartan and amlodipine from the Sumitomo Dainippon Pharma Co, Japan, and received a research fund and donation from the company.

Appendix A. Supplementary data

Supplementary data to this article can be found online at <http://dx.doi.org/10.1016/j.jmcc.2014.09.021>.

References

- [1] White HD, Chew DP. Acute myocardial infarction. *Lancet* 2008;372:570–84.
- [2] Antman EM. ST-segment elevation myocardial infarction: pathology, pathophysiology, and clinical features. In: Libby P, Bonow RO, Mann D, Zipes DP, editors. *Braunwald's Heart Disease*. 9th ed. Philadelphia: Elsevier Saunders; 2012. p. 1087–110.
- [3] Antman EM, Loscalzo J. ST-segment elevation myocardial infarction. In: Longo DL, Fauci AS, Kasper DL, Hauser SL, Jameson JL, Loscalzo J, editors. *Harrison's Principles of Internal Medicine*. 18th ed. New York: Mc Graw Hill Medical; 2012. p. 2012–35.
- [4] Brecht DS, Snyder SH. Nitric oxide: a physiological messenger molecule. *Annu Rev Biochem* 1994;63:175–95.
- [5] Ignarro LJ. Biosynthesis and metabolism of endothelium-derived nitric oxide. *Annu Rev Pharmacol Toxicol* 1990;30:535–60.
- [6] Moncada S, Palmer RMJ, Higgs EA. Nitric oxide: physiology, pathophysiology, and pharmacology. *Pharmacol Rev* 1991;43:109–42.
- [7] Murad F. What are the molecular mechanisms for the antiproliferative effects of nitric oxide and cGMP in vascular smooth muscle? *Circulation* 1997;95:1101–3.
- [8] Shimokawa H. Primary endothelial dysfunction: atherosclerosis. *J Mol Cell Cardiol* 1999;31:23–37.
- [9] Tsutsui M, Shimokawa H, Otsuji Y, Yanagihara N. Pathophysiological relevance of NO signaling in the cardiovascular system: novel insight from mice lacking all NO synthases. *Pharmacol Ther* 2010;128:499–508.
- [10] Morishita T, Tsutsui M, Shimokawa H, Sabanai K, Tasaki H, Suda O, et al. Nephrogenic diabetes insipidus in mice lacking all nitric oxide synthase isoforms. *Proc Natl Acad Sci U S A* 2005;102:10616–21.
- [11] Nakata S, Tsutsui M, Shimokawa H, Suda O, Morishita T, Shibata K, et al. Spontaneous myocardial infarction in mice lacking all nitric oxide synthase isoforms. *Circulation* 2008;117:2211–23.
- [12] Coresh J, Selvin E, Stevens LA, Manzi J, Kusek JW, Eggers P, et al. Prevalence of chronic kidney disease in the United States. *JAMA* 2007;298:2038–47.
- [13] Lopez-Novoa JM, Martinez-Salgado C, Rodriguez-Pena AB, Lopez-Hernandez FJ. Common pathophysiological mechanisms of chronic kidney disease: therapeutic perspectives. *Pharmacol Ther* 2010;128:61–81.
- [14] Ninomiya T, Kiyohara Y, Kubo M, Tanizaki Y, Doi Y, Okubo K, et al. Chronic kidney disease and cardiovascular disease in a general Japanese population: the Hisayama Study. *Kidney Int* 2005;68:228–36.
- [15] Ninomiya T, Kiyohara Y, Tokuda Y, Doi Y, Arima H, Harada A, et al. Impact of kidney disease and blood pressure on the development of cardiovascular disease: an overview from the Japan Arteriosclerosis Longitudinal Study. *Circulation* 2008;118:2694–701.
- [16] Shoji T, Abe T, Matsuo H, Egusa G, Yamasaki Y, Kashihara N, et al. Chronic kidney disease, dyslipidemia, and atherosclerosis. *J Atheroscler Thromb* 2012;19:299–315.
- [17] Miyazaki-Anzai S, Levi M, Kratzer A, Ting TC, Lewis LB, Miyazaki M. Farnesoid X receptor activation prevents the development of vascular calcification in ApoE^{-/-} mice with chronic kidney disease. *Circ Res* 2010;106:1807–17.

- [18] Pelletier CC, Koppe L, Croze ML, Kalbacher E, Vella RE, Guebre-Egziabher F, et al. White adipose tissue overproduces the lipid-mobilizing factor zinc alpha2-glycoprotein in chronic kidney disease. *Kidney Int* 2013;83:878–86.
- [19] Schober A, Knarren S, Lietz M, Lin EA, Weber C. Crucial role of stromal cell-derived factor-1alpha in neointima formation after vascular injury in apolipoprotein E-deficient mice. *Circulation* 2003;108:2491–7.
- [20] Moreno Junior H, Nathan LP, Metze K, Costa SK, Antunes E, Hyslop S, et al. Non-specific inhibitors of nitric oxide synthase cause myocardial necrosis in the rat. *Clin Exp Pharmacol Physiol* 1997;24:349–52.
- [21] Ono Y, Ono H, Matsuoka H, Fujimori T, Frohlich ED. Apoptosis, coronary arterial remodeling, and myocardial infarction after nitric oxide inhibition in SHR. *Hypertension* 1999;34:609–16.
- [22] Verhagen AM, Hohbach J, Joles JA, Braam B, Boer P, Koomans HA, et al. Unchanged cardiac angiotensin II levels accompany losartan-sensitive cardiac injury due to nitric oxide synthase inhibition. *Eur J Pharmacol* 2000;400:239–47.
- [23] Ikeda K, Nara Y, Tagami M, Yamori Y. Nitric oxide deficiency induces myocardial infarction in hypercholesterolaemic stroke-prone spontaneously hypertensive rats. *Clin Exp Pharmacol Physiol* 1997;24:344–8.
- [24] Suda O, Tsutsui M, Morishita T, Tanimoto A, Horiuchi M, Tasaki H, et al. Long-term treatment with N(omega)-nitro-L-arginine methyl ester causes arteriosclerotic coronary lesions in endothelial nitric oxide synthase-deficient mice. *Circulation* 2002;106:1729–35.
- [25] Braun A, Trigatti BL, Post MJ, Sato K, Simons M, Edelberg JM, et al. Loss of SR-BI expression leads to the early onset of occlusive atherosclerotic coronary artery disease, spontaneous myocardial infarctions, severe cardiac dysfunction, and premature death in apolipoprotein E-deficient mice. *Circ Res* 2002;90:270–6.
- [26] Zhang S, Picard MH, Vasile E, Zhu Y, Raffai RL, Weisgraber KH, et al. Diet-induced occlusive coronary atherosclerosis, myocardial infarction, cardiac dysfunction, and premature death in scavenger receptor class B type I-deficient, hypomorphic apolipoprotein ER61 mice. *Circulation* 2005;111:3457–64.
- [27] Nakagawa-Toyama Y, Zhang S, Krieger M. Dietary manipulation and social isolation alter disease progression in a murine model of coronary heart disease. *PLoS One* 2012;7:e47965.
- [28] Taddei S, Virdis A, Ghiadoni L, Magagna A, Favilla S, Pompella A, et al. Restoration of nitric oxide availability after calcium antagonist treatment in essential hypertension. *Hypertension* 2001;37:943–8.
- [29] Tsuji H, Venditti Jr FJ, Manders ES, Evans JC, Larson MG, Feldman CL, et al. Reduced heart rate variability and mortality risk in an elderly cohort. The Framingham Heart Study. *Circulation* 1994;90:878–83.
- [30] Baylis C. Nitric oxide deficiency in chronic kidney disease. *Am J Physiol Renal Physiol* 2008;294:F1–9.
- [31] Schmidt RJ, Baylis C. Total nitric oxide production is low in patients with chronic renal disease. *Kidney Int* 2000;58:1261–6.
- [32] Wever R, Boer P, Hijmering M, Stroes E, Verhaar M, Kastelein J, et al. Nitric oxide production is reduced in patients with chronic renal failure. *Arterioscler Thromb Vasc Biol* 1999;19:1168–72.
- [33] Lu TM, Chung MY, Lin CC, Hsu CP, Lin SJ. Asymmetric dimethylarginine and clinical outcomes in chronic kidney disease. *Clin J Am Soc Nephrol* 2011;6:1566–72.
- [34] Piatti P, Di Mario C, Monti LD, Fragasso G, Sgura F, Caumo A, et al. Association of insulin resistance, hyperleptinemia, and impaired nitric oxide release with in-stent restenosis in patients undergoing coronary stenting. *Circulation* 2003;108:2074–81.
- [35] Cooke JP. ADMA: its role in vascular disease. *Vasc Med* 2005;10(Suppl. 1):S11–7.
- [36] Cook S. Coronary artery disease, nitric oxide and oxidative stress: the “Yin-Yang” effect, a Chinese concept for a worldwide pandemic. *Swiss Med Wkly* 2006;136:103–13.
- [37] Shamseddin MK, Parfrey PS. Sudden cardiac death in chronic kidney disease: epidemiology and prevention. *Nat Rev Nephrol* 2011;7:145–54.
- [38] Sata M, Saiura A, Kunisato A, Tojo A, Okada S, Tokuhisa T, et al. Hematopoietic stem cells differentiate into vascular cells that participate in the pathogenesis of atherosclerosis. *Nat Med* 2002;8:403–9.
- [39] Shimizu K, Sugiyama S, Aikawa M, Fukumoto Y, Rabkin E, Libby P, et al. Host bone-marrow cells are a source of donor intimal smooth-muscle-like cells in murine aortic transplant arteriopathy. *Nat Med* 2001;7:738–41.
- [40] Ceradini DJ, Kulkarni AR, Callaghan MJ, Tepper OM, Bastidas N, Kleinman ME, et al. Progenitor cell trafficking is regulated by hypoxic gradients through HIF-1 induction of SDF-1. *Nat Med* 2004;10:858–64.
- [41] Zhang LN, Wilson DW, da Cunha V, Sullivan ME, Vergona R, Rutledge JC, et al. Endothelial NO synthase deficiency promotes smooth muscle progenitor cells in association with upregulation of stromal cell-derived factor-1alpha in a mouse model of carotid artery ligation. *Arterioscler Thromb Vasc Biol* 2006;26:765–72.
- [42] Mason RP, Walter MF, Trumbore MW, Olmstead Jr EG, Mason PE. Membrane antioxidant effects of the charged dihydropyridine calcium antagonist amlodipine. *J Mol Cell Cardiol* 1999;31:275–81.



Usefulness of the apparent diffusion coefficient (ADC) for predicting the consistency of intracranial meningiomas



Akira Yogi ^{a,*}, Tomomi Koga ^a, Kimei Azama ^a, Daichi Higa ^a, Kazuhiko Ogawa ^{a,b}, Takashi Watanabe ^c, Shogo Ishiuchi ^c, Sadayuki Murayama ^a

^a Department of Radiology, Graduated School of Medical Science, University of the Ryukyus, Okinawa, Japan

^b Department of Radiation Oncology, Osaka University Graduate School of Medicine, Osaka, Japan

^c Neurosurgery, Graduated School of Medical Science, University of the Ryukyus, Okinawa, Japan

ARTICLE INFO

Article history:

Received 27 December 2013

Received in revised form 4 June 2014

Accepted 24 June 2014

Keywords:

Meningioma

Consistency

DWI

ADC

ABSTRACT

Meningioma consistency is an important factor for surgical treatment. Tumor cellularity and fibrous tissue contribute to the consistency of tumors, and it is proposed that the minimum apparent diffusion coefficient (ADC) value is significantly correlated with meningioma consistency. Twenty-seven consecutive patients with 28 meningiomas were retrospectively enrolled. Minimum ADC values in meningiomas with a hard consistency were significantly lower than those with a soft consistency. The minimum ADC value might have clinical use as a predictor of meningioma consistency.

© 2014 Elsevier Inc. All rights reserved.

1. Introduction

Meningiomas are one of the most common intracranial benign neoplasms in adults; they arise from meningotheial cells of the arachnoid layer. The incidence of meningiomas has been increasing [1–3], in part due to technological advancement of radiologic imaging in the ability to detect small meningiomas [1,3,4]. Typical meningiomas are seen as a sharply circumscribed isodense masses that are isodense to cortex on computed tomography (CT) images. On magnetic resonance imaging (MRI), a meningiomas are often isointense or slightly hypointense on T1-weighted images (T1WI), and variably hypointense to hyperintense on T2-weighted images (T2WI). This variability of signal change depends on the amount of tumor calcification, fibrous tissue, necrosis, vascularity, and histological cell types [5]. Marked and relatively homogeneous contrast enhancement with a dural tail sign is also typically seen.

Surgical resection is often the treatment of choice for symptomatic meningiomas. The consistency of meningiomas is an important factor in developing the strategy of surgical resection and predicting the degree of removal; soft tumors are easily curetted by suctioning, whereas hard tumors frequently require a lengthy and tedious dissection. A noninvasive technique that enables surgeons to preoperatively assess the mechanical properties of meningiomas

could provide valuable information affecting risk assessment, patient management, and workflow optimization. In the case of hard meningiomas, preoperative transarterial embolization is a useful method to soften tumors and facilitate resection, especially when they are located at a complex site such as cavernous sinus, clivus, cerebellopontine angle, and sellar lesion [4,6]. Though some investigators have employed T1WI and T2WI for this purpose, it remains inaccurate because amount of water is not the only factor affecting tumor consistency [6–9].

Diffusion weighted image (DWI) and the apparent coefficient (ADC) map, derived from DWI, can provide information of water diffusion. Some studies in glioma suggest that ADC value has a strong correlation with tumor cellularity, and therefore it also strongly correlates with World Health Organization (WHO) grade, treatment effect, and prognosis [9,10,13–15]. Furthermore, it has been reported that the ADC value also correlates with the amount of fibrous tissue [16,17]. Both tumor cellularity and the amount of fibrous tissue contribute the consistency of tumors, and it is supposed that the intratumoral ADC value has a significant correlation with the consistency of meningiomas. Nevertheless, to our knowledge, there have been no reports regarding the relationship between the quantitatively measured ADC value and the consistency of meningiomas. Although some studies reported the usefulness of diffusion tensor imaging and MR elastography to predict the consistency of tumor [18–23], these advanced MR techniques require special equipment and software, and are not still commonly used in clinical purpose. In contrast, DWI is now commonly accepted as a part of conventional MR examination in most institutes. For these reason, it is

* Corresponding author. Department of Radiology, Graduate School of Medical Science, University of the Ryukyus, 207 Uehara, Nishihara-cho, Nakagami-gun Okinawa, 903–0215, Japan. Tel.: +81 98 895 1162; fax: +81 98 895 1420.

E-mail address: jxo98ayg@med.u-ryukyu.ac.jp (A. Yogi).

Table 1
Summary of cases

Case	Location	Histologic subtypes	ADC _{min} ($\times 10^{-3}$ mm ² /s)	ADC _{max} ($\times 10^{-3}$ mm ² /s)	ADC _{mean} ($\times 10^{-3}$ mm ² /s)	Consistency
1	CPA	Psammomatous	0.477	1.470	0.796	Hard
2	CPA	Fibroblastic	0.451	3.530	0.865	Hard
3	Sphenoid ridge	Meningothelial	0.519	1.283	0.814	Hard
4	Convexity	Meningothelial	0.595	1.286	1.812	Hard
5	Petroclival	Meningothelial	0.584	2.402	1.128	Hard
6	Convexity	Angiomatous	0.633	1.957	0.977	Hard
7	Convexity	Fibroblastic	0.253	1.162	0.892	Hard
8	Petroclival	Meningothelial	0.702	1.978	1.133	Hard
9	Convexity	Transitional	0.449	2.235	0.832	Hard
10	Convexity	Meningothelial	0.560	1.635	0.936	Hard
11	Tuberculum sellae	Meningothelial	0.109	2.129	0.877	Hard
12	Parasagittal	Transitional	0.615	1.771	0.850	Hard
13	Sphenoid ridge	Secretory	0.553	2.342	1.233	Hard
14	CPA	Meningothelial	0.465	2.861	1.330	Hard
15	Sphenoid ridge	Meningothelial	0.582	1.298	0.834	Hard
16	Sphenoid ridge	Meningothelial	0.684	2.337	1.034	Hard
17	Parasagittal	Meningothelial	0.628	1.692	0.769	Hard
18	Sphenoid ridge	Atypical	0.538	3.038	0.885	Soft
19	Sphenoid ridge	Angiomatous	0.802	2.863	1.521	Soft
20	CPA	Fibroblastic	0.597	2.036	0.905	Soft
21	Sphenoid ridge	Transitional	0.729	2.589	0.958	Soft
22	Parasagittal	Angiomatous	0.666	2.395	1.314	Soft
23	Sphenoid ridge	Meningothelial	0.638	1.136	0.830	Soft
24	Tuberculum sellae	Angiomatous	0.950	2.945	1.179	Soft
25	Parasagittal	Meningothelial	0.736	1.507	0.982	Soft
26	CPA	Transitional	0.741	1.076	0.872	Soft
27	Tuberculum sellae	Meningothelial	0.815	1.717	1.065	Soft
28	CPA	Meningothelial	1.488	2.108	1.708	Soft

ADC_{min}: minimum ADC.ADC_{max}: maximum ADC.ADC_{mean}: mean ADC.

CPA; cerebellopontine angle.

important to investigate the relationship between ADC value and consistency of tumors. Thus, the purpose of the present study is to evaluate the usefulness of ADC value in predicting the consistency of meningiomas.

2. Materials and methods

2.1. Patient selection

The present study protocol was approved by the institutional ethics committee, and written informed consent was waived because of the retrospective nature of the investigation. For this retrospective study, all consecutive patients with intracranial meningiomas who were referred to our institute between October 2009 and August 2010 were included. A total of 27 patients with 28 meningiomas (4 men and 23 women; mean age, 55.1 years; range, 28–74 years) were enrolled in this study. The locations of meningiomas included eight in the sphenoid ridge, six in the cerebellopontine angle (CPA), five in the convexity, four in the parasagittal region, three in the tuberculum sellae, and two in the petroclival region. Histological subtypes based on World Health Organization (WHO) classification consisted of 27 grade I tumors (meningothelial; 14, transitional; four, angiomatous; four, fibroblastic; three, psammomatous; one, and secretory; one) and one WHO grade II tumors (atypical). Calcification and intratumoral hemorrhage were not confirmed in CT and conventional MRI.

2.2. Magnetic resonance imaging examination

All patients underwent MRI with a 1.5T clinical imager (MAGNETOM Avanto; Siemens, Munich, Germany) and a quadrature head coil. All patients underwent conventional MRI including axial spine-echo T1WI sequence [repetition time (ms)/echo time (ms)=3000/90; section thickness, 5 mm; and matrix size 320×260] and an axial turbo spin-echo

T2WI sequence (repetition time (ms)/echo time (ms)=4200/108; section thickness, 5 mm; and matrix size 448×108). DWI was acquired in the axial plane, with diffusion gradients applied along the three principal orthogonal axes, in turn, by using single-shot spin-echo echo-planar (EP) sequences. The following parameters were used: matrix, 232×256; field of view, 230mm; section thickness, 5mm; intersection gap, 2.5 mm; maximum gradient strength, 33 mT/m; acquisition time, 35s; and *b* values, 0 and 1000 s/mm². ADC maps were also generated.

2.3. Image analysis

The data of DWI and ADC map were transferred to the workstation (NUMERIS/4 syngoMR B17, Siemens, Munich, Germany). Two neuroradiologists (T.K. and D.H., with ten and three years of experience of brain MRI, respectively) who were blinded to the clinical and pathological details create the regions-of-interest (ROIs) on T2WI by consensus. All ROIs were manually drawn along with the tumor contour. The position of every ROI was therefore brought back on all the other images including ADC map, T1WI, DWI with *b* values of 0 and 1000 s/mm². Cystic degeneration, flow void, bone, and susceptibility artifacts derived from air and bone were intentionally avoided. ROIs were drawn on all slices where the lesion was visualized and the minimum (ADC_{min}), maximum (ADC_{max}), and mean ADC (ADC_{mean}) values were determined.

2.4. Surgery

All patients underwent surgical resection of the meningiomas. A neurosurgeon with sixteen years of experience in brain surgery who was blinded to the analysis of ADC value evaluated the consistency of the tumors, and classified them into two groups: meningiomas with a

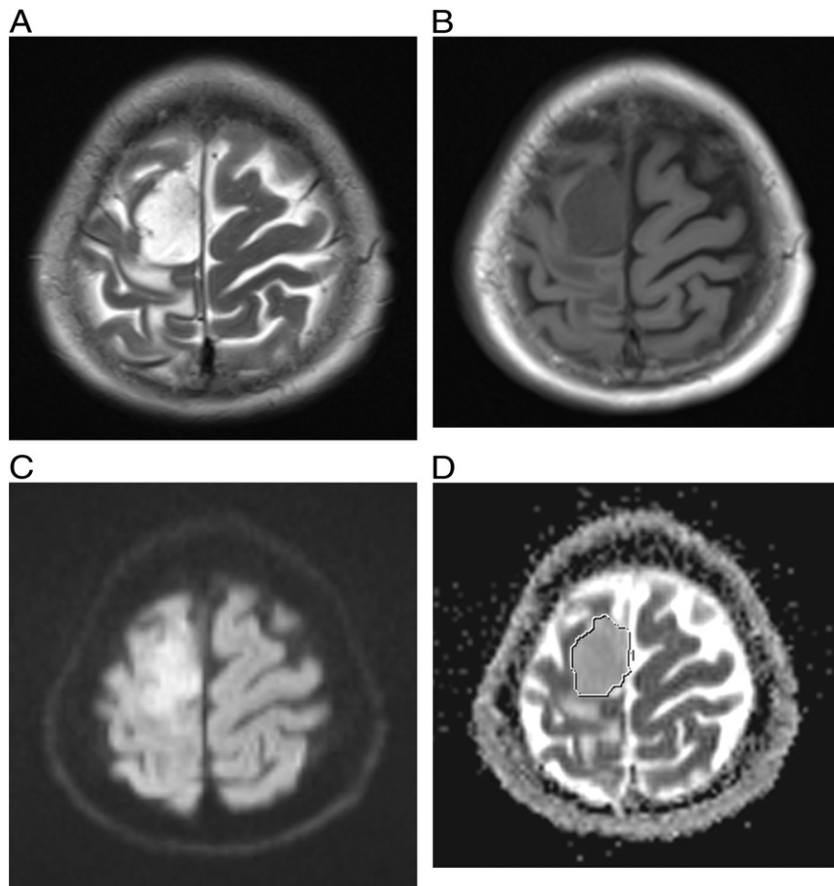


Fig. 1. A 60-year-old woman with angiomatous meningioma at right frontal parasagittal region. The tumor shows hyperintensity on T2WI (A), hypointensity on T1WI (B), and slight hyperintensity on DWI (C). The ROI was drawn around the tumor on the ADC map (D). The calculated ADC_{min} , ADC_{max} , and ADC_{mean} values were $0.66 \times 10^{-3} \text{ mm}^2/\text{s}$, $2.40 \times 10^{-3} \text{ mm}^2/\text{s}$, and $1.31 \times 10^{-3} \text{ mm}^2/\text{s}$, respectively. The ADC_{min} value was above the cut-off value ($0.64 \times 10^{-3} \text{ mm}^2/\text{s}$). Total removal was performed and the consistency was classed as soft.

“soft” consistency (removed by suction probe only) and meningiomas with a “hard” consistency (not removable through suction but excised).

2.5. Statistical analyses

Statistical analysis was achieved by statistical software (GraphPad Prism 6). Mann–Whitney *U* test and unpaired *t* test were used for analysis of ADC values between soft and hard groups. Sensitivity and specificity were calculated by receiver operating characteristics (ROC) curve analysis, and the best cut-off value was determined. The area under the curve (AUC) was elevated to assess test accuracy. In addition, all meningiomas were divided into two groups according to whether they occurred at skull base or not. All ADC values were compared between these two location groups using Mann–Whitney *U* test. A difference with a threshold *P* value of less than .05 was considered statistically significant.

3. Results

3.1. Surgical findings

At surgery, 17 meningiomas were classified as hard and 11 as soft. The hard group consisted of 10 meningothelial, two fibroblastic, two transitional, one psammomatous, one angiomatous, and one secretory meningioma. The soft group consisted of four meningothelial, three angiomatous, two transitional, one fibroblastic and one atypical. Two meningiomas demonstrated cystic components on MRI and which were confirmed at surgery.

3.2. Imaging findings and analyses

All meningiomas were clearly visualized on every MRI sequence and all ROI could be drawn accurately. Cystic degeneration and susceptibility artifacts were successfully avoided.

All ADC values of all cases are shown in Table 1. ADC_{min} , ADC_{max} , and ADC_{mean} values of all meningiomas were 0.63 ± 0.24 (range 0.11–1.49), 2.03 ± 0.65 (range 1.08–3.53), and 1.05 ± 0.27 (range 0.77–1.81) $\times 10^{-3} \text{ s/mm}^2$, respectively. For the hard group, these values were 0.52 ± 0.15 (range 0.11–0.70), 1.96 ± 0.63 (range 1.16–3.53), and 1.01 ± 0.26 (range 0.77–1.81) $\times 10^{-3} \text{ s/mm}^2$, respectively (Fig. 1) and for the soft group, these values were 0.79 ± 0.26 (range 0.54–1.49), 2.13 ± 0.71 (range 1.08–3.04), and 1.11 ± 0.29 (range 0.83–1.71) $\times 10^{-3} \text{ s/mm}^2$, respectively (Fig. 2). Statistical analysis indicated that ADC_{min} value of hard group was significantly lower than that of soft group ($P < .001$) (Fig. 3). ADC_{max} and ADC_{mean} values showed no significant difference between two groups though these values of hard group tended to be lower ($P = .52$ and $.21$, respectively). According to ADC_{min} value, the ROC curve revealed $0.64 \times 10^{-3} \text{ mm}^2/\text{s}$ as the best cut off value (Fig. 4). According to this cut-off value, sensitivity and specificity were calculated as 88% and 81%, respectively, and the AUC was 0.9.

Nineteen meningiomas were located at skull base; eight in the sphenoid ridge, six in the CPA, two in the tuberculum sella, and two in the petroclival region (meningothelial; 10, fibroblastic; two, transitional; one, angiomatous; one, and atypical; one), and nine meningiomas were located at supratentorial region; five in the convexity and four in the parasagittal region (meningothelial; four, transitional; two, angiomatous; two, and fibroblastic; one). All ADC

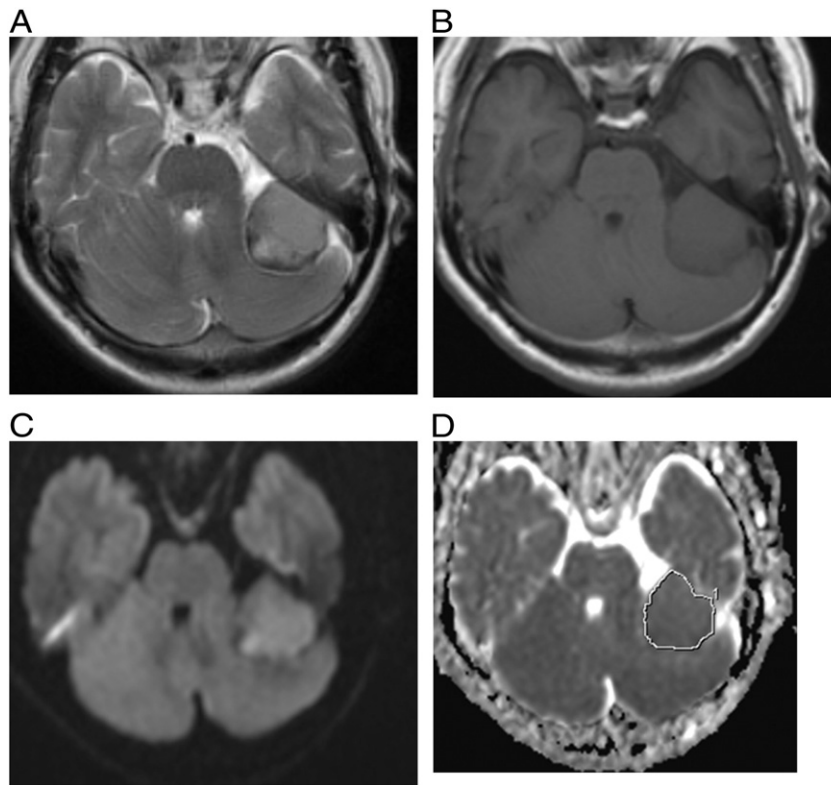


Fig. 2. A 58-year-old woman with a fibroblastic meningioma at left cerebellopontine angle. On T2WI (A), the periphery of the tumor shows hypointensity, and the inside of the tumor shows hyperintensity. The tumor shows slight hypointensity to isointensity on T1WI (B). The tumor shows hyperintensity on DWI (C). The ROI was drawn around the tumor on ADC map (D). The calculated ADC_{min} , ADC_{max} , and ADC_{mean} values were $0.45 \times 10^{-3} \text{ mm}^2/\text{s}$, $3.53 \times 10^{-3} \text{ mm}^2/\text{s}$, and $0.87 \times 10^{-3} \text{ mm}^2/\text{s}$, respectively. The ADC_{min} value was under the cut-off value ($0.64 \times 10^{-3} \text{ mm}^2/\text{s}$). Total removal was performed and the consistency was classed as hard.

values showed no significant difference between these two location groups ($P=.55, .11, \text{ and } .75$, respectively).

4. Discussion

It has been reported that there is a significant correlation between MR signal intensity and the consistency of meningiomas. Recently, Hoover et al. and Sitthinamsuwan et al. found a strong relationship between the signal intensity of T2WI and the consistency of meningiomas [24,25]. Yamaguchi et al. reported that meningiomas which showed hyperintensity on T2WI and proton density weighted images were soft, and they postulated that the water content of meningiomas is an important factor related to consistency [21]. Maiuri et al. reported that meningiomas with more hyperintensity than the cortex on T2WI were usually soft, more vascular, and more frequently were of the syncytial or angioblastic subtype, whereas meningiomas with more hypointensity than the cortex on T2WI tended to be hard and more frequently of the fibroblastic subtype [8]. These reports concluded that the amount of water or fibrous tissue resulted in a soft or hard consistency, and hyperintensity or hypointensity on T2WI, respectively [8,21,24,25].

However, this correlation has not been consistently demonstrated. Carpeggiani et al. did not find any statistically significant correlation between signal intensity and the consistency of meningioma, although they agreed that hyperintense meningioma on T2WI was unlikely to be fibroblastic or hard [12]. Besides, Kasoff et al. didn't find any relationship between MRI findings with the consistency and water content of meningiomas [11].

Tumor cellularity and the amount of fibrous tissue are important factors of tumor consistency. Meningioma cells are characterized by interdigitations connected with junctional complexes and extracellular cisterns, and it is supposed that meningiomas with higher

cellularity have stronger cell adhesion [21]. Fibrous tissue and high cellularity with a low nucleus-to-cytoplasm ratio reduce the signal intensity on T2WI, whereas extracellular space with interstitial fluid may increase the signal intensity on T2WI. Each of these mechanisms can have a different contribution to signal intensity on T2WI and may therefore limit the diagnostic utility in predicting the consistency. It has been suggested that the ADC value inversely correlates with tumor cellularity and the amount of fibrous tissue within heterogeneous tumors [9,14,15,26]. Thus, it is supposed that tumors, including meningiomas, with low ADC value have a hard consistency. In this

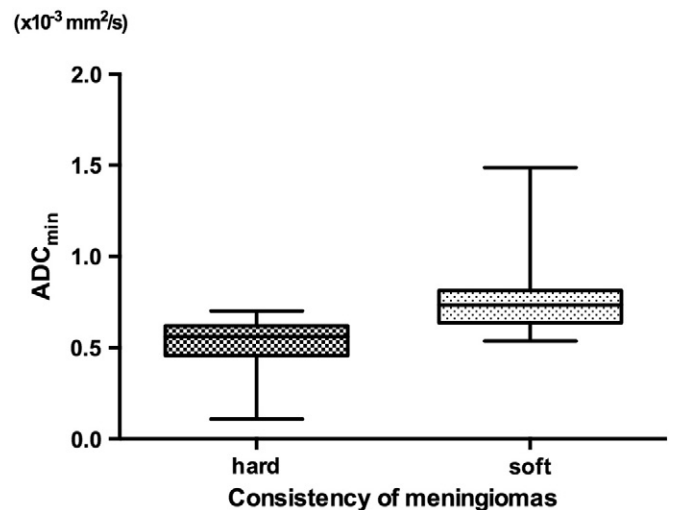


Fig. 3. Box plots showing the consistency of the meningioma and the ADC_{min} value. ADC_{min} value in the hard group was significantly lower ($P<.001$).

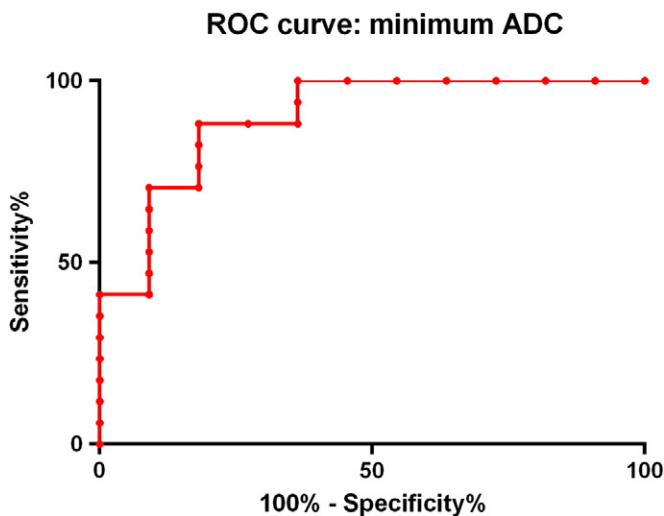


Fig. 4. Graph shows the ROC curves of ADC_{min} . The ROC curve calculated the best cut off value as $0.64 \times 10^{-3} \text{ mm}^2/\text{s}$. For this cut-off value, sensitivity and specificity were calculated 88% and 81%, respectively. The AUC was 0.9.

study, the minimum ADC values of hard group showed significantly lower ADC values than those of soft group, which consistent with this theory. Maximum ADC values and mean ADC values, on the other hand, showed no significant difference between hard and soft groups though mean ADC were reported to be related to some histologic subtypes [27]. It is because we divided meningiomas into soft or hard group according to if they were completely resected by suction probe only. In this classification, if a small component of meningioma could not be removed by suction probe only, the meningioma was classified as “hard” group even though most parts were easily removed. Though this division is not directly associated with whole histologic feature, it is useful to determine which surgical devices will be needed for complete resection.

Recently, Hoover et al. reported that T1WI and T2WI predicted the consistency of meningiomas, but DWI and ADC maps were not correlated with tumor consistency [24]. They, however, performed only qualitative analysis and did not measure ADC values of the meningioma. In contrast, we performed a quantitative analysis using ROIs. These ROIs were constructed by contouring the tumor with all slices and avoiding cystic degeneration, flow void, bone, and susceptibility artifacts. Thus, this method can better reflect the entire tumor tissue.

As hemosiderin deposition was not confirmed in present study, it is not common in meningioma unlike pituitary macroadenomas, in which intratumoral hemorrhage often occurs and results in preventing calculating ADC values accurately [17]. Thus, intrinsic susceptibility artifacts were less common in meningiomas, excepting the cases with calcification.

On DWI, abnormal signal change and spatial distortion often occurs by the susceptibility artifacts derived by air, bone, and hemorrhage, which could result in showing inadequate ADC values. Though meningiomas occur in supratentorial region more commonly than in skull base [4] where susceptibility artifacts often exist [28], about two thirds of cases were located at skull base in the present study. Because there was no significant difference in ADC values between these two location groups, it is supposed that potential susceptibility artifacts did not significantly affect the ADC values.

Present study has several limitations. The principle limitation of our study is its relatively small number of patients. Second, because there was a lack of direct histopathological correlation with ADC values, we could not clarify which was the main factor accounting for decreasing ADC values, high cellularity or rich fibrous tissue. Third, all ROIs were drawn manually and were susceptible to bias. Two blinded

observers, however, drew ROIs by consensus, which should have minimized it. Fourth, all DWI were performed by using EP sequences, which often suffered by susceptibility artifacts at skull base. As mentioned above, we drew ROIs avoiding artifacts, and ADC values showed no significant difference between skull base lesion and supratentorial lesion. Thus, it is supposed that there was little influence that intrinsic susceptibility artifact affected ADC values in this study. Further study using advanced DWI technique including readout-segmented EP imaging [29], periodically rotated overlapping parallel lines with enhanced reconstruction (PROPELLER) DWI [17], and 3D turbo field echo with diffusion-sensitized driven-equilibrium preparation [30], which has higher spatial resolution and fewer susceptibility artifacts, might elucidate the relationship between ADC values and meningioma consistency. Finally, we didn't confirm prospectively if minimum ADC value would really give surgeon useful information in making decision of management. There is still an overlap of the ADC values between two groups, and it could be misleading in determining consistency. It might be more useful to combine the results of signal intensity of other sequences including T2WI, T1WI, and so on, and further studies are needed.

5. Conclusions

The present study suggests that the minimum ADC value can be a promising tool to predict the consistency of intracranial meningiomas. Meningiomas with low minimum ADC are considered to have a hard consistency. It is very important and beneficial to predict the meningioma consistency for surgical planning and selection of the surgical devices, especially if the tumors are located in complex regions. Because DWI is available in many institutes, the minimum ADC may be a tool for predicting the consistency of meningiomas. Furthermore, with inclusion of more study cases and analysis across modalities, ADC values may help select cases for preoperative embolization in future.

Conflicts of interest

None.

Acknowledgments

We received no acknowledgement of grants, disclosures, or other assistance.

References

- [1] Dobes M, Khurana VG, Shadbolt B, Jain S, Smith SF, Smee R, Dexter M, Cook R. Increasing incidence of glioblastoma multiforme and meningioma, and decreasing incidence of Schwannoma (2000–2008): findings of a multicenter Australian study. *Surg Neurol Int* 2011;2:176. <http://dx.doi.org/10.4103/2152-7806.90696>.
- [2] Hoffman SPJ, McCarthy BJ. Temporal trends in incidence of primary brain tumors in the United States, 1985–1999. *Neuro Oncol* 2009;8:27–37.
- [3] Klæboe L, Lonn S, Scheie D, Auvinen A, Christensen HC, Feychting M, Johansen C, Salminen T, Tynes T. Incidence of intracranial meningiomas in Denmark, Finland, Norway and Sweden, 1968–1997. *Int J Cancer* 2005;20:996–1001.
- [4] Belinda A, Campbell MBBS, Jhamb A, Manguir JA, Toyota B, Roy M. Meningiomas in 2009: controversies and future challenges. *Am J Clin Oncol* 2009;32:73–85.
- [5] Majda M, Thurnher MD, editors. *Diagnostic imaging: brain*. 2nd ed. Salt Lake City: Amirsy; 2010.
- [6] Eis M, Els T, Hoehn-Berlage M, Hossmann KA. Quantitative diffusion MR imaging of cerebral tumor and edema. *Acta Neurochir Suppl (Wien)* 1994;60:344–6.
- [7] Chen TC, Zee CS, Miller CA, Weiss MH, Tang G, Chin L, Levy ML, Apuzzo ML. Magnetic resonance imaging and pathological correlates of meningiomas. *Neurosurgery* 1992;31:1015–22.
- [8] Maiuri F, Iaconetta G, de Divitiis O, Cirillo S, Di Salle F, De Caro ML. Intracranial meningiomas: correlations between MR imaging and histology. *Eur J Radiol* 1997;31:69–75.
- [9] Guo AC, Cummings TJ, Dash RC, Provenzale JM. Lymphomas and high-grade astrocytomas: comparison of water diffusibility and histologic characteristics. *Radiology* 2002;224:177–83.
- [10] Castillo M, Smith JK, Kwock L, Wilber K. Apparent diffusion coefficients in the evaluation of high-grade cerebral gliomas. *AJNR Am J Neuroradiol* 2001;22:60–4.

- [11] Eis M, Els T, Hoehn-Berlage M. High resolution quantitative relaxation and diffusion MRI on three different experimental brain tumors in rat. *Magn Reson Med* 1995;34:835–44.
- [12] Eis M, Els T, Hoehn-Berlage M, Hossmann KA. Quantitative diffusion MR imaging of cerebral tumor and oedema. *Acta Neurochir Suppl (Wien)* 1994;60:344–6.
- [13] Gauvain KM, McKinstry RC, Mukherjee P, Perry A, Neil JJ, Kaufman BA, Hayashi RJ. Evaluating pediatric brain tumor cellularity with diffusion-tensor imaging. *AJR Am J Roentgenol* 2001;177:449–54.
- [14] Kono K, Inoue Y, Nakayama K, Shakudo M, Morino M, Ohata K, Wakasa K, Yamada R. The role of diffusion-weighted imaging in patients with brain tumors. *AJNR Am J Neuroradiol* 2001;22:1081–8.
- [15] Sugahara T, Korogi Y, Kochi M, Ikushima I, Shigematu Y, Hirai T, Okuda T, Liang L, Ge Y, Komohara Y, Ushio Y, Takahashi M. Usefulness of diffusion-weighted MRI with echo-planar technique in the evaluation of cellularity in gliomas. *J Magn Reson Imaging* 1999;9:53–60.
- [16] Fujimoto K, Tonan T, Azuma S, Kage M, Nakashima O, Johkoh T, Hayabuchi N, Okuda K, Kawaguchi T, Sata M, Qayyum A. Evaluation of the mean and entropy of apparent diffusion coefficient values in chronic hepatitis C: correlation with pathologic fibrosis stage and inflammatory activity grade. *Radiology* 2011;258(3):739–48.
- [17] Mahmoud OM, Tominaga A, Amatya VJ, Ohtaki M, Sugiyama K, Sakoguchi T, Kinoshita Y, Takeshima Y, Abe N, Akiyama Y, El-Ghoriyan AI, Abd Alla AK, El-Sharkawy MA, Arita K, Kurisu K, Yamasaki F. Role of PROPELLER diffusion-weighted imaging and apparent diffusion coefficient in the evaluation of pituitary adenomas. *Eur J Radiol* 2011;80(2):412–7.
- [18] Kashimura H, Inoue T, Ogasawara K, Arai H, Otawara Y, Kanbara Y, Ogawa A. Prediction of meningioma consistency using fractional anisotropy value measured by magnetic resonance imaging. *J Neurosurg* 2007;107(4):784–7.
- [19] Le Bihan D, Mangin JF, Poupon C, Clark CA, Pappata S, Molko N, Chabriat H. Diffusion tensor imaging: concepts and applications. *J Magn Reson Imaging* 2001;13(4):534–46.
- [20] Muthupillai R, Lomas DJ, Rossman PJ, Greenleaf JF, Manduca A, Ehman RL. Magnetic resonance elastography by direct visualization of propagating acoustic strain waves. *Science* 1995;269:1854–7.
- [21] Muthupillai R, Rossman PJ, Lomas DJ, Greenleaf JF, Riederer SJ, Ehman RL. Magnetic resonance imaging of transverse acoustic strain waves. *Magn Reson Med* 1996;36:266–74.
- [22] Pierpaoli C, Basser PJ. Toward a quantitative assessment of diffusion anisotropy. *Magn Reson Med* 1996;36(6):893–906.
- [23] Tropine A, Dellani PD, Glaser M, Bohl J, Plöner T, Vucurevic G, Perneczky A, Stoeter P. Differentiation of fibroblastic meningiomas from other benign subtypes using diffusion tensor imaging. *J Magn Reson Imaging* 2007;25(4):703–8.
- [24] Hoover JM, Morris JM, Meyer FB. Use of preoperative magnetic resonance imaging T1 and T2 sequences to determine intraoperative meningioma consistency. *Surg Neurol Int* 2011;2:142. <http://dx.doi.org/10.4103/2152-7806.85983>.
- [25] Sitthinamsuwan B, Khampalikit I, Nunta-aree S, Srirabheebhat P, Witthiwej T, Nitising A. Predictors of meningioma consistency: A study in 243 consecutive cases. *Acta Neurochir (Wien)* 2012;154(8):1383–9.
- [26] Higano S, Yun X, Kumabe T, Watanabe M, Mugikura S, Umetsu A, Sato A, Yamada T, Takahashi S. Malignant astrocytic tumors: clinical importance of apparent diffusion coefficient in prediction of grade and prognosis. *Radiology* 2006;241:839–46.
- [27] Yin B, Liu L, Ahang BY, Li YX, Geng DY. Correlating apparent diffusion coefficients with histopathologic findings on meningiomas. *Eur J Radiol* 2012;81(12):4050–6.
- [28] Le Bihan D, Poupon C, Amadon A, Lethimonnier F. Artifacts and pitfalls in diffusion MRI. *J Magn Reson Imaging* 2006;24(3):478–88 [Review].
- [29] Holdsworth SJ, Yeom K, Skare S, Gentles AJ, Barnes PD, Bammer R. Clinical application of readout-segmented-echo-planar imaging for diffusion-weighted imaging in pediatric brain. *AJNR Am J Neuroradiol* 2011;32(7):1274–9.
- [30] Hiwatashi A, Yoshiura T, Togao K, Yamashita K, Kikuchi K, Kobayashi M, Ohga S, Sonoda S, Honda H, Obara M. Evaluation of diffusivity in the anterior lobe of the pituitary gland: 3D turbo field echo with diffusion-sensitized driven-equilibrium preparation. *AJNR Am J Neuroradiol* 2014;35:95–8.

Enhanced expression of proapoptotic and autophagic proteins involved in the cell death of glioblastoma induced by synthetic glycans

Laboratory investigation

AHMAD FARIED, M.D., PH.D.,¹ MUHAMMAD ZAFRULLAH ARIFIN, M.D., PH.D.,¹
SHOGO ISHIUCHI, M.D., PH.D.,² HIROYUKI KUWANO, M.D., PH.D.,³ AND SHIN YAZAWA, PH.D.^{3,4}

¹Department of Neurosurgery, Faculty of Medicine, Universitas Padjadjaran–Dr. Hasan Sadikin Hospital, Bandung, Indonesia; ²Department of Neurosurgery, Faculty of Clinical Medicine, the University of Ryukyus, Nakagami-gun, Okinawa; ³Department of General Surgical Science, Faculty of Medicine, Gunma University, Maebashi; and ⁴Tokushima Research Institute, Otsuka Pharmaceutical Co. Ltd., Tokushima, Japan

Object. Glioblastoma is the most aggressive malignant brain tumor, and overall patient survival has not been prolonged even by conventional therapies. Previously, the authors found that chemically synthesized glycans could be anticancer agents against growth of a series of cancer cells. In this study, the authors examined the effects of glycans on the growth of glioblastoma cells both in vitro and in vivo.

Methods. The authors investigated not only the occurrence of changes in the cell signaling molecules and expression levels of various proteins related to cell death, but also a mouse model involving the injection of glioblastoma cells following the administration of synthetic glycans.

Results. Synthetic glycans inhibited the growth of glioblastoma cells, induced the apoptosis of the cells with cleaved poly (adenosine diphosphate-ribose) polymerase (PARP) expression and DNA fragmentation, and also caused autophagy, as shown by the detection of autophagosome proteins and monodansylcadaverine staining. Furthermore, tumor growth in the in vivo mouse model was significantly inhibited. A dramatic induction of programmed cell death was found in glioblastoma cells after treatment with synthetic glycans.

Conclusions. These results suggest that synthetic glycans could be a promising novel anticancer agent for performing chemotherapy against glioblastoma.

(<http://thejns.org/doi/abs/10.3171/2014.1.JNS131534>)

KEY WORDS • synthetic glycan • glioblastoma • apoptosis • autophagy • oncology

GLIOLASTOMA is the most aggressive and lethal malignancy of the CNS, and patients with glioblastoma have an average life expectancy of 1 year after the standard treatment of surgery followed by radiation therapy.^{26,45} Recently, clinical studies have shown

that chemotherapy in addition to radiation therapy could increase patient survival up to 2 years.⁴⁵ The continuing problems caused by glioblastoma and the failure of conventional therapy for this advanced invasive brain tumor indicate that novel strategies and anticancer drugs are critically needed to improve the prognosis.

Glioblastoma cells are naturally resistant to cell death,^{16,26} which has been considered to be attributable to the activation of phosphatidylinositol 3-kinase (PI3K) by growth factors and the subsequent hyperactivation of its downstream targets, the serine/threonine kinases protein kinase B (Akt) and mammalian target of rapamycin (mTOR). These targets are known to release a variety of

Abbreviations used in this paper: Akt = protein kinase B; AMPA = α -amino-3-hydroxy-5-methyl-4-isoxazolepropionic acid; CPI = cell proliferation inhibition; HP- β -CD = hydroxypropyl- β -cyclodextrin; Gal β Chol = D-galactose β cholestanol; GChol = GlcNAc β Chol; GGChol = GlcNAc β 1,3 Gal β Chol; GlcNAc β 1,3 = N-acetyl-D-glucosamine β 1,3; GluR1 = glutamate receptor 1; GluR4 = glutamate receptor 4; HO342 = Hoechst 33342; MDC = monodansylcadaverine; mTOR = mammalian target of rapamycin; PARP = poly (adenosine diphosphate-ribose) polymerase; PI3K = phosphatidylinositol 3-kinase; Z-VAD-FMK = benzylloxycarbonyl-Val-Ala-Asp(OMe)-fluoromethylketone.

This article contains some figures that are displayed in color online but in black-and-white in the print edition.

Cell death of glioblastoma induced by glycans

antiapoptotic signals, thereby promoting the proliferation of the tumor cells.^{26,34,39} Growing evidence is accumulating that glioblastoma cells exploit glutamate for their proliferation and migration ability. The released glutamate may stimulate glioblastoma cell growth and migration through the autocrine and/or paracrine activation of glutamate receptors.^{20,21} In addition, the expression of Rho GTPase family members has been demonstrated in a wide variety of malignancies^{9,12,18,23} and in high-grade glioma as a hallmark of cell migration and as a predictor of the clinical prognosis.⁴⁷

Programmed cell death plays an important role during tissue development and homeostasis. Aberrations in this process result in the pathology of numerous disorders, such as malignancy. Apoptosis is the most common form of programmed cell death, but recently, alternative cell death programs have received increased attention, with autophagy proposed as an important nonapoptotic cell death mechanism.^{6,33}

In our previous studies, using chemically synthesized glycans consisting of sugar cholestanols with mono-, di-, and trisaccharides attached to cholestanols, we showed both strong inhibitory activity against the proliferation of a series of mouse and human cancer cells from the digestive system and antitumor effects in a mouse model of peritoneal dissemination.^{8,14,15} The sugar cholestanols added to the cell culture were rapidly taken up via the lipid rafts/microdomains on the cell surface.¹⁵ The uptake of sugar cholestanols in mitochondria increased gradually and was followed by the activation of apoptotic signals via the caspase cascade, leading to apoptotic cell death.^{8,14,15} Furthermore, the examination of sugar cholestanols in a mouse model of peritoneal dissemination showed a dramatic reduction of tumor growth and a prolonged survival time of the mice.¹⁵ The sugar cholestanols described in our previous studies, therefore, appeared to have clinical potential as novel anticancer agents. However, the cell death pathways in malignant glioma cells induced by the same compounds remain an open question. In this study, we investigated the programmed cell death induced by the sugar cholestanols in glioblastoma cells and its anticancer effect on growth in nude mice.

Methods

Cell Lines and Culture Condition

Human glioblastoma cell lines, CGNH-89 and CGNH-NM, were established as described previously.^{19,20} The morphology of CGNH cells is epithelial and adherent type, and their doubling time is 24 hours. CGNH cells were established through resection from the tumor at the right frontal lobe of female patients according to the explant method by Nichols et al.³⁶ It has been demonstrated that the CGNH cells have glioblastoma morphological characteristics, and they grow very fast (highly cellular) and are relatively monotonous, while some are multinucleated giant cells with slight nuclear pleomorphism, marked atypical nucleus, and brisk mitotic activity.^{19,20} The cells were maintained at 37°C in DMEM (Nissui) supplemented with 10% fetal bovine serum (Invitrogen) and 3% L-glutamine in a humidified atmosphere of 5% CO₂ in air. When they

were confluent, the cells were exposed in 0.05% trypsin and subcultured in the same growth medium.

Compounds

N-acetyl-D-glucosamine (GlcNAc) β1,3 D-galactose (Gal) β cholestanol, or GGChol, and GlcNAc β cholestanol, or GChol, were synthesized and prepared^{13,15} as an inclusion complexation with 20% of hydroxypropyl-β-cyclodextrin (HP-β-CD; BICO) and used for the experiment as previously described.^{8,15}

Antibodies and Chemical Reagents

Anti-GluR1 (glutamate receptor 1) and GluR4 (glutamate receptor 4) were obtained from Chemicon. Anti-RhoA, RhoC, Beclin-1, and LC3 were obtained from Santa Cruz Biotech, Inc. Anti-pAkt at ser473, pmTOR at ser2448, p53 at ser46, Bcl-2 family, caspase family, and poly (adenosine diphosphate-ribose) polymerase (PARP) were obtained from Cell Signaling. 3-Methyladenine (3-MA; Sigma), was used as an inhibitor of autophagy. 3-MA (30 mg) was dissolved with 1 ml dH₂O to make a 200 mM stock solution and kept at room temperature. Benzoyloxycarbonyl-Val-Ala-Asp(OMe)-fluoromethylketone (Z-VAD-FMK, or just Z-VAD; BD Biosciences), a general caspase inhibitor, was used to inhibit apoptosis. Z-VAD was dissolved in dimethylsulfoxide for a stock solution. And 1 mM of 3-MA and 10 μM of Z-VAD were diluted separately in DMEM to obtain the desired concentration. The autofluorescent agent monodansylcadaverine (MDC; Sigma) was introduced as a specific autophagolysosome marker to analyze the autophagic process.³² The fluorescence of MDC has been reported to be a specific marker for autophagic vacuoles.¹ Monodansylcadaverine was dissolved in methanol (10 mg/ml) and used to observe autophagy.

Cell Proliferation Inhibition and Nuclear Fragmentation Assays

Cell proliferation inhibition with each compound was conducted in the presence of serially diluted compounds as described previously.^{8,15} DNA binding dyes, Hoechst 33342 (HO342), in addition to propidium iodide fluorescence, were used for determination of apoptosis.¹⁷ Cells were exposed to HO342 (10 μM) and propidium iodide (10 μM), and each fluorescence intensity was examined using a fluorescence microscope with ultraviolet excitation at 340–380 nm. The apoptotic index (AI) was calculated as follows:

$$AI = \frac{\text{apoptotic cell number}}{\text{apoptotic cell number} + \text{necrotic cell number} + \text{viable cell number}} \times 100\%$$

Protein Extraction and Western Blot Analysis

All cells were harvested at approximately 80% confluent growth. Protein concentrations of the cell lysate were determined with a bicinchoninic acid protein assay kit (Pierce) using bovine serum albumin as a standard. Each sample (50 μg protein/line) was run on a 5%–20% ReadyGel (Bio-Rad) and the gel was then electrotransferred to a hybrid-enhanced chemiluminescence nitrocellulose

membrane (Amersham Pharmacia Biotech). Changes in expression levels of corresponding (apoptosis and autophagy) proteins after treatment with sugar cholestanol were analyzed by Western blotting; β -actin was used as a loading control. Bands on the membrane were detected using an enhanced chemiluminescence detection system, and horizontal scanning densitometry was performed using Photoshop software (version 3.0, Adobe), and analyzed by Quantity One software (BioRad).

Analysis of Autophagy

The analysis of autophagy was performed with the aid of MDC and counted as previously described.³² Autophagic vacuoles were labeled with MDC, and the fluorescent images were obtained with an epifluorescence microscope (BX-50, Olympus). The quantification of intracellular MDC accumulation was measured by fluorometry. Cells (2×10^4) were incubated with 0.05 mM MDC in phosphate-buffered saline at 37°C for 10 minutes and collected in 10 mM Tris-HCl, pH 8.0, containing 0.1% Triton X-100. Fluorescence was measured at a 380-nm excitation wavelength with a 530-nm emission filter, using an MTP-600 microplate reader (Corona Electric). Monodansylcadaverine expression was measured using a relative unit to show the ratio of the amount on intensity from fluorescence imaging.

Antitumor Effect of Sugar Cholestanols on Nude Mice Injected With CGNH-89 Cells

The effect of sugar cholestanols on CGNH-89 cell growth was evaluated quantitatively in a subcutaneous tumor. Cell suspensions (2×10^7 cells/200 μ l) were injected subcutaneously in the flanks of 5- to 6-week-old nude mice (Clea Laboratories). One hundred microliters of 2 μ mol of GChol dissolved in HP- β -CD was administered intratumorally 3 times (at 14, 15, and 16 days) after tumor inoculation with a 27-gauge needle. The same treatment of HP- β -CD without GChol was conducted as control. Tumor volume was calculated as follows: (length \times width²)/2.

At the end of each experiment, tumor tissues were subjected to histological analysis. Five mice were used for each group, and the experiment was approved by the Animal Care and Experimentation Committee of Gunma University. Experiments using patient tissues from glioblastoma cells were approved by the Ethical Committee of Gunma University.

Statistical Analysis

Statistical analysis was performed using StatView software (version 5.0, SAS Institute). Differences were considered significant when p was < 0.05 .

Results

Cell Proliferation Inhibition of Glioblastoma Cells by Sugar Cholestanols

The effects of sugar cholestanols on the viability of glioblastoma cells were evaluated at various concentrations. Sugar cholestanols such as GGChol and GChol showed considerable inhibiting activities against the pro-

liferation of glioblastoma cells in a dose-dependent manner (Fig. 1). However, β Chol itself, without the sugar moiety, showed very low activity only at a high concentration in CGNH cells (data not shown). The minimum concentrations of sugar cholestanols producing 50% cell proliferation inhibition (CPI₅₀) were determined in the glioblastoma cells, and no clear differences were observed (Table 1). The sugar cholestanols clearly induced cell death in glioblastoma cells.

Nuclear Fragmentation

Nuclear fragmentation was clearly observed in CGNH cells treated with GGChol but not in the control cells (Fig. 2 left). Staining of the glioblastoma cells (CGNH-89 and CGNH-NM) with HO342 and propidium iodide indicated that GGChol induced nuclear fragmentation (a hallmark of apoptosis) in approximately 17% and 23% of the total cells, respectively, and were counted as apoptotic (Fig. 2 right).

Western Blot Analysis of Caspase Cascade and PARP Activation

Caspase signaling pathways consisting of a death receptor-dependent extrinsic pathway and death receptor-independent intrinsic pathway were examined in the glioblastoma cells treated with GGChol. The expression levels of active caspase-8 for the extrinsic pathway, caspase-9 for the intrinsic pathway, and caspase-3 were found to increase in the CGNH-89 and CGNH-NM cells in a time-dependent manner (Fig. 3). The expression levels of PARP, one of the best biomarkers of apoptosis, were analyzed in CGNH cells during the 24 hours after the treatment with GGChol. The N-terminal fragment of PARP, possessing an 89-kDa peptide cleaved from the full-sized PARP (116 kDa), was detected as early as 2 hours in the CGNH cells after the treatment with sugar cholestanols (Fig. 3). These results suggested that GGChol induced apoptotic cell death through both extrinsic and intrinsic pathways.

Analysis of Autophagy, Apoptosis, and the Inhibition of Both

We examined the changes in autophagy activity in both CGNH-89 and CGNH-NM cells treated with GGChol. The treatment of both cell types with GGChol induced not only apoptosis but also an autophagic response (Fig. 4). In both cell types, the number of distinct dot-like structures distributed within the cytoplasm or localized in the perinuclear regions was higher than in the control (Fig. 4A and B, left). The level of MDC incorporated into the CGNH-89 and CGNH-NM cells was increased 1.4- and 1.5-fold, respectively, after being treated with GGChol compared with that in the untreated cells (Fig. 4A and B, right). The cell viability of glioblastoma cells was reduced in the presence of GGChol up to 60% but was restored after the addition of 3-MA and Z-VAD to the culture medium (Fig. 4C). Our results showed that 3-MA and Z-VAD can block autophagy and apoptosis from 17%–20% and 38%–41%, respectively. The combination of inhibitors against both autophagy and apoptosis can fully block the cell death induced by GGChol (45%–

Cell death of glioblastoma induced by glycans

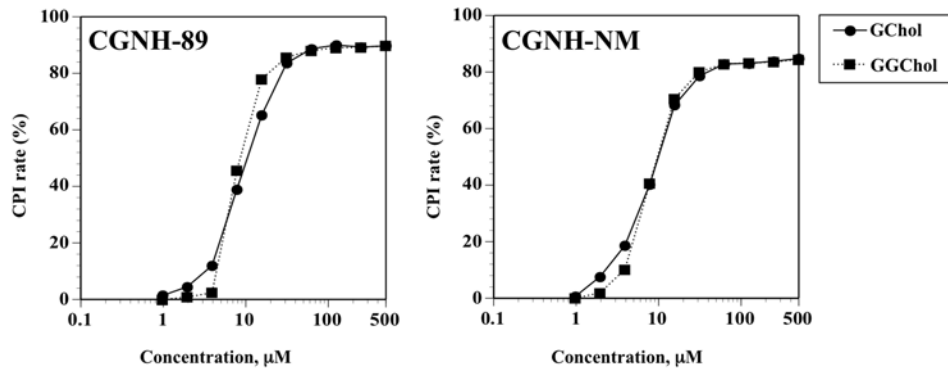


Fig. 1. Line graphs showing the effect of sugar cholestanols on the viability of glioblastoma cells. The CGNH-89 and CGNH-NM cells were treated with various concentrations of sugar cholestanols for 24 hours.

48% increase). When 3-MA and Z-VAD were added at the same time to the cell culture, the cell viability in the GGChol-treated cells was as high as that of the untreated control cells. However, no effect was observed when either agent was added individually to the cell culture (Fig. 4C).

Western Blot Analysis of the Bcl-2 Family

The expression levels of Bcl-2 family members, consisting of both proapoptosis and antiapoptosis factors, were then analyzed in the CGNH cells treated with GGChols. A slightly increased expression of Bax (proapoptosis) was detected in the CGNH-89 and CGNH-NM cells in a time-dependent manner, and a slightly decreased expression of Bcl-xL (antiapoptosis) was detected in the same cells (Fig. 5). We also evaluated the expression level of p53 (ser46), one of the initiators that activates Bax and/or downregulates Bcl-xL. Our results showed that glioblastoma cells treated with GGChol increased the expression of p53 (ser46) in a time-dependent manner (Fig. 5).

Western Blot Analysis of Autophagy

Using Western blot analysis and MDC staining, we found that GGChol increased the expression of apoptosis-related proteins and slightly increased the expression of LC3-II and Beclin-1 (Fig. 5). All these results suggest that sugar cholestanols induced both apoptosis and autophagic cell death in glioblastoma cells.

Western Blot Analysis of Survival Pathways

The expression of survival signaling proteins was

TABLE 1: Minimum amounts of each compound producing 50% cell proliferation inhibition of various cells*

Compounds	CPI ₅₀ (µM)	
	CGNH-89	CGNH-NM
GGChol	14.8	15.6
GChol	15.6	17.2
cholestanol	>1000	>1000

* The 3(4,5-dimethylthiazol-2-yl)2,5-diphenyltetrazolium bromide (MTT) assay was conducted after 24 hours of incubation under the presence of each compound diluted from 500 µM to 0.98 µM (in a gradual manner).

evaluated in glioblastoma cells in response to sugar cholestanols. The treatment of both CGNH cell types with GGChol indicated inhibition of Akt activation and expression of both phosphorylated Akt (ser473) and phosphorylated mTOR (ser2448), the downstream targets of Akt in glioblastoma cells (Fig. 6A). The expression levels of the upstream molecules related to Akt/mTOR were also analyzed in CGNH cells treated with GGChol, and the decreased expression of both GluR1 and GluR4 was detected in CGNH cells treated with GGChol in a time-dependent manner (Fig. 6A). However, the expression levels of RhoA and RhoC in CGNH cells treated with GGChol were revealed to be suppressed in a time-dependent manner (Fig. 6B).

Antitumor Effect of Sugar Cholestanols in a Mouse Model

Nude mice were subcutaneously inoculated with CGNH-89 cells and tumors formed within 2 weeks in all

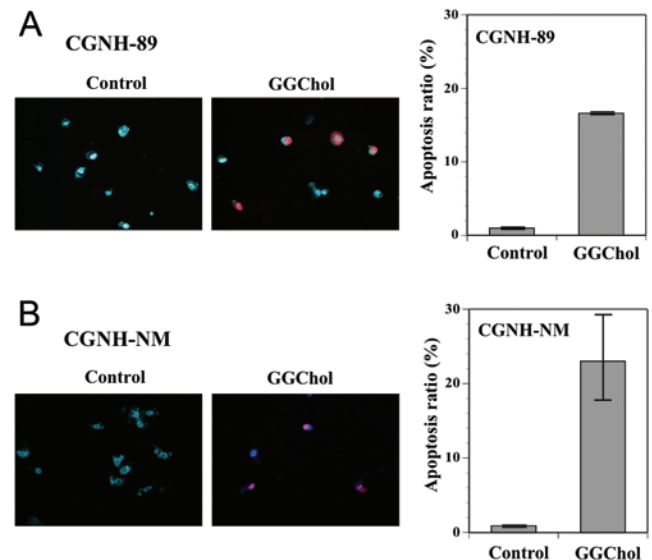


Fig. 2. Left: Induction of apoptotic cell death in CGNH-89 (A) and CGNH-NM (B) cells after treatment with GGChol. The cells were analyzed by the HO342 combined with propidium iodide assay. Original magnification $\times 200$. Right: The apoptosis index (mean \pm SEM) was calculated in each cell line. All results were from 3 independent experiments.

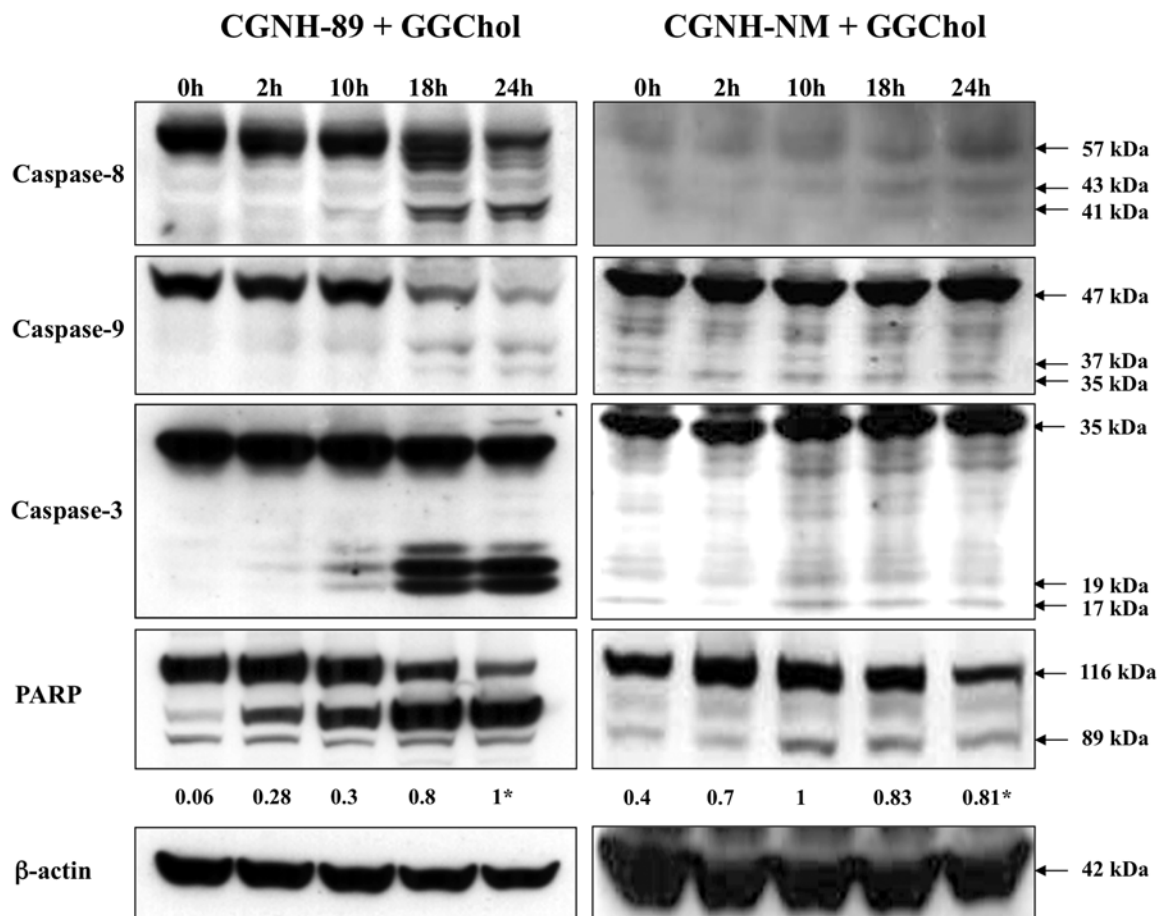


FIG. 3. Western blot analysis of glioblastoma cells treated with GGChol. The cells were treated with 30 μ M of GGChol for 24 hours, and the values given below the caspase-8, -9, -3, and PARP figures indicate the calculation of the active form band (41–43 kDa, 35–37 kDa, 17–19 kDa, and 89 kDa, respectively) after normalization of its expression to that of β -actin, shown as a percentage compared with the control. Asterisk = significant increase for the active form of cleaved PARP (89 kDa) measured using densitometric analysis.

mice. Tumor formation was significantly suppressed ($p < 0.05$) in the mice treated with GChol in HP- β -CD intratumorally 3 times at 14, 15, and 16 days after inoculation of tumor cells. However, no significant suppression was observed in the mice treated only with HP- β -CD (Fig. 7). The histological analysis of GChol-treated mice revealed the presence of high degrees of tumor anaplasia including nuclear and cytoplasmic pleomorphism, tumor necrosis, and vascular proliferation. However, in the control mice, large numbers of mitotic cells were observed (data not shown), as hallmarks of the glioblastoma cells.

Discussion

Temozolomide is commonly used in the treatment of primary or recurrent high-grade gliomas, including anaplastic astrocytoma and glioblastoma.^{2,48} To date, the prognosis of patients with malignant gliomas has been poor.⁴ It is clear that tumor cells with drug-resistant ability will not respond to chemotherapy treatment. The mechanism by which temozolomide mediates cell death in malignant tumor cells has been characterized, and it was shown to induce autophagy, not apoptosis, in glioblastoma.²⁴ In the

cancer field, autophagy is a new concept for the defense mechanisms of malignant cells,^{38,40} and they are eliminated, in some cases, due to the induction of a nonapoptotic mechanism, also known as autophagic cell death.³ However, the triggers for the induction of autophagy and apoptosis and their roles remain unclear.

In our previous studies, novel glycans consisting of a series of sugar cholestanols were chemically synthesized and evaluated as anticancer drugs in both in vitro and in vivo experiments.^{8,14,15} In this study, the expression levels of a series of molecules related to programmed cell death (apoptosis and autophagy) were investigated in glioblastoma cells treated with the same sugar cholestanols. We used CGNH-type glioblastoma cells, cell lines showing epithelial morphology and adhesive capacity. These cell lines possess glial fibrillary acidic protein, vimentin, A2B5, O4, and myelin basic protein.⁴² The mRNAs for the glutamate-AMPA receptors (GluR1 and GluR4) were analyzed in CGNH cells using reverse transcriptase-polymerase chain reaction; the cells expressed GluR1 and GluR4.²⁰ As previously described, these cell lines have the same profile as that of the primary glioblastoma cells de novo.

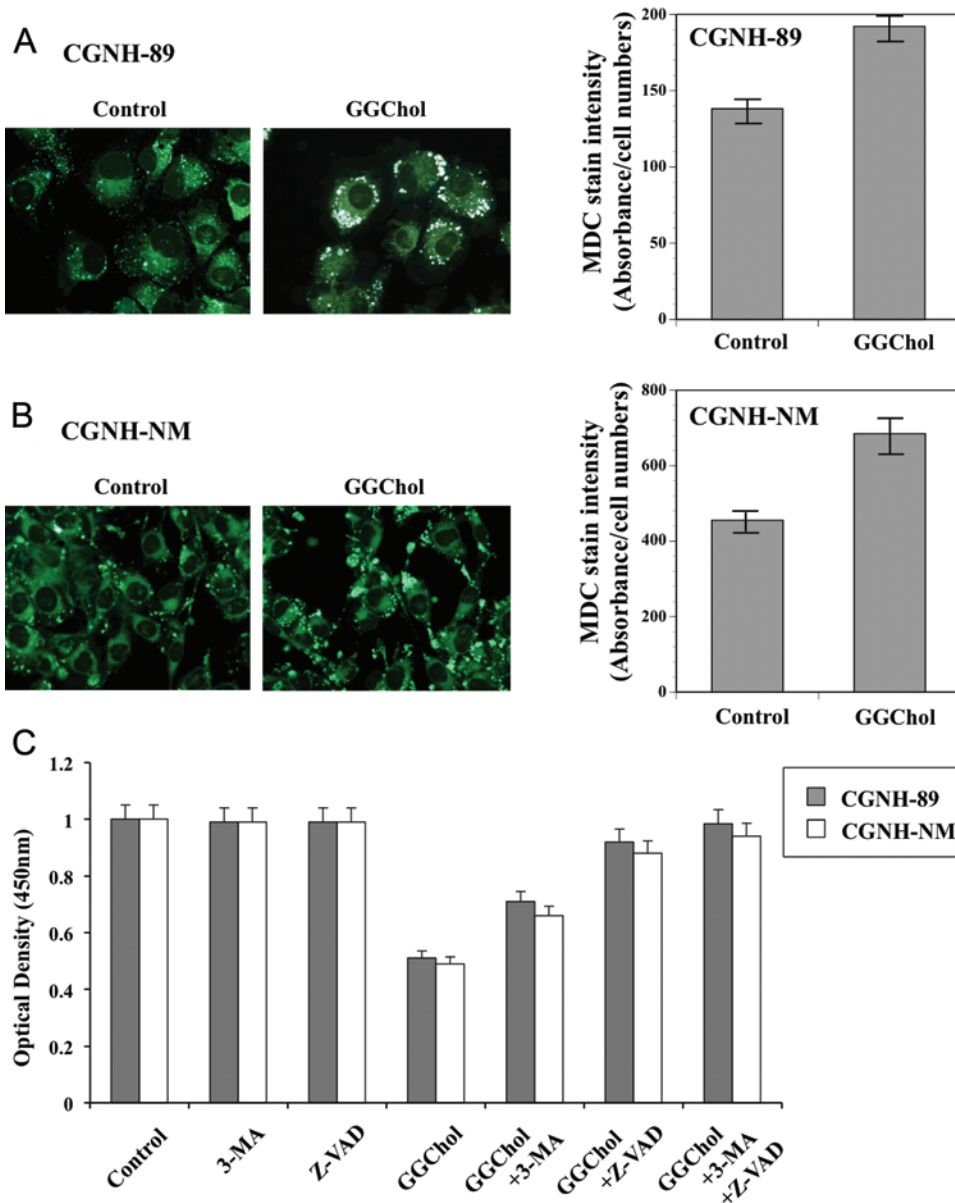


Fig. 4. Fluorescence microscope images showing induction of autophagic cell death in CGNH-89 (A) and CGNH-NM (B) cells. Original magnification $\times 200$. Bar graph (C) demonstrates cell viability in the glioblastoma cells treated with GGChol measured in the presence of antiapoptosis and antiautophagy reagents. Monodansylcadaverine incorporation was quantified and presented as the fold increase \pm SEM compared with the control (bar graph, upper right). The figures and values are from 3 independent experiments.

In glioblastoma cells treated with sugar cholestanols, the activation of the initiator caspases (extrinsic caspase-8 and intrinsic caspase-9) followed by the activation of the executor caspase (caspase-3) occurred in the glioblastoma cells after treatment with sugar cholestanols. Accordingly, the activation of the cascade involving such caspases induced PARP cleavage, resulting in nuclear fragmentation. Furthermore, the induction of the apoptosis signaling pathway in glioblastoma cells treated with sugar cholestanols appeared to suppress the expression of Bcl-xL and to enhance the expression of Bax in antiapoptotic and proapoptotic manners, respectively. Therefore, the induction of apoptosis appeared to be caused by the disruption of a

balance between these anti- and proapoptotic molecules, as described previously.^{8,14,15}

One of the most important survival-signaling pathways is mediated by PI3K and its downstream targets, such as Akt and mTOR.²⁹ Recently, Akt was reported to play an important role in determining the chemosensitivity of many types of cells.^{7,10,35} The induction of autophagy requires the activation of Beclin-1 and its interacting partner, Class III PI3K, resulting in the generation of phosphatidylinositol-3'phosphates. This induction is negatively regulated by Class I PI3K via the Akt/mTOR pathway.^{41,44,46} In contrast, Beclin-1, a mammalian homolog of the yeast autophagy-related gene Atg6, was observed to be

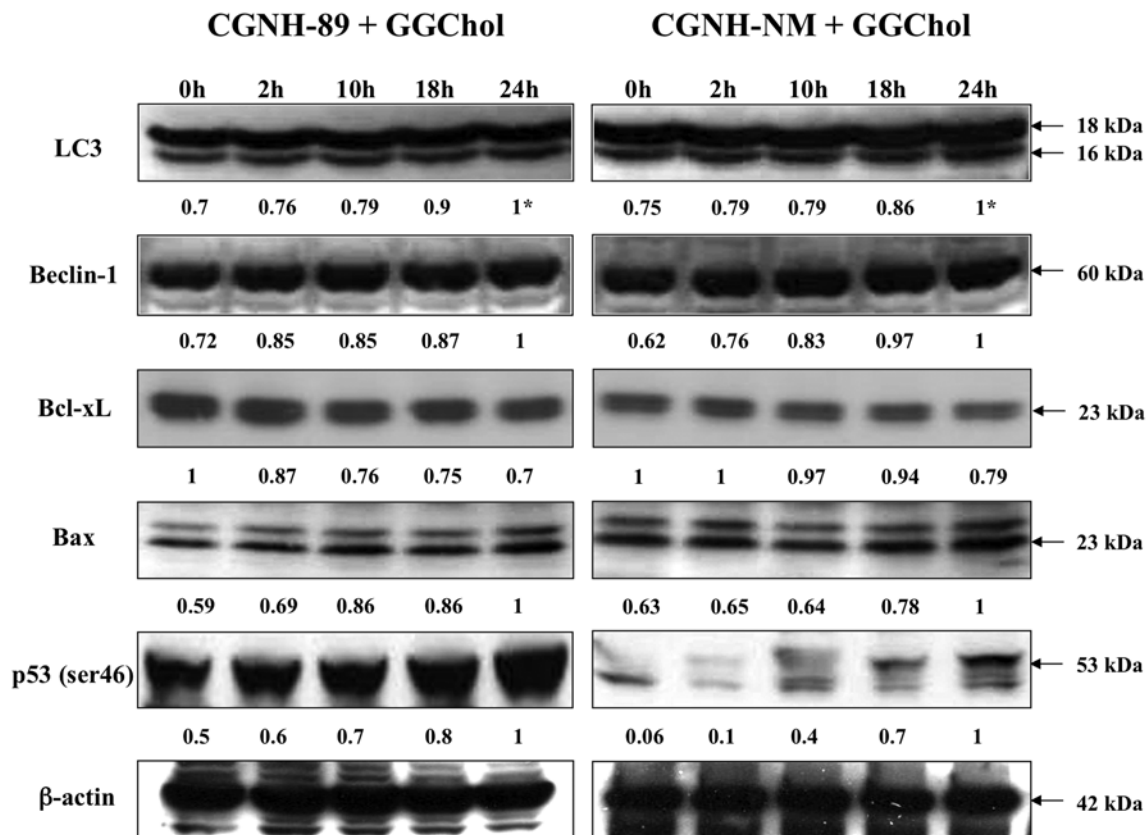


Fig. 5. Western blot analysis in the glioblastoma cells treated with GGChol. Changes in the expression of the autophagy activation, Bcl-2 family members, p53 (ser46) in the CGNH-89 and CGNH-NM cells are shown. The cells were treated with 30 μ M of GGChol for 24 hours, and values given below each figure indicate the calculation of each band, and the LC3 active form band (16 kDa), after normalization of their expression to that of β -actin, shown as a percentage compared with the control. There was a significant increase in the active form of LC3 (16 kDa) measured using densitometric analysis.

deleted in breast and prostate cancer cells, and its expression was shown to induce autophagy and inhibit tumorigenicity in MCF-7 breast cancer cells.²⁷ Furthermore, the microtubule associated protein 1 light chain 3, designated as LC3, exists in 2 forms, which are LC3-I and LC3-II, located in the cytosol and autophagosomal membranes, respectively. LC3 is the first protein that was reported to specifically localize to autophagosome membranes and was later designated as LC3-II (16 kDa), the inner limiting membrane of the autophagosome. During the process of autophagy, cleaved LC3-I conjugates with phosphatidylethanolamine to form LC3-II, which is an important step for autophagosome formation.²⁵ Immunofluorescence staining of endogenous LC3 can detect autophagy (Fig. 4). The expression of Beclin-1 in glioblastoma cells was slightly increased after treatment with sugar cholestanols along with the decreased expression of the members of the Akt/mTOR pathway. In addition, LC3-II expression was increased, and this hallmark could be used to estimate the abundance of autophagosomes before they are destroyed via fusion with lysosomes.

Recently, p53 has also been revealed to activate autophagy.²² Several groups have reported the localization of p53 to the outer layer of the mitochondrial membrane and the activation of apoptosis through direct binding to

the Bcl-2 family members Bax, Bak, or Bcl-xL.^{5,30} The overexpression of p53 was also reported to increase Bax expression in several cell types following the induction of apoptosis.^{31,43} The binding of p53 to p53AIP1, which appears to be important for the apoptotic response, is selectively enhanced by the phosphorylation of ser46.³⁷ We also observed that, in fact, p53 at ser46 was increased in glioblastoma cells after treatment with sugar cholestanols. In addition, the stimulation of cell death controlled by apoptosis and/or at least partially by autophagy was observed in glioblastoma cells treated with sugar cholestanols and cotreated with inhibitors of caspases and autophagy. Therefore, we provided evidence that sugar cholestanols induced apoptosis and autophagic cell death in the same glioblastoma cells. The occurrence of cell death induced by apoptosis was also observed in colorectal cancer cells treated with the same sugar cholestanols (S. Yazawa et al., unpublished observation, 2008).

The mechanism of drug-induced cell death has been accepted to be governed not only by the upregulation of proapoptotic, proautophagic factors or tumor suppressors, but also by the modulation of the survival-signaling pathways.¹¹ As we previously showed, CGNH cells express Ca^{2+} -permeable AMPA receptors assembled mainly from the GluR1 and/or GluR4 subunits, which contribute to the

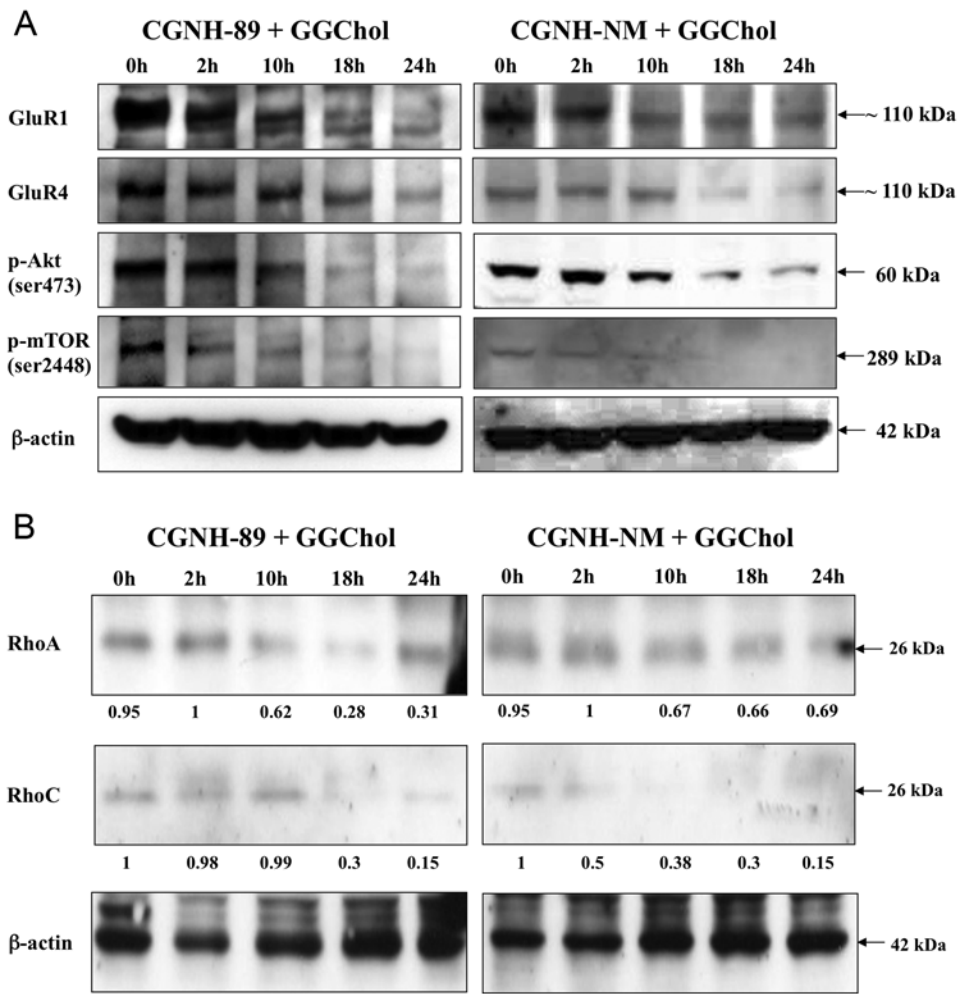


Fig. 6. Western blot analysis of glioblastoma cells treated with GGChol. Changes in the expression levels of the glutamate receptors (GluR1 and GluR4), p-Akt, and p-mTOR (**A**) and Rho GTPases (**B**) in the CGNH-89 and CGNH-NM cells are shown. The CGNH cells were treated with 30 μ M of GGChol for 24 hours. The values given below the Rho GTPase figures indicate the calculation of each band after normalization of the expression to that of β -actin, shown as a percentage compared with the control.

invasive and aggressive behavior of glioblastoma.²⁰ Cell growth appeared to be suppressed in cancer cells treated with the sugar cholestanols, particularly through the activation of the Akt/mTOR pathway (A. Faried et al., unpublished observation, 2009). As reported previously, there is an important survival-signaling pathway that is mediated by the Akt/mTOR pathway²⁹ and its upstream target, the AMPA receptors.²¹

Our results demonstrated that the sugar cholestanols inhibit the activation of the Akt/mTOR pathway, as shown by the downregulation of phosphorylated Akt at ser473 and phosphorylated mTOR at ser2448. Therefore, we analyzed the expression of the glutamate-AMPA receptors as an upstream target of Akt/mTOR in glioblastoma cells. As expected, we found that the sugar cholestanols inhibited the activation of the glutamate-AMPA receptors, GluR1 and GluR4, in both glioblastoma cell types tested. Taken together, our results suggest that the activation of the glutamate-AMPA receptors–Akt/mTOR pathway was downregulated after treatment with sugar cholestanols.

Ca²⁺-permeable AMPA receptors and Rho GTPase

family members facilitate the migration ability of human glioblastomas.^{20,47} In addition, we also evaluated the expression of Rho GTPases (RhoA and RhoC) because they were reported to be related to the degree of malignancy in glioblastoma.^{28,47} Furthermore, the inhibition of Rho GTPase signaling has been reported to decrease glioblastoma cell migration.²⁸ In this study, we showed that the expression of both RhoA and RhoC was decreased after treatment with the sugar cholestanols in a time-dependent manner. Overall, our results showed that different processes of cell death were induced by the sugar cholestanols and that the survival, proliferation, or metastatic properties of glioblastoma cells were affected by some other oncogenic factors (Fig. 8).

Our *in vivo* experiment using nude mice showed that the sugar cholestanols suppressed tumor growth of CGNH-89 cells that were injected into subcutaneous tissue, possessing the features of human glioblastomas in terms of histological tissue organization. This experiment may provide a reliable *in vivo* model for studying the response of human glioblastomas to our potential synthetic

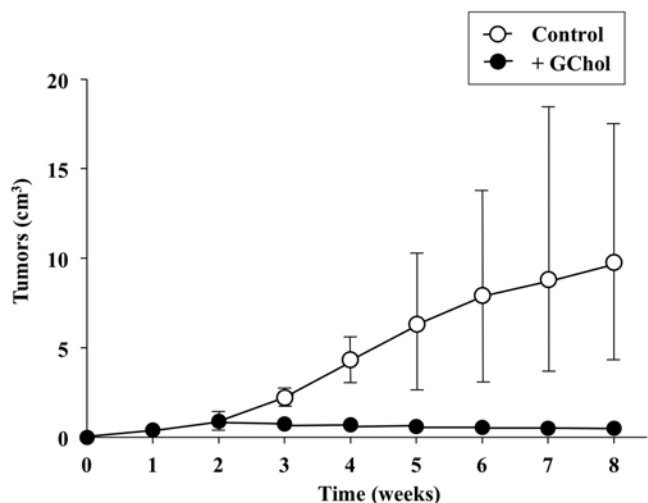


Fig. 7. Line graph showing the anticancer effect of sugar cholestanols on the subcutaneously formed tumors with glioblastoma cells. CGNH-89 cells (2×10^7 cells) were subcutaneously injected into nude mice. Injections of 120 μ l of GChol or phosphate-buffered saline only (as a control) were administered intratumorally 3 times (at 14, 15, and 16 days). The values of tumor volumes given indicate the mean \pm SD of 5 mice in each group.

glycans (sugar cholestanols). The sugar cholestanol injections reduced the incidence of intratumoral bleeding in the treated mice compared with the untreated mice, accompanied by the suppression of tumor growth and induction of apoptosis. These results indicate that programmed cell death controlled by apoptosis and/or at least partially by autophagy in CGNH cells was stimulated by treatment with our novel synthetic glycans (sugar cholestanols). It remains to be seen whether the sugar cholestanols could be applicable to an in vivo experiment using an intracranial glioma model to investigate their usefulness in chemotherapy against the expected blood-brain barrier.

Conclusions

The activation of programmed cell death in human malignant brain tumor cells induced by treatment with the sugar cholestanols may be involved in not only apoptosis, as we previously demonstrated in several tumor cell lines, but also autophagy, which was demonstrated here for the first time. The sugar cholestanols represent potential pharmaceutical agents against glioblastoma cells.

Disclosure

This work was supported partly by the 21st Century COE

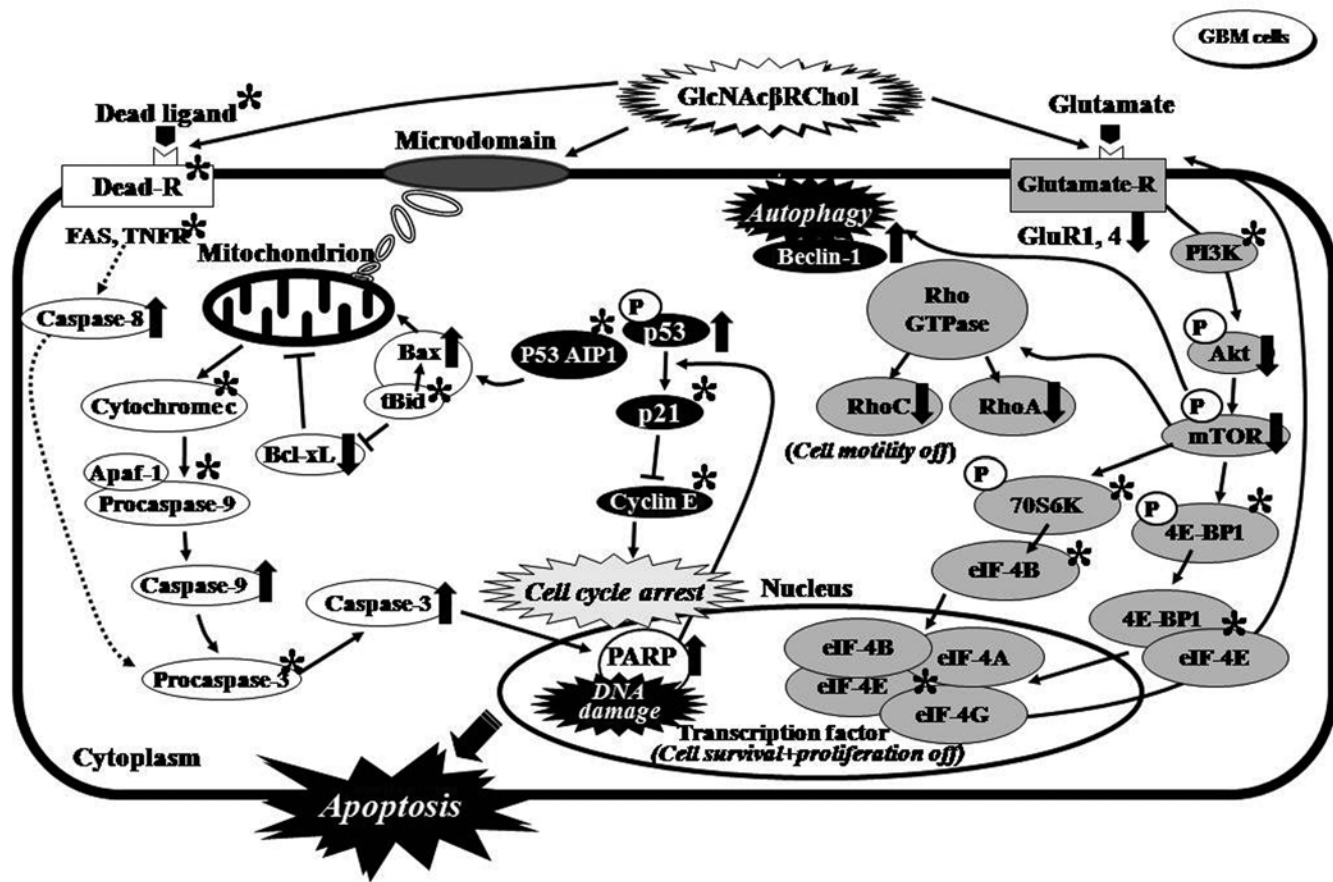


Fig. 8. The predicted effects of sugar cholestanols on cell death inducing both apoptosis and autophagy in the glioblastoma cells resulting from continuous activations and/or suppressions in the expressions of their related molecules. Molecules flagged with an asterisk were not examined in this study, but their details have been described in our previous studies.^{8-10,14,15,21} TNFR = tumor necrosis factor receptor.

Cell death of glioblastoma induced by glycans

Program, Japan; the Japan Society for the Promotion of Science; and a research grant for collaboration research to Dr. Faried from the Faculty of Medicine at Universitas Padjadjaran.

Author contributions to the study and manuscript preparation include the following. Conception and design: Faried, Arifin, Yazawa. Acquisition of data: Faried, Yazawa. Analysis and interpretation of data: Faried, Yazawa. Drafting the article: Faried, Yazawa. Critically revising the article: all authors. Reviewed submitted version of manuscript: all authors. Approved the final version of the manuscript on behalf of all authors: Faried.

References

1. Biederbick A, Kern HF, Elsässer HP: Monodansylcadaverine (MDC) is a specific *in vivo* marker for autophagic vacuoles. **Eur J Cell Biol** **66**:3–14, 1995
2. Bower M, Newlands ES, Bleehen NM, Brada M, Begent RJ, Calvert H, et al: Multicentre CRC phase II trial of temozolomide in recurrent or progressive high-grade glioma. **Cancer Chemother Pharmacol** **40**:484–488, 1997
3. Bursch W, Ellinger A, Gerner C, Fröhwein U, Schulte-Hermann R: Programmed cell death (PCD). Apoptosis, autophagic PCD, or others? **Ann N Y Acad Sci** **926**:1–12, 2000
4. Chamberlain MC, Kormanik PA: Practical guidelines for the treatment of malignant gliomas. **West J Med** **168**:114–120, 1998
5. Chipuk JE, Kuwana T, Bouchier-Hayes L, Droin NM, Newmeyer DD, Schuler MM, et al: Direct activation of Bax by p53 mediates mitochondrial membrane permeabilization and apoptosis. **Science** **303**:1010–1014, 2004
6. Edinger AL, Thompson CB: Death by design: apoptosis, necrosis and autophagy. **Curr Opin Cell Biol** **16**:663–669, 2004
7. Fahy BN, Schlieman MG, Virudachalam S, Bold RJ: Inhibition of AKT abrogates chemotherapy-induced NF-kappaB survival mechanisms: implications for therapy in pancreatic cancer. **J Am Coll Surg** **198**:591–599, 2004
8. Faried A, Faried LS, Nakagawa T, Yamauchi T, Kitani M, Sasabe H, et al: Chemically synthesized sugar-cholestanols possess a preferential anticancer activity involving promising therapeutic potential against human esophageal cancer. **Cancer Sci** **98**:1358–1367, 2007
9. Faried A, Faried LS, Usman N, Kato H, Kuwano H: Clinical and prognostic significance of RhoA and RhoC gene expression in esophageal squamous cell carcinoma. **Ann Surg Oncol** **14**:3593–3601, 2007
10. Faried LS, Faried A, Kanuma T, Nakazato T, Tamura T, Kuwano H, et al: Inhibition of the mammalian target of rapamycin (mTOR) by rapamycin increases chemosensitivity of CaSki cells to paclitaxel. **Eur J Cancer** **42**:934–947, 2006
11. Fraser M, Leung B, Jahani-Asl A, Yan X, Thompson WE, Tsang BK: Chemoresistance in human ovarian cancer: the role of apoptotic regulators. **Reprod Biol Endocrinol** **1**:66, 2003
12. Fritz G, Just I, Kaina B: Rho GTPases are over-expressed in human tumors. **Int J Cancer** **81**:682–687, 1999
13. Goto J, Suzuki K, Nambara T: Synthesis of conjugated cholesterol and cholestanols. **Chem Pharm Bull (Tokyo)** **27**:1926–1931, 1979
14. Hashimoto S, Tsuboi K, Asao T, Kuwano H, Nishimura T, Nakagawa T, et al: Anti-tumor effect of chemically synthesized novel glycoconjugates. **Glycoconj J** **22**:311, 2005
15. Hahimoto S, Yazawa S, Asao T, Faried A, Nishimura T, Tsuboi K, et al: Novel sugar-cholestanols as anticancer agents against peritoneal dissemination of tumor cells. **Glycoconj J** **25**:531–544, 2008
16. Hoelzinger DB, Mariani L, Weis J, Woyke T, Berens TJ, McDonough WS, et al: Gene expression profile of glioblastoma multiforme invasive phenotype points to new therapeutic targets. **Neoplasia** **7**:7–16, 2005
17. Hoorens A, Van de Castele M, Klöppel G, Pipeleers D: Glucose promotes survival of rat pancreatic beta cells by activating synthesis of proteins which suppress a constitutive apoptotic program. **J Clin Invest** **98**:1568–1574, 1996
18. Horiuchi A, Imai T, Wang C, Ohira S, Feng Y, Nikaido T, et al: Up-regulation of small GTPases, RhoA and RhoC, is associated with tumor progression in ovarian carcinoma. **Lab Invest** **83**:861–870, 2003
19. Ishiuchi S, Nakazato Y, Iino M, Ozawa S, Tamura M, Ohye C: *In vitro* neuronal and glial production and differentiation of human central neurocytoma cells. **J Neurosci Res** **51**:526–535, 1998
20. Ishiuchi S, Tsuzuki K, Yoshida Y, Yamada N, Hagimura N, Okado H, et al: Blockage of Ca²⁺-permeable AMPA receptors suppresses migration and induces apoptosis in human glioblastoma cells. **Nat Med** **8**:971–978, 2002
21. Ishiuchi S, Yoshida Y, Sugawara K, Aihara M, Ohtani T, Watanabe T, et al: Ca²⁺-permeable AMPA receptors regulate growth of human glioblastoma via Akt activation. **J Neurosci** **27**:7987–8001, 2007
22. Jin S: p53, autophagy and tumor suppression. **Autophagy** **1**:171–173, 2005
23. Kamai T, Tsujii T, Arai K, Takagi K, Asami H, Ito Y, et al: Significant association of Rho/ROCK pathway with invasion and metastasis of bladder cancer. **Clin Cancer Res** **9**:2632–2641, 2003
24. Kanzawa T, Germano IM, Komata T, Ito H, Kondo Y, Kondo S: Role of autophagy in temozolomide-induced cytotoxicity for malignant glioma cells. **Cell Death Differ** **11**:448–457, 2004
25. Kondo Y, Kanzawa T, Sawaya R, Kondo S: The role of autophagy in cancer development and response to therapy. **Nat Rev Cancer** **5**:726–734, 2005
26. Lefranc F, Brotchi J, Kiss R: Possible future issues in the treatment of glioblastomas: special emphasis on cell migration and the resistance of migrating glioblastoma cells to apoptosis. **J Clin Oncol** **23**:2411–2422, 2005
27. Liang XH, Jackson S, Seaman M, Brown K, Kempkes B, Hibshoosh H, et al: Induction of autophagy and inhibition of tumorigenesis by beclin 1. **Nature** **402**:672–676, 1999
28. Manning TJ Jr, Parker JC, Sontheimer H: Role of lysophosphatidic acid and rho in glioma cell motility. **Cell Motil Cytoskeleton** **45**:185–199, 2000
29. McCormick F: Cancer: survival pathways meet their end. **Nature** **428**:267–269, 2004
30. Mihara M, Erster S, Zaika A, Petrenko O, Chittenden T, Pantoska P, et al: p53 has a direct apoptogenic role at the mitochondria. **Mol Cell** **11**:577–590, 2003
31. Miyashita T, Krajewski S, Krajewska M, Wang HG, Lin HK, Liebermann DA, et al: Tumor suppressor p53 is a regulator of bcl-2 and bax gene expression *in vitro* and *in vivo*. **Oncogene** **9**:1799–1805, 1994
32. Munafó DB, Colombo MI: A novel assay to study autophagy: regulation of autophagosome vacuole size by amino acid deprivation. **J Cell Sci** **114**:3619–3629, 2001
33. Nelson DA, White E: Exploiting different ways to die. **Genes Dev** **18**:1223–1226, 2004
34. Newton HB: Small-molecule and antibody approaches to molecular chemotherapy of primary brain tumors. **Curr Opin Investig Drugs** **8**:1009–1021, 2007
35. Nguyen DM, Chen GA, Reddy R, Tsai W, Schrupp WD, Cole G Jr, et al: Potentiation of paclitaxel cytotoxicity in lung and esophageal cancer cells by pharmacologic inhibition of the phosphoinositide 3-kinase/protein kinase B (Akt)-mediated signaling pathway. **J Thorac Cardiovasc Surg** **127**:365–375, 2004
36. Nichols WW, Murphy DG, Cristofalo VJ, Toji LH, Greene AE, Dwight SA: Characterization of a new human diploid cell strain, IMR-90. **Science** **196**:60–63, 1977
37. Oda K, Arakawa H, Tanaka T, Matsuda K, Tanikawa C, Mori T, et al: p53AIP1, a potential mediator of p53-dependent apoptosis

- tosis, and its regulation by Ser-46-phosphorylated p53. *Cell* **102**:849–862, 2000
38. Ogier-Denis E, Codogno P: Autophagy: a barrier or an adaptive response to cancer. *Biochim Biophys Acta* **1603**:113–128, 2003
 39. Osaki M, Oshimura M, Ito H: PI3K-Akt pathway: its functions and alterations in human cancer. *Apoptosis* **9**:667–676, 2004
 40. Paglin S, Hollister T, Delohery T, Hackett N, McMahon M, Sphicas E, et al: A novel response of cancer cells to radiation involves autophagy and formation of acidic vesicles. *Cancer Res* **61**:439–444, 2001
 41. Petiot A, Ogier-Denis E, Blommaert EF, Meijer AJ, Codogno P: Distinct classes of phosphatidylinositol 3'-kinases are involved in signaling pathways that control macroautophagy in HT-29 cells. *J Biol Chem* **275**:992–998, 2000
 42. Sasaki A, Tamura M, Hasegawa M, Ishiuchi S, Hirato J, Nakazato Y: Expression of interleukin-1beta mRNA and protein in human gliomas assessed by RT-PCR and immunohistochemistry. *J Neuropathol Exp Neurol* **57**:653–663, 1998
 43. Selvakumaran M, Lin HK, Miyashita T, Wang HG, Krajewski S, Reed JC, et al: Immediate early up-regulation of bax expression by p53 but not TGF beta 1: a paradigm for distinct apoptotic pathways. *Oncogene* **9**:1791–1798, 1994
 44. Shintani T, Klionsky DJ: Autophagy in health and disease: a double-edged sword. *Science* **306**:990–995, 2004
 45. Stupp R, Mason WP, van den Bent MJ, Weller M, Fisher B, Taphoorn MJ, et al: Radiotherapy plus concomitant and adjuvant temozolomide for glioblastoma. *N Engl J Med* **352**:987–996, 2005
 46. Wang CW, Klionsky DJ: The molecular mechanism of autophagy. *Mol Med* **9**:65–76, 2003
 47. Yan B, Chour HH, Peh BK, Lim C, Salto-Tellez M: RhoA protein expression correlates positively with degree of malignancy in astrocytomas. *Neurosci Lett* **407**:124–126, 2006
 48. Yung WK, Prados MD, Yaya-Tur R, Rosenfeld SS, Brada M, Friedman HS, et al: Multicenter phase II trial of temozolomide in patients with anaplastic astrocytoma or anaplastic oligoastrocytoma at first relapse. *J Clin Oncol* **17**:2762–2771, 1999

Manuscript submitted July 16, 2013.

Accepted January 23, 2014.

Please include this information when citing this paper: published online March 28, 2014; DOI: 10.3171/2014.1.JNS131534.

Address correspondence to: Ahmad Faried, M.D., Ph.D., Department of Neurosurgery, Faculty of Medicine, Universitas Padjadjaran–Dr. Hasan Sadikin Hospital, Jl. Pasteur No. 38, Bandung, West Java 40161, Indonesia. email: faried.fkup@gmail.com.

神経膠芽腫に対する Akt を標的とした分子標的療法

渡邊 孝, 菅原健一, 長嶺英樹, 石内勝吾

琉球大学医学部 脳神経外科

Targeted Molecular Therapy Against the Multiple Akt-mediated Signaling Pathways in Glioblastoma

Takashi Watanabe, MD, PhD., Kenichi Sugawara, MD, PhD.
Hideki Nagamine, MD and Shogo Ishiuchi, MD, PhD.

*Department of Neurosurgery, Graduate School of Medicine,
University of the Ryukyus, Okinawa, Japan*

ABSTRACT

Glioblastoma multiforme is the most malignant tumor occurring in the central nervous system and is incurable by current therapeutic strategies. The serine/threonine-specific protein kinase, Akt, is frequently dysregulated and affects cell survival and proliferation in many human cancers, including glioblastoma. Inhibition of Akt phosphorylation has demonstrated therapeutic potential against glioblastoma. Many inhibitors of the PI3K-Akt signaling pathway and α -amino-3-hydroxy-5-methyl-4-isoxazolepropionate (AMPA)-Akt signaling pathway are in clinical use and have demonstrated preliminary activity against various tumor types. This review describes the limitations of therapy against glioblastoma targeting single dysregulated pathways because of the presence of diverse signaling pathways that regulate the coactivation of multiple tyrosine kinases in most malignant gliomas, and the requirement for combined approaches targeting the multiple Akt-mediated signaling pathways based on the findings of clinical trials and earlier investigations. *Ryukyu Med. J., 33 (1~3) 1~8, 2014*

Key words: AMPA, Akt, glioblastoma, PI3K, platelet-derived growth factor

はじめに

神経膠芽腫は、中枢神経系で最も悪性度が高く、予後不良な疾患である。極めて高い増殖能と浸潤能により、開頭術で完全に摘出することが困難であるため、放射線治療、化学療法を組み合わせた集学的治療が必要であるが、現在の標準治療では治癒困難である¹⁻³⁾。

拡大局所放射線治療 (60Gy/30Fr) と Temozolomide (TMZ) 75mg/m²・42 間投与を行った後、TMZ 150-200mg/m²・5 日間を 28 日周期で投与し、6 周期投与する治療法 (Stupp regimen) を用いた第三相臨

床試験において、全生存期間中央値 (median overall survival: mOS) が放射線治療単独の 12.1 ヶ月と比較し、放射線治療・TMZ 併用投与で 14.6 ヶ月と有意な延長を示した。このことから、この regimen が、現在の神経膠芽腫に対する標準的治療法となっているが、2 年生存率 27.2% 及び 5 年生存率 9.8% と低率であり、依然として十分な効果が得られていないのが現状である²⁾。

その後の研究で、DNA 修復酵素である O6-methylguanine-DNA methyltransferase (MGMT) の発現率が高いと、TMZ の効果が減弱することが判明した⁴⁾。これに対し、Interferon (INF)- β が、腫瘍抑制

遺伝子である p53 を介して MGMT の発現を抑制する効果を有することが示された⁵⁾。Stupp regimen に INF- β 300 万単位を併用投与した臨床試験 (INTEGRA study) が本邦において行われ、明らかな有害事象の増加がなく、mOS が 17.1 ヶ月と延長し、12 ヶ月の無増悪生存期間 (progression free survival: PFS) が 50% と治療効果の改善がみられた⁶⁾。

本邦でも、2013 年より Bevacizumab (アバスタン[®]) が悪性神経膠腫に対して保険適応となった。初発神経膠芽腫に対する bevacizumab の効果を検証する大規模第三相試験 (AVA glioblastoma 試験と、RTOG 0825 試験) は、標準治療 (Stupp regimen) に Bevacizumab を追加投与し、プラセボと比較した二重盲検無作為化比較検討試験である。その結果において、PFS は、bevacizumab 投与群で AVA glioblastoma 試験 10.6 ヶ月、RTOG 0825 試験 10.7 ヶ月であり、プラセボ群と比較して 3-4 ヶ月延長したが、mOS は、Bevacizumab 投与群で、AVA glioblastoma 試験 16.8 ヶ月、RTOG 0825 試験 15.7 ヶ月であり、どちらもプラセボ群と比べて有意な延長効果は得られなかった^{7,8)}。

以上のように、現在本邦で、神経膠芽腫、悪性神経膠腫に対して主に用いられている化学療法薬は、TMZ (INF- β 併用) と Bevacizumab であり、これまでの治療法の進歩により、OS, PFS の延長が認められてきたが、mOS は、15-17 ヶ月と限定的であった。このため、新たな治療薬や治療方法の開発が切望されており、その中で分子標的療法が注目されている。複数のシグナル伝達経路の中で、Akt を介するシグナル伝達経路が重要視されてきており、他の固形癌に対しても、このシグナル伝達経路を標的とした治療法が盛んに開発されている。本稿では、認容性が良好で、様々な悪性腫瘍に対して臨床的に使用可能となっている Akt を標的とした分子標的療法の神経膠芽腫に対する臨床応用について概説する。

Akt を介する分子標的療法

Akt は、Plekstrin Homology (PH) ドメインを有するセリン/スレオニンキナーゼであり、腫瘍細胞の生存、増殖、分化、遊走、血管新生において重要な役割を果たしている。近年の研究から、神経膠芽腫の生存、増殖、遊走、血管新生に Akt の活性化が関与していることが判明し、治療の標的として注目を集めてきた^{3,9-15)}。Akt は、PI3K-Akt シグナル伝達経路の中心に位置し、Thr-308 と Ser-473 でリン酸化されて活性化され、抗アポトーシス活性による腫瘍細胞の生存や増殖に関与するといわれている^{11,16-21)}。神経膠芽腫細胞では、epidermal growth factor receptor (EGFR), platelet-derived growth factor receptor (PDG-

FR) といったチロシンキナーゼ受容体の増幅による PI3K-Akt シグナル伝達経路の活性化が認められている²²⁻²⁶⁾。また、神経膠芽腫には vascular endothelial growth factor (VEGF) が過剰発現し、腫瘍の血管新生や悪性度、予後に関与しており、VEGF に対する抗体が神経膠芽腫の腫瘍形成を抑制することが判明している²⁷⁾。神経膠芽腫細胞は、主に GluR1 と GluR4 サブユニットで構成されるカルシウム透過型 α -amino-3-hydroxy-5-methyl-4-isoxazolepropionate (AMPA) 型グルタミン酸受容体を発現している^{28,29)}。この受容体を介する細胞内カルシウム濃度の上昇による Ser-473 での Akt のリン酸化が神経膠芽腫の増殖、浸潤に関与することが解明され、このシグナル伝達経路は、PI3K-Akt シグナル伝達経路とは独立していることが判明した^{9,30)}。Phosphatase and tensin homolog Deleted from Chromosome 10 (PTEN) を欠失した神経膠芽腫では、Sonic Hedgehog (shh) シグナル伝達経路が活性化され、p70 S6 kinase (S6K) の活性化を介して、腫瘍細胞の生存や増殖に関与していることが明らかとなっている³¹⁾。

神経膠芽腫は、腫瘍増殖や血管新生に関する複数のシグナル伝達経路を有し、相互に活性化していることが知られており、単剤での抗腫瘍効果が制限される原因と考えられている^{3,32)}。このため、複数のシグナル伝達経路を抑制する多剤併用療法が重要視されている³²⁾。Akt を中心としたシグナル伝達経路も複数存在し、相互に密接に関連しているため、複数のシグナル伝達経路を標的とした多剤併用分子標的療法が必要と考えられる (Fig 1)。近年、これらのシグナル伝達経路を標的とした分子標的薬が次々に開発され、様々な固形癌に対する臨床試験が行われて実用化されている。認容性が良好である分子標的療法薬は、将来的に神経膠芽腫に臨床応用が可能となる可能性があり、これらの効果を検証する研究が重要である。

臨床試験における単剤投与の限界

AMPA 受容体拮抗薬

カルシウム透過型 AMPA 受容体拮抗薬である 2,3-dihydroxy-6-nitro-7-sulfamoyl-benzo-(F)-quinoxaline (NBQX) は、Ser-473 での Akt のリン酸化を抑制し、神経膠芽腫細胞株の増殖と遊走を抑制することが判明している。しかし、NBQX は、静脈内投与を行うと腎尿細管で凝結するため現実的ではない。[2,3-dioxo-7-(1H-imidazol-1-yl)-6-nitro-1,2,3,4-tetrahydroquinoxalin-1-yl]-acetic acid monohydrate (YM872) は、経口摂取が可能であり、水に溶解性であり、生体に投与するという点では現実的である³³⁾。Talampanel は、認容性が良好で、経口摂取が可能で、

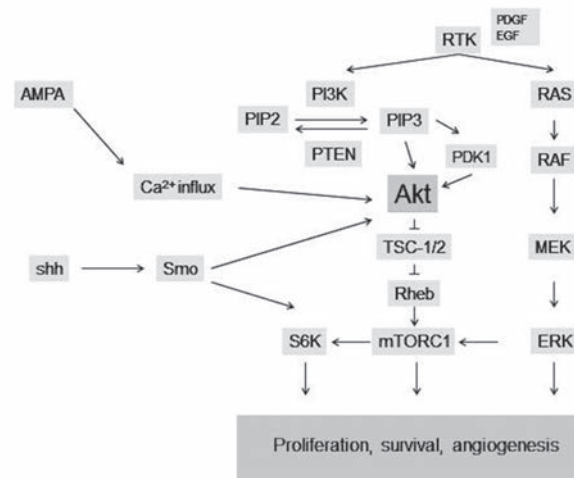


Fig. 1 Schematic representation of the Akt signaling pathway and its main components

EGF, epidermal growth factor; PDGF, platelet-derived growth factor; RTK, receptor tyrosine kinase; RAS, rat sarcoma oncogene; RAF, murine sarcoma viral oncogene; MEK, mitogen-activated protein kinase; ERK, extracellular signal-related kinase; mTORC1, mammalian target of rapamycin complex 1; PI3K, phosphatidylinositol 3-kinase; PIP2, phosphatidylinositol 4,5-bisphosphate; PIP3, phosphatidylinositol 3,4,5-trisphosphate; PDK1, 3-phosphoinositide dependent protein kinase-1; PTEN, phosphatase and tensin homolog; TSC-1/2, tuberous sclerosis complex-1/2; Rheb, RAS homologue enriched in brain; S6K, S6 kinase; AMPA, α -amino-3-hydroxy-5-methyl-4-isoxazolepropionate; shh, sonic hedgehog; Smo, smoothened.

非競合性のカルシウム透過型 AMPA 受容体拮抗薬で、中枢神経への移行性も優れている薬剤であり、臨床試験で使用されている³⁴⁾。多施設共同研究による第二相臨床試験では、新規神経膠芽腫症例（年齢 18 歳から 70 歳）60 例に対して、Stupp regimen に talampanel (25mg × 3 / 日から 75mg × 3 / 日へ 1 週間ごとに増量) を連日併用投与した結果、mOS 20.3 ヶ月、2 年生存率 41.7% であり、Stupp regimen による標準治療の結果 (mOS 14.6 ヶ月、2 年生存期間 26.5%) と比較して、有害事象を増加させることなく、生存期間を延長させた³⁵⁾。しかし、再発悪性神経膠腫（神経膠芽腫 22 例、退形成性神経膠腫 8 例）に対し、talampanel (25-75mg × 3 / 日) を連日単剤投与した第二相臨床試験では、partial response が膠芽腫 1 例 (5%) のみであり、6 ヶ月の PFS は、膠芽腫 4.6%、退形成性神経膠腫 0%、median PFS は、膠芽腫 5.9 週、退形成性神経膠腫 8.9 週であった。倦怠感、めまい、失調といった有害事象は軽度であったが、有意な抗腫瘍効果を認めておらず、多数のシグナル伝達経路を有する悪性神経膠腫に対する単剤投与での治療の困難さを示している³⁶⁾。

PDGF 受容体拮抗薬

メシル酸イマチニブ (Imatinib mesylate) は、Bcl-

Abl, PDGF α 受容体, PDGF β 受容体, c-kit チロシンキナーゼ活性を阻害する抗腫瘍薬である。慢性骨髄性白血病と消化管間質腫瘍で臨床的に使用されており³⁷⁻³⁹⁾、神経膠芽腫に対する治療薬としても期待された。しかし、55 例の再発悪性神経膠芽腫（膠芽腫 34 例、退形成性神経膠腫 21 例）に対してメシル酸イマチニブ 600 ~ 800mg / 日を単剤投与した第二相臨床試験では、6 ヶ月 PFS は、膠芽腫 3%、退形成性神経膠腫 10% であり、5 例で腫瘍内出血が認められた⁴⁰⁾。また、112 例の再発悪性神経膠芽腫（膠芽腫 51 例、退形成性星細胞腫 25 例、退形成性乏突起膠腫 36 例）に対してメシル酸イマチニブ 600 ~ 800mg / 日を単剤投与した第二相臨床試験では、6 ヶ月 PFS は、膠芽腫 16%、退形成性星細胞腫 9%、退形成性乏突起膠腫 4% であり、いずれの臨床試験においても単剤投与の効果は低く限定的であるという結果に終わった。

抗 VEGF 受容体抗体

再発膠芽腫に対する bevacizumab 単剤投与 (10mg/kg, 2 ~ 3 週間毎) を行った第二相臨床試験では、Bevacizumab 投与により、脳浮腫の軽減とステロイド投与量を減量できるという点が有利であったが、6 ヶ月の PFS: 25-42.6%, median PFS: 2.7 ~ 4.2 ヶ月、mOS: 6.4 ~ 10.5 ヶ月であり、Bevacizumab の単剤

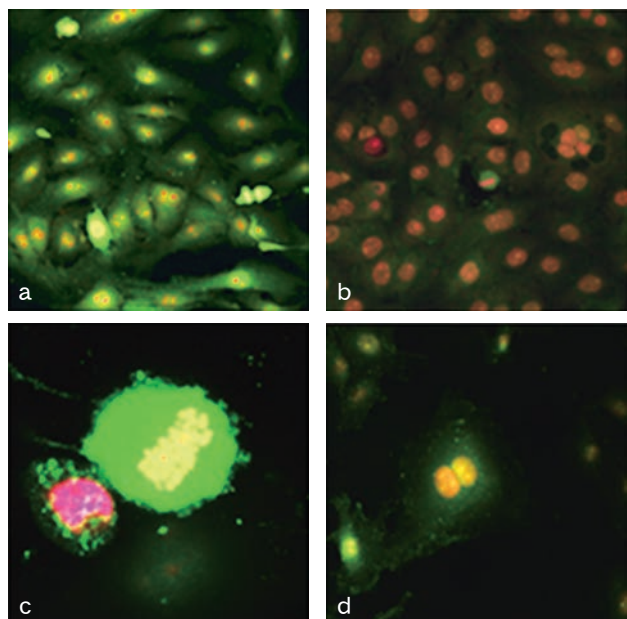


Fig. 2

Fig. 2 Effect of combination therapy targeting the AMPA-Akt signaling pathway and PI3K-Akt signaling pathway in vitro

Human glioblastoma cells were treated with PBS (control; left column), or calcium-permeable AMPA receptor antagonist (YM872 at 20 μ M) and PDGF receptor antagonist (AG1296 at 20 μ M) (right column). Immunofluorescence staining is shown for phosphorylated Akt in green, for Ki-67 in blue, and for propidium iodide in red.

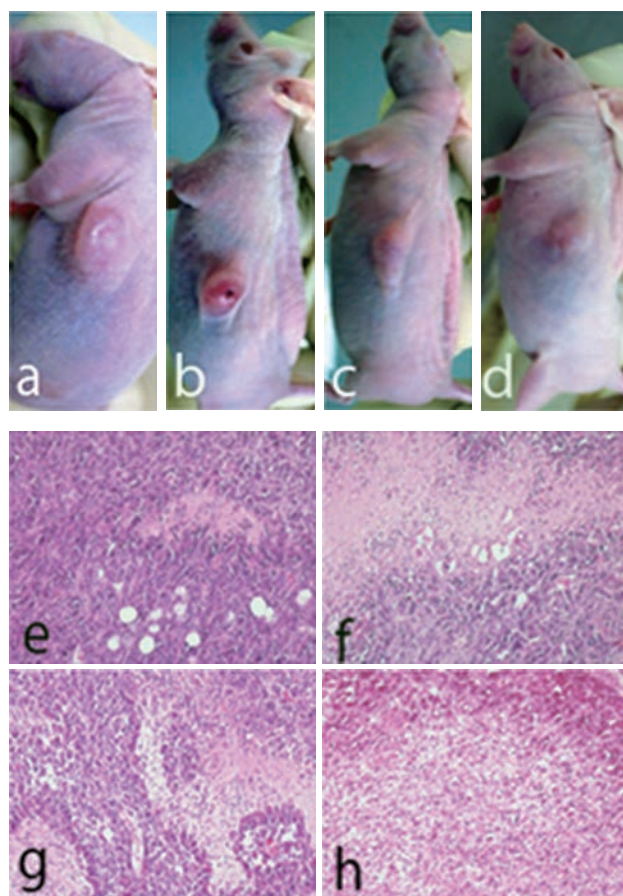


Fig. 3

Fig. 3 Effect of combination therapy targeting the AMPA-Akt signaling pathway and PI3K-Akt signaling pathway in vivo

a-d: Glioblastoma cell suspensions were injected subcutaneously into the flank of nude mice. Inhibition of tumor growth was observed after daily intraperitoneal injection of PBS (control; a), calcium-permeable AMPA receptor antagonist (YM872 at 25 mg/kg; b), PDGF receptor antagonist (AG1296 at 1.25 mg/kg; c), or the combination of both antagonists (d) for 2 weeks.

e-h: Photomicrographs of sections of tumor tissue taken 36 days after inoculation, treated with PBS (e), 25 mg/kg YM872 (f), 1.25 mg/kg AG1296 (g), and the combination of both agents (h). Extensive necrosis in the tumor tissue was found after treatment with YM872, AG1296, and the combination of both agents. Hematoxylin and eosin stain, original magnification: $\times 200$.

投与による効果は限定的であった⁴¹⁻⁴³。これまで臨床試験で使用されてきた悪性神経膠腫に対する分子標的治療薬は、認容性は良好であったが、単剤投与での効果はどれも限定的なものであった。

多剤併用化学療法の効果

AMPA-Akt シグナル伝達経路と PI3K-Akt シグナル伝達経路の両シグナル伝達経路を標的とし

た我々の最新の研究において、神経膠芽腫細胞株 (CGNH-89,U87,HKG) にカルシウム透過型 AMPA 受容体拮抗薬である YM872 と PDGF 受容体拮抗薬である AG1296 を併用投与した場合、AG1296 投与群、YM872 投与群と併用投与群では、control と比較し、腫瘍増殖及び Akt のリン酸化ともに有意に抑制された。この効果は正常マウス海馬神経細胞では認められず、正常神経細胞を阻害することなく、腫瘍増殖を抑

制することが判明した (Fig 2). In vitro では, この抑制効果には, 単独投与と併用投与の間での有意差が認められなかったが, ヒト神経膠芽腫をヌードマウスに移植した異種移植モデルを用いた解析では, control と比較し, AG1296 投与群, YM872 投与群, 併用群で腫瘍体積の減少, 壊死巣の増加及び細胞密度の減少が認められた (Fig.3). また, Ki-67 標識率及び CD34 で標識した腫瘍血管数は, 各治療群で有意に減少し, 併用投与における相乗効果が認められた. このことから, 異種移植モデルにおいて併用投与群の抗腫瘍効果が増強したのは, vascular niche の抑制によるものと考えられた⁴⁴⁾. PDGF 受容体拮抗薬である Imatinib mesylate や AMPA 受容体拮抗薬である Talampanel は, 単独投与での効果は限定的であるが, 併用投与による効果が期待される. また, PTEN が欠失して PI3K シグナル伝達経路が活性化された神経膠芽腫細胞に, 経口 PI3K 阻害薬である BKM120(Buparlisib) と Smoothened (Smo) の阻害薬で Sonic Hedgehog (shh) シグナル伝達経路を抑制する LDE225 (sonidegib) を併用投与した最近の研究では, 併用投与により腫瘍の増殖抑制とアポトーシス誘導に相乗効果が認められた³¹⁾. BKM120 は, 手術不能局所進行性または転移性乳癌に対する臨床試験に使用されており, LDE225 は, 基底細胞癌や, 再発・難治性髄芽腫に対する臨床試験に使用されているため, 今後, 神経膠芽腫への臨床応用が期待される薬剤である.

まとめ

Akt を標的とする分子標的療薬が開発され, 多くの悪性腫瘍の治療薬として, 認容性が良好な治療薬が登場し, 臨床応用されるようになってきており, 神経膠芽腫への応用が期待される. 一方で, 神経膠芽腫は, 複雑で多様なシグナル伝達経路を有し, 単剤投与の限界も確認されてきているのが現状である. 神経膠芽腫に対する治療成績向上のためには, 複数のシグナル伝達経路を抑制する多剤併用分子標的療法の効果を検証する preclinical study が重要であると考えられる.

謝辞

執筆の機会を与您いただきました前琉球医学会長上里 博先生に謝意を表します.

REFERENCES

- 1) Maher EA, Furnari FB, Bachoo RM, et al. Malignant glioma: genetics and biology of a grave matter. *Genes Dev.* 15:1311-1333, 2001.
- 2) Stupp R, Mason WP, van den Bent MJ, et al. Radiotherapy plus concomitant and adjuvant temozolomide for glioblastoma. *N Engl J Med.* 352:987-996, 2005.
- 3) Wen PY, Kesari S. Malignant gliomas in adults. *N Engl J Med.* 359:492-507, 2008.
- 4) Hegi ME, Diserens AC, Gorlia T, et al. MGMT gene silencing and benefit from temozolomide in glioblastoma. *N Engl J Med.* 352:997-1003, 2005.
- 5) Natsume A, Ishii D, Wakabayashi T, et al. IFN-beta down-regulates the expression of DNA repair gene MGMT and sensitizes resistant glioma cells to temozolomide. *Cancer Res.* 65:7573-7579, 2005.
- 6) Wakabayashi T, Kayama T, Nishikawa R, et al. A multicenter phase I trial of combination therapy with interferon-beta and temozolomide for high-grade gliomas (INTEGRA study): the final report. *J Neurooncol.* 104:573-577, 2011.
- 7) Chinot OL, Wick W, Mason W, et al. Bevacizumab plus radiotherapy-temozolomide for newly diagnosed glioblastoma. *N Engl J Med.* 370:709-722, 2014.
- 8) Gilbert MR, Dignam JJ, Armstrong TS, et al. A randomized trial of bevacizumab for newly diagnosed glioblastoma. *N Engl J Med.* 370:699-708, 2014.
- 9) Ishiuchi S, Yoshida Y, Sugawara K, et al. Ca²⁺-permeable AMPA receptors regulate growth of human glioblastoma via Akt activation. *J Neurosci.* 27:7987-8001, 2007.
- 10) Choe G, Horvath S, Cloughesy TF, et al. Analysis of the phosphatidylinositol 3'-kinase signaling pathway in glioblastoma patients in vivo. *Cancer Res.* 63:2742-2746, 2003.
- 11) Datta SR, Brunet A, Greenberg ME. Cellular survival: a play in three Akts. *Genes Dev.* 13:2905-2927, 1999.
- 12) Datta SR, Dudek H, Tao X, et al. Akt phosphorylation of BAD couples survival signals to the cell-intrinsic death machinery. *Cell.* 91:231-241, 1997.
- 13) Holland EC. Gliomagenesis: genetic alterations and mouse models. *Nat Rev Genet.* 2:120-129, 2001.
- 14) Holland EC, Celestino J, Dai C, Schaefer L, Sawaya RE, Fuller GN. Combined activation of

1) Maher EA, Furnari FB, Bachoo RM, et al.

- Ras and Akt in neural progenitors induces glioblastoma formation in mice. *Nat Genet.* 25:55-57, 2000.
- 15) Bochet P, Audinat E, Lambolez B, et al. Subunit composition at the single-cell level explains functional properties of a glutamate-gated channel. *Neuron.* 12:383-388, 1994.
 - 16) Cully M, You H, Levine AJ, Mak TW. Beyond PTEN mutations: the PI3K pathway as an integrator of multiple inputs during tumorigenesis. *Nat Rev Cancer.* 6:184-192, 2006.
 - 17) Engelman JA, Luo J, Cantley LC. The evolution of phosphatidylinositol 3-kinases as regulators of growth and metabolism. *Nat Rev Genet.* 7:606-619, 2006.
 - 18) Alessi DR, Cohen P. Mechanism of activation and function of protein kinase B. *Curr Opin Genet Dev.* 8:55-62, 1998.
 - 19) Williams MR, Arthur JS, Balendran A, et al. The role of 3-phosphoinositide-dependent protein kinase 1 in activating AGC kinases defined in embryonic stem cells. *Curr Biol.* 10:439-448, 2000.
 - 20) Maehama T, Dixon JE. The tumor suppressor, PTEN/MMAC1, dephosphorylates the lipid second messenger, phosphatidylinositol 3,4,5-trisphosphate. *J Biol Chem.* 273:13375-13378, 1998.
 - 21) Blume-Jensen P, Hunter T. Oncogenic kinase signalling. *Nature.* 411:355-365, 2001.
 - 22) Joensuu H, Pupa M, Sihto H, Tynninen O, Nupponen NN. Amplification of genes encoding KIT, PDGFR α and VEGFR2 receptor tyrosine kinases is frequent in glioblastoma multiforme. *J Pathol* 207:224-231, 2005.
 - 23) Hermanson M, Funa K, Hartman M, et al. Platelet-derived growth factor and its receptors in human glioma tissue: expression of messenger RNA and protein suggests the presence of autocrine and paracrine loops. *Cancer Res.* 52:3213-3219, 1992.
 - 24) Guha A, Dashner K, Black PM, Wagner JA, Stiles CD. Expression of PDGF and PDGF receptors in human astrocytoma operation specimens supports the existence of an autocrine loop. *Int J Cancer* 60:168-173, 1995.
 - 25) Lokker NA, Sullivan CM, Hollenbach SJ, Israel MA, Giese NA. Platelet-derived growth factor (PDGF) autocrine signaling regulates survival and mitogenic pathways in glioblastoma cells: evidence that the novel PDGF-C and PDGF-D ligands may play a role in the development of brain tumors. *Cancer Res.* 62:3729-3735, 2002.
 - 26) Berdel WE, de Vos S, Maurer J, et al. Recombinant human stem cell factor stimulates growth of a human glioblastoma cell line expressing c-kit protooncogene. *Cancer Res.* 52:3498-3502, 1992.
 - 27) Jansen M, de Witt Hamer PC, Witmer AN, Troost D, van Noorden CJ. Current perspectives on antiangiogenesis strategies in the treatment of malignant gliomas. *Brain research Brain research reviews.* 45:143-163, 2004.
 - 28) Seeburg PH, Osten P. Neurobiology: a thorny issue. *Nature.* 424:627-628, 2003.
 - 29) Yoshida Y, Tsuzuki K, Ishiuchi S, Ozawa S. Serum-dependence of AMPA receptor-mediated proliferation in glioma cells. *Pathol Int.* 56:262-271, 2006.
 - 30) Ishiuchi S, Tsuzuki K, Yoshida Y, et al. Blockage of Ca²⁺-permeable AMPA receptors suppresses migration and induces apoptosis in human glioblastoma cells. *Nat Med.* 8:971-978, 2002.
 - 31) Gruber Filbin M, Dabral SK, Pazyra-Murphy MF, et al. Coordinate activation of Shh and PI3K signaling in PTEN-deficient glioblastoma: new therapeutic opportunities. *Nat Med.* 19:1518-1523, 2013.
 - 32) Stommel JM, Kimmelman AC, Ying H, et al. Coactivation of receptor tyrosine kinases affects the response of tumor cells to targeted therapies. *Science.* 318:287-290, 2007.
 - 33) Shimizu-Sasamata M, Kano T, Rogowska J, Wolf GL, Moskowitz MA, Lo EH. YM872, a highly water-soluble AMPA receptor antagonist, preserves the hemodynamic penumbra and reduces brain injury after permanent focal ischemia in rats. *Stroke.* 29:2141-2148, 1998.
 - 34) Howes JF, Bell C. Talampanel. *Neurotherapeutics.* 4:126-129, 2007.
 - 35) Grossman SA, Ye X, Chamberlain M, et al. Talampanel with standard radiation and temozolomide in patients with newly diagnosed glioblastoma: a multicenter phase II trial. *J Clin Oncol.* 27:4155-4161, 2009.
 - 36) Iwamoto FM, Kreisl TN, Kim L, et al. Phase 2 trial of talampanel, a glutamate receptor

- inhibitor, for adults with recurrent malignant gliomas. *Cancer*. 116:1776-1782, 2010.
- 37) Savage DG, Antman KH. Imatinib mesylate--a new oral targeted therapy. *N Engl J Med*. 346:683-693, 2002.
- 38) Druker BJ, Guilhot F, O'Brien SG, et al. Five-year follow-up of patients receiving imatinib for chronic myeloid leukemia. *N Engl J Med*. 355:2408-2417, 2006.
- 39) Druker BJ, Talpaz M, Resta DJ, et al. Efficacy and safety of a specific inhibitor of the BCR-ABL tyrosine kinase in chronic myeloid leukemia. *N Engl J Med*. 344:1031-1037, 2001.
- 40) Wen PY, Yung WK, Lamborn KR, et al. Phase I/II study of imatinib mesylate for recurrent malignant gliomas: North American Brain Tumor Consortium Study 99-08. *Clin Cancer Res*. 12:4899-4907, 2006.
- 41) Friedman HS, Prados MD, Wen PY, et al. Bevacizumab alone and in combination with irinotecan in recurrent glioblastoma. *J Clin Oncol*. 27:4733-4740, 2009.
- 42) Nagane M, Nishikawa R, Narita Y, et al. Phase II study of single-agent bevacizumab in Japanese patients with recurrent malignant glioma. *Japanese journal of clinical oncology*. 42:887-895, 2012.
- 43) Raizer JJ, Grimm S, Chamberlain MC, et al. A phase 2 trial of single-agent bevacizumab given in an every-3-week schedule for patients with recurrent high-grade gliomas. *Cancer*. 116:5297-5305, 2010.
- 44) Watanabe T, Ohtani T, Aihara M, Ishiuchi S. Enhanced antitumor effect of YM872 and AG1296 combination treatment on human glioblastoma xenograft models. *Journal of neurosurgery* 118:838-845, 2013.



Clinical Study

SLC44A1–PRKCA fusion in papillary and rosette-forming glioneuronal tumors



Masaya Nagaishi^{a,b,*}, Sumihito Nobusawa^b, Nozomi Matsumura^b, Fumihiko Kono^c, Shogo Ishiuchi^d, Tatsuya Abe^e, Michimasa Ebato^f, Yin Wang^g, Akio Hyodo^a, Hideaki Yokoo^b, Yoichi Nakazato^b

^a Department of Neurosurgery, Dokkyo Medical University Koshigaya Hospital, 2-1-50 Minami-Koshigaya, Koshigaya-shi, Saitama 343-8555, Japan

^b Department of Human Pathology, Gunma University Graduate School of Medicine, Maebashi-shi, Gunma, Japan

^c Department of Diagnostic Pathology, Kyoto University Hospital, Mibu, Nakagyo-ku, Kyoto, Japan

^d Department of Neurosurgery, University of the Ryukyus Graduate School of Medicine, Nishihara-cho, Okinawa, Japan

^e Department of Neurosurgery, Oita University School of Medicine, Hasama-machi, Yufu-shi, Oita, Japan

^f Department of Neurosurgery, Koshigaya Municipal Hospital, Koshigaya-shi, Saitama, Japan

^g Department of Neuropathology, Institute of Neurology and Huashan Hospital of Fudan University, Shanghai, China

ARTICLE INFO

Article history:

Received 3 January 2015

Accepted 11 April 2015

Keywords:

Fluorescence *in situ* hybridization

Papillary glioneuronal tumor

Rosette-forming glioneuronal tumor

SLC44A–PRKCA fusion

ABSTRACT

We investigated the fused protein of solute carrier family 44 choline transporter member 1 (*SLC44A1*) and protein kinase C alpha (*PRKCA*) in three patients with papillary glioneuronal tumors (PGNT). PGNT and rosette-forming glioneuronal tumors (RGNT) are recently identified, unusual glioneuronal tumor variants which were categorized as novel tumor entities in the 2007 World Health Organization classification system. The molecular background of these tumors remains poorly understood due to the paucity of studies. The *SLC44A1–PRKCA* fusion was recently detected in three cases of PGNT. We investigated for the *SLC44A1–PRKCA* fusion protein in the three PGNT patients and a further two with RGNT using fluorescence *in situ* hybridization. Two out of the three PGNT patients had a fused signal (paired red–green signal) representing a rearrangement on chromosomes 9 and 17. A normal signal pattern was observed in the third PGNT patient. Neither of the two RGNT patients demonstrated a fused signal. This suggests that the *SLC44A1–PRKCA* fusion is a characteristic alteration in PGNT but not RGNT. Therefore, it is a potential biomarker of PGNT. The paired red–green signal that was observed in the PGNT patients implies the presence of a different breakpoint than that previously reported in the 9q31 and 17q24 genes.

© 2015 Elsevier Ltd. All rights reserved.

1. Introduction

Glioneuronal tumors of the central nervous system are rare low grade tumors that consist of glial and neuronal cells at varying stages of differentiation. Papillary glioneuronal tumors (PGNT) and rosette-forming glioneuronal tumors (RGNT) have been recently identified as unusual glioneuronal tumor variants, and were categorized as novel tumor entities in the 2007 World Health Organization (WHO) classification system [1]. PGNT are characterized by a prominent pseudopapillary structure composed of small glial cells arranged around hyalinized blood vessels along with sheets or focal collections of synaptophysin-positive neurocytes. Oligodendroglia-like cells (OLC) expressing oligodendrocyte transcription factor (Olig2) are also sometimes present in parts of

this tumor [2,3]. RGNT display uniform neurocytes that form neurocytic rosettes and/or perivascular pseudorosettes. The glial tumor component in RGNT resembles pilocytic astrocytoma. OLC have also been detected in inter-rosette spaces. Therefore, the histopathology of RGNT shares common features with PGNT.

In spite of the morphological features of the glial elements, none of the reported PGNT and RGNT patients have had a 1p19q codeletion, *KIAA–BRAF* fusion, or *BRAF* V600E mutation [4–7]. The molecular features and histogenesis of these glioneuronal tumors have not yet been elucidated in detail. Bridge et al. recently described a solute carrier family 44 choline transporter member 1 (*SLC44A1*)–protein kinase C alpha (*PRKCA*) fusion as the defining genetic alteration in PGNT. They observed it in all three of their PGNT patients, and investigated it with fluorescence *in situ* hybridization (FISH) [8]. Although they suggested that this genetic alteration was the defining molecular feature and may be responsible for the pathogenesis of PGNT, the analysis of a larger number

* Corresponding author. Tel.: +81 48 965 1111; fax: +81 48 965 8682.

E-mail address: nagaishi-nsu@umin.ac.jp (M. Nagaishi).

of PGNT patients is needed. In RGNT, the phosphatidylinositol-4,5-bisphosphate 3-kinase catalytic subunit alpha and fibroblast growth factor receptor 1 mutations that are predominantly seen in glial tumors have recently been demonstrated [7,9]. However, the *SLC44A1-PRKCA* fusion has not been analyzed in this tumor type. Therefore, the aim of the present study was to confirm the FISH findings from the previously reported PGNT patients, and to investigate this fusion in another type of glioneuronal tumor, RGNT.

2. Materials and methods

2.1. Tumor samples

Formalin fixed paraffin embedded (FFPE) tissue samples from three PGNT and two RGNT patients were obtained from the following institutions: Department of Neurosurgery, Ryukyu University, Japan; Department of Pathology, Kyoto City Hospital, Japan; Department of Neurosurgery, Oita University Hospital, Japan; Department of Neurosurgery, Koshigaya Municipal Hospital; Department of Neuropathology, Huashan Hospital, China. All of the samples were from primarily developed intracranial tumors and were diagnosed on the basis of the 2007 WHO Classification [1]. All clinical samples were analyzed according to a protocol approved by the Medical Ethics Committee of Gunma University (based on the principles detailed in the Declaration of Helsinki). All patient information associated with this study was obtained in a deidentified format.

2.2. FISH

A dual color interphase FISH analysis was performed on 5 micron thick FFPE tissue sections, using previously published probes and methods [8,10]. Briefly, following deparaffinization

and pretreatment, the sections were incubated in 0.35% pepsin/0.01 normal hydrochloric acid for 30 min, and then in 0.1% nonionic polyoxyethylene surfactant 40/2 × standard sodium citrate for 30 min. DNA was denatured using 70% formamide/2 × standard sodium citrate for 5 min at 75°C. An 8 μl aliquot mixture of two labeled probes was applied to the glass slide with a cover slip. The latter probe was prepared from bacterial artificial chromosomes (RP11-1036114 for *PRKCA*, RP11-9507 for *SLC44A1*; GenoTechs, Tsukuba, Japan) using a DNA purification kit (Qiagen Plasmid Kit Midi; Qiagen, Germantown, MD, USA) and labeled using Spectrum Green or Spectrum Orange (Vysis Nick Translation Kit; Abbott Laboratories, Abbott Park, IL, USA). The samples were intermittently irradiated at intervals of 3 s on and 2 s off (42°C; 300 W) for 2 h using a microwave processor, and then incubated for 3 nights. 4,6-diamidino-2-phenylindole (DAPI I; 1,000 ng/ml; Vysis; Abbott Laboratories) was used for nuclear counterstaining. The signals were evaluated in more than 200 non-overlapping intact nuclei of the tumor cells. A previous study detected a dual fusion signal in >68% of tumor cells in all the PGNT samples [8]. Based on this finding, we intentionally defined >60% of the neoplastic cells per tissue section as positive for a dual fusion signal.

3. Results

The microscopic examination revealed a distinctive pseudopapillary morphology with hyalinized vessels and glial cells characterized by round nuclei and scant cytoplasm in all three PGNT samples. The neuronal cells were scattered in the interpapillary area and were strongly immunostained by synaptophysin. Differently sized neuronal cells, including ganglion and ganglioid cells, were occasionally noted in each sample. Olig2-positive cells were observed around the pseudopapillary structure (Fig. 1A–D). Both RGNT samples displayed typical neurocytic rosettes with central fibrillary stroma that were immunoreactive to synaptophysin.

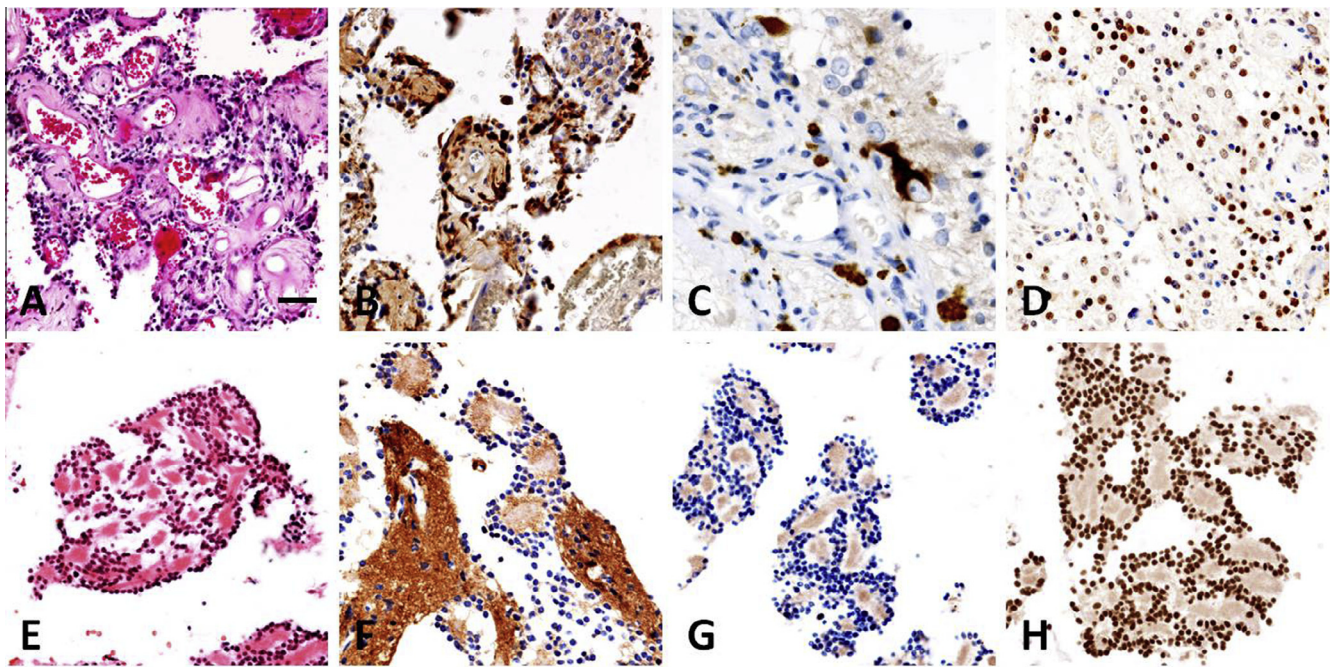


Fig. 1. Representative morphological and immunohistochemical features from tumor sections of papillary glioneuronal tumors (PGNT; A–D) and rosette-forming glioneuronal tumors (RGNT; E–H). PGNT showing a pseudopapillary structure (A; hematoxylin and eosin [H&E] staining) circumscribed by glial fibrillary acidic protein (GFAP)-positive astrocytic cells (B) and scattered neuronal cells, highlighted by synaptophysin immunostaining (C). Oligodendrocyte transcription factor (Olig2)-positive cells were present among blood vessels (D). RGNT consisted of astrocytic tumor cells (E; H&E staining) expressing GFAP (F) and neurocytes forming rosettes with a synaptophysin-positive neuropil core (G). Rosette-forming cells expressed Olig2 (H). The scale bar in part A represents the following scales for each image: 100 μm (A); 25 μm (C); 50 μm (B, D–H).

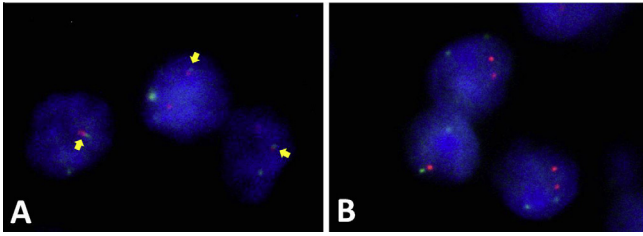


Fig. 2. Fluorescence *in situ* hybridization (FISH) images of papillary glioneuronal tumors (PGNT) and rosette-forming glioneuronal tumors (RGNT). A FISH analysis for protein kinase C alpha (*PRKCA*; green) and solute carrier family 44 choline transporter member 1 (*SLC44A1*; red) probes showed a fused signal pattern (paired red–green signal) in PGNT (A; arrow) and a normal, unfused signal pattern in RGNT (B).

The neurocytic tumor cells had small round nuclei that were stained by Olig2, and scant cytoplasm. The glial component of RGNT was dominated by spindle astroglial cells resembling pilocytic astrocytomas (Fig. 1E–H). All the PGNT and RGNT samples had Rosenthal fibers and eosinophilic granular bodies, and both lacked necrosis and mitotic activity in the tumor cells.

With the dual color probe, the normal cell nuclei showed separate red and green signals (two of each). Two out of three PGNT samples showed one fused signal (paired red–green) representing the rearrangement of chromosomes 9 and 17. However, neither displayed a completely fused yellow signal (Fig. 2A). A normal signal pattern was observed in the third PGNT sample. On the other hand, neither of the two RGNT samples demonstrated a fused signal (Fig. 2B).

4. Discussion

A novel translocation between chromosomes 9 and 17 was recently described in three PGNT patients [8]. FISH data revealed two juxtaposed red–green signals, indicating breakpoints in the 9q31 and 17q24 genes, and a sequence analysis of the reverse transcription polymerase chain reaction-generated transcript identified the fusion point in *SLC44A1* exon 15 and *PRKCA* exon 9. *PRKCA* is a member of a family of serine and threonine-specific protein kinases that contain the *BRAF* gene, which is involved in tumor-promoting signaling pathways [11]. *SLC44A1* has a role in sodium-independent choline transport and is widely expressed throughout the nervous system in both neurons and oligodendrocytes [12]. The deregulation of *PRKCA* and/or high activity of the *SLC44A1* promoter were previously proposed to be involved in the tumorigenesis of PGNT [8].

In our study, the fusion of chromosomes 9 and 17 was confirmed in two PGNT tissue samples by FISH, using one of the two probe sets described by Bridge et al. [8]. The FISH analysis with the other probe set did not result in an informative fluorescence signal. One of the PGNT samples did not show the *SLC44A1*–*PRKCA* fusion. In addition, in our samples, the fusion signals were a paired red–green signal but not an overlapping yellow signal, which may indicate different breakpoints than those that were previously reported within the chromosomal regions 9q31 and 17q24. A sequence analysis previously identified two different

breakpoints on the *SLC44A1* gene [8]. Further analysis is needed to identify the localization of the different breakpoints and investigate the PGNT that didn't have this fusion. We were unable to perform this analysis due to the small size of the surgical specimens.

PGNT and RGNT are characterized by a biphasic pattern with neuronal and glial components. The neuronal component is mainly comprised of neurocytes, similar to the central neurocytoma. In both PGNT and RGNT, OLC are a characteristic feature and have recently been suggested to derive from common progenitor cells with the neurocytes [10]. Therefore, the cellular characteristics of the neuronal component in RGNT bear some similarities to those of the neuronal components in PGNT. The *SLC44A1*–*PRKCA* fusion may be histopathologically associated with papillary formation, which is a characteristic of PGNT but not RGNT.

In summary, PGNT and RGNT have recently been categorized as unusual variants of glioneuronal tumors, with molecular features that remain poorly understood. We verified the existence of the recently identified *SLC44A1*–*PRKCA* fusion in two out of our three PGNT patients. The fusion was not present in either of the RGNT patients, which adds support to its potential as a biomarker for PGNT.

Conflicts of Interest/Disclosures

The authors declare that they have no financial or other conflicts of interest in relation to this research and its publication.

Acknowledgment

We would like to thank Mr. Koji Isoda and Ms. Machiko Yokota for their technical support.

References

- [1] Louis DN, Ohgaki H, Wiestler OD. The 2007 WHO classification of tumours of the central nervous system. *Acta Neuropathol* 2007;114:97–109.
- [2] Vajtai I, Kappeler A, Lukes A, et al. Papillary glioneuronal tumor. *Pathol Res Pract* 2006;202:107–12.
- [3] Izzycka-Swieszewska E, Majewska H, Szurawska E, et al. Papillary glioneuronal tumour of the precentral gyrus. *Folia Neuropathol* 2008;46:158–63.
- [4] Faria C, Miguens J, Antunes JL, et al. Genetic alterations in a papillary glioneuronal tumor. *J Neurosurg Pediatr* 2008;1:99–102.
- [5] Gessi M, Waha A, Setty P, et al. Analysis of KIAA1549-BRAF fusion status in a case of rosette-forming glioneuronal tumor of the fourth ventricle (RGNT). *Neuropathology* 2011;31:654–7.
- [6] Myung JK, Byeon SJ, Kim B, et al. Papillary glioneuronal tumors: a review of clinicopathologic and molecular genetic studies. *Am J Surg Pathol* 2011;35:1794–805.
- [7] Ellezam B, Theeler BJ, Luthra R, et al. Recurrent PIK3CA mutations in rosette-forming glioneuronal tumor. *Acta Neuropathol* 2012;123:285–7.
- [8] Bridge JA, Liu XQ, Sumegi J, et al. Identification of a novel, recurrent *SLC44A1*–*PRKCA* fusion in papillary glioneuronal tumor. *Brain Pathol* 2013;23:121–8.
- [9] Gessi M, Moneim YA, Hammes J, et al. FGFR1 mutations in Rosette-forming glioneuronal tumors of the fourth ventricle. *J Neuropathol Exp Neurol* 2014;73:580–4.
- [10] Tanaka Y, Yokoo H, Komori T, et al. A distinct pattern of Olig2-positive cellular distribution in papillary glioneuronal tumors: a manifestation of the oligodendroglial phenotype? *Acta Neuropathol* 2005;110:39–47.
- [11] Michie AM, Nakagawa R. The link between PKCalpha regulation and cellular transformation. *Immunol Lett* 2005;96:155–62.
- [12] Michel V, Bakovic M. The ubiquitous choline transporter *SLC44A1*. *Cent Nerv Syst Agents Med Chem* 2012;12:70–81.

RESEARCH PAPER

A novel insulinotropic mechanism of whole grain-derived γ -oryzanol via the suppression of local dopamine D₂ receptor signalling in mouse islet

Correspondence

Professor Hiroaki Masuzaki, Division of Endocrinology, Diabetes and Metabolism, Hematology, Rheumatology (Second Department of Internal Medicine), Graduate School of Medicine, University of the Ryukyus, 207 Uehara, Nishihara, Nakagami-gun, Okinawa 903-0215, Japan. E-mail: hiroaki@med.u-ryukyu.ac.jp

Received

4 March 2015

Revised

16 June 2015

Accepted

20 June 2015

Chisayo Kozuka¹, Sumito Sunagawa¹, Rei Ueda¹, Moritake Higa^{1,2}, Yuzuru Ohshiro^{1,3}, Hideaki Tanaka^{1,4}, Chigusa Shimizu-Okabe⁵, Chitoshi Takayama⁵, Masayuki Matsushita⁶, Masato Tsutsui⁷, Shogo Ishiuchi⁸, Masanori Nakata⁹, Toshihiko Yada⁹, Jun-ichi Miyazaki¹⁰, Seiichi Oyadomari¹¹, Michio Shimabukuro¹² and Hiroaki Masuzaki¹

¹Division of Endocrinology, Diabetes and Metabolism, Hematology, Rheumatology (Second Department of Internal Medicine), Departments of ⁵Molecular Anatomy, ⁶Molecular and Cellular Physiology, ⁷Pharmacology, ⁸Neurosurgery, Graduate School of Medicine, University of the Ryukyus, Okinawa, Japan, ²The Diabetes and Life-Style Related Disease Center, Tomishiro Central Hospital, Okinawa, Japan, ³Okinawa Daiichi Hospital, Okinawa, Japan, ⁴Tanaka Clinic, Okinawa, Japan, ⁹Division of Integrative Physiology, Department of Physiology, Jichi Medical University School of Medicine, Tochigi, Japan, ¹⁰Division of Stem Cell Regulation Research, Osaka University Graduate School of Medicine, Osaka, Japan, ¹¹Institute for Genome Research, University of Tokushima, Tokushima, Japan, and ¹²Department of Cardio-Diabetes Medicine, Institute of Biomedical Sciences, Tokushima University Graduate School, Tokushima, Japan

BACKGROUND AND PURPOSE

γ -Oryzanol, derived from unrefined rice, attenuated the preference for dietary fat in mice, by decreasing hypothalamic endoplasmic reticulum stress. However, no peripheral mechanisms, whereby γ -oryzanol could ameliorate glucose dyshomeostasis were explored. Dopamine D₂ receptor signalling locally attenuates insulin secretion in pancreatic islets, presumably via decreased levels of intracellular cAMP. We therefore hypothesized that γ -oryzanol would improve high-fat diet (HFD)-induced dysfunction of islets through the suppression of local D₂ receptor signalling.

EXPERIMENTAL APPROACH

Glucose metabolism and regulation of molecules involved in D₂ receptor signalling in pancreatic islets were investigated in male C57BL/6J mice, fed HFD and treated with γ -oryzanol. In isolated murine islets and the beta cell line, MIN6, the effects of γ -oryzanol on glucose-stimulated insulin secretion (GSIS) was analysed using siRNA for D₂ receptors and a variety of compounds which alter D₂ receptor signalling.

KEY RESULTS

In islets, γ -oryzanol enhanced GSIS via the activation of the cAMP/PKA pathway. Expression of molecules involved in D₂ receptor signalling was increased in islets from HFD-fed mice, which were reciprocally decreased by γ -oryzanol. Experiments with siRNA for D₂ receptors and D₂ receptor ligands *in vitro* suggest that γ -oryzanol suppressed D₂ receptor signalling and augmented GSIS.

CONCLUSIONS AND IMPLICATIONS

γ -Oryzanol exhibited unique anti-diabetic properties. The unexpected effects of γ -oryzanol on D₂ receptor signalling in islets may provide a novel; natural food-based, approach to anti-diabetic therapy.

Abbreviations

[Ca²⁺]_i, cytosolic Ca²⁺ concentration; CCK-8, cholecystokinin-octapeptide; DAT, dopamine transporter; GLP-1, glucagon-like peptide 1; GSIS, glucose-stimulated insulin secretion; GTT, glucose tolerance test; HFD, high-fat diet; IHC, immunohistochemical; siRNA, small interfering RNA; TH, L-tyrosine hydroxylase; VMAT2, vesicular monoamine transporter 2

Tables of Links

TARGETS
GPCRs^a
Dopamine D ₂ receptor
GPR119
GPR120
Transporters^b
DAT, dopamine transporter
VMAT2, vesicular monoamine transporter 2
Enzymes^c
PKA
TH, tyrosine hydroxylase

LIGANDS	
cAMP	Haloperidol
CCK-8, cholecystokinin-octapeptide	Insulin
L-DOPA	Oleoylethanolamide
GLP-1, glucagon-like peptide 1	Palmitic acid
Glucagon	Quinpirole
GW 9508	Somatostatin
H-89	

These Tables list key protein targets and ligands in this article which are hyperlinked to corresponding entries in <http://www.guidetopharmacology.org>, the common portal for data from the IUPHAR/BPS Guide to PHARMACOLOGY (Pawson *et al.*, 2014) and are permanently archived in the Concise Guide to PHARMACOLOGY 2013/14 (^{a,b,c}Alexander *et al.*, 2013a,b,c).

Introduction

Dopamine is a major catecholamine neurotransmitter that controls a wide range of biological processes important in neurological, cardiovascular and metabolic homeostasis. Previous reports have demonstrated that in patients with Parkinson's disease, glucose metabolism was markedly impaired by treatment with L-DOPA, a dopamine precursor, in a dose-dependent manner (Sirtori *et al.*, 1972; Marsden and Parkes, 1977). Importantly, molecules involved in dopamine receptor signalling are expressed in both murine and human pancreatic islets (Rubi *et al.*, 2005; Simpson *et al.*, 2012). Notably, a recent study on isolated pancreatic islets from humans demonstrated that pancreatic islet-derived dopamine did attenuate insulin secretion in an autocrine or paracrine fashion via its receptors (Simpson *et al.*, 2012). In particular, studies in dopamine D₂ receptor knockout mice suggest a critical role of dopaminergic suppression in function and replication of pancreatic beta cells during development in mice (Garcia-Tornadu *et al.*, 2010).

It is well recognized that two distinct signalling pathways contribute to the control of insulin secretion from pancreatic

beta cells, namely the ATP-sensitive K⁺ channel-dependent pathway (triggering pathway) and the cAMP/PKA pathway (amplifying pathway) (Henquin, 2000; Kahn *et al.*, 2006). Two major incretin hormones, glucagon-like peptide 1 (GLP-1) and glucose-dependent insulinotropic polypeptide, are crucial regulators for glucose-stimulated insulin secretion (GSIS) through an increase in intracellular cAMP level, thereby activating the cAMP/PKA pathway. On the other hand, dopamine is known to substantially decrease intracellular cAMP level mainly via D₂ receptors in striatum and pituitary gland in the brain in rats, pigs and humans (Missale *et al.*, 1998; Vallone *et al.*, 2000).

Based on the notion that chronic feeding with a high fat diet (HFD) causes dysfunction of pancreatic islets and results in whole body glucose dysmetabolism (Giacca *et al.*, 2011), we hypothesized that dopamine receptor signalling would be activated locally in pancreatic islets from HFD-fed mice, thereby causing dyshomeostasis of islet functions, at least partly, through a decrease in intracellular cAMP level. On the other hand, it has been shown that expression of genes involved in D₂ receptor signalling in the brain reward system (e.g. striatum, ventral tegmental area) was considerably

decreased in HFD-induced obese rodents, resulting in profound addiction to fatty foods (Li *et al.*, 2009; Johnson and Kenny, 2010). This finding suggested that decreased local synthesis of dopamine in the brain could be relevant to this deviation in feeding behaviour.

γ -Oryzanol, derived from unrefined rice, is a unique bioactive substance, consisting of a mixture of ferulic acid esters with phytosterols or triterpene alcohols (Lerma-Garcia *et al.*, 2009; Kozuka *et al.*, 2013). An earlier study in humans demonstrated that replacement of white rice by brown rice reduced the incidence of type 2 diabetes mellitus (Sun *et al.*, 2010). Based on this report and our interventional trial assessing the metabolically beneficial impact of brown rice on pre-diabetic obese humans (Sun *et al.*, 2010; Shimabukuro *et al.*, 2014), we recently reported in mouse experiments that γ -oryzanol acted directly on the hypothalamus and attenuated preference for dietary fat by decreasing hypothalamic endoplasmic reticulum (ER) stress, thereby ameliorating HFD-induced obesity (Kozuka *et al.*, 2012). We also demonstrated that long-term administration of γ -oryzanol considerably ameliorated HFD-induced glucose dyshomeostasis, independently of body weight and food intake (Kozuka *et al.*, 2012). Moreover, although γ -oryzanol (3.2 mg·g⁻¹ body weight) given orally to mice was distributed predominantly to the brain (83.8 mg per 100 g tissue); it also accumulated particularly in the pancreas (3.5 mg per 100 g tissue) 1 h after supplementation (Kozuka *et al.*, 2015). However, the full mechanism whereby γ -oryzanol ameliorates glucose dysmetabolism throughout the body remained to be elucidated.

In rats, γ -oryzanol increased the dopamine content of the medial basal hypothalamus (Ieiri *et al.*, 1982). This effect was suppressed by an inhibitor of L-tyrosine hydroxylase (TH), the rate-limiting enzyme in dopamine synthesis (Ieiri *et al.*, 1982), suggesting a potential interaction of γ -oryzanol between dopamine metabolism and signalling via dopamine receptors. Based on all these findings, we tested if γ -oryzanol would improve dysfunction of pancreatic islets through the inhibition of D₂ receptor signalling in murine experimental models.

Methods

Animals

All animal care and experimental procedures were approved by the Animal Experiment Ethics Committee of the University of the Ryukyus (Nos. 5352, 5718 and 5943). All studies involving animals are reported in accordance with the ARRIVE guidelines for reporting experiments involving animals (Kilkenny *et al.*, 2010; McGrath *et al.*, 2010). A total of 204 animals were used in the experiments described here.

Eight-week-old male C57BL/6J mice obtained from Charles River Laboratories Japan, Inc. (Kanagawa, Japan) were housed at 24°C under a 12 h/12 h light/dark cycle. The mice were allowed free access to food and water.

Administration of γ -oryzanol

γ -Oryzanol (Wako Pure Chemical Industries, Ltd., Osaka, Japan) was dissolved in 0.5% methyl cellulose solution. γ -Oryzanol (20, 80 or 320 μ g·g⁻¹ body weight) was delivered

into the stomach by a gavage needle every day during feeding with a HFD (Western Diet; Research Diets Inc., New Brunswick, NJ, USA) for 13 weeks. HFD and HFD containing 0.4% γ -oryzanol were manufactured as pellets by Research Diets (Research Diets Inc.). Daily intake of γ -oryzanol by mice, as estimated by mean food intake, was approximately 320 μ g·g⁻¹ body weight. The doses of γ -oryzanol were determined as described (Kozuka *et al.*, 2012).

Metabolic parameters

Whole blood was taken from the tail vein and blood glucose was measured using an automatic glucometer (Medisafe Mini; Terumo, Tokyo, Japan). Occasional blood samples were taken from the retro-orbital venous plexuses or tail vein. Plasma insulin, glucagon and active GLP-1 levels were measured using ELISA kits (Shibayagi Co. Ltd., Gunma, Japan; Wako Pure Chemical Industries, Ltd.; and Morinaga Institute of Biological Science, Inc., Tokyo, Japan). For glucose tolerance tests (GTTs), mice were intraperitoneally injected with 2.0 g·kg⁻¹ glucose after an 18 h fast. Blood glucose levels were measured at the indicated times.

Sub-diaphragmatic vagotomy

Sub-diaphragmatic vagotomy, or sham surgery, was performed as described earlier (Miyamoto *et al.*, 2012) and mice were used for experiments 2 weeks after the surgery. To test the success of the vagotomy, we assessed the satiety induced by CCK-8 (Bachem, Bubendorf, Switzerland), which is mediated by the abdominal vagus nerves (Smith *et al.*, 1981; 1985). Sham-treated and vagotomized mice were injected i.p. with PBS or 8 μ g·kg⁻¹ CCK-8 after an 18 h fast.

Immunohistochemical (IHC) analyses

The pancreas was carefully dissected and fixed in 4% paraformaldehyde, embedded in paraffin and sectioned. The paraffin-embedded sections were stained with haematoxylin and eosin or immunostained for insulin (A0654; Dako Japan, Tokyo, Japan), glucagon (A0565; Dako Japan), somatostatin (AB5495; Merck Millipore, Billerica, MA), dopamine transporter (DAT) (AB1591P; Merck Millipore) and TH (AB152; Merck Millipore). The mean size and ratio of glucagon-positive α -cells, DAT-positive and TH-positive cell areas to the total islet area were calculated based on >100 islets per group using Photoshop (Adobe, San Jose, CA, USA).

Isolation of pancreatic islets and assessment of insulin/glucagon secretion

Pancreatic islets were isolated from mice by collagenase digestion (Liberase TL; Roche Diagnostics GmbH, Mannheim, Germany) and purified on a Histopaque gradient (Histopaque 1077; Sigma-Aldrich, St Louis, MO, USA) as described by Zmuda *et al.*, (2011). Insulin secretion from isolated islets and from a murine pancreatic beta cell line, MIN6 cells, (Miyazaki *et al.*, 1990), was measured as described earlier (Wei *et al.*, 2005). Briefly, the islets were incubated with or without γ -oryzanol (0.2, 2 or 20 μ g·mL⁻¹), forskolin (10 mM), Rp-8-Br-cAMPS (10 μ M), H-89 (10 μ M), haloperidol (1, 10 μ M; Wako Pure Chemical Industries, Ltd.), a D₂ receptor antagonist, 10 μ M L-DOPA, a dopamine precursor, or 5 μ M quinpirole, a potent D₂ receptor agonist (Sigma-Aldrich), for 1 h, and

stimulated with glucose for an additional 1 h with or without γ -oryzanol, haloperidol, L-DOPA or quinpirole. The doses of each compound were decided as described (Simpson *et al.*, 2012). MIN6 cells and an α -cell line (α -TC cells) were seeded at a density of 2.0×10^5 cells·mL⁻¹ on 24-well plates. After 48 h of culture, MIN6 cells were incubated with Krebs–Ringer bicarbonate buffer (KRB; composition; 119 mM NaCl, 4.74 mM KCl, 2.54 mM CaCl₂, 1.19 mM MgCl₂, 1.19 mM KH₂PO₄, 25 mM NaHCO₃, 0.5 % BSA, 25 mM HEPES, pH 7.4.) containing 2.5 mM glucose for 2 h, subsequently incubated in KRB with or without γ -oryzanol (0.2, 2 or 10 μ g·mL⁻¹) for 1 h. The cells were also incubated with a series of insulin secretagogues with or without γ -oryzanol for 2 h. α -TC cells were incubated with KRB containing 16.7 mM glucose for 1 h, subsequently incubated with or without palmitic acid (0.25 or 0.5 mM; Sigma-Aldrich), γ -oryzanol (2 or 10 μ g·mL⁻¹) or haloperidol (10 μ M) for 2 h. Insulin or glucagon secretion was normalized by cellular protein content. Levels of cAMP and PKA activity were determined by the cyclic AMP EIA Kit (Cayman Chemical, Ann Arbor, MI, USA) and PKA kinase activity kit (Enzo Life Sciences, Farmingdale, NY, USA) respectively. To measure insulin content of islets, 10 islets were placed in 1 mL of acid-ethanol (90 mM HCl in 70% ethanol). Insulin was extracted overnight at -20°C after sonication, as previously described (Ariyama *et al.*, 2008). The acid-ethanol extract was neutralized with 1 M Tris (pH 7.5) and insulin levels were measured using an ELISA kit.

Measurement of cytosolic Ca²⁺ concentration ([Ca²⁺]_i) in isolated islets

[Ca²⁺]_i in isolated islets was measured by fura-2 microfluorometry as described (Nakata *et al.*, 2010). Briefly, islets on coverslips were incubated with 1 μ M fura-2/acetoxymethylester (Dojin Chemical Co., Kumamoto, Japan) for 1 h at 37°C in KRB containing 2.8 mM glucose with or without γ -oryzanol or haloperidol. Islets were subsequently mounted in a chamber and superfused at a rate of 1 mL·min⁻¹ at 37°C in KRB with or without γ -oryzanol or haloperidol. Fluorescence following excitation at 340 nm (F340) and that at 380 nm (F380) was measured, and [Ca²⁺]_i was expressed by the ratio (F340/F380).

RNA interference

The small interfering RNA (siRNA) for D₂ receptors (the *Drd2* gene) and a control scrambled siRNA were designed and purchased from Sigma-Aldrich. Pancreatic islets and MIN6 cells were transfected with each siRNA using Lipofectamine RNAi/MAX (Life technologies, Tokyo, Japan) according to the manufacturer's protocol. Insulin secretion from MIN6 cells was normalized against cellular DNA content.

Agonist activity assay

Recruitment of β -arrestin to GPCRs, induced by γ -oryzanol was tested by the PathHunter β -Arrestin Assay obtained from DiscoverRx (Fremont, CA, USA). Luminescence was analysed with Envision (PerkinElmer, Waltham, MA, USA) and % activity was expressed as the relative luminescence units of 10 μ M γ -oryzanol in comparison with that of each positive ligand. Antagonist activity (% inhibition) was measured against approximately EC₅₀ concentrations of agonists. Duplicate

data were obtained. The Z-factor, a parameter of quality control in high throughput screening assays (Zhang *et al.*, 1999), was determined by the following equation: Z-factor = $1 - 3(SD_{\text{sample}} + SD_{\text{control}})/|\text{mean}_{\text{sample}} - \text{mean}_{\text{control}}|$. SD_{sample} and SD_{control} refer to standard deviation of sample and positive control regions respectively.

Western blotting

Western blotting was performed as described (Tanaka *et al.*, 2007) with antibodies against D₂ receptors (AB5084P; Merck Millipore), DAT, TH and β -actin (ab6276; Abcam, Cambridge, MA, USA).

Quantitative real-time PCR

Gene expression was examined as described (Kozuka *et al.*, 2012). Total RNA was extracted using Trizol reagent (Life technologies) and cDNA was synthesized using an iScriptTM cDNA Synthesis Kit (Bio-Rad, Hercules, CA, USA). Quantitative real-time PCR was performed using a StepOnePlusTM Real-Time PCR System and Fast SYBR Green Master Mix (Life Technologies). The mRNA levels were normalized against *Rn18s* (18S rRNA). The primer sets used for the quantitative real-time PCR analyses are summarized in Table 1.

Table 1

The primer sets used for quantitative real-time PCR analysis

Gene	GenBank Accession No.	Primer (5'–3')
<i>Drd2</i> (D2R)	NM_010077	<i>f</i> CCA TTG TCT GGG TCC TGT CC
		<i>r</i> GTG GGT ACA GTT GCC CTT GA
<i>Drd3</i> (D3R)	NM_007877	<i>f</i> GCA GTG GTC ATG CCA GTT CAC TAT CAG
		<i>r</i> CCT GTT GTG TTG AAA CCA AAG AGG AGA GG
<i>Slc6a3</i> (DAT)	NM_010020	<i>f</i> GCA CTA CTT CTT CTC CTC CT
		<i>r</i> CCT GAA GTC TTT ACT CCC TTC C
<i>Th</i> (TH)	NM_009377	<i>f</i> CCC TAC CAA GAT CAA ACC TAC C
		<i>r</i> GAG CGC ATG CAG TAG TAA GA
<i>Slc18a2</i> (VMAT2)	NM_172523	<i>f</i> GTC TGT CTA TGG GAG TGT GTA T
		<i>r</i> GGG TAC GGC TGG ACA TTA TT
<i>Rn18s</i> (18S rRNA)	NR_003278	<i>f</i> TTC TGG CCA ACG GTC TAG ACA AC
		<i>r</i> CCA GTG GTC TTG GTG TGC TGA

Forward and reverse primers are designated by *f* and *r* respectively. D2R, dopamine D₂ receptor; D3R, dopamine D₃ receptor.

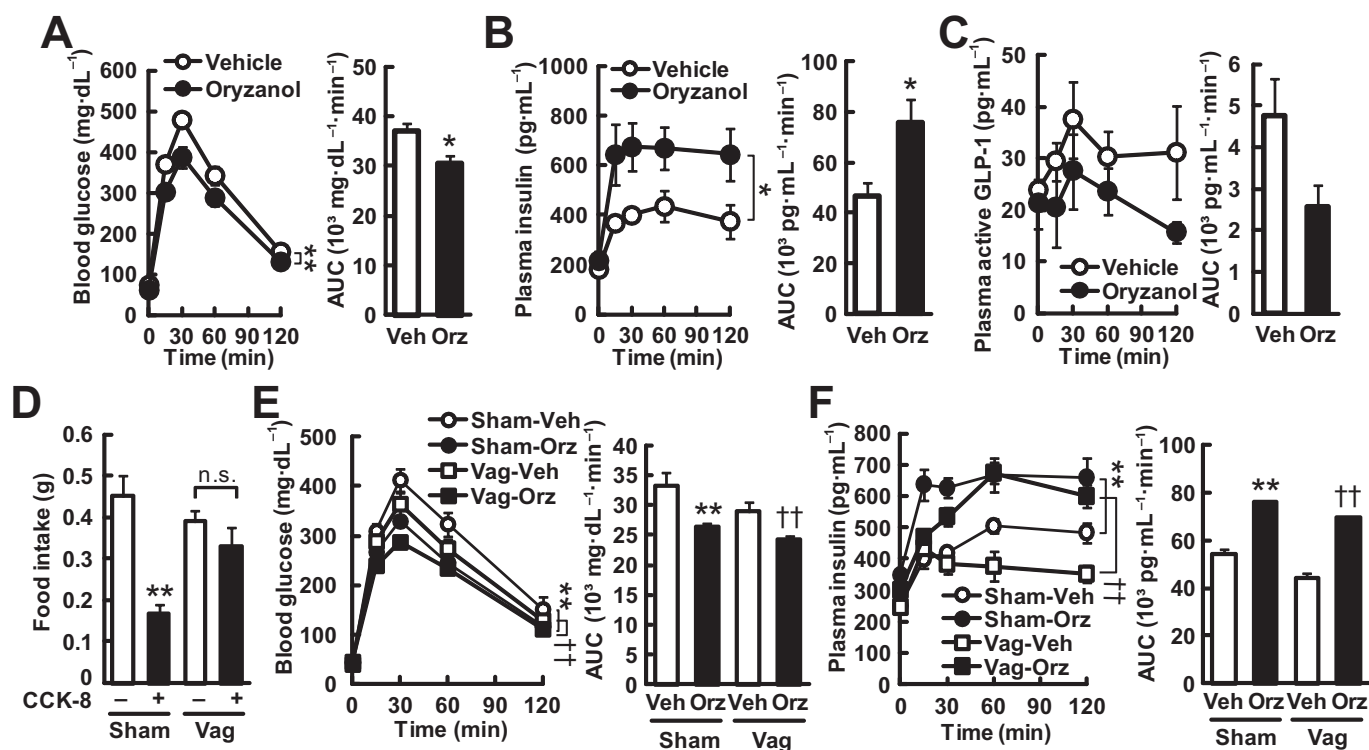


Figure 1

γ -Oryzanol enhances GSIS in mice. (A–C, E, F) Mice on a chow diet were treated with a single oral dose of γ -oryzanol (320 μ g·g⁻¹). The concentrations and AUCs of blood glucose (A, E), plasma insulin (B, F) and plasma active GLP-1 (C) during ipGTTs ($n = 8$) are shown. Chow-fed mice (A–C) and vagotomized mice (Vag) (E, F) were analysed. (D) Satiety effects of CCK-8 were tested in sham-treated mice (Sham) and vagotomized mice (Vag). Sub-diaphragmatic vagotomy abolished the satiety effect of CCK-8. * $P < 0.05$, ** $P < 0.01$ versus unoperated or sham-operated mice treated with vehicle (Vehicle or Sham-Veh). †† $P < 0.01$ versus vehicle-treated vagotomized mice (Vag-Veh). Data are expressed as means \pm SEM.

Data analysis

Data are expressed as the mean \pm SEM from n independent experiments. One-way ANOVA and repeated-measures ANOVA followed by multiple comparison tests (Bonferroni/Dunn method) were used where applicable. Student's t -test was used to analyse the differences between two groups. Differences were considered significant at $P < 0.05$.

Results

γ -Oryzanol acts directly on pancreatic islets and enhances GSIS in vivo

As a first step in exploring the effects of γ -oryzanol on GSIS in chow-fed mice, the effects of a single oral dose of γ -oryzanol (320 μ g·g⁻¹ body weight) on blood glucose and insulin levels were examined during i.p. GTTs (ipGTTs). γ -Oryzanol augmented GSIS and significantly enhanced glucose tolerance even in normal mice (Figure 1A,B). γ -Oryzanol showed a trend towards a decrease in the plasma GLP-1 level, but the change was not statistically significant ($P = 0.11$) (Figure 1C). To see if γ -oryzanol would enhance GSIS independently of GLP-1 receptors, we evaluated, using PathHunter β -arrestin assays,

the agonist activities of γ -oryzanol on GLP-1 receptors and on two other GPCRs, GPR119 and GPR120, both of which potently stimulate GLP-1 secretion (Hirasawa *et al.*, 2005; Chu *et al.*, 2007; Lauffer *et al.*, 2009). γ -Oryzanol did not show agonist activities on these GPCRs [0% of exendin-4, a potent GLP-1 receptor agonist, Z-factor (a parameter of quality control in high throughput screening assays) (Zhang *et al.*, 1999) was 0.81; 9% of oleoylethanolamide, a potent GPR119 agonist, Z-factor was 0.41; -2% of GW 9508, a potent GPR120 agonist, Z-factor was 0.75 respectively].

To exclude the possibility that γ -oryzanol augments GSIS via a central mechanism, we carried out sub-diaphragmatic vagotomy in mice. Cholecystokinin-octapeptide (CCK-8) reduced the food intake in 1 h by 63% in sham-operated mice, while sub-diaphragmatic vagotomy abolished the satiety effect of CCK-8 (Figure 1D), indicating that the vagotomy was successful. In both sham-operated and vagotomized mice, a single oral dose of γ -oryzanol significantly lowered the blood glucose levels and the AUC of glucose during ipGTTs (Figure 1E). Noticeably, in both sham-operated and vagotomized mice, γ -oryzanol markedly increased plasma insulin levels and the AUC of insulin during ipGTTs (Figure 1F). These results suggest that γ -oryzanol acted directly on the pancreatic islets to enhance GSIS.

γ -Oryzanol enhances GSIS through activation of the cAMP/PKA pathway via the suppression of D₂ receptor signalling

In both isolated murine islets and MIN6 cells, γ -oryzanol markedly enhanced GSIS in a dose-dependent fashion (Figure 2A,E). Furthermore, in both cellular systems, γ -oryzanol significantly increased intracellular cAMP levels and PKA activity (Figure 2B,C,F,G). Similarly, augmentation of PKA activity by γ -oryzanol was abolished by H-89, a PKA inhibitor (Figure 2C,G). To explore the underlying mechanism, isolated murine islets and MIN6 cells were exposed to (i) forskolin, which increases intracellular cAMP level; (ii) Rp-8-Br-cAMPS, a cAMP antagonist; or (iii) H-89 respectively. In both cellular systems, γ -oryzanol augmented forskolin-enhanced insulin secretion (Figure 2D,H), while both Rp-8-Br-cAMPS and H-89 abolished such stimulatory effects of γ -oryzanol on GSIS (Figure 2I–K). These findings suggest that γ -oryzanol reinforces GSIS via the cAMP/PKA amplifying pathway in pancreatic islets.

On the other hand, haloperidol, a D₂ receptor antagonist, significantly enhanced GSIS (Figure 3A) through the elevation of intracellular cAMP (Figure 3B) but γ -oryzanol showed no additive effect with haloperidol (Figure 3C,D), supporting the notion that γ -oryzanol increased intracellular cAMP levels and enhanced GSIS through suppression of D₂ receptor signalling. Furthermore, both L-DOPA, a dopamine precursor, and quinpirole, a potent D₂ receptor agonist, abolished γ -oryzanol-induced enhancement of GSIS (Figure 3E–G). Of note, the inhibition by L-DOPA and quinpirole was concentration-dependent (Figure 3F,G). To further confirm the involvement of D₂ receptor signalling in enhancing GSIS by γ -oryzanol, *Drd2* was silenced *in vitro* by incubating the tissues or cells with specific siRNA for 2 days. In both pancreatic islets and MIN6 cells treated with *Drd2* siRNA, the expression of *Drd2* was attenuated by $71.4 \pm 0.1\%$ and $69.5 \pm 0.1\%$ compared with scrambled siRNA-treated cells respectively (Figure 3H,K). There were no significant changes in the expression of *Drd3* (dopamine D₃ receptor) in both systems (Figure 3H,K). Either γ -oryzanol or haloperidol enhanced GSIS accompanied by the elevation of intracellular cAMP level in cells treated with the scrambled siRNA. In contrast, in *Drd2* siRNA-treated cells, γ -oryzanol and haloperidol did not increase GSIS and intracellular cAMP level (Figure 3I,J,L). These results suggest that γ -oryzanol augments GSIS via the suppression of D₂ receptor signalling in pancreatic beta cells. Of note, data from the PathHunter β -arrestin assays suggested that there was no significant agonist or antagonist activities of γ -oryzanol for any of the dopamine receptors (Table 2).

γ -Oryzanol increases insulin biosynthesis and [Ca²⁺]_i in islets

Elevation of intracellular cAMP enhances the biosynthesis of insulin (Fehmann and Habener, 1992) and insulin secretion induced by increased [Ca²⁺]_i in the presence of insulinotropic glucose concentrations (Yada *et al.*, 1993). We therefore assessed the effect of γ -oryzanol and haloperidol on the biosynthesis of insulin and its secretion in response to increased [Ca²⁺]_i in murine-isolated islets. Both γ -oryzanol and haloperidol significantly increased intracellular insulin contents and the [Ca²⁺]_i response (Figure 4). Of note, both γ -oryzanol

and haloperidol enhanced the first phase of [Ca²⁺]_i responses to high glucose (Figure 4B,C). These results also reinforce the notion that γ -oryzanol increases intracellular cAMP levels and subsequently enhances GSIS through suppression of D₂ receptor signalling.

γ -Oryzanol suppresses D₂ receptor signalling in pancreatic islets from HFD-fed mice

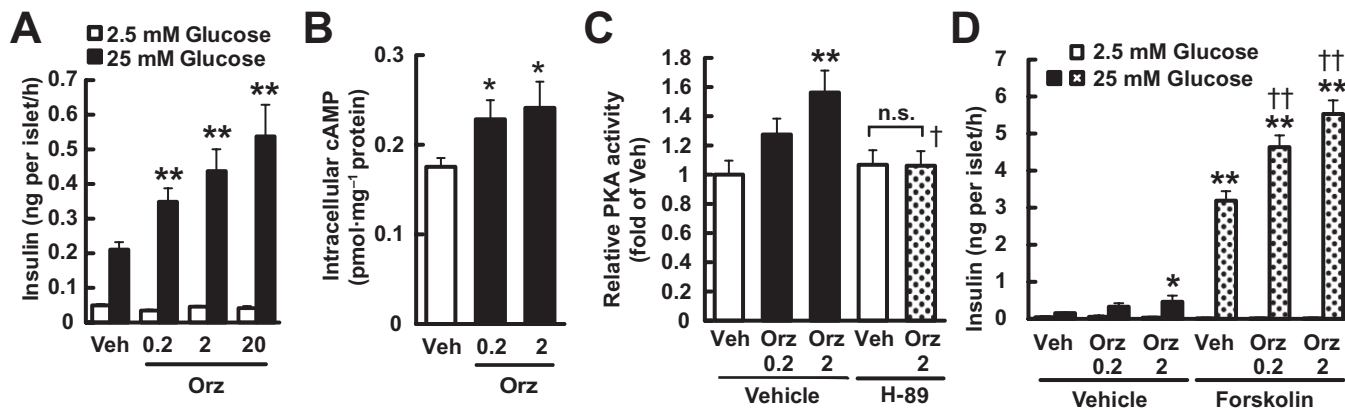
Following treatment of γ -oryzanol (320 $\mu\text{g}\cdot\text{g}^{-1}$ per body weight per day) for 13 weeks, glucose level in mice on a HFD was $1280 \pm 50 \text{ mg}\cdot\text{L}^{-1}$, which was significantly decreased compared with those in mice on the HFD alone ($1570 \pm 80 \text{ mg}\cdot\text{L}^{-1}$, $P < 0.01$). Body weight in mice fed HFD with γ -oryzanol was $31.7 \pm 0.8 \text{ g}$, which was comparable to that in mice fed HFD alone ($30.4 \pm 1.2 \text{ g}$). Areas of islet cells stained with antibody to TH, the rate-limiting enzyme of dopamine synthesis (Figure 5A), and antibody to DAT, which mediates dopamine uptake (Figure 5B), were increased in pancreatic islets from HFD-fed mice, whereas the stained areas were markedly decreased after treatment with γ -oryzanol. Consequently, the ratio of TH-positive or DAT-positive cell areas to the total islet area was significantly increased in HFD-fed mice, and was substantially decreased by the treatment with γ -oryzanol (Figure 5C,D). IHC analyses suggested that TH was localized in beta cells, while DAT was not confined to α -cells, beta cells or δ -cells (Figure 6).

We assessed protein and mRNA expression levels of genes involved in D₂ receptor signalling including D₂ receptors (*Drd2*), TH (*Th*), DAT (*Slc6a3*) and the vesicular monoamine transporter type 2 (VMAT2; *Slc18a2*), which transports dopamine into vesicles. In pancreatic islets from HFD-fed mice, the mRNA levels of *Drd2*, *Th* and *Slc6a3* were considerably elevated, while that of *Slc18a2*, also known as a functional marker of insulin production (Harris *et al.*, 2008), was markedly decreased (Figure 5E–H). Importantly, administration of γ -oryzanol depressed the mRNA levels of these genes (Figure 5E–H). In parallel with mRNA levels, protein levels of D₂ receptors, TH and DAT were concomitantly decreased by γ -oryzanol (Figure 5I–L).

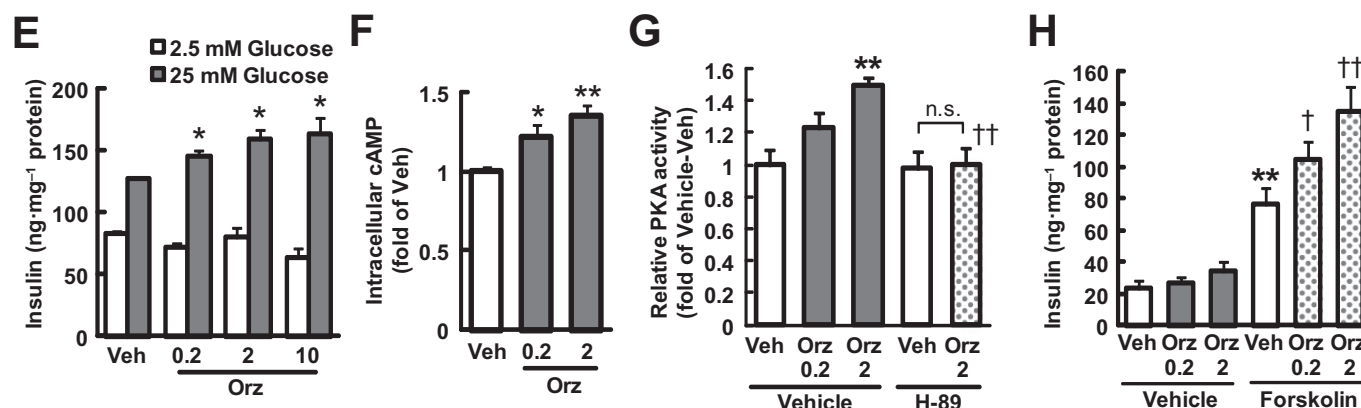
γ -Oryzanol decreases glucagon secretion from murine islets

γ -Oryzanol significantly decreased glucagon levels in plasma of HFD-fed mice (Figure 7A) and in media of isolated islet cultures (Figure 7B). To test the possibility that γ -oryzanol directly acted on α -cells, a murine α -cell line, α -TC cells, was treated with γ -oryzanol. As shown in Figure 7C, glucagon secretion from α -TC cells was reduced, concentration-dependently, by glucose. It should be noted that mRNA level of *Drd2* in α -TC cells was extremely low, compared with those in isolated islets and MIN6 cells, while that of *Drd3* was about the same in the three types of cells (Figure 7D,E). In α -TC cells, γ -oryzanol and haloperidol did not affect glucagon secretion in both basal and palmitate-stimulated conditions (Figure 7F,G). IHC analyses of pancreatic islets from mice on a HFD demonstrated that γ -oryzanol augmented the intensity of insulin staining, while attenuating the average size of pancreatic islets, as well as the ratio of α -cells to the total islet area (Figure 7H–J). These results raised the possibility that γ -oryzanol reduced the increased secretion of glucagon via mechanisms independent of α -cells.

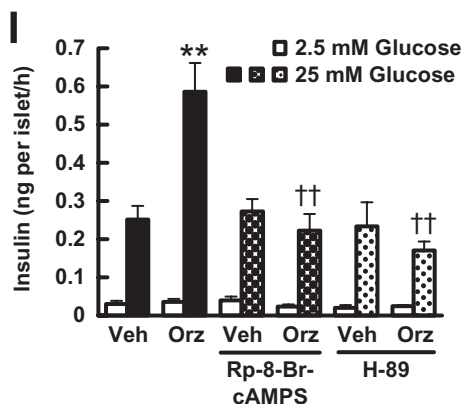
Isolated islets



MIN6 cells



Isolated islets



MIN6 cells

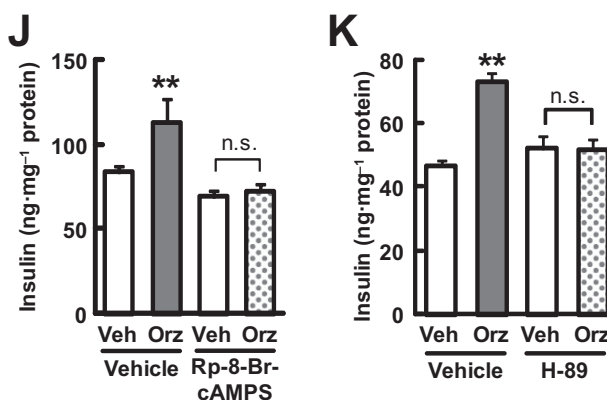


Figure 2

γ -Oryzanol enhances GSIS through activation of the cAMP/PKA pathway in murine isolated islets and MIN6 cells. Murine isolated islets (A–D, I) and MIN6 cells (E–H, J, K) were treated with the indicated concentrations of γ -oryzanol (Orz; 0.2, 2, 10 or 20 μ g·mL⁻¹). (A, E) Insulin secretion was assessed following 25 mM glucose treated in murine-isolated islets ($n = 10$) (A) and MIN6 cells ($n = 8$) (E). (B, C, F, G) γ -Oryzanol (Orz; 0.2 or 2 μ g·mL⁻¹) increased intracellular cAMP levels (B, F) and PKA activity (C, G) following 25 mM glucose in islets ($n = 12$) (B, C) and MIN6 cells ($n = 8$) (F, G). (D, H) Effects of γ -oryzanol (Orz; 0.2 or 2 μ g·mL⁻¹) on insulin secretion enhanced by 10 μ M forskolin in islets ($n = 10$) (D) and MIN6 cells following 2.5 mM glucose ($n = 8$) (H). (I–K) GSIS by 25 mM glucose was suppressed by 10 μ M Rp-8-Br-cAMPS or 10 μ M H-89 in islets ($n = 10$) (I) and MIN6 cells ($n = 8$) (J, K) treated with γ -oryzanol (Orz; 2 μ g·mL⁻¹). Islets used in each experiment were isolated from eight mice, and they were pooled and divided into indicated number of groups. * $P < 0.05$, ** $P < 0.01$ versus vehicle (Veh)-treated islets. † $P < 0.01$ versus cells treated with vehicle (Veh) and γ -oryzanol (2 μ g·mL⁻¹). n.s., not significant. Data are expressed as means \pm SEM.

Isolated islets

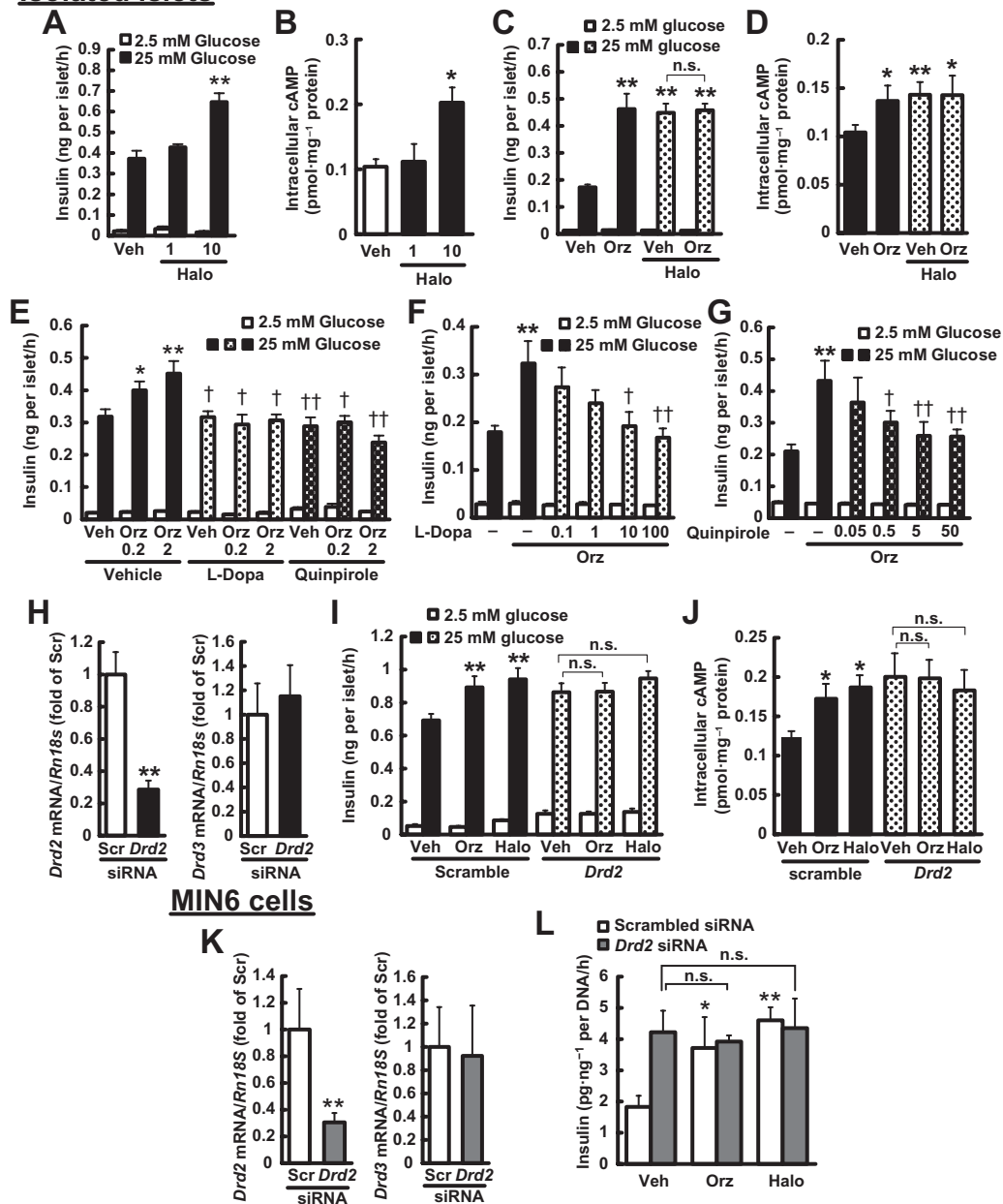


Figure 3

γ -Oryzanol enhances GSIS through the suppression of D₂ receptor signalling in murine isolated islets and MIN6 cells. (A, B) Haloperidol (1, 10 μ M) increased insulin secretion (A) and intracellular cAMP levels (B) in isolated islets following 25 mM glucose ($n = 12$). (C, D) γ -Oryzanol (Orz; 2 μ g·mL⁻¹) and haloperidol (10 μ M) had no additive effect on insulin secretion ($n = 12$) (C) and intracellular cAMP levels ($n = 24$) (D) in isolated islets following 25 mM glucose. Islets used in each experiment were isolated from six mice, and they were pooled and divided into indicated number of groups. (E) Insulin secretion enhanced by the indicated concentrations of γ -oryzanol (Orz; 0.2 or 2 μ g·mL⁻¹) was suppressed by 10 μ M L-DOPA or 5 μ M quinpirole and in isolated islets ($n = 10$; islets isolated from 12 mice were pooled and divided into indicated number of groups). (F, G) Insulin secretion in isolated islets treated with γ -oryzanol (Orz; 2 μ g·mL⁻¹) was suppressed by the indicated concentrations of L-DOPA (0.1, 1, 10 or 100 μ M) (F) or quinpirole (0.05, 0.5, 5 or 50 μ M) (G) ($n = 10$ –14; islets isolated from eight mice were pooled and divided into indicated number of groups). * $P < 0.05$, ** $P < 0.01$ versus islets treated with vehicle (Veh). † $P < 0.05$, †† $P < 0.01$ versus islets treated with vehicle (Veh) and γ -oryzanol. (H–L) Isolated pancreatic islets (H–J) and MIN6 cells (K, L) were treated with *Drd2* siRNA. (H, K) Level of mRNA expression for *Drd2* and *Drd3*. The levels were normalized against those of *Rn18s*. ** $P < 0.01$ versus scrambled siRNA-transfected islets or cells (Scr). (I, L) Insulin secretion in siRNA-treated islets (I) and MIN6 cells (L) was not enhanced by γ -oryzanol (Orz; 2 μ g·mL⁻¹) or haloperidol (10 μ M) ($n = 15$ –20). (J) γ -Oryzanol (Orz; 2 μ g·mL⁻¹) and haloperidol (Halo; 10 μ M) had no effect on intracellular cAMP levels in siRNA-treated islets ($n = 10$). Islets isolated from eight mice were pooled and divided into indicated number of groups. ** $P < 0.01$ versus scrambled siRNA-transfected islets treated with vehicle (Veh). n.s., not significant. Amount of insulin secretion from MIN6 cells was normalized against the cellular protein content. Data are expressed as means \pm SEM.

Table 2Agonist or antagonist activities of γ -oryzanol for dopamine receptors (DRD1–DRD5)

	Agonist		Antagonist	
	% Activity	Z-factor	% Inhibition	Z-factor
DRD1	0	0.73	10	0.84
DRD2L	1	0.79	–5	0.81
DRD2S	2	0.81	5	0.91
DRD3	13	0.48	–13	0.79
DRD4	1	0.86	–2	0.77
DRD5	–2	0.75	9	0.87

Percentage of activity in γ -oryzanol for each dopamine receptor was calculated relative to the basal or maximal agonist values of dopamine. Percentage of inhibition by γ -oryzanol for each dopamine receptor was calculated relative to the basal or EC_{80} values for dopamine (antagonist activity). GPCR targets: DRD1, dopamine D_1 receptor; DRD2L, long form of the dopamine D_2 receptor; DRD2S, short form of the dopamine D_2 receptor; DRD3, dopamine D_3 receptor; DRD4, dopamine D_4 receptor; DRD5, dopamine D_5 receptor.

Discussion and conclusions

The major findings in the present study are summarized by the scheme shown in Figure 8. Here, we have demonstrated that, in mice, γ -oryzanol acted directly on pancreatic islets and enhanced GSIS *in vivo* and *in vitro* (Figures 1 and 2). Such a reinforcement of GSIS by γ -oryzanol was mediated by the local activation of the cAMP/PKA amplifying pathway (Figures 2 and 4). Along with chemical agonists for a variety of fatty acid receptors, cAMP/PKA amplifying pathways in pancreatic beta cells are promising drug targets for the treatment of type 2 diabetes (Drucker, 2006; Rayasam *et al.*, 2007; Ohishi and Yoshida, 2012). In this context, γ -oryzanol may be potentially useful as an alternative or a partner of combination therapies with incretin-related drugs.

To our knowledge, the present study is the first to demonstrate that protein and mRNA expression of molecules involved in D_2 receptor signalling was considerably elevated in pancreatic islets from mice fed on a HFD. Moreover, supplementation with γ -oryzanol corrected the dysregulation of these molecules *in vivo* (Figure 5). As increased signal transduction by D_2 receptors in pancreatic beta cells suppresses the secretion of insulin (Rubi *et al.*, 2005; Simpson *et al.*, 2012), such an effect of γ -oryzanol may be beneficial for individuals with glucose intolerance and type 2 diabetes. To date, how transcription of *Drd2* is regulated is largely undefined. It is possible that consensus element of NF- κ B in the promoter region of *Drd2* (Bontempi *et al.*, 2007) is related to the HFD-induced dysregulation of D_2 receptors in isolated islets. Apart from the direct action of γ -oryzanol on pancreatic islets, it is also possible that improvement of hyperglycaemia *per se* may influence the expression of molecules involved in D_2 receptor signalling. In this context, further studies are necessary to elucidate fully the molecular mechanisms involved.

Intriguingly, in HFD-induced obese rodents, expression of genes involved in D_2 receptor signalling in the brain reward system (e.g. striatum, ventral tegmental area) was clearly decreased, resulting in a profound addiction to fatty foods (Li

et al., 2009; Johnson and Kenny, 2010). Furthermore, recent studies in rodents demonstrated that HFD-induced decrement in D_2 receptor expression in the brain reward system was closely associated with the hyper-methylation in the promoter region of the *Drd2* gene (Vucetic *et al.*, 2012). Studies are ongoing in our laboratory to investigate whether there is HFD-induced epigenetic dysregulation of the D_2 receptor signalling in pancreatic islets or beta cells.

In isolated islets and MIN6 cells, experiments with RNA interference for *Drd2* and with exogenous D_2 receptor ligands demonstrated that γ -oryzanol augmented GSIS via the suppression of D_2 receptor signalling (Figure 3). Enhancement of GSIS by γ -oryzanol was suppressed by L-DOPA (Figure 3E,F), while γ -oryzanol has neither agonist nor antagonist activities at D_2 receptors (Table 2). These findings suggest that γ -oryzanol has inhibitory effects on local dopamine synthesis.

In the pathophysiology of diabetes mellitus, exaggerated secretion of glucagon from pancreatic α -cells contributes to the vicious cycle of glucose dyshomeostasis (Holst, 2007). We demonstrated that γ -oryzanol substantially ameliorated the exaggerated secretion of glucagon in both HFD-fed mice and murine-isolated islets (Figure 7). As D_2 receptors are confined to beta cells in pancreatic islets in mice (Rubi *et al.*, 2005), our data raise the possibility that γ -oryzanol would not directly affect glucagon secretion from α -cells. To support this notion, we demonstrated in an α -cell line, α -TC cells, that γ -oryzanol and haloperidol did not affect glucagon secretion in either basal or palmitate-stimulated conditions (Figure 7E,G). The secretion of glucagon is known to be regulated by the central and peripheral nervous system as well as intra-islet paracrine factors including insulin, GABA and somatostatin (Ishihara *et al.*, 2003; Kawamori *et al.*, 2009; Walker *et al.*, 2011). For instance, postprandial glucagon release is strongly suppressed by GLP-1 and the effect of GLP-1 is mediated, at least partly, by somatostatin (Holst, 2007; Seino *et al.*, 2010). In this context, our results raise the possibility that γ -oryzanol may reduce increased secretion of glucagon via α -cell-independent, intra-islet paracrine factors.

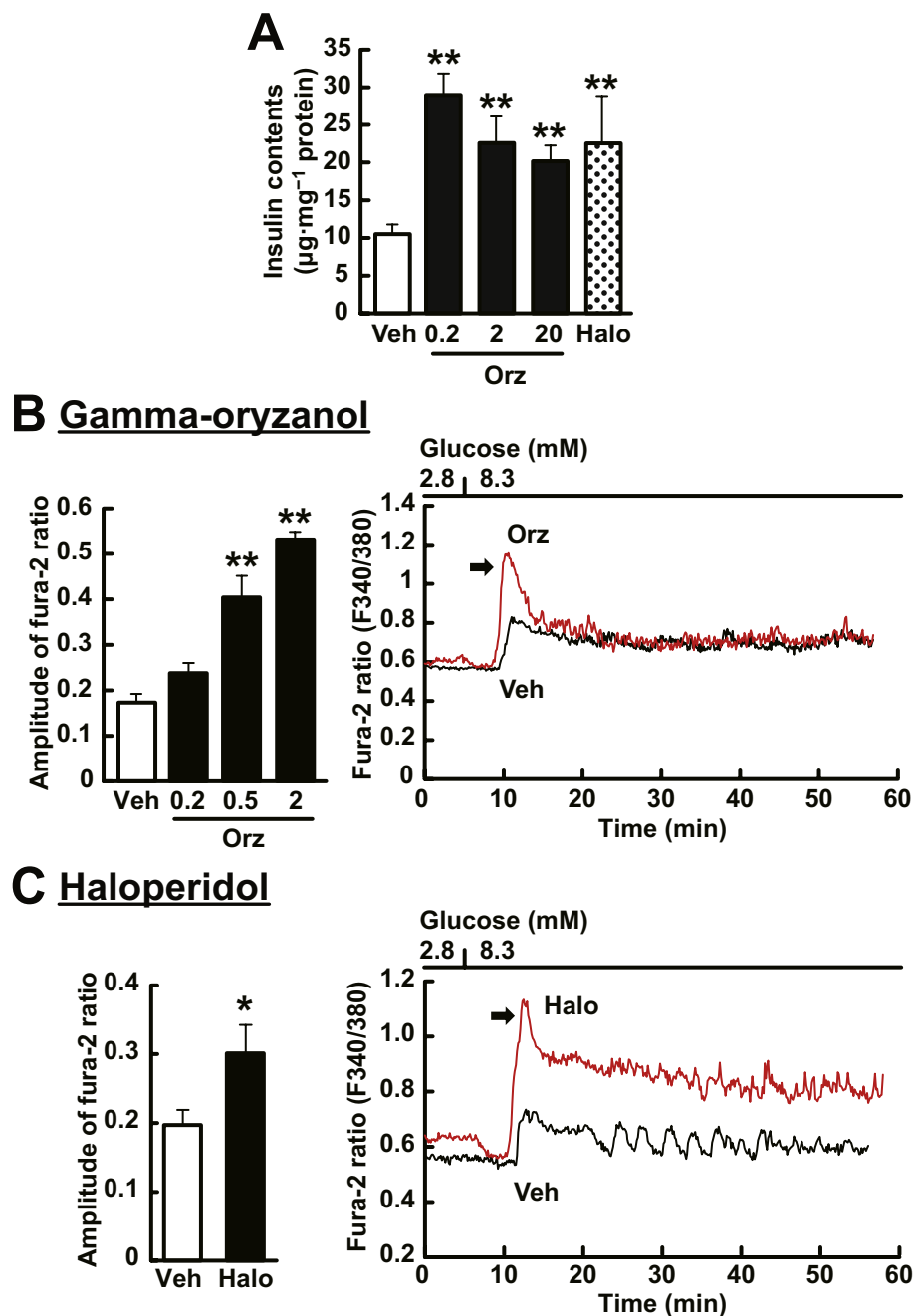


Figure 4

γ -Oryzanol increases intracellular insulin contents and $[Ca^{2+}]_i$ in murine isolated islets. (A) γ -Oryzanol (Orz; 0.2, 2 or 20 $\mu\text{g}\cdot\text{mL}^{-1}$) and haloperidol (Halo; 10 μM) increased intracellular insulin contents ($n = 14$). (B, C) The representative $[Ca^{2+}]_i$ responses to 8.3 mM glucose in islets incubated with γ -oryzanol or haloperidol. Both 2 $\mu\text{g}\cdot\text{mL}^{-1}$ γ -oryzanol (B) and 10 μM haloperidol (C) potentiated the first-phase $[Ca^{2+}]_i$ response to 8.3 mM glucose in murine single islet. The peak amplitude of $[Ca^{2+}]_i$ responses was significantly enhanced by γ -oryzanol (Orz; 0.2, 0.5 or 2 $\mu\text{g}\cdot\text{mL}^{-1}$) (B) (Veh, $n = 8$, Orz 0.2, $n = 12$, Orz 0.5, $n = 5$, Orz 2, $n = 3$; islets isolated from three mice were pooled and divided into indicated number of groups) and haloperidol (C) (Veh, $n = 12$, Halo, $n = 10$; islets isolated from two mice were pooled and divided into indicated number of groups). * $P < 0.05$, ** $P < 0.01$ versus vehicle (Veh)-treated islets. Data are expressed as means \pm SEM.

Regarding the effects of γ -oryzanol on food intake in mice, we previously reported that γ -oryzanol did not affect the total amount of food intake (chow: 16.8 ± 0.5 g per week, HFD: 16.4 ± 0.4 g per week, HFD + γ -oryzanol: 16.2 ± 0.5 g per

week). However, γ -oryzanol does reduce the preference for fatty foods in mice (Kozuka *et al.*, 2012). Based on these findings, in the current experimental settings, the insulinotropic effects of γ -oryzanol on pancreatic islets should be

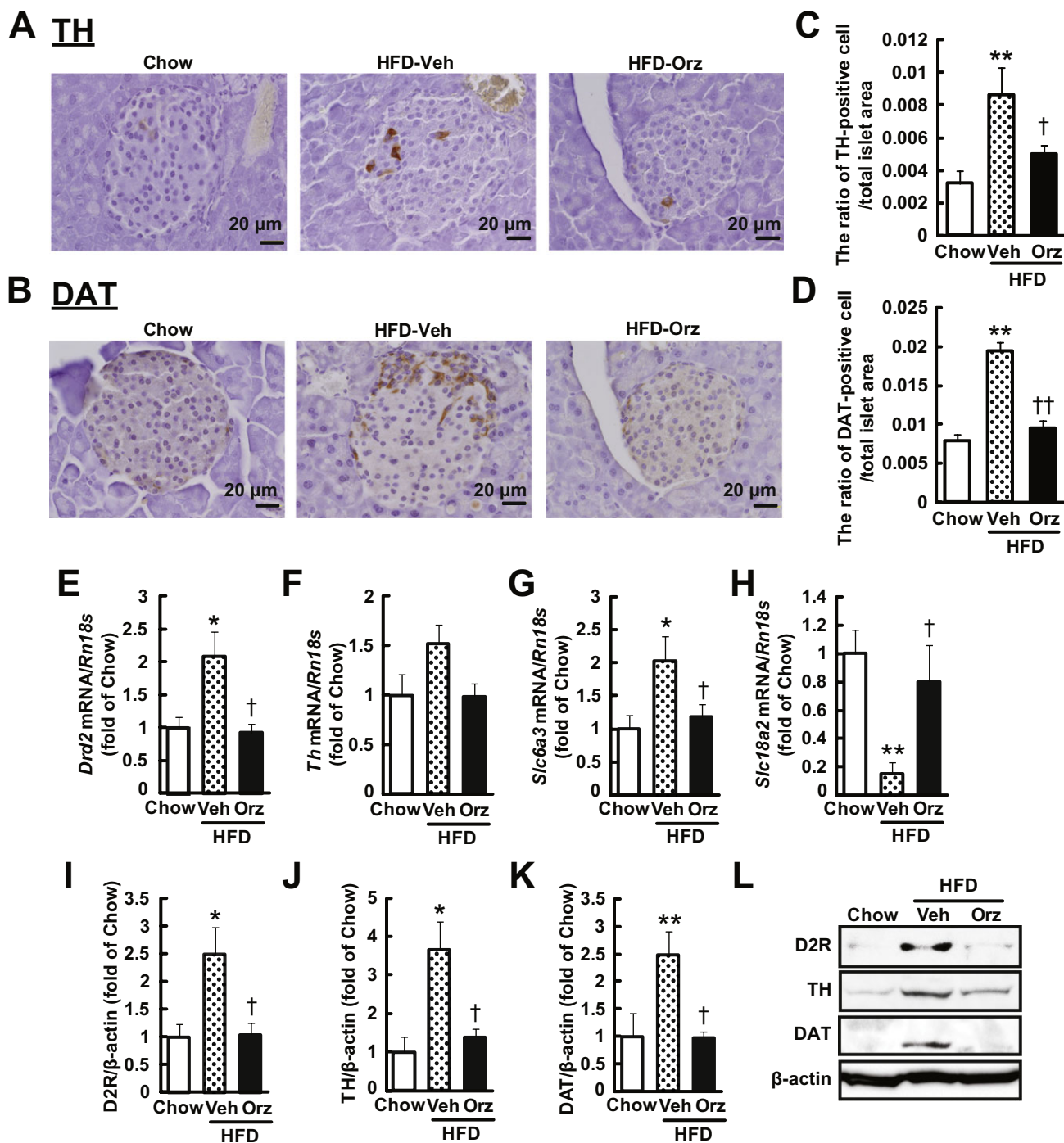


Figure 5

γ -Oryzanol suppresses the expression of molecules involved in D_2 receptor signalling in murine pancreatic islets from mice fed HFD. (A, B) IHC analyses of pancreatic islets from HFD-fed mice treated with γ -oryzanol (Orz). Paraffin-embedded sections were stained with anti-TH (A) or anti-DAT (B) antibodies. Scale bar, 20 μ m; magnification, $\times 400$. (C, D) The ratios of TH-positive (C) and DAT-positive (D) cell area to the total islet area were attenuated by the treatment with γ -oryzanol in HFD-fed mice (chow, $n = 6$, HFD-Veh, $n = 8$, HFD-Orz, $n = 8$). $**P < 0.01$ versus chow-fed mice. $^\dagger P < 0.05$, $^\ddagger P < 0.01$ versus vehicle (Veh)-treated HFD-fed mice. (E–H) Expression levels of *Drd2* (E), *Th* (F), *Slc6a3* (DAT) (G) and *Slc18a2* (VMAT2) (H) mRNAs in pancreatic islets from HFD-fed mice were decreased by γ -oryzanol (Orz; 320 μ g \cdot g $^{-1}$ per body weight per day) ($n = 6$). The mRNA levels were determined by real-time PCR. The levels were normalized by those of *Rn18s* (18S rRNA). (I–L) Protein levels of D_2 receptors (I), TH (J) and DAT (K) in pancreatic islets from HFD-fed mice were decreased by γ -oryzanol ($n = 6$). Protein levels were determined by Western blotting. The values were normalized against those of β -actin protein. $*P < 0.05$, $**P < 0.01$ versus chow-fed mice. $^\dagger P < 0.05$ versus vehicle (Veh)-treated HFD-fed mice. Data are expressed as means \pm SEM.

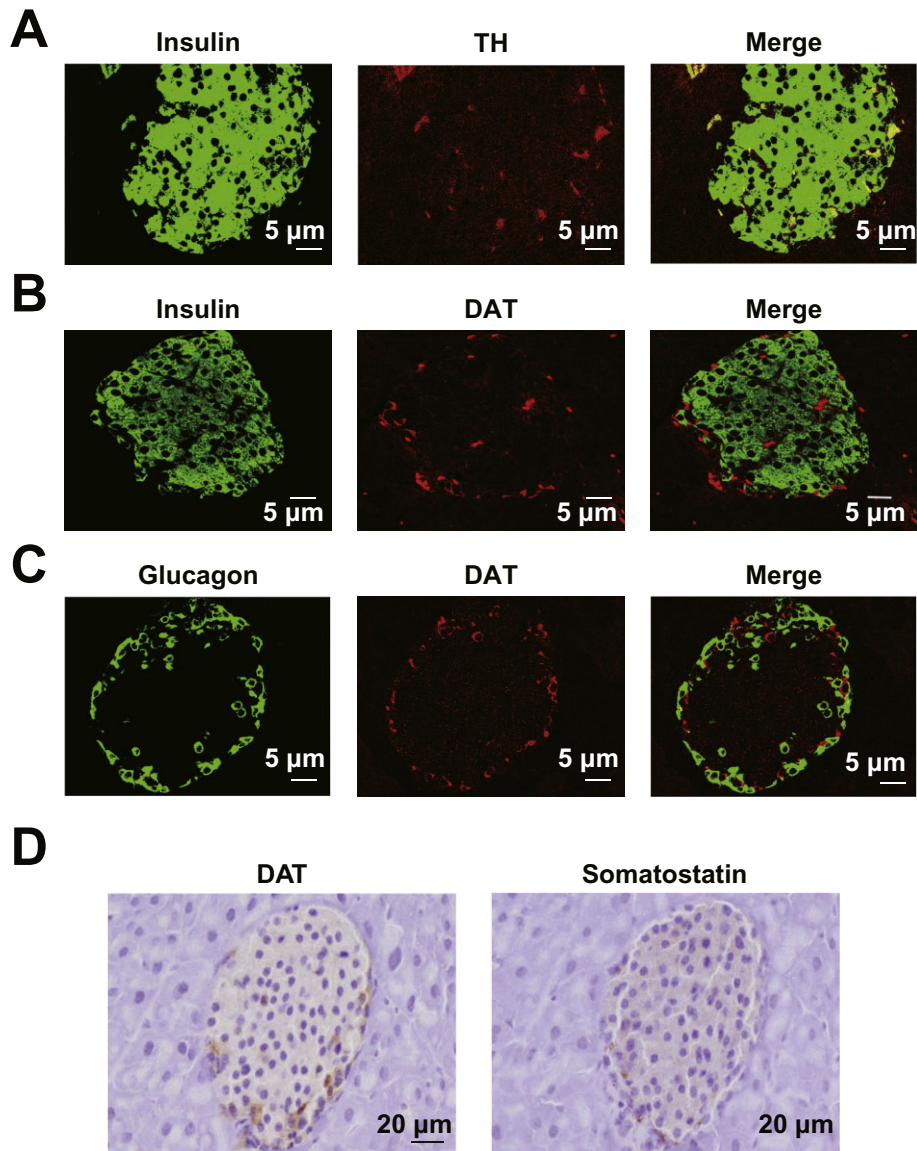


Figure 6

TH was localized in beta cells, whereas DAT was not confined to α -cells, beta cells or δ -cells. IHC analyses of pancreatic islets from HFD-fed mice. Paraffin-embedded sections were co-stained with anti-TH (red) and anti-insulin (green) (A), anti-DAT (red) and anti-insulin (green) (B), or anti-DAT (red) and anti-glucagon (green) (C) antibodies. Scale bar, 5 μ m; magnification, $\times 600$. (D) Serial paraffin-embedded sections were stained with anti-DAT and anti-somatostatin antibodies. Scale bar, 20 μ m; magnification, $\times 400$.

largely attributed to its direct mechanism. Moreover, as demonstrated in Figure 1, oral administration of γ -oryzanol to mice fed chow diet did not increase plasma GLP-1 level. The results of β -arrestin assays also support the notion that γ -oryzanol did not act as a ligand for GLP-1 receptor. Notably, secretion of GLP-1 is controlled strongly by a vagal nerve-mediated central mechanism (Drucker, 2006). However, even in vagotomized mice, γ -oryzanol markedly increased the plasma insulin levels during ipGTTs (Figure 1). These data suggest that γ -oryzanol acts directly on pancreatic

islets and enhances GSIS independently of GLP-1 receptor signalling. Furthermore, we recently demonstrated that γ -oryzanol protects beta cells against ER stress-induced apoptosis in HFD-fed mice (Kozuka *et al.*, 2015). Taken together, γ -oryzanol exhibited metabolically beneficial effects on glucose homeostasis in a GLP-1 independent, unique insulintropic manner.

The present study unveiled the mechanism, at least in part, whereby γ -oryzanol protects pancreatic islets against HFD-induced dysfunction and augments GSIS via the

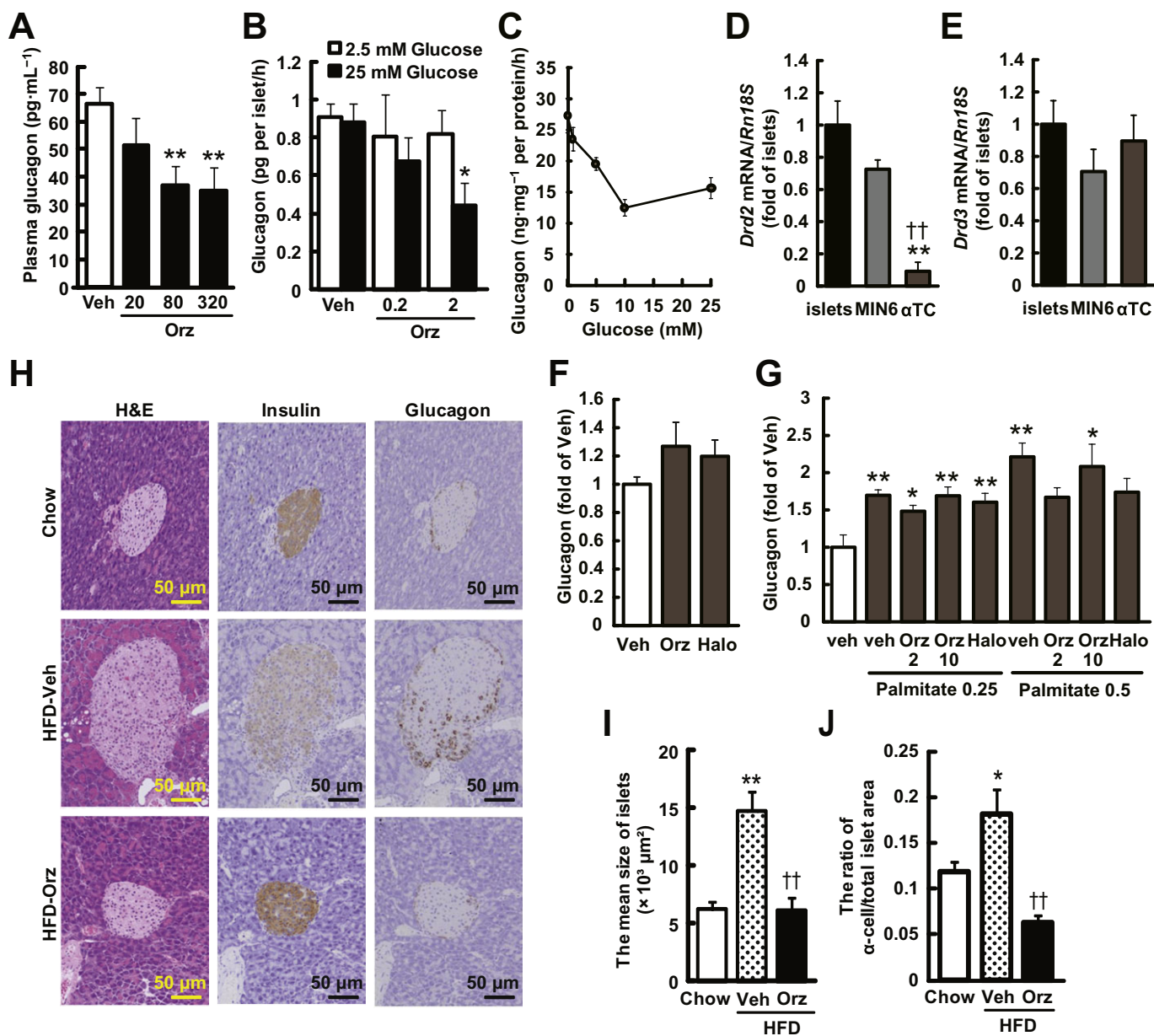


Figure 7

γ -Oryzanol ameliorates increased secretion of glucagon in HFD-fed mice and from murine isolated islets. (A) Plasma glucagon levels in HFD-fed mice treated with the indicated doses of γ -oryzanol (Orz) after a 4 h fast (20, 80 or 320 μ g·g⁻¹ per body weight per day; $n = 6$). (B) Glucagon secretion in isolated pancreatic islets was decreased by γ -oryzanol (Orz; 0.2 or 2 μ g·mL⁻¹) following the exposure to 25 mM glucose ($n = 10$; islets isolated from three mice were pooled and divided into indicated number of groups). (C) Glucagon secretion was stimulated by indicated concentrations of glucose (0, 1, 5, 10 and 25 mM). Amount of glucagon secretion was normalized against the cellular protein content. (D, E) Expression level of *Drd2* and *Drd3* in isolated islets, MIN6 and α -TC cells. Levels of mRNA expression for *Drd2* (D) and *Drd3* (E) in three types of cells ($n = 12$). The mRNA levels were determined by real-time PCR. The levels were normalized against those of *Rn18s*. ** $P < 0.01$ versus islets, †† $P < 0.01$ versus MIN6 cells. (F, G) In α -TC cells treated with γ -oryzanol (Orz; 2 or 10 μ g·mL⁻¹) or haloperidol (10 μ M), glucagon secretion was assessed following 5 mM glucose (F) or palmitate (0.25 and 0.5 mM following 16.7 mM glucose (G)). * $P < 0.05$, ** $P < 0.01$ versus HFD-fed mice, islets, or α -TC cells treated with vehicle (Veh). (H) IHC analyses of isolated pancreatic islets from HFD-fed mice treated with γ -oryzanol (Orz; 320 μ g·g⁻¹·day⁻¹). Serial paraffin-embedded sections were stained with haematoxylin and eosin (H&E) (upper panel) or anti-insulin (middle panel), anti-glucagon (lower panel) antibodies. Scale bar, 50 μ m; magnification, $\times 200$. (I, J) The mean sizes of islets (I) and ratios of glucagon-positive α -cell areas to the total islet area (J) were calculated ($n = 6-8$). * $P < 0.05$, ** $P < 0.01$ versus chow-fed mice. †† $P < 0.01$ versus HFD-fed mice treated with vehicle (Veh). Data are expressed as means \pm SEM.

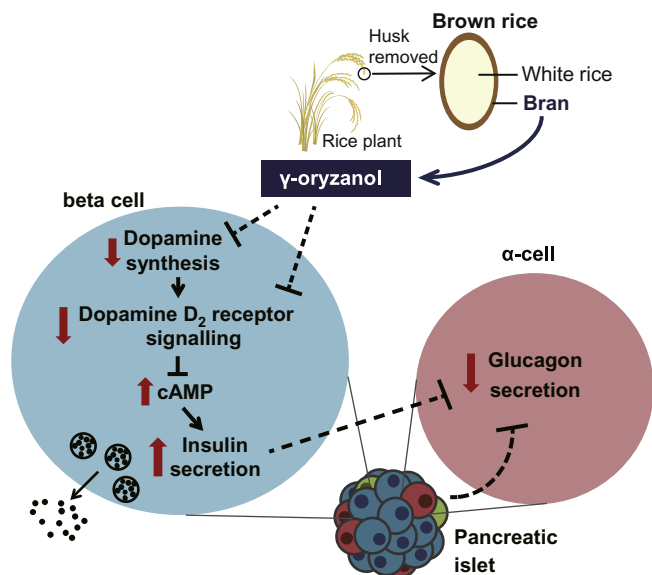


Figure 8

Scheme illustrating the effects of γ -oryzanol on pancreatic islets in mice. In pancreatic islets and beta cells, γ -oryzanol suppresses D₂ receptor signalling, at least partly via the inhibition of local dopamine synthesis, leading to an increase in the intracellular cAMP level. Consequently, GSIS is augmented via the cAMP/PKA pathway (amplifying pathway). On the other hand, γ -oryzanol ameliorates exaggerated secretion of glucagon from pancreatic α -cells, not via the direct action on α -cells, but presumably via some intra-islet paracrine factors.

attenuation of local D₂ receptor signalling in mice. This series of unexpected actions of γ -oryzanol may lead to a novel, natural food-based preventive treatment for type 2 diabetes.

Acknowledgements

We thank M. Takaki (University of the Ryukyus, Japan) and F. Y. Wei (Kumamoto University, Japan) for technical help. We are grateful to M. Hirata, I. Asato and C. Noguchi (University of the Ryukyus, Japan) for assistance. The α -TC cells were kindly provided by T. Kitamura (Gunma University, Japan). This work was supported in part by Grants-in-Aid from Japan Society for the Promotion of Science (JSPS; KAKENHI Grant Nos. 24591338 and 25-9668), Council for Science, Technology and Innovation (CSTI), Cross-ministerial Strategic Innovation Promotion Program (SIP), 'Technologies for creating next-generation agriculture, forestry and fisheries', Takeda Science Foundation (Specified Research Grant), Society for Woman's Health Science Research (13-A1-001), the Nestlé Nutrition Council Japan, Narishige Neuroscience Research Foundation, Lotte Foundation, Leave a Nest Grants, Metabolic Syndrome Foundation and Specified Project 'Establishing a research hub toward the development of an intellectual cluster in Okinawa Prefecture' (2011–2014). C. K. is a Research Fellow of JSPS.

Author contributions

C. K., C. S.-O. and M. N. performed the research. C. K. and H. M. designed the research study. S. S., R. U., M. H., Y. O., H. T., C. S.-O., C. T., M. M., M. T., S. I., M. N., T. Y., J. M., S. O. and M. S. provided invaluable advice on research design and data interpretation. J. M. and S. O. contributed essential reagents or tools. C. K. analysed the data. C. K. and H. M. wrote the paper.

Conflict of interest

We declare that we have no conflict of interest.

References

- Alexander SP, Benson HE, Faccenda E, Pawson AJ, Sharman JL, Spedding M *et al.* (2013a). The concise guide to PHARMACOLOGY 2013/14: G protein-coupled receptors. *Br J Pharmacol* 170: 1459–1581.
- Alexander SPH, Benson HE, Faccenda E, Pawson AJ, Sharman JL Spedding M *et al.* (2013b). The concise guide to PHARMACOLOGY 2013/14: Transporters. *Br J Pharmacol* 170: 1706–1796.
- Alexander SPH, Benson HE, Faccenda E, Pawson AJ, Sharman JL Spedding M *et al.* (2013c). The concise guide to PHARMACOLOGY 2013/14: Enzymes. *Br J Pharmacol* 170: 1797–1867.
- Ariyama Y, Tanaka Y, Shimizu H, Shimomura K, Okada S, Saito T *et al.* (2008). The role of CHOP messenger RNA expression in the link between oxidative stress and apoptosis. *Metabolism* 57: 1625–1635.
- Bontempi S, Fiorentini C, Busi C, Guerra N, Spano P, Missale C (2007). Identification and characterization of two nuclear factor-kappaB sites in the regulatory region of the dopamine D2 receptor. *Endocrinology* 148: 2563–2570.
- Chu ZL, Jones RM, He H, Carroll C, Gutierrez V, Lucman A *et al.* (2007). A role for beta-cell-expressed G protein-coupled receptor 119 in glycemic control by enhancing glucose-dependent insulin release. *Endocrinology* 148: 2601–2609.
- Drucker DJ (2006). The biology of incretin hormones. *Cell Metab* 3: 153–165.
- Fehmann HC, Habener JF (1992). Insulinotropic hormone glucagon-like peptide-I(7–37) stimulation of proinsulin gene expression and proinsulin biosynthesis in insulinoma beta TC-1 cells. *Endocrinology* 130: 159–166.
- Garcia-Tornadu I, Ornstein AM, Chamson-Reig A, Wheeler MB, Hill DJ, Arany E *et al.* (2010). Disruption of the dopamine d2 receptor impairs insulin secretion and causes glucose intolerance. *Endocrinology* 151: 1441–1450.
- Giacca A, Xiao C, Oprescu AI, Carpentier AC, Lewis GF (2011). Lipid-induced pancreatic beta-cell dysfunction: focus on in vivo studies. *Am J Physiol Endocrinol Metab* 300: E255–E262.
- Harris PE, Ferrara C, Barba P, Polito T, Freeby M, Maffei A (2008). VMAT2 gene expression and function as it applies to imaging beta-cell mass. *J Mol Med (Berl)* 86: 5–16.

- Henquin JC (2000). Triggering and amplifying pathways of regulation of insulin secretion by glucose. *Diabetes* 49: 1751–1760.
- Hirasawa A, Tsumaya K, Awaji T, Katsuma S, Adachi T, Yamada M *et al.* (2005). Free fatty acids regulate gut incretin glucagon-like peptide-1 secretion through GPR120. *Nat Med* 11: 90–94.
- Holst JJ (2007). The physiology of glucagon-like peptide 1. *Physiol Rev* 87: 1409–1439.
- Ieiri T, Kase N, Hashigami Y, Kobori H, Nakamura T, Shimoda S (1982). [Effects of gamma-oryzanol on the hypothalamo-pituitary axis in the rat]. *Nihon Naibunpi Gakkai Zasshi* 58: 1350–1356.
- Ishihara H, Maechler P, Gjinovci A, Herrera PL, Wollheim CB (2003). Islet beta-cell secretion determines glucagon release from neighbouring alpha-cells. *Nat Cell Biol* 5: 330–335.
- Johnson PM, Kenny PJ (2010). Dopamine D2 receptors in addiction-like reward dysfunction and compulsive eating in obese rats. *Nat Neurosci* 13: 635–641.
- Kahn SE, Hull RL, Utzschneider KM (2006). Mechanisms linking obesity to insulin resistance and type 2 diabetes. *Nature* 444: 840–846.
- Kawamori D, Kurpad AJ, Hu J, Liew CW, Shih JL, Ford EL *et al.* (2009). Insulin signaling in alpha cells modulates glucagon secretion in vivo. *Cell Metab* 9: 350–361.
- Kilkenny C, Browne W, Cuthill IC, Emerson M, Altman DG (2010). Animal research: Reporting in vivo experiments: the ARRIVE guidelines. *Br J Pharmacol* 160: 1577–1579.
- Kozuka C, Yabiku K, Sunagawa S, Ueda R, Taira SI, Ohshiro H *et al.* (2012). Brown rice and its component, gamma-oryzanol, attenuate the preference for high-fat diet by decreasing hypothalamic endoplasmic reticulum stress in mice. *Diabetes* 61: 3084–3093.
- Kozuka C, Yabiku K, Takayama C, Matsushita M, Shimabukuro M, Masuzaki H (2013). Natural food science based novel approach toward prevention and treatment of obesity and type 2 diabetes: recent studies on brown rice and γ -oryzanol. *Obes Res Clin Pract* 7: e165–e172.
- Kozuka C, Sunagawa S, Ueda R, Higa M, Tanaka H, Shimizu-Okabe C *et al.* (2015). Gamma-oryzanol protects pancreatic beta-cells against endoplasmic reticulum stress in male mice. *Endocrinology* 156: 1242–1250.
- Lauffer LM, Iakoubov R, Brubaker PL (2009). GPR119 is essential for oleoylethanolamide-induced glucagon-like peptide-1 secretion from the intestinal enteroendocrine L-cell. *Diabetes* 58: 1058–1066.
- Lerma-Garcia MJ, Herrero-Martinez JM, Simo-Alfonso EF, Mendonca CRB, Ramis-Ramos G (2009). Composition, industrial processing and applications of rice bran gamma-oryzanol. *Food Chem* 115: 389–404.
- Li Y, South T, Han M, Chen J, Wang R, Huang XF (2009). High-fat diet decreases tyrosine hydroxylase mRNA expression irrespective of obesity susceptibility in mice. *Brain Res* 1268: 181–189.
- Marsden CD, Parkes JD (1977). Success and problems of long-term levodopa therapy in Parkinson's disease. *Lancet* 1: 345–349.
- McGrath J, Drummond G, McLachlan E, Kilkenny C, Wainwright C (2010). Guidelines for reporting experiments involving animals: the ARRIVE guidelines. *Br J Pharmacol* 160: 1573–1576.
- Missale C, Nash SR, Robinson SW, Jaber M, Caron MG (1998). Dopamine receptors: from structure to function. *Physiol Rev* 78: 189–225.
- Miyamoto L, Ebihara K, Kusakabe T, Aotani D, Yamamoto-Kataoka S, Sakai T *et al.* (2012). Leptin activates hepatic 5' AMP-Activated Protein Kinase through sympathetic nervous system and alpha1 adrenergic receptor: a potential mechanism for improvement of fatty liver in lipodystrophy by leptin. *J Biol Chem* 287: 40441–40447.
- Miyazaki J, Araki K, Yamato E, Ikegami H, Asano T, Shibasaki Y *et al.* (1990). Establishment of a pancreatic beta cell line that retains glucose-inducible insulin secretion: special reference to expression of glucose transporter isoforms. *Endocrinology* 127: 126–132.
- Nakata M, Shintani N, Hashimoto H, Baba A, Yada T (2010). Intra-islet PACAP protects pancreatic beta-cells against glucotoxicity and lipotoxicity. *J Mol Neurosci* 42: 404–410.
- Ohishi T, Yoshida S (2012). The therapeutic potential of GPR119 agonists for type 2 diabetes. *Expert Opin Investig Drugs* 21: 321–328.
- Pawson AJ, Sharman JL, Benson HE, Faccenda E, Alexander SP, Buneman OP *et al.*; NC-IUPHAR (2014). The IUPHAR/BPS Guide to PHARMACOLOGY: an expert-driven knowledge base of drug targets and their ligands. *Nucl Acids Res* 42 (Database Issue): D1098–D1106.
- Rayasam GV, Tulasi VK, Davis JA, Bansal VS (2007). Fatty acid receptors as new therapeutic targets for diabetes. *Expert Opin Ther Targets* 11: 661–671.
- Rubi B, Ljubcic S, Pournourmohammadi S, Carobbio S, Armanet M, Bartley C *et al.* (2005). Dopamine D2-like receptors are expressed in pancreatic beta cells and mediate inhibition of insulin secretion. *J Biol Chem* 280: 36824–36832.
- Seino Y, Fukushima M, Yabe D (2010). GIP and GLP-1, the two incretin hormones: similarities and differences. *J Diabetes Investig* 1: 8–23.
- Shimabukuro M, Higa M, Kinjo R, Yamakawa K, Tanaka H, Kozuka C *et al.* (2014). Effects of the brown rice diet on visceral obesity and endothelial function: the BRAVO study. *Br J Nutr* 111: 310–320.
- Simpson N, Maffei A, Freeby M, Burroughs S, Freyberg Z, Javitch J *et al.* (2012). Dopamine-mediated autocrine inhibitory circuit regulating human insulin secretion in vitro. *Mol Endocrinol* 26: 1757–1772.
- Sirtori CR, Bolme P, Azarnoff DL (1972). Metabolic responses to acute and chronic L-dopa administration in patients with parkinsonism. *N Engl J Med* 287: 729–733.
- Smith GP, Jerome C, Cushin BJ, Eterno R, Simansky KJ (1981). Abdominal vagotomy blocks the satiety effect of cholecystokinin in the rat. *Science* 213: 1036–1037.
- Smith GP, Jerome C, Norgren R (1985). Afferent axons in abdominal vagus mediate satiety effect of cholecystokinin in rats. *Am J Physiol* 249: R638–641.
- Sun Q, Spiegelman D, van Dam RM, Holmes MD, Malik VS, Willett WC *et al.* (2010). White rice, brown rice, and risk of type 2 diabetes in US men and women. *Arch Intern Med* 170: 961–969.
- Tanaka T, Masuzaki H, Yasue S, Ebihara K, Shiuchi T, Ishii T *et al.* (2007). Central melanocortin signaling restores skeletal muscle AMP-activated protein kinase phosphorylation in mice fed a high-fat diet. *Cell Metab* 5: 395–402.
- Vallone D, Picetti R, Borrelli E (2000). Structure and function of dopamine receptors. *Neurosci Biobehav Rev* 24: 125–132.

Vucetic Z, Carlin JL, Totoki K, Reyes TM (2012). Epigenetic dysregulation of the dopamine system in diet-induced obesity. *J Neurochem* 120: 891–898.

Walker JN, Ramracheya R, Zhang Q, Johnson PR, Braun M, Rorsman P (2011). Regulation of glucagon secretion by glucose: paracrine, intrinsic or both? *Diabetes Obes Metab* 13 (Suppl. 1): 95–105.

Wei FY, Nagashima K, Ohshima T, Saheki Y, Lu YF, Matsushita M *et al.* (2005). Cdk5-dependent regulation of glucose-stimulated insulin secretion. *Nat Med* 11: 1104–1108.

Yada T, Itoh K, Nakata M (1993). Glucagon-like peptide-1-(7–36) amide and a rise in cyclic adenosine 3',5'-monophosphate increase

cytosolic free Ca²⁺ in rat pancreatic beta-cells by enhancing Ca²⁺ channel activity. *Endocrinology* 133: 1685–1692.

Zhang JH, Chung TDY, Oldenburg KR (1999). A simple statistical parameter for use in evaluation and validation of high throughput screening assays. *J Biomol Screen* 4: 67–73.

Zmuda EJ, Powell CA, Hai T (2011). A method for murine islet isolation and subcapsular kidney transplantation. *J Vis Exp* 50: e2096.

γ -Oryzanol Protects Pancreatic β -Cells Against Endoplasmic Reticulum Stress in Male Mice

Chisayo Kozuka, Sumito Sunagawa, Rei Ueda, Moritake Higa, Hideaki Tanaka, Chigusa Shimizu-Okabe, Shogo Ishiuchi, Chitoshi Takayama, Masayuki Matsushita, Masato Tsutsui, Jun-ichi Miyazaki, Seiichi Oyadomari, Michio Shimabukuro, and Hiroaki Masuzaki

Division of Endocrinology, Diabetes and Metabolism, Hematology, Rheumatology (Second Department of Internal Medicine) (C.K., S.S., R.U., M.H., H.T., M.S., H.M.), Graduate School of Medicine, University of the Ryukyus, Okinawa 903-0215, Japan; The Diabetes and Life-Style Related Disease Center (M.H.), Tomishiro Central Hospital, Okinawa 901-0243, Japan; Tanaka Clinic (H.T.), Okinawa 901-0244, Japan; Department of Molecular Anatomy (C.S.-O., C.T.), Graduate School of Medicine, University of the Ryukyus, Okinawa 903-0215, Japan; Department of Neurosurgery (S.I.), Graduate School of Medicine, University of the Ryukyus, Okinawa 903-0215, Japan; Department of Molecular and Cellular Physiology (M.M.), Graduate School of Medicine, University of the Ryukyus, Okinawa 903-0215, Japan; Department of Pharmacology (M.T.), Graduate School of Medicine, University of the Ryukyus, Okinawa 903-0215, Japan; Division of Stem Cell Regulation Research (J.-i.M.), Osaka University Graduate School of Medicine, Osaka 565-0871, Japan; Institute for Genome Research (S.O.), University of Tokushima, Tokushima 770-8506, Japan; and Department of Cardio-Diabetes Medicine (M.S.), University of Tokushima Graduate School of Health Biosciences, Tokushima 770-8503, Japan

Endoplasmic reticulum (ER) stress is profoundly involved in dysfunction of β -cells under high-fat diet and hyperglycemia. Our recent study in mice showed that γ -oryzanol, a unique component of brown rice, acts as a chemical chaperone in the hypothalamus and improves feeding behavior and diet-induced dysmetabolism. However, the entire mechanism whereby γ -oryzanol improves glucose metabolism throughout the body still remains unclear. In this context, we tested whether γ -oryzanol reduces ER stress and improves function and survival of pancreatic β -cells using murine β -cell line MIN6. In MIN6 cells with augmented ER stress by tunicamycin, γ -oryzanol decreased exaggerated expression of ER stress-related genes and phosphorylation of eukaryotic initiation factor-2 α , resulting in restoration of glucose-stimulated insulin secretion and prevention of apoptosis. In islets from high-fat diet-fed diabetic mice, oral administration of γ -oryzanol improved glucose-stimulated insulin secretion on following reduction of exaggerated ER stress and apoptosis. Furthermore, we examined the impact of γ -oryzanol on low-dose streptozotocin-induced diabetic mice, where exaggerated ER stress and resultant apoptosis in β -cells were observed. Also in this model, γ -oryzanol attenuated mRNA level of genes involved in ER stress and apoptotic signaling in islets, leading to amelioration of glucose dysmetabolism. Taken together, our findings demonstrate that γ -oryzanol directly ameliorates ER stress-induced β -cell dysfunction and subsequent apoptosis, highlighting usefulness of γ -oryzanol for the treatment of diabetes mellitus. (*Endocrinology* 156: 1242–1250, 2015)

ISSN Print 0013-7227 ISSN Online 1945-7170

Printed in U.S.A.

Copyright © 2015 by the Endocrine Society

Received September 9, 2014. Accepted January 9, 2015.

First Published Online January 16, 2015

Abbreviations: *Bcl2*, B cell leukemia/lymphoma 2; CAD, caspase-activated DNase; *Casp3*, caspase-3; *Cdkn1a*, cyclin-dependent kinase inhibitor 1A; Chop, CCAAT/enhancer-binding protein-homologous protein; eIF2 α , eukaryotic initiation factor-2 α ; ER, endoplasmic reticulum; ERdj4, ER resident DNAJ 4; GLP-1, glucagon-like peptide-1; GSIS, glucose-stimulated insulin secretion; HFD, high-fat diet; IHC, immunohistochemical; 4-PBA, 4-phenylbutyrate; PCNA, proliferating cell nuclear antigen; PI, propidium iodide; PKA, protein kinase A; *Rn18s*, 18S rRNA; STZ, streptozotocin; *Xbp1s*, spliced form of X box binding protein 1.

γ -Oryzanol is a unique bioactive substance exclusively and abundantly found in brown rice (1), comprising of a mixture of ferulic acid esters with phytosterols or triterpene alcohols (2). We recently reported that γ -oryzanol decreases endoplasmic reticulum (ER) stress in hypothalamus and attenuates the preference for dietary fat, thereby ameliorating high-fat diet (HFD)-induced obesity in mice (3). In accordance with this finding, our recent clinical studies highlight metabolically beneficial impact of brown rice on prediabetic obese humans (4). However, the entire mechanism whereby brown rice prevents type 2 diabetes still remains obscure.

In subjects with type 2 diabetes, exaggerated ER stress in pancreatic islets is linked to progressive β -cell dysfunction and resultant apoptosis (5). Recent studies clarified the importance of IL-1 β and nucleotide-binding oligomerization domain like receptor family, pyrin domain-containing 3 inflammasome in ER stress-induced apoptosis in β -cell (6, 7). In response to unfolded proteins, 3 kinds of ER transmembrane proteins, including protein kinase R-like ER kinase, activating transcription factor-6, and inositol-requiring enzyme-1, are initially activated (8). Besides inositol-requiring enzyme-1 α , protein kinase R-like ER kinase/eukaryotic initiation factor-2 α (eIF2 α) signaling strongly augments active form of IL-1 β via activation of nucleotide-binding oligomerization domain like receptor family, pyrin domain-containing 3 inflammasome, and expression level of *Il1b*, leading to apoptosis (7). Of note, an antidiabetic incretin hormone, glucagon-like peptide-1 (GLP-1) protects β -cells against ER stress-induced apoptosis via the cAMP/protein kinase A (PKA) pathway (9). These findings led us to hypothesize that γ -oryzanol would protect β -cells against ER stress-induced apoptosis. Notably, exendin-4, a long-acting GLP-1 agonist, also ameliorates glucose intolerance in diabetic rats via the proliferation of β -cells (10). In this context, using murine pancreatic β -cell line MIN6 (11) as well as HFD- or streptozotocin (STZ)-induced diabetic murine models, we tested whether γ -oryzanol would improve dysfunction of pancreatic islets through reduction of ER stress and enhancement of β -cell proliferation.

Materials and Methods

Animals

Eight-week-old male C57BL/6J mice obtained from Charles River Laboratories Japan, Inc were housed at 24°C under a 12-hour light, 12-hour dark cycle. The mice were allowed free access to food and water. Body weights were measured weekly. All animal experiments were approved by the Animal Experiment Ethics Committee of the University of the Ryukyus (No. 5352, 5718).

Administration of γ -oryzanol

γ -Oryzanol (Wako Pure Chemical Industries, Ltd) was orally administered as described (3). Briefly, γ -oryzanol was dissolved in 0.5% methyl cellulose solution. γ -oryzanol (20, 80, or 320 μ g/g body weight) was delivered into the stomach by a gavage needle every day during feeding with a HFD (Western Diet; Research Diets, Inc) for 13 weeks. For immunohistochemical (IHC) analyses, mice were treated for 6 months. The doses of γ -oryzanol used were as described (3).

Metabolic parameters

Blood samples were taken from the retro-orbital venous plexuses. Plasma insulin and proinsulin levels were measured using ELISA kits (Shibayagi Co, Ltd and Morinaga Institute of Biological Science, Inc). For oral glucose tolerance tests, the mice were orally administered with 2.0 g/kg body weight glucose after an 18-hour fast. Blood glucose levels were measured at the indicated times.

Treatment of STZ

To create a model of augmented ER stress in pancreatic β -cells (12, 13), mice were single injected with low-dose STZ (100 μ g/g body weight ip; Sigma-Aldrich) after 4 hours of fasting. γ -Oryzanol (320 μ g/g body weight⁻¹ d⁻¹) was orally administered daily for 14 days 1 day before the treatment of STZ.

Assessment of tissue distribution of γ -oryzanol

At 1 hour after the single oral administration of γ -oryzanol (3.2 mg/g body weight), tissues were sampled, and their total lipids were extracted according to the procedure of Folch and Lebaron (14). Tissue contents of γ -oryzanol were quantified by HPLC (LC-20AT, SPD-20AV; Shimadzu) with UV detection at 315 nm using XBridge C18 column (particle size 5 μ m; Waters).

Isolation of pancreatic islets and assessment of insulin secretion

Pancreatic islets were isolated from mice by collagenase digestion (Liberase TL; Roche Diagnostics GmbH) and purified on a Histopaque gradient (Histopaque 1077; Sigma-Aldrich) as described (15). Amount of insulin secretion from MIN6 cells, a representative murine pancreatic β -cell line (11), were seeded at a density of 2.0×10^5 cells/mL on 24-well plates. After 48 hours of culture, the cells were incubated with Krebs-Ringer bicarbonate buffer containing 2.5mM glucose for 2 hours, subsequently incubated in Krebs-Ringer bicarbonate buffer with or without γ -oryzanol (0.2, 2, or 10 μ g/mL) for 1 hour. Insulin secretion was normalized by cellular protein content.

Assessment of cell viability and apoptosis

MIN6 cells were treated with tunicamycin and γ -oryzanol for 24 hours. Cell viability was evaluated by a colorimetric procedure with Cell Count Reagent SF (Nacalai Tesque, Inc). To assess the extent of apoptosis, cells were stained with Hoechst 33342 and propidium iodide (PI). Morphological changes of the nuclei were observed under a fluorescence microscope. Caspase-3 activity was determined by Caspase-Glo 3/7 Assay (Promega) at 24 hours after the treatment.

Luciferase reporter assay

The potential chaperone activity of ferulic acid was investigated as described (3).

Western blotting

Western blotting was performed as described (16) with antibodies against eIF2 α and phospho-eIF2 α (9722 and 9721; Cell Signaling Technology) (17) (see Table 1). Protein extracted from MIN6 cells treated with or without tunicamycin were used as positive or negative control, respectively.

Quantitative real-time PCR

Total RNA was extracted using TRIzol reagent (Invitrogen) and cDNA was synthesized using an iScript cDNA Synthesis kit (Bio-Rad). Quantitative real-time PCR was performed using a StepOnePlus Real-Time PCR System, Fast SYBR Green Master Mix and TaqMan Fast Advanced Master Mix (Applied Biosystems). The mRNA levels were normalized by 18S rRNA (*Rn18s*). Primers used were summarized in Supplemental Table 1.

IHC analyses

The dissected pancreas was fixed in 4% paraformaldehyde, embedded in paraffin, and sectioned. The sections were immunostained for insulin (N1542; Dako Japan), phospho-eIF2 α , cleaved caspase-3 (9661; Cell Signaling Technology), and proliferating cell nuclear antigen (PCNA) (13110; Cell Signaling Technology) (18) (see Table 1). The ratios of insulin-positive and cleaved caspase-3-positive area to the total islet area were calculated based on more than 65 islets per group using Photoshop (Adobe).

Statistical analysis

Data are expressed as the mean \pm SEM. One-way ANOVA, repeated-measures ANOVA, and repeated-measures ANOVA followed by multiple comparison tests (Bonferroni/Dunn method) were used where applicable. Student's *t* test was used to analyze the differences between 2 groups. Differences were considered significant at $P < .05$.

Results

Tissue distribution of γ -oryzanol after oral administration in mice

Based on a previous report showing that orally administered γ -oryzanol was rapidly absorbed from the

intestine and reached a maximum plasma concentration in less than or equal to 1 hour (2), tissue contents of γ -oryzanol were assessed at 1 hour after single oral administration of γ -oryzanol (3.2 mg/g body weight). As reported (2), γ -oryzanol was distributed dominantly in the brain, whereas γ -oryzanol was also accumulated considerably in pancreas comparable with kidney and adipose tissue (Figure 1A). On the other hand, little accumulation of γ -oryzanol was observed in liver (Figure 1A). Considering that metabolites of γ -oryzanol were distributed mainly in liver (2), it is likely that γ -oryzanol is metabolized by liver.

γ -Oryzanol ameliorates ER stress-induced β -cell dysfunction both in vitro and in vivo

To examine the possible effect of γ -oryzanol on ER stress in β -cells, we assessed the expression levels of ER stress-responsive genes, including *Ddit3* (CCAAT/enhancer-binding protein-homologous protein [Chop]), *Dnajb9* (ER resident DNAJ 4 [ERdj4]), and spliced form of X box binding protein 1 (*Xbp1s*). In islets, mRNAs of ER stress-responsive genes were substantially increased after 13 weeks of HFD feeding (Figure 1B). Noticeably, oral administration of γ -oryzanol significantly decreased the expression levels of ER stress-responsive genes in islets from HFD-fed mice (Figure 1B). Also in MIN6 cells, increment of expression of these genes induced by tunicamycin was reversed by the supplementation of γ -oryzanol (Figure 1C). Similarly, phosphorylation of eIF2 α in response to ER stress was markedly reduced by γ -oryzanol in pancreatic β -cells both in vivo (Figure 1D) and in vitro (Figure 1E). γ -Oryzanol also decreased mRNA level of *Il1b* in islets from HFD-fed mice and tunicamycin-treated MIN6 cells (Figure 1, B and C). As reported (19), glucose-stimulated insulin secretion (GSIS) was significantly decreased in MIN6 cells treated with tunicamycin (Figure 1F). In contrast, both γ -oryzanol and 4-phenylbutyrate (4-PBA), a potent chemical chaperone, restored GSIS even in tunicamycin-treated cells (Figure 1F).

In addition, to explore whether ferulic acid, a partial structure of γ -oryzanol, would also decrease ER stress, we examined its possible effect on the activities of reporter

Table 1. Antibodies Used for Western Blots and IHC Analyses

Peptide/ Protein Target	Antigen Sequence (If Known)	Name of Antibody	Manufacturer, Catalog Number, and/or Name of Individual Providing the Antibody	Species Raised in; Monoclonal or Polyclonal	Dilution Used
Insulin		Guinea pig antiinsulin	Dako Japan, N1542	Guinea pig polyclonal	1:3 (IHC)
eIF2 α		eIF2 α Antibody	Cell Signaling Technology, 9722	Rabbit polyclonal	1:500 (WB)
Phospho-eIF2 α (Ser51)		Phospho-eIF2 α (Ser51) antibody	Cell Signaling Technology, 9721	Rabbit polyclonal	1:500 (WB), 1:500 (IHC)
Cleaved caspase-3		Cleaved caspase-3 (Asp175) antibody	Cell Signaling Technology, 9661	Rabbit polyclonal	1:1000 (IHC)
PCNA		PCNA (D ³ H8P) XP rabbit mAb	Cell Signaling Technology, 13110	Rabbit monoclonal	1:200 (IHC)

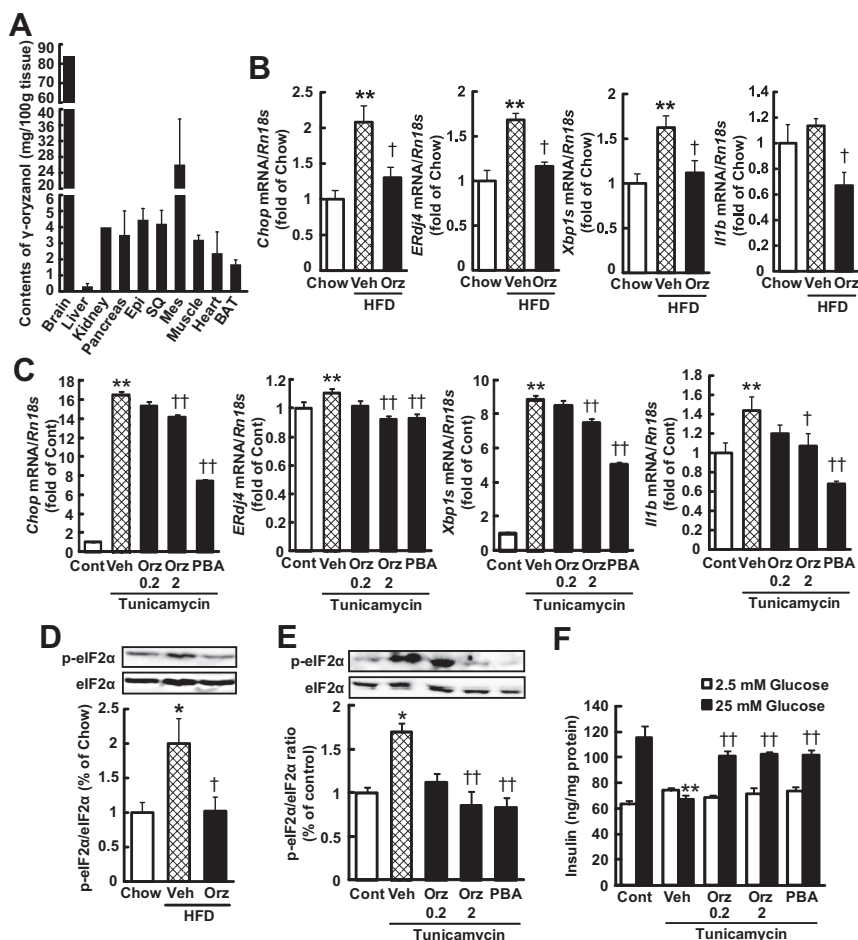


Figure 1. γ -Oryzanol (Orz) ameliorates ER stress-induced β -cell dysfunction. A, Tissue contents of Orz (mg/100 g tissue) were examined at 1 hour after single oral administration of Orz (3.2 mg/g body weight) in C57BL/6J mice ($n = 10$ – 70 ; 3 independent experiments). Epi, epididymal fat; SQ, sc fat; Mes, mesenteric fat; BAT, brown adipose tissue. HFD-fed mice were treated with Orz (320 μ g/g body weight $^{-1}$ d $^{-1}$) for 13 weeks, and pancreatic islets were isolated. MIN6 cells were treated with tunicamycin (0.5 μ g/mL) and Orz (0.2 or 2 μ g/mL) or 4-PBA (PBA) (5mM) for 24 hours. B and C, Expression levels of ER stress-responsive genes such as *Chop*, *ERdj4*, *Xbp1s*, and *Irf1b* in pancreatic islets from HFD-fed mice (B) ($n = 6$) and tunicamycin-treated MIN6 cells (C) ($n = 10$). The levels were determined by real-time PCR and normalized by those of *Rn18s*. D and E, Phosphorylation (Ser51) of eIF2 α (p-eIF2 α) in pancreatic islets from HFD-fed mice (D) and tunicamycin-treated MIN6 cells (E) ($n = 6$). F, Effects of Orz on GSIS in tunicamycin-treated MIN6 cells. Data are expressed as mean \pm SEM. *, $P < .05$; **, $P < .01$, vs chow-fed mice or control cells (Cont); †, $P < .05$; ††, $P < .01$, vs vehicle-treated HFD-fed mice or cells treated with tunicamycin and vehicle (Veh).

genes carrying ER stress-responsive *cis*-acting elements such as ER stress-responsive elements and unfolded protein response element upstream of the luciferase gene. Consequently, ferulic acid did not suppress the tunicamycin-induced activation of the *cis*-acting elements in luciferase reporter assays in human embryonic kidney 293 cells (Supplemental Figure 1), suggesting the importance of full-structure of γ -oryzanol as a chemical chaperone.

γ -Oryzanol ameliorates ER stress-induced apoptosis in β -cells

To further investigate whether γ -oryzanol prevents ER stress-induced apoptosis in β -cells, MIN6 cells were stained

with Hoechst 33342 and PI. Although the number of apoptotic cells (PI-negative cells with chromatin condensation) was increased by replenishing tunicamycin, γ -oryzanol ameliorated the ER stress-induced apoptosis in tunicamycin-treated MIN6 cells (Figure 2, A and B). γ -Oryzanol also reduced the caspase-3 activity in tunicamycin-treated MIN6 cells (Figure 2C). To explore antiapoptotic potential of γ -oryzanol in vivo, expression levels of apoptosis-related genes, including caspase-3 (*Casp3*), B cell leukemia/lymphoma 2 (*Bcl2*), and *Dffb* (caspase-activated DNase [CAD]), were examined. In islets from HFD-fed mice, mRNA levels of apoptosis-related genes were substantially decreased by the treatment with γ -oryzanol (Figure 2D). Observed changes in mRNA levels were reproduced in tunicamycin-treated MIN6 cells (Supplemental Figure 2). IHC analyses also showed that positive cells for phospho-eIF2 α (ER stress marker), cleaved caspase-3 (apoptosis marker), or PCNA (proliferative marker) were increased in HFD-fed mice, whereas the changes were restored by the treatment of γ -oryzanol (Figure 2, E and H). The quantification of cleaved caspase-3-positive area to total islet area as well as cleaved caspase-3-positive β -cell area to total β -cell area further reinforced the notion above (Figure 2, G and I). Moreover, γ -oryzanol augmented the intensity of insulin staining and increased the ratio of insulin-positive area to total islet area in mice on a HFD (Figure 2, E and F). In HFD-fed mice, γ -oryzanol dose dependently lowered plasma insulin level (vehicle, 511 ± 73 pg/mL; γ -oryzanol 20 μ g/g body weight $^{-1}$ d $^{-1}$, 358 ± 58 pg/mL; γ -oryzanol 80 μ g/g body weight $^{-1}$ d $^{-1}$, 351 ± 100 pg/mL; and γ -oryzanol 320 μ g/g body weight $^{-1}$ d $^{-1}$, 262 ± 34 pg/mL, 18-h fasting) and the proinsulin/insulin ratio, a marker of β -cell function (20) (Figure 2J), further supporting the notion that γ -oryzanol protects β -cells against ER stress in vivo.

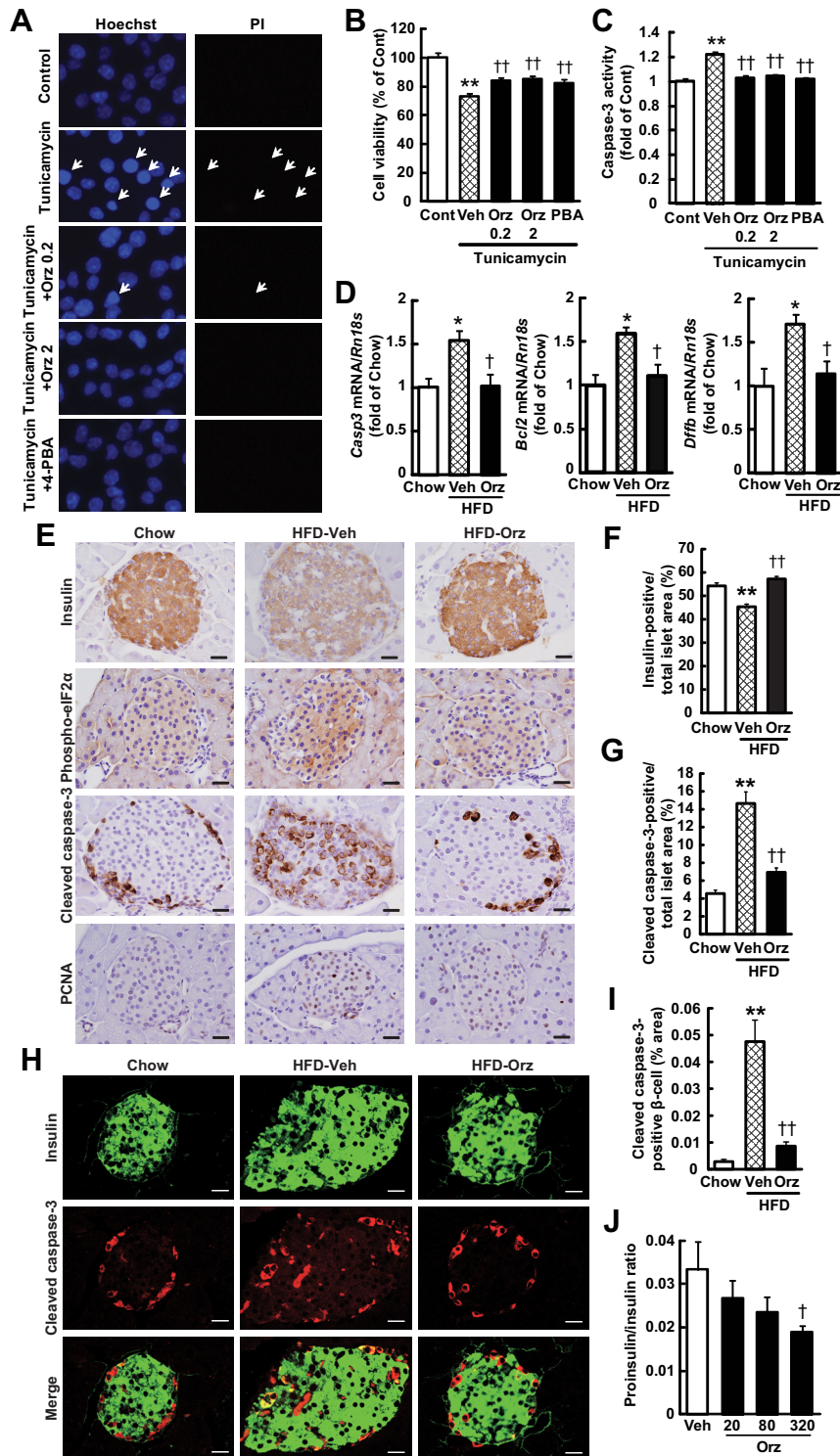


Figure 2. γ -Oryzanol (Orz) ameliorates ER stress-induced β -cell apoptosis. A–C, Effects of Orz (0.2 or 2 μ g/mL) or 4-PBA (PBA) (5mM) on apoptotic nuclear morphological changes visualized by staining with Hoechst 33342 and PI (A), viability (B), and caspase-3 activity (C) in tunicamycin-treated MIN6 cells (n = 8–10). D, Expression levels of mRNA for *Casp3*, *Bcl2*, and *CAD (Dffb)* in pancreatic islets from Orz-treated HFD-fed mice (320 μ g/g body weight⁻¹ d⁻¹; n = 6). E, IHC analyses of isolated pancreatic islets from HFD-fed mice treated with Orz (320 μ g/body weight⁻¹ d⁻¹). Serial paraffin-embedded sections were stained with antiinsulin, antiphospho-eIF2 α , anticlaved caspase-3, and anti-PCNA antibodies. Scale bar, 20 μ m; magnification, \times 400. F and G, The ratios of insulin-positive area (F) and cleaved caspase-3-positive area (G) to the total islet area were calculated (n = 3; 108–144 islets). Data are expressed as mean \pm SEM. **, P < .01, vs chow-fed mice; ††, P < .01, vs HFD-fed mice treated with vehicle (Veh). H, Paraffin-embedded pancreatic sections were costained with antiinsulin (green) and anticlaved caspase-3 (red) antibodies. Scale bar, 20 μ m; magnification, \times 600. I, The ratio of cleaved caspase-3-positive β -cell area to total β -cell area was calculated (n = 3; 108–118 islets). J, Proinsulin/insulin ratio in Orz-treated HFD-fed mice (20, 80, or 320 μ g/g body weight⁻¹ d⁻¹; n = 6). Data are expressed as mean \pm SEM. *, P < .05; **, P < .01, vs chow-fed mice or control cells (Cont); †, P < .05; ††, P < .01, vs vehicle-treated HFD-fed mice or cells treated with tunicamycin and vehicle (Veh).

γ -Oryzanol ameliorates β -cell dysfunction and apoptosis in STZ-treated mice

To endorse the protective effects of γ -oryzanol on β -cell in vivo, we administrated γ -oryzanol orally to low-dose

STZ-induced diabetic mice. Treatment of low-dose STZ induces the partial destruction of pancreatic β -cell and insulinopenia (12), leading to exaggerated ER stress in β -cell by increased demand of insulin (21). In low-dose

STZ-treated mice, fasting plasma insulin level was significantly decreased (Figure 3A), resulting in the elevation of fasting blood glucose levels (Figure 3B). In this model, γ -oryzanol significantly ameliorated glucose dysmetabolism (Figure 3, A–C) and augmented considerably plasma insulin levels (Figure 3A). IHC analyses by antibody against insulin revealed that insulin-positive β -cell area was considerably decreased in islets of STZ-treated mice, whereas the decrement was restored by γ -oryzanol (Figure 3, D and E). In islets of STZ-treated mice, intensity of phospho-eIF2 α and cleaved caspase-3-positive cells were also increased, indicating that ER stress and resultant apoptosis were augmented by the treatment of STZ (Figure 3, D and G). The cleaved caspase-3-positive area to total β -cell area as well as cleaved caspase-3-positive β -cell area to total β -cell area further reinforced the notion above (Figure 3, F and H). Of note, phospho-eIF2 α , cleaved caspase-3, and PCNA were colocalized in β -cells (Supplemental Figure 3). In this experimental setting, γ -oryzanol increased insulin-positive area and decreased the intensities of phospho-eIF2 α and cleaved caspase-3-positive area in islets (Figure 3, D–H), whereas γ -oryzanol did not increase PCNA-positive proliferating cells (Figure 3D). Expression levels of genes involved in ER stress signaling and apoptosis were significantly decreased by γ -oryzanol in islets from STZ-treated mice (Figure 3I).

γ -Oryzanol has no effect on gene expression related to β -cell survival and proliferation in HFD- or STZ-induced diabetic mice

To explore the potential of γ -oryzanol on β -cell survival and proliferation, we assessed the expression levels

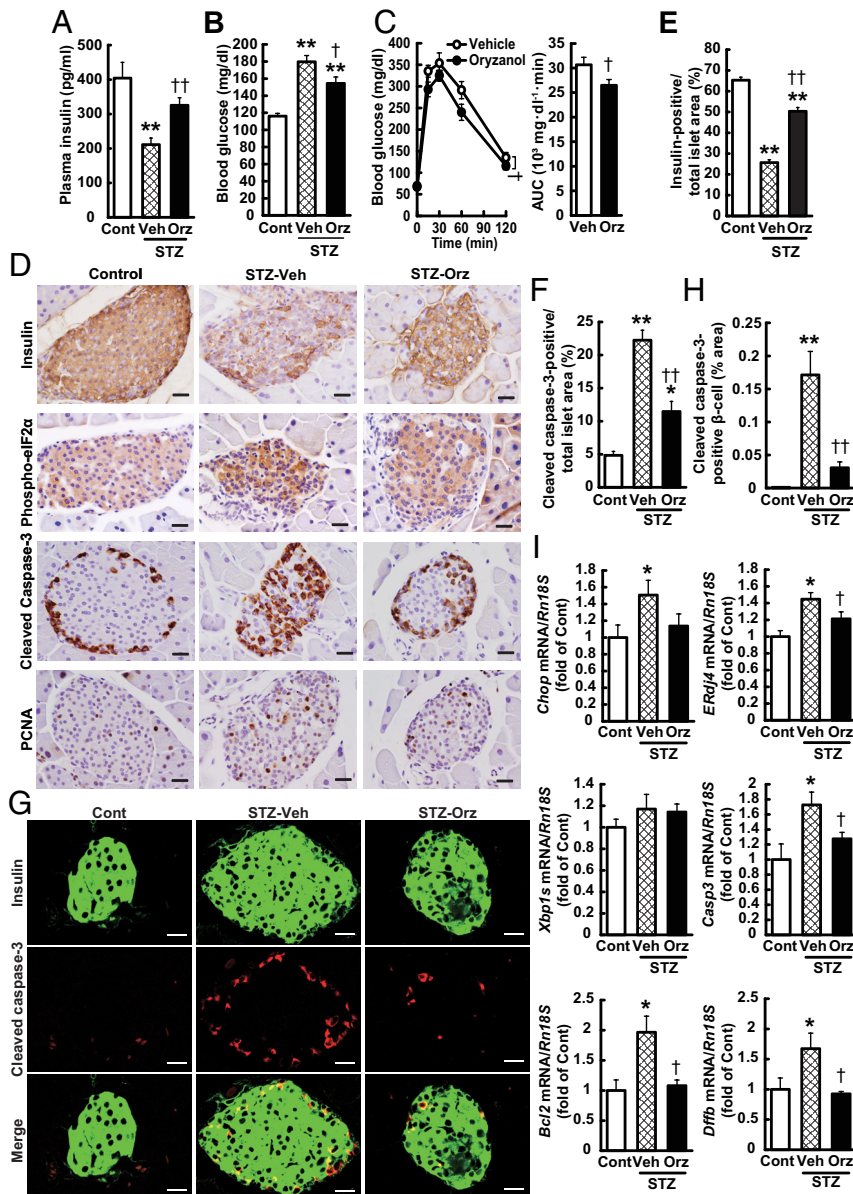


Figure 3. γ -Oryzanol ameliorates β -cell dysfunction and apoptosis in STZ-treated mice. A–C, Effects of γ -oryzanol (320 μ g/g body weight⁻¹ d⁻¹) on plasma insulin levels (A) ($n = 7$) and blood glucose levels (B) ($n = 7$) after a 4-h fasting were measured at 2 weeks after the STZ treatment. Blood glucose levels and the AUC of blood glucose during the oral glucose tolerance test (C) ($n = 7$). D, IHC analyses of pancreatic islets from STZ-treated mice treated with γ -oryzanol. Serial paraffin-embedded sections were stained with antiinsulin, antiphospho-eIF2 α , cleaved caspase-3, PCNA antibodies. Scale bar, 20 μ m; magnification, $\times 400$. E and F, The ratios of insulin-positive area (E) and cleaved caspase-3-positive area (F) to the total islet area were calculated ($n = 2$; 84–111 islets). G, Paraffin-embedded pancreatic sections were costained with antiinsulin (green) and anticlaved caspase-3 (red) antibodies. Scale bar, 20 μ m; magnification, $\times 600$. (H) The ratio of cleaved caspase-3-positive β -cell area to total β -cell area was calculated ($n = 2$; 66–116 islets). (I) Expression levels of mRNA for *Chop*, *ERdj4*, *Xbp1s*, *Casp3*, *Bcl2*, and *Dffb* (CAD) in pancreatic islets from STZ-treated mice ($n = 5$). The mRNA levels were determined by real-time PCR and normalized by those of *Rn18s*. Data are expressed as mean \pm SEM. *, $P < .05$; **, $P < .01$, vs chow-fed or control (Cont) mice; †, $P < .05$; ††, $P < .01$, vs STZ mice treated with vehicle (Veh).

of genes related to β -cell survival and proliferation, including *pancreatic and duodenal homeobox 1*, *v-maf musculoaponeurotic fibrosarcoma oncogene family, protein A*, *neurogenin 3*, *Ins1*, *Ins2*, and *cyclin-dependent kinase inhibitor 1A* (22) in islets from HFD-fed mice and STZ-treated diabetic mice. In HFD-fed mice, mRNA levels of these genes showed a trend to increase, whereas the trend was cancelled by γ -oryzanol (Figure 4A). Also in STZ-treated mice, γ -oryzanol did not increase the expression levels of these genes (Figure 4B). In tunicamycin-treated MIN6 cells, there was no change in mRNA levels of these genes (Supplemental Figure 4).

Discussion

In the present study, we demonstrated that γ -oryzanol ameliorated ER stress-induced β -cell apoptosis and glucose intolerance in both HFD-fed mice and STZ-treated mice (Figures 1–3 and Supplemental Figure 3). Also in MIN6 cells, tunicamycin-induced ER stress and after apoptosis were restored by γ -oryzanol (Figures 1 and 2 and Supplemental Figure 2). On the other hand, γ -oryzanol did not show apparent effects on β -cell survival and proliferation both in vivo and in vitro (Figure 4 and Supplemental Figure 4), suggesting that γ -oryzanol ameliorates β -cell function mainly via reduction of ER stress-induced

apoptosis. ER stress plays a critical role in regulating function of β -cells and in the pathophysiology of type 2 diabetes (5, 23). Excess free fatty acid, chronic inflammation, and hyperglycaemia are known to provoke ER stress in β -cells, leading to suppression of insulin biosynthesis, impaired GSIS, and resultant apoptosis (23). Even without apparent reduction of β -cell mass, isolated pancreatic islets from HFD-fed mice showed a pronounced aggravation of GSIS (24). We recently demonstrated that γ -oryzanol acts as a chemical chaperone in primary murine neuronal cells (3). In the present study, we demonstrated that γ -oryzanol reduced ER stress also in pancreatic β -cells, thereby improving GSIS and preventing apoptosis from β -cells both in vivo and in vitro (Figures 1–3 and Supplemental Figures 2 and 3). These data suggest that γ -oryzanol has therapeutic potential for the prevention and treatment of type 2 diabetes. Importantly, ferulic acid, a partial structure of γ -oryzanol, did not exhibit the chaperone activity in luciferase reporter assays (Supplemental Figure 1). These findings reinforce the significance of full structure of γ -oryzanol in its variety of biological actions.

A series of previous studies showed that elevation of intracellular cAMP by GLP-1, forskolin, and 3-isobutyl-1-methyl xanthine prevent β -cells from apoptosis (9, 25, 26). For example, β -cell apoptosis induced by palmitate, a potent inducer of ER stress, is rescued by GLP-1 through

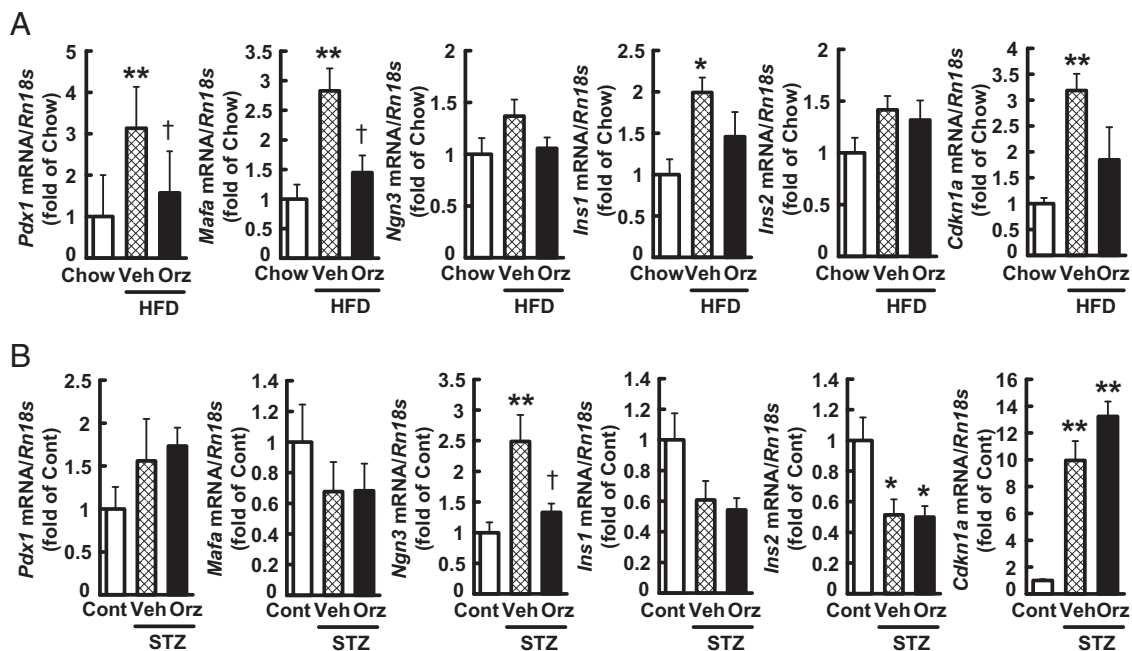


Figure 4. Effect of γ -oryzanol on expression levels of genes related to β -cell survival and proliferation factors in diabetic mice. Expression levels of mRNA for pancreatic and duodenal homeobox 1 (*Pdx1*), v-maf musculoaponeurotic fibrosarcoma oncogene family, protein A (*Mafa*), neurogenin 3 (*Ngn3*), *Ins1*, *Ins2*, and cyclin-dependent kinase inhibitor 1A (*Cdkn1a*) in pancreatic islets from γ -oryzanol-treated HFD-fed (A) ($n = 6$) or STZ-treated mice (B) ($n = 5$). The mRNA levels were determined by real-time PCR and normalized by those of *Rn18s*. Data are expressed as mean \pm SEM. *, $P < .05$; **, $P < .01$, vs chow-fed or control (Cont) mice; †, $P < .05$; ††, $P < .01$, vs HFD-fed or STZ mice treated with vehicle (Veh).

activation of the cAMP/PKA pathway in rat β -cell line, RINm5F (9). On the other hand, via the decrease in intracellular cAMP level, dopamine provokes apoptosis in various types of neuronal and lactotrope cells (27, 28). We recently found that γ -oryzanol enhances GSIS through activation of the cAMP/PKA pathway by suppression of dopamine D2 receptor signaling (C. Kozuka, S. Sunagawa, R. Ueda, M. Higa, Y. Ohshiro, H. Tanaka, C. Shimizu-Okabe, C. Takayama, M. Matsushita, M. Tsutsui, S. Ishiuchi, M. Nakata, T. Yada, J. Miyazaki, S. Oyadomari, M. Shimabukuro, and H. Masuzaki, unpublished data). To our knowledge, the present study is the first demonstration that γ -oryzanol directly improves the survival and function of murine pancreatic islets in a similar manner to GLP-1. Experiments to explore the potential target molecule for γ -oryzanol are underway in our laboratory.

The present study unveiled the enigma on the molecular mechanism whereby γ -oryzanol protects pancreatic islets in a diabetic status. Because the phenotype of ER stress-based genetic models of diabetes such as *Akita* mice is extremely severe (29, 30), we used HFD- and STZ-induced diabetic mice. We think it critical to assess the impact of γ -oryzanol on glucose metabolism in models relevant to life style-related human diseases. Our novel findings that γ -oryzanol acts as a potent ER stress eraser in pancreatic β -cells may open a fresh avenue for natural food-based approaches toward the prevention and treatment of type 2 diabetes in humans.

Acknowledgments

We thank M. Takaki (University of the Ryukyus) and J. Yamakawa, M. Okayasu, S. Okayasu (Okayasu shouten Co, Ltd, Saitama, Japan) for technical help. We also thank M. Hirata, I. Asato, and C. Noguchi (University of the Ryukyus) for assistance. C.K. is a Research Fellow of the Japan Society for the Promotion of Science.

Address all correspondence and requests for reprints to: Hiroaki Masuzaki, MD, PhD, Division of Endocrinology, Diabetes and Metabolism, Hematology, Rheumatology (Second Department of Internal Medicine), Graduate School of Medicine, University of the Ryukyus, 207 Uehara, Nishihara, Nakagami-gun, Okinawa 903-0215, Japan. E-mail: hiroaki@med.u-ryukyu.ac.jp.

This work was supported in part by Grants-in-Aid from Japan Society for the Promotion of Science (JSPS KAKENHI Grant Numbers 24591338 and 25·9668), Takeda Science Foundation (Specified Research Grant), Society for Woman's Health Science Research (13-A1-001), Leave a Nest grants, Metabolic Syndrome Foundation, Specified Project "Establishing a research hub toward the development of an intellectual cluster in Okinawa Prefecture" (2011–2014), and Council for Science Technology and Innovation, Cross-ministerial Strategic Innovation

Promotion Program, "Technologies for creating next-generation agriculture, forestry and fisheries."

Disclosure Summary: The authors have nothing to disclose.

References

1. Lerma-Garcia MJ, Herrero-Martinez JM, Simo-Alfonso EF, Mendonca CRB, Ramis-Ramos G. Composition, industrial processing and applications of rice bran γ -oryzanol. *Food Chem*. 2009;115(2):389–404.
2. Kozuka C, Yabiku K, Takayama C, Matsushita M, Shimabukuro M. Natural food science based novel approach toward prevention and treatment of obesity and type 2 diabetes: recent studies on brown rice and γ -oryzanol. *Obesity Research, Clinical Practice*. 2013;7(3):e165–e172.
3. Kozuka C, Yabiku K, Sunagawa S, et al. Brown rice and its component, γ -oryzanol, attenuate the preference for high-fat diet by decreasing hypothalamic endoplasmic reticulum stress in mice. *Diabetes*. 2012;61(12):3084–3093.
4. Shimabukuro M, Higa M, Kinjo R, et al. Effects of the brown rice diet on visceral obesity and endothelial function: the BRAVO study. *Br J Nutr*. 2014;111(2):310–320.
5. Cnop M, Foufelle F, Velloso LA. Endoplasmic reticulum stress, obesity and diabetes. *Trends Mol Med*. 2012;18(1):59–68.
6. Lerner AG, Upton JP, Praveen PV, et al. IRE1 α induces thioredoxin-interacting protein to activate the NLRP3 inflammasome and promote programmed cell death under irremediable ER stress. *Cell Metab*. 2012;16(2):250–264.
7. Osowski CM, Hara T, O'Sullivan-Murphy B, et al. Thioredoxin-interacting protein mediates ER stress-induced β cell death through initiation of the inflammasome. *Cell Metab*. 2012;16(2):265–273.
8. Mori K. Tripartite management of unfolded proteins in the endoplasmic reticulum. *Cell*. 2000;101(5):451–454.
9. Kwon G, Pappan KL, Marshall CA, Schaffer JE, McDaniel ML. cAMP dose-dependently prevents palmitate-induced apoptosis by both protein kinase A- and cAMP-guanine nucleotide exchange factor-dependent pathways in β -cells. *J Biol Chem*. 2004;279(10):8938–8945.
10. Xu G, Stoffers DA, Habener JF, Bonner-Weir S. Exendin-4 stimulates both β -cell replication and neogenesis, resulting in increased β -cell mass and improved glucose tolerance in diabetic rats. *Diabetes*. 1999;48(12):2270–2276.
11. Ishihara H, Asano T, Tsukuda K, et al. Pancreatic β cell line MIN6 exhibits characteristics of glucose metabolism and glucose-stimulated insulin secretion similar to those of normal islets. *Diabetologia*. 1993;36(11):1139–1145.
12. Kusakabe T, Tanioka H, Ebihara K, et al. Beneficial effects of leptin on glycaemic and lipid control in a mouse model of type 2 diabetes with increased adiposity induced by streptozotocin and a high-fat diet. *Diabetologia*. 2009;52(4):675–683.
13. Zhang R, Kim JS, Kang KA, Piao MJ, Kim KC, Hyun JW. Protective mechanism of KIOM-4 in streptozotocin-induced pancreatic β -cells damage is involved in the inhibition of endoplasmic reticulum stress. *Evid Based Complement Alternat Med*. 2011;2011:231938.
14. Folch J, Lebaron FN. The isolation from brain tissue of a trypsin-resistant protein fraction containing combined inositol, and its relation to neurokeratin. *J Neurochem*. 1956;1(2):101–108.
15. Zmuda EJ, Powell CA, Hai TA. Method for murine islet isolation and subcapsular kidney transplantation. *J Vis Exp*. 2011(50):e2096.
16. Tanaka T, Masuzaki H, Yasue S, et al. Central melanocortin signaling restores skeletal muscle AMP-activated protein kinase phosphorylation in mice fed a high-fat diet. *Cell Metab*. 2007;5(5):395–402.
17. Akerfeldt MC, Howes J, Chan JY, et al. Cytokine-induced β -cell death is independent of endoplasmic reticulum stress signaling. *Diabetes*. 2008;57(11):3034–3044.
18. Chakravarthy MV, Zhu Y, Wice MB, et al. Decreased fetal size is

- associated with β -cell hyperfunction in early life and failure with age. *Diabetes*. 2008;57(10):2698–2707.
19. Lee AH, Heidman K, Hotamisligil GS, Glimcher LH. Dual and opposing roles of the unfolded protein response regulated by IRE1 α and XBP1 in proinsulin processing and insulin secretion. *Proc Natl Acad Sci USA*. 2011;108(21):8885–8890.
 20. Bergman RN, Finegood DT, Kahn SE. The evolution of β -cell dysfunction and insulin resistance in type 2 diabetes. *Eur J Clin Invest*. 2002;32(suppl 3):35–45.
 21. Scheuner D, Kaufman RJ. The unfolded protein response: a pathway that links insulin demand with β -cell failure and diabetes. *Endocr Rev*. 2008;29(3):317–333.
 22. Jourdan T, Godlewski G, Cinar R, et al. Activation of the Nlrp3 inflammasome in infiltrating macrophages by endocannabinoids mediates β cell loss in type 2 diabetes. *Nat Med*. 2013;19(9):1132–1140.
 23. Volchuk A, Ron D. The endoplasmic reticulum stress response in the pancreatic β -cell. *Diabetes Obes Metab*. 2010;12(suppl 2):48–57.
 24. Peyot ML, Pepin E, Lamontagne J, et al. β -Cell failure in diet-induced obese mice stratified according to body weight gain: secretory dysfunction and altered islet lipid metabolism without steatosis or reduced β -cell mass. *Diabetes*. 2010;59(9):2178–2187.
 25. Li L, El-Kholy W, Rhodes CJ, Brubaker PL. Glucagon-like peptide-1 protects β cells from cytokine-induced apoptosis and necrosis: role of protein kinase B. *Diabetologia*. 2005;48(7):1339–1349.
 26. Jhala US, Canettieri G, Screaton RA, et al. cAMP promotes pancreatic β -cell survival via CREB-mediated induction of IRS2. *Genes Dev*. 2003;17(13):1575–1580.
 27. Radl DB, Ferraris J, Boti V, Seilicovich A, Sarkar DK, Pisera D. Dopamine-induced apoptosis of lactotropes is mediated by the short isoform of D2 receptor. *Plos One*. 2011;6(3):e18097.
 28. Bozzi Y, Borrelli E. Dopamine in neurotoxicity and neuroprotection: what do D2 receptors have to do with it? *Trends Neurosci*. 2006;29(3):167–174.
 29. Oyadomari S, Koizumi A, Takeda K, et al. Targeted disruption of the Chop gene delays endoplasmic reticulum stress-mediated diabetes. *J Clin Invest*. 2002;109(4):525–532.
 30. Yoshioka M, Kayo T, Ikeda T, Koizumi A. A novel locus, Mody4, distal to D7Mit189 on chromosome 7 determines early-onset NIDDM in nonobese C57BL/6 (Akita) mutant mice. *Diabetes*. 1997;46(5):887–894.

Review

カルシウム透過性AMPA型グルタミン酸受容体と神経膠芽腫
Ca²⁺-permeable AMPA -type glutamate receptors and glioblastomas

石内 勝吾

Shogo Ishiuchi

琉球大学大学院 医学研究科脳神経科教授

Professor and Chairman Department of Neurosurgery, University of the Ryukyus, Graduate school of Medicine

略 歴

1985年3月 群馬大学医学部医学科卒業
1999年1月 科学技術振興事業団「脳を知る」(CREST)研究員
1999年7月 群馬大学医学部脳神経外科助手
2002年9月 群馬大学医学部脳神経外科講師
2009年6月 琉球大学医学部脳神経外科教授
2011年1月 琉球大学医学部副医学部長
2012年8月 琉球大学医学部附属病院長特別補佐
2014年1月 琉球大学医学部附属病院長副病院長



そ の 他

時実利彦記念脳研究基金 1992年
第11回日本脳腫瘍学会「星野賞」受賞 2003年
第42回高松宮妃癌研究基金 2013年
President of the 3rd International Society of Radiation Neurobiology conference 2013年

Abstract

Glioblastoma cells release and exploit glutamate for proliferation and migration by autocrine or paracrine loops through Ca²⁺-permeable α -amino-3-hydroxy-5-methyl-4-isoxazolepropionate -type glutamate receptors (CP-AMPA). Here we show the molecular mechanism behind glioblastoma cells expressing CP-AMPA, and refer to its role for gliomagenesis.

Key words : calcium-permeable AMPA type glutamate receptor, glioblastoma, invasive growth behavior, gliomagenesis

はじめに

グルタミン酸は、ヒトの認知、知覚、記憶および学習など興奮性シナプス伝達に関与する重要な興奮性伝達物質である。一方、脳虚血、外傷、てんかん、神経変性・代謝疾患など中枢系の様々な疾患において、細胞外に過剰放出されたグルタミン酸は、興奮毒性という共通の現象を引き起こし病勢の根幹に関与することが古くから知られている。これらの現象の背景に重要な役割を果たすのがグルタミン酸受容体の中のイオンチャンネル型受容体(ionotropic glutamate receptor; iGluR)に分類されるNMDA(N-methyl-D-aspartic acid)型とAMPA(α -amino-3-hydroxy-5-methyl-4-isoxazolepropionate)型受容体である。NMDA型受容体を介するカルシウムの急速な細胞内流入が病態生理としてよく知られている一方でAMPA型グルタミン酸受容体は一般的に不透過型として理解されてきた。近年、カルシウム透過性(calcium permeable)AMPA(CP-AMPA)型受容体の存在が認識され、このチャンネルが多様な疾患の病態生理に重要な役割を果たす事が判明し注目されている。本稿では脳腫瘍ことに神経膠芽腫における役割について概説する。

グルタミン酸受容体

1) グルタミン酸受容体の分類

グルタミン酸受容体は、イオンチャンネル型受容体

(ionotropic glutamate receptor; iGluR)と代謝調節型受容体(metabotropic glutamate receptor; mGluR)の2種類に大別される。イオンチャンネル型受容体(iGluR)はさらにアゴニスト特異性により、NMDA型、AMPA型とカイニン酸型の3つのサブタイプに分類され、リガンドが同定されていないOrphan型もその分子構造の相同性からこの中に入る。AMPA型受容体はGluA1-4の4つのサブユニットから形成され、受容体はこれらのサブユニットの単独または様々な組み合わせからなる4量体で形成されている。カルシウム透過性という機能的観点からはGRIA2遺伝子にコードされるGluA2サブユニットの発現の有無が重要である。すなわち、GluA2発現の無い場合は、カルシウム透過性を示し、逆にGluA2が発現しているとカルシウム不透過性となる。GluA2の変異体はGluA2(Q)と呼ばれている。野生型または編集型GluA2はイオン透過性に関わる細胞膜のM2部(Q/R部位)がアルギニンで陽性に帯電しているため細胞外のカルシウムをほとんど通さないが、変異型または未編集型GluA2(Q)はグルタミンで中性であるために、陽イオンであるカルシウムとは反撥せずチャンネルは強いカルシウム透過性を示すことになる(Table. 1)。AMPA型受容体のチャンネルの透過性を考える上でGRIA1遺伝子にコードされるGluA1受容体の細胞膜へのtrafficking機構も重要である。これはcGMP-dependent kinase II(cGKII)依存性にGluA1のリン酸化が促進されることにより生じる。

Table. 1 The size of four AMPA receptor subunits including GluA1, GluA2, GluA3, and GluA4 are similar in approximate 900 amino acids, and they share high amino acid sequence identity. Importantly, receptor permeability for calcium is depend upon a transmembrane portion of the AMPA receptor GluA2 subunit called Q/Rsite. A glutamine residue (Q; CGA) in M2 is encoded in the genes for GluRA1, A3, and GluA4, however, GluA2 contains an arginine (R; CGG) at this position termed the Q/R site indicating by voxel in the figure. This codon change due to the adenosine (A)-to-guanosine (G) alteration is generated by site-directed nuclear RNA editing, and mature brain contained abundant edited form of GluA2, and the unedited immature GluA2, namely GluA2(Q) was present in fetal brain. A point mutagenesis at the Q/R site from guanosine (G)-to-adenosine (A) transformed GluA2(R) to GluA2(Q), which in contrast induces high calcium permeability.

Amino acid sequences of the M2 segments of AMPA receptor subunits.

GluA1 NE-FGIFNSLWFSLGAFMQQGC-DIS
 GluA2 NE-FGIFNSLWFSLGAFMRQGC-DIS
 GluA3 NE-FGIFNSLWFSLGAFMQQGC-DIS
 GluA4 NE-FGIFNSLWFSLGAFMQQGC-DIS

↑
 Q/R site

以上まとめると従来カルシウム透過性を示すイオン型グルタミン酸受容体はもっぱら NMDA 型受容体と考えられ AMPA 型受容体は不透過とされてきたがカルシウム透過性を示す CP-AMPA 型受容体の存在が近年確認された。その分子機構として 1)GRIA2 遺伝子のサイレンシングによる GluA2 発現が欠落した場合 2)mRNA 翻訳機構の異常から GluA2(Q)が発現する場合 3)GluA1 の細胞膜への trafficking が促進された場合の 3 型が認められる。CP-AMPA 型受容体と脳腫瘍ことに神経膠芽腫との関連について次項で述べてみたい。

2) 脳腫瘍細胞での発現様式とその機能

1990 年代から、新鮮な手術摘出腫瘍より準備された初代培養系においてグルタミン酸やカイニン酸の投与により電気生理学的応答や細胞内カルシウムの上昇の現象が捉えられ¹⁾、これらの応答は AMPA 型グルタミン酸受容体の拮抗薬 CNQX により抑制されるという知見が報告された。2001 年には神経細胞に豊富に認められる NMDA 受容体遺伝子サブユニット NR1、NR2A、NR2B、NR2C や AMPA 型受容体 GluA2 サブユニットは神経膠芽腫においては、神経細胞に比較して著しくその発現が低下しているという報告がなされた²⁾。2002 年に著者らは、手術にて摘出した腫瘍細胞の初代培養とその樹立株の解析から AMPA 型グルタミン酸受容体が神経膠芽腫に発現していることを報告した³⁾。解析した 16 例中 12 例症例で GluA2 の蛋白発現がないこと、またカルシウム測光による解析から腫瘍細胞は 100 μ M の AMPA agonist にて細胞内カルシウムの上昇を認め AMPA 型受容体拮抗薬 NBQX でこの反応が完全に遮断されることから機能的にカルシウム透過性であることを示した。また独自に樹立したヒトグリオーマ細胞を用いた in vitro および in vivo 疾患モデルにおいて、編集型 GluA2 の強制導入により腫瘍の移動性と増殖性が阻害され、逆に変異型 GluA2(Q)を強制発現させると遊走性の亢進と細胞死の抑制が認められたことより、このチャンネルを介するカルシウムの流入によって引き起こされる緩徐な細胞内カルシウムの上昇が腫瘍細胞の浸潤と増殖に関与していることをはじめて明らかにした (Fig. 1 & Fig. 2)。16 症例中 4 例、2 割の症例で mRNA レベルでの未編集型と編集型の共発現が見られた。このように神経膠腫細胞が発現する AMPA 型受容体は GluA2 サブユニットを欠くものと、GluA2 の変異型 GluA2(Q)を発現するもの⁴⁾とがありいずれもその受容体の機能はカルシウム透過型である。さらに摘出腫瘍から培養され樹立された培養株では GluA2 が消失し GluA1 の発現が有意となる。これは bFGF (basic fibroblast growth factor) や PDGF (platelet

derived growth factor) などの様々な environmental cue により GluA1 の trafficking が促進された事によると考えられている。

神経膠芽腫の浸潤性増殖に対する治療への応用

1) グルタミン酸 / カルシウム透過性 AMPA 型受容体 / Akt シグナリング

グリオーマに対する分子標的治療としては上皮増殖因子受容体 (EGFR)⁵⁾、血管内皮増殖因子 (VEGF)、血小板増殖因子受容体 (PDGFR)⁶⁾ などに対する拮抗薬や中和抗体が臨床応用されている⁷⁾。成長因子 (GF) を介するチロシンキナーゼの活性化は最終的には Akt のリン酸化を促進する^{8), 9), 10)}。分子標的剤は成長因子 (GF) を介するチロシンキナーゼの活性化を抑制することにより Akt の脱リン酸化を目指すものである。神経膠芽腫細胞に発現するカルシウム透過性 AMPA 型グルタミン酸受容体は、Akt のリン酸化に関与し glutamate-AMPA 受容体-Akt pathway を通じて新たな増殖と浸潤を促進する¹¹⁾。神経膠芽腫では、EGFR からのシグナルが phosphatidylinositol-3-OH kinase (PI3K) を活性化し phosphatidylinositol (4,5)-biphosphate (PIP2) は phosphatidylinositol(3,4,5)-triphosphate (PIP3) に変換され、phosphatase/tensin homolog on chromosome 10 (PTEN) 欠失がさらにこの変換を促進する^{12), 13), 14), 15)}。PIP3 は Akt をリン酸化する。Akt のリン酸化は kinase domain にある Thr-308 と C-terminal regulatory alignment の Ser-473 部位により制御され、それぞれ PDK-1、PDK-2¹⁶⁾ がそのリン酸化にかかわる。神経膠芽腫では、通常 PDK-1 は常時リン酸化されており、GF-PI3K-PDK1-Akt signaling はグリオーマの浸潤性増殖に関与している。PI3K 阻害剤である wortmannin や LY294002 を高濃度で投与すると Akt のリン酸化は抑制される。著者らは高濃度の PI3K 阻害剤下でも、AMPA 受容体を刺激すると Akt のリン酸化が認められることを見出し、glutamate-AMPA 型受容体-Akt pathway という新たな cascade を突き止めた。この pathway は現在分子標的の主たる対象となっている tyrosine kinase を介する PI3K-PDK1¹⁷⁾ を介して Akt を活性化する経路の側副路と考えている。tyrosine kinase を標的とした各種拮抗薬を用いた治療では短時間で大多数の症例で治療不応、薬剤耐性が認められ¹⁸⁾、その一因を説明するものと思われる。実際に AMPA 型受容体に対する拮抗薬 YM872 と増殖因子 PDGFR, c-kit に対する拮抗薬 AG1296 を併用して使用するとヒト

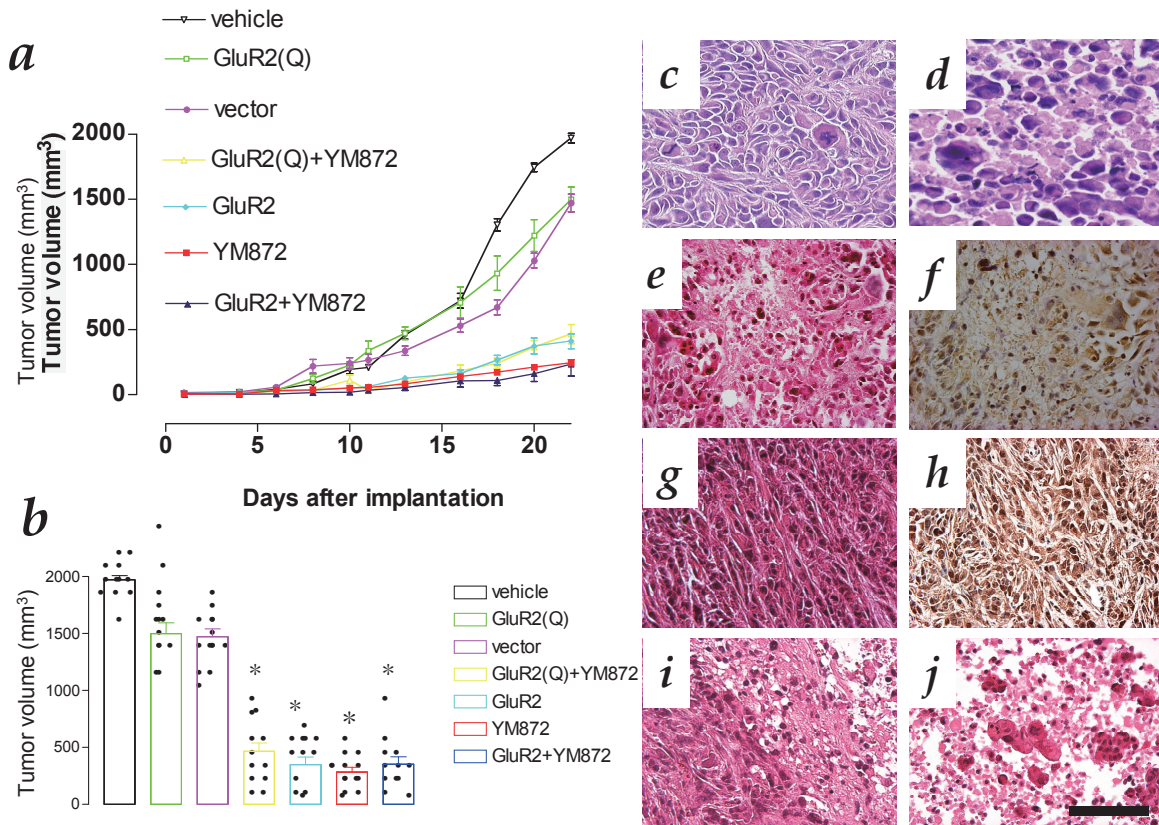


Fig. 1 Effects of manipulation of AMPA receptors on tumor growth. **a**, Effects of various treatments on growth rate of tumors grafted into the subcutaneous tissue of nude mice: injection of PBS (vehicle as control for application of YM872, a non-competitive AMPAR antagonist, inverted triangles); expression of GluA2(Q) (open squares); injection of AxCALN1GluA2 without AxCANCre (vector as control for expression of GluA2 and GluA2(Q), filled circles); expression of GluA2(Q) plus application of YM872 (open triangles); expression of GluA2 (filled diamonds); application of YM872 (filled squares); and expression of GluA2 plus application of YM872 (filled triangles). For each treatment, 12 animals were used. Each plot represents the mean \pm s.e.m. (n = 12) of the tumor volume. **b**, Plots of tumor volumes measured 22 days after inoculation. For each treatment, raw data obtained from 12 animals are plotted. * indicates significant difference at $p < 0.001$ relative to control (either vehicle or vector). **c-f**, Histology of tumor tissues treated with the vehicle (**c**) and YM872 (**d**), and of those to which the GluR2 gene was delivered (**e**, **f**). **c**, **d** and **e**, HE staining. **f**, Immunostaining with anti-GluA2 antibody. **g-h**, HE staining (**g**) and immunostaining with anti-GluA2 antibody (**h**) in tumor tissues to which the GluA2(Q) gene was delivered. **i**, HE staining of tumor tissues expressing GluA2(Q) and treated with YM872. **j**, HE staining of tumor tissues expressing GluA2 and treated with YM872. The tissues in **c-j** were taken 22 days after tumor inoculation. Scale bar in **j** 50 μ m for **c-j**. Note in **a** & **b**, GluR2 equally means GluA2.

glioblastoma の動物モデルで効果的に増殖抑制が達成された¹⁹⁾。

2) グルタミン酸産生の機序

神経伝達物質であるグルタミン酸は神経細胞のシナプス前極から分泌され、シナプス後極のグルタミン酸受容体を興奮させる。余剰のグルタミン酸は先に述べたように強い興奮毒性をもたらすため、正常星細胞のグルタミ

ン酸トランスポーターによって厳密に排除される。実際グリオーマ細胞はグルタミンからグルタミン酸を de novo で産生する事が出来る。樹立培養株では、グルタミン酸を透析することでグルタミンおよびグルタミン酸を含まない培養液中で発育させると、数日で培養液中のグルタミン酸とグルタミンはともに 100 μ M 以上の濃度に達する¹¹⁾。またアミノ酸がなくともブドウ糖があれば TCA サイクルを回してグルタミン酸を産生すること

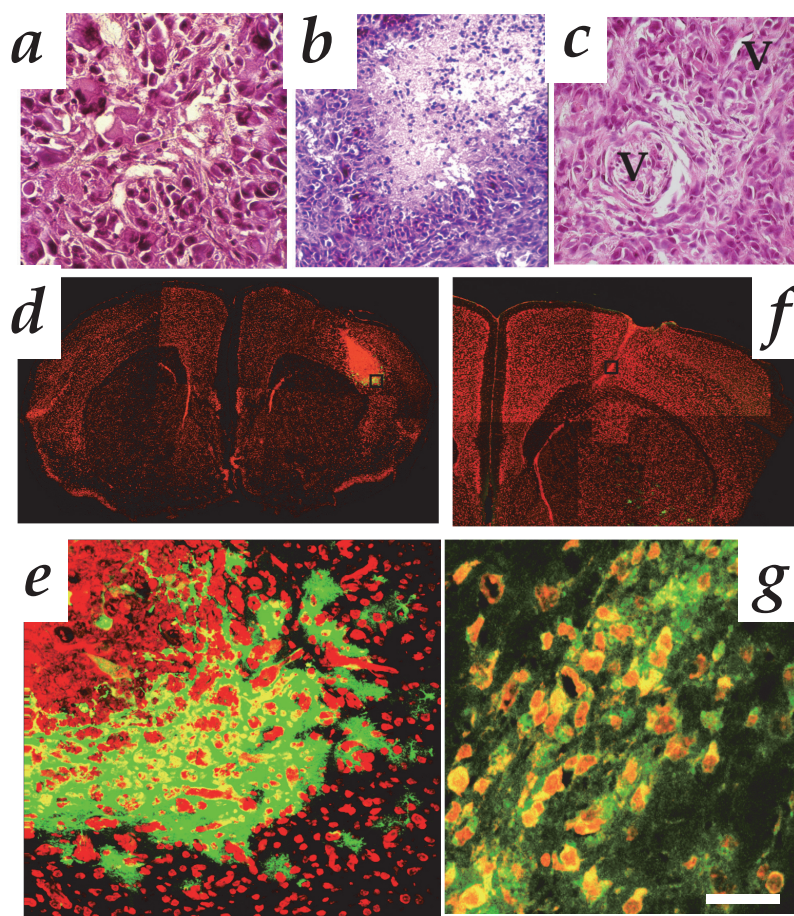


Fig. 2 Effects of GluA2 expression on tumor transplantation. **a-c**, Histopathology of the tumor formed by transplantation of cultured glioblastoma cells into the nude mouse. The tumor was characterized by pleomorphism (**a**), necrosis with pseudopalisading (**b**), and microvascular proliferation (**c**). 'v' indicates tumor vessels (HE staining). **d**, Tumor formation at 9 days after transplantation of 2×10^5 cultured glioblastoma cells into the subcortical area of the nude mouse cerebrum. The cultured cells had been infected with AxCAGFP and AxCALNLGluA2 each at MOI 5 for expression of GFP (green) two days before transplantation, and stained by PI (red). **e**, Higher magnification view of the boxed area in **d**. **f**, Cells at 14 days after transplantation of 2×10^5 cultured glioblastoma cells. The cultured cells had been infected with AxCAGFP and AxCALNLGluR2 together with AxCANCre each at MOI 5 for expression of both GFP and GluR2 two days before transplantation. **g**, Higher magnification view of the boxed area in **f**. Note apoptotic nuclear morphology caused by expression of GluR2. Scale bar in **g** represents $50 \mu\text{m}$ for **a**, **e** and **g**, $100 \mu\text{m}$ for **b**, $75 \mu\text{m}$ for **c**, $1500 \mu\text{m}$ for **d**, and $1000 \mu\text{m}$ for **f**.

ができる。細胞外シスチンを投与すると細胞外グルタミン酸濃度が上昇する事から腫瘍細胞膜に存在するシスチン・グルタミン酸エキスチェンジャーの関与も指摘されている²⁰⁾。このチャネルの拮抗薬は潰瘍性大腸炎やクローン病の治療薬であるサラゾピリンであり、脳腫瘍動物モデルで抗腫瘍効果が確認されている²¹⁾。Glutamate transporter 1 (GLT1)²²⁾や excitatory amino acid transporter 2 (EAAT-2)²³⁾などのグルタミン酸トランスポーターの発現低下が悪性度の高いグリオーマでは認められており、細胞外グルタミン酸の過剰状態に拍車を

かけることになる。実験的に GLT1 や EAAT-2 を強制発現させると腫瘍増殖が抑制される。以上より、グリオーマ細胞は細胞外にグルタミン酸を放出して周囲の脳組織を興奮性神経細胞死させることで空間拡大に利用するだけでなく、グルタミン酸をリガンドとして自ら受容体を賦活化しオートクラインおよびパラクラインに増殖と浸潤に悪用する事で浸潤性増殖を促進することが判明した¹¹⁾。神経細胞体の中には mM 単位のグルタミン酸が存在するため興奮性神経細胞死に陥った細胞から細胞外にこぼれ落ちるグルタミン酸を利用してグリオーマはさ

らに脳深部へと浸潤する。最近、シナプス間隙から分泌される Neuroligin-3 も PI3-K-mTOR を活性化することで glutamate 同様にグリオーマの増殖を促進することが報告されている²⁴⁾。

発生母細胞に関する研究

以上概説したように、我々はイオン共役型グルタミン酸受容体の一つであるカルシウム透過性 AMPA 型受容体が悪性神経膠腫の増殖と遊走に重要な役割を担うことを解明してきた^{3), 11), 25)}。最終項では、グリオーマの発生母細胞及び gliomagenesis に関する我々の仮説に言及したい。悪性グリオーマの発生母細胞に関しては文献的に神経幹細胞およびグリア前駆細胞が提示されている。神経幹細胞からがん幹細胞への逸脱を惹起する最初の分子メカニズムの正体が何か解明されれば根治療法の樹立につながるはずである。先に述べた AMPA 型受容体のカルシウム透過性に重要な役割を担う GluA2 受容体は正常細胞では胎生初期に RNA editing により CAG:glutamine(Q) codon が CGG:arginine(R) codon に変化することで受容体膜様部(Q/R site)における中性のグルタミンから陽電荷のアルギニンへの変換により同じく陽イオンを有するカルシウムを不透過にさせるという分子機構により制御されていることを述べた。すなわち正常細胞では胎生初期には未編集型 GluA2Q であるが誕生後には RNA editing により全て GluA2R の翻訳型となるわけである。またヒト生検材料を用いた解析からは神経膠芽腫がカルシウム透過性を獲得する分子機構については GluA2(Q) を保有するものが2割、残り8割は GRIA2 の pre-mRNA level での epigenetic なサイレンシングにより GluA2 を欠く AMPA 受容体が形成される場合である。これ等の変化は腫瘍内で起こるわけであるが、腫瘍の階層的構築を考慮すると、本来カルシウム不透過型の AMPA 型受容体を有する正常神経幹細胞が機能的な変容を引き起こし CP-AMPA 型に改変する事で増殖と遊走の亢進を来した細胞群がグリオーマ幹細胞ではないかと思われる。さらにこの GluA2 のサイレンシングの機序に関しては REST (Repressor element-1 silencing transcription factor) が重要である。REST は同時にミトコンドリアの電子輸送に重要な cytochrome C oxidase が GRIA2 同様に抑制される事が判明している²⁶⁾。エネルギー代謝経路とグルタミン酸受容体遺伝子双方に共通の repressor の同定は発生母細胞レベルにおけるがん化のメカニズムの理解を促進し今後根本治療の理論的背景の形成につながる可能性を秘めており大変興味深い。

終わりに

AMPA 受容体拮抗薬は、てんかん、パーキンソン病などの神経疾患ですでに臨床治験が施行されているので安全性が確認されている薬剤が複数存在し臨床応用が可能である。実際 AMPA 型受容体拮抗薬は前臨床試験で抗腫瘍効果を持つことが判明しており^{3), 11)}、神経膠芽腫治療剤として有望であることが認識され、より安全性が高く治療効果の高い薬剤の開発と臨床治験が行われた。AMPA 型受容体拮抗剤はその構造によりキノキサリンジオン型(YM872, NBQX)²⁷⁾、ピリドチアジン型(YM928)²⁸⁾、ベンゾジアゼピン型(GYKI52466, Talampanel)²⁹⁾の3系統に分類される。グリオーマに対する抗腫瘍効果は著者らの研究開発からいずれの系統の薬剤でも同等の薬効が確認されている。AMPA 型受容体拮抗薬はまた、競合的拮抗薬と非競合的拮抗薬に分類される。前者では、作用時間が短く多量なグルタミン酸の存在するところでは薬効が低下する。悪性度の高いグリオーマでは、特に浸潤最先端部では、グリオーマ細胞から直接放出されるグルタミン酸と細胞死に陥った神経細胞より漏れ出す過剰なグルタミン酸が高濃度に認められることから、非競合的拮抗薬が浸潤機構の病態生理を考えると有利である。より合理的に CP-AMPA 型受容体を選択的に拮抗する化合物もあるが毒性や安全性から臨床治験にはあがってきておらず現時点での実用化は成功していない。経口非競合的拮抗薬タランパネルについては米国にて2005年12月から2007年7月に登録された72例の初発神経膠芽腫患者に対して多施設共同による第2相試験が行われた³⁰⁾。症例は、平均年齢60歳(37歳-85歳)で70歳以上が17%と高齢者が多く、平均KPS 90(70-100)、生検のみの症例が23%含まれているにも拘らず平均生存中央値は17.9ヶ月、比較対照群では14.6ヶ月と良好な生存期間の延長をもたらした。現行の悪性グリオーマの標準治療剤はいずれもがん幹細胞から派生する多様な clonal progeny を攻撃対象とする薬剤が用いられているが今後はがん幹細胞自体を標的にする、さらに踏み込んで正常幹細胞からがん幹細胞への逸脱を予防する治療剤の創出も望まれる。

引用文献

1. **Labrakis C, Patt S, Hartman J, and Kettenmann H:** Glutamate receptor activation can trigger electrical activity in human glioma cells. *Eur. J. Neurosci.* 10: 2153-62, 1998.
2. **Markert JM, Fuller CM, Gillespie GY, Bubien JK, McLean LA, Hong RL, Lee K, Gullans SR, Mapstone TB, Benos DJ:** Differential gene expression profiling in human brain tumors. *Physiol Genomics.* 5: 21-33, 2001.
3. **Ishiuchi S, Tsuzuki K, Yoshida Y, Yamada N, Hagimura N, Okado H, Miwa A, Kurihara H, Nakazato Y, Tamura M, Sasaki T, Ozawa S:** Blockage of Ca²⁺-permeable AMPA receptors suppresses migration and induces apoptosis in human glioblastoma cells. *Nat. Med.* 8 : 971-978, 2002.
4. **Maas, S, Patt S, Schrey M, Rich A:** Underediting of glutamate receptor GluR-B mRNA in malignant gliomas. *Proc Natl Acad Sci USA* 98: 14687-92, 2001.
5. **Smith JS, Tachibana I, Passe SM, Huntley BK, Borell TJ, Iturria N, O'Fallon JR, Schaefer PL, Scheithauer BW, James CD, Buckner JC, Jenkins RB:** PTEN mutation, EGFR amplification, and outcome in patients with anaplastic astrocytoma and glioblastoma multiforme. *J. Natl. Cancer Inst.* 93: 1246-1256, 2001.
6. **Lokker NA, Sullivan CM, Hollenbach SJ, Israel MA, Giese NA:** Platelet-derived growth factor (PDGF) autocrine signaling regulates survival and mitogenic pathways in glioblastoma cells: evidence that the novel PDGF-C and PDGF-D ligands may play a role in the development of brain tumors. *Cancer Res.* 62: 3729-3735, 2002.
7. **Shawver LK, Salmon D, Ullrich HM:** Smart drugs : tyrosine kinase inhibitors in cancer therapy. *Cancer Cell* 1: 117-123, 2002.
8. **Datta SR, Brunet A, Greenberg ME:** Cellular survival: a play in three Akts. *Genes Dev.* 13: 2905-2927, 1999.
9. **Alessi DR, Cohen P:** Mechanism of activation and function of protein kinase B. *Curr. Opin. Genet. Dev.* 8: 55-62, 1998.
10. **Osaki M, Oshimura M, Ito H:** PI3K-Akt pathway: its functions and alterations in human cancer. *Apoptosis* 9: 667-676, 2004.
11. **Ishiuchi S, Yoshida Y, Sugawara K, Aihara M, Ohtani T, Watanabe T, Saito N, Tsuzuki K, Okado H, Miwa A, Nakazato Y, Ozawa S:** Ca²⁺-permeable AMPA receptors regulate growth of human glioblastoma via akt activation. *J Neurosci* 27: 7987-8001, 2007.
12. **Cantley LC, Neel BG:** New insights into tumor suppression: PTEN suppresses tumor formation by restraining the phosphoinositide 3-kinase/AKT pathway. *Proc. Natl. Acad. Sci. USA* 96: 4240-4245, 1999.
13. **Li J, Yen C, Liaw D, Podsypanina K, Bose S, Wang SI, Puc J, Miliareis C, Rodgers L, McCombie R, Bigner SH, Giovanella BC, Ittmann M, Tycko B, Hibshoosh H, Wigler MH, Parsons R:** PTEN, a putative protein tyrosine phosphatase gene mutated in human brain, breast, and prostate cancer. *Science* 275: 1943-1947, 1997.
14. **Maehama T, Dixon JE:** The tumor suppressor, PTEN/MMAC1, dephosphorylates the lipid second messenger, phosphatidylinositol 3,4,5-trisphosphate. *J. Biol. Chem.* 273: 13375-13378, 1998.
15. **Choe G, Horvath S, Cloughesy TF, Crosby K, Seligson D, Palotie A, Inge L, Smith BL, Sawyers CL, Mischel PS:** Analysis of the phosphatidylinositol 3'-kinase signaling pathway in glioblastoma patients in vivo. *Cancer Res.* 63: 2742-2746, 2003.
16. **Toker A, Newton AC et al:** Akt/protein kinase B is regulated by autophosphorylation at the hypothetical PDK-2 site. *J. Biol. Chem.* 275: 8271-8274, 2000.
17. **Vanhaesebroeck B, Alessi DR et al:** The PI3K-PDK1 connection: more than just a road to PKB. *Biochem. J.* 346: 561-576, 2000.
18. **Mellinghoff IK, Wang MD, Vivanco I, Haas-Kogan DA, Zhu S, Dia EQ, Lu KV, Yoshimoto K, Huang JH, Chute DJ, Riggs BL, Horvath S, Liau LM, Cavenee WK, Rao PN, Beroukhim R, Peck TC, Lee JC, Sellers WR, Stokoe D, Prados M, Cloughesy TF, Sawyers CL, Mischel PS:** Molecular determinants of the response of glioblastomas to EGFR kinase inhibitors. *N. Engl. J. Med.* 353: 2012-2024, 2005.

19. **Watanabe T, Ohtani T, Aihara M, Ishiuchi S:** Enhanced antitumor effect of YM872 and AG1296 combination treatment on human glioblastoma xenograft models. *J Neurosurg.* 118: 838-45. 2013.
20. **Ye ZC, Rothstein JD, Sontheimer H:** Compromised glutamate transport in human glioma cells: reduction-mislocalization of sodium-dependent glutamate transporters and enhanced activity of cystine-glutamate exchange. *J Neurosci.* 19: 10767-77, 1999.
21. **Chung WJ, Sontheimer H:** Sulfasalazine inhibits the growth of primary brain tumors independent of nuclear factor-kappaB. *J Neurochem.* 110: 182-93, 2009.
22. **Vanhoutte N, Hermans E:** Glutamate-induced glioma cell proliferation is prevented by functional expression of the glutamate transporter GLT-1. *FEBS Letters* 582: 1847-1852, 2008.
23. **de Groot JF, Liu TJ, Fuller G, Yung WK:** The excitatory amino acid transporter-2 induces apoptosis and decreases glioma growth in vitro and in vivo. *Cancer Res.* 65: 1934-40, 2005.
24. **Venkatesh HS, Johung TB, Caretti V, Noll A, Tang Y, Nagaraja S, Gibson EM, Mount CW, Polepalli J, Mitra SS, Woo PJ, Malenka RC, Vogel H, Bredel M, Mallick P, Monje M.** Neuronal Activity Promotes Glioma Growth through Neuroligin-3 Secretion *Cell.* 7 ; 161: 803-16. 2015.
25. **Ishiuchi S.** New roles of glutamate receptors in glias and gliomas. *Brain Nerve.* 61: 753-64. 2009.
26. **Priya A, Johar K, Wong-Riley MT.** Nuclear respiratory factor 2 regulates the expression of the same NMDA receptor subunit genes as NRF-1: both factors act by a concurrent and parallel mechanism to couple energy metabolism and synaptic transmission. *Biochim Biophys Acta.* 1833: 48-58. 2013.
27. **Kohara A, Okada M, Tsutsumi R, Ohno K, Takahashi M, Shimizu-Sasamata M, Shishikura J, Inami H, Sakamoto S, Yamaguchi T:** In vitro characterization of YM872, a selective, potent and highly water-soluble α -amino-3-hydroxy-5-methylisoxazole-4-propionate receptor antagonist. *J. Pharm. Pharmacol.* 50: 795-801, 1998.
28. **Yamashita H, Ohno K, Amada Y, Imai H, Shishikura J, Sakamoto S, Okada M, Yamaguchi T:** Effect of YM928, a novel AMPA receptor antagonist, on seizures in EL mice and kainite-induced seizures in rats. *Naunyn schmiedebergs Arch Pharmacol* 370: 99-105, 2004.
29. **Langan YM, Lucas R, Jewell H, Toublanc N, Schaefer H, Sander JW, Patsalos PN:** Talampanel, a new antiepileptic drug: single- and multi-dose pharmacokinetics and initial 1-week experience in patients with chronic intractable epilepsy. *Epilepsia* 44: 46-53, 2003.
30. **Grossman SA, Ye X, Chamberlain MC, Mikkelsen T, Batchelor T, Desideri S, Piantadosi S, Fisher J, Fine HA:** Talampanel With Standard Radiation and Temozolomide in Patients With Newly Diagnosed Glioblastoma: A Multicenter Phase II Trial *J Clin Oncol* 27: 4155-4161, 2009.

Case Report

A case of high-grade astrocytoma with *BRAF* and *ATRX* mutations following a long-standing course over two decades

Satoshi Nakata,^{1,2} Keishi Horiguchi,² Shogo Ishiuchi,³ Yuhei Yoshimoto,² Seiji Yamada,¹
Sumihito Nobusawa,¹ Hayato Ikota,¹ Junko Hirato⁴ and Hideaki Yokoo¹

Departments of ¹Human Pathology, and ²Neurosurgery, Gunma University Graduate School of Medicine, and ⁴Department of Pathology, Gunma University Hospital, Maebashi and ³Department of Neurosurgery, University of the Ryukyus Graduate School of Medicine, Nishihara-cho, Okinawa, Japan

Pediatric high-grade gliomas are rare and occasionally hard to classify. These tumors often feature a well-demarcated histology and are expected to have a better outcome than ordinary diffuse high-grade gliomas in adults. We herein report a case of circumscribed high-grade glioma that showed a distinct molecular profile and followed an excellent course for 26 years. The patient, a 3-year-old boy at onset, presented with a contrast-enhancing mass in the right temporal lobe and underwent resection. Histologically, the tumor mainly consisted of compact bundles of GFAP-positive spindle cells. With its malignant features including brisk mitotic activity and pseudopallisading necrosis, a diagnosis of high-grade astrocytoma was made and adjuvant chemoradiotherapy was administered. After a disease-free period of two decades, the tumor recurred locally. The resected tumor was histologically identical to the primary tumor and additionally contained pleomorphic cells, but lacked eosinophilic granular bodies and reticulin networks. The primary and recurrent tumors both harbored the *BRAF* V600E mutation, and the recurrent tumor was immunonegative for *ATRX*. Combined *BRAF* and *ATRX* mutations are rare in gliomas, with only a pediatric case of glioblastoma being reported in the literature. However, our case cannot be regarded as glioblastoma because of its well-demarcated histology and excellent course. The distinction of either a diffuse or localized nature in gliomas is important, particularly in children, for predicting prognoses and selecting adjuvant therapies that consequently affect life-long health care. The present case provides novel insights into pediatric high-grade astrocytomas.

Key words: *ATRX*, *BRAF* V600E, diffuse glioma, pediatric, pleomorphic xanthoastrocytoma.

INTRODUCTION

Pediatric and young adult gliomas are variegated, with some being histologically hard to classify in the setting of malignant features. In addition to grades III and IV diffuse astrocytic and oligodendroglial tumors in the revised 4th edition of the WHO classification,¹ anaplastic variants of pleomorphic xanthoastrocytoma (PXA) and pilocytic astrocytoma (PA) occur in this population.^{2–4} Despite their strong proliferative activities, anaplastic PXA/PA generally follow less aggressive courses than diffuse high-grade gliomas,^{2,3} and this may be due to their less invasive nature into the brain parenchyma. If a given glioma harbors anaplastic features such as brisk mitotic activity, microvascular proliferation and necrosis, but lacks the typical features of PXA/PA, a diagnosis of diffuse high-grade glioma is initially proposed. Under these conditions, the distinction between a diffuse and circumscribed nature is important, particularly in children, for predicting prognoses and selecting adjuvant therapies, including the timing and field of radiotherapy, which consequently affect life-long health care.⁵ However, it is challenging for pathologists to accurately evaluate the invasiveness of each glioma.

We herein present a case of pediatric high-grade astrocytoma predominantly composed of compact bundles of spindle cells devoid of the features of PXA/PA. This case followed an excellent clinical course and recurred locally after a long-term latency of more than two decades.

CLINICAL SUMMARY

A 3-year-old boy with impaired consciousness was admitted to a hospital. Computed tomography revealed a hemorrhagic mass in the right temporal lobe, which was

Correspondence: Satoshi Nakata, MD, Department of Human Pathology, Gunma University Graduate School of Medicine, 3-39-22, Showa-machi, Maebashi, Gunma, 371-8511, Japan. Email: nakata3104@gmail.com

Received 29 November 2016; revised and accepted 12 January 2017.

heterogeneously enhanced and was considered to be a malignant glioma (Fig. 1A). The tumor was completely resected, and extended focal radiotherapy of 33 Gy and platinum-based concomitant and maintenance chemotherapy were administered based on the pathological diagnosis of high-grade astrocytoma.

Although slight enhancement around the surgical cavity persisted in the subsequent 20 years, no evidence of recurrence was detected (Fig. 1B). However, the patient visited the hospital with a worsening headache at the age of 26 years. MRI revealed the recurrence of a large tumor. Despite the large size (7×5 cm) of the enhanced mass (Fig. 1C), the volume of surrounding edema on T2-weighted images was limited (Fig. 1D). The recurrent tumor was resected and histopathologically confirmed to be identical to the primary tumor. The patient received chemotherapy with temozolomide and bevacizumab and has maintained his quality of life without further recurrence for more than 2 years.

MATERIALS AND METHODS

Tissue specimens were fixed in 10% formalin and embedded in paraffin. Paraffin blocks were cut at a thickness of 2.5 μ m and stained with HE. An immunohistochemical examination was performed on paraffin-embedded sections using

the biotin-streptavidin immunoperoxidase method (Histofine Kit, Nichirei, Tokyo, Japan). Primary antibodies against the following antigens were used: GFAP (polyclonal, 1:5000; our own), Olig2 (polyclonal, 1:100; IBL, Takasaki, Japan), nestin (monoclonal, 1:200; Merck Millipore, Tokyo, Japan), neurofilament (RMd0-20; 1:100; Invitrogen, Camarillo, CA, USA), CD34 (NU-4A1; 1:200; Nichirei), p53 protein (monoclonal, 1:50; Leica Microsystems, Wetzlar, Germany), ATRX (polyclonal, 1:500; Sigma, St. Louis, MO, USA), and Ki-67 (MIB-1; 1:100; Dako, Glostrup, Denmark). After visualization with diaminobenzidine, tissue sections were briefly counterstained with hematoxylin.

In direct DNA sequencing, genomic DNA was extracted from the primary and recurrent tumors, then amplified by PCR and sequenced using primers for *BRAF*, the telomerase reverse transcriptase (*TERT*) promoter, and isocitrate dehydrogenase-1/2 (*IDH1/2*), as previously described.⁶

This study was approved by our Institutional Review Board.

RESULTS

In the first tumor, intersecting bundles of spindle cells formed a compact, polynodular mass that entrapped a medium-sized muscular artery presumably in the

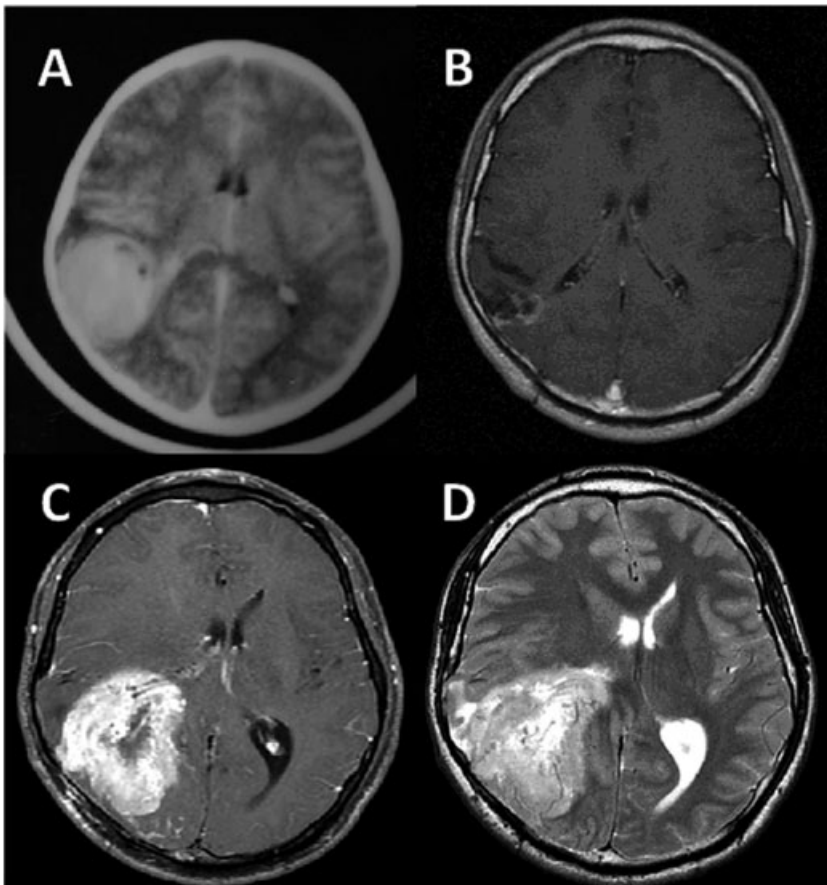


Fig. 1 Axial CT and MRIs. **(A)** Contrast-enhanced CT image at the onset showing a hemorrhagic mass within the right temporal lobe. **(B)** On a gadolinium-enhanced T1-weighted image (Gd-T1WI) when the patient was 22 years old, slight enhancement around the surgical cavity remained unchanged. **(C)** Gd-T1WI at recurrence shows a solid heterogeneously enhanced mass that is 7×5 cm in size in the same region. **(D)** On the T2-weighted image at recurrence, surrounding edema is limited despite the volume of the tumor.

subarachnoid space. Malignant features including pseudopalisading necrosis (Fig. 2A) and high mitotic activity (Fig. 2B) with up to 4/10 high-power fields were observed. In the adjacent brain parenchyma, tumor cells partly intermingled with normal glial cells and neurons, whereas the subpial and perineuronal accumulation of tumor cells was not detected, which is in contrast to that in diffuse gliomas (Fig. 2C). Tumor cells showed moderate cellular pleomorphism and xanthic changes, which indicated

PXA. Furthermore, lower-grade areas that consisted of loosely textured bipolar or multipolar cells (Fig. 2D) and frequent hyalinized vessels (Fig. 2E) appeared to be analogous to PA. However, neither Rosenthal fibers nor eosinophilic granular bodies (EGBs) were observed and reticulin fibers were poor (Fig. 2F). In immunohistochemistry, tumor cells were partially positive for GFAP (Fig. 2G), diffusely positive for Olig2 and nestin, and negative for CD34. Rare plump tumor cells were immunoreactive for neurofilaments;

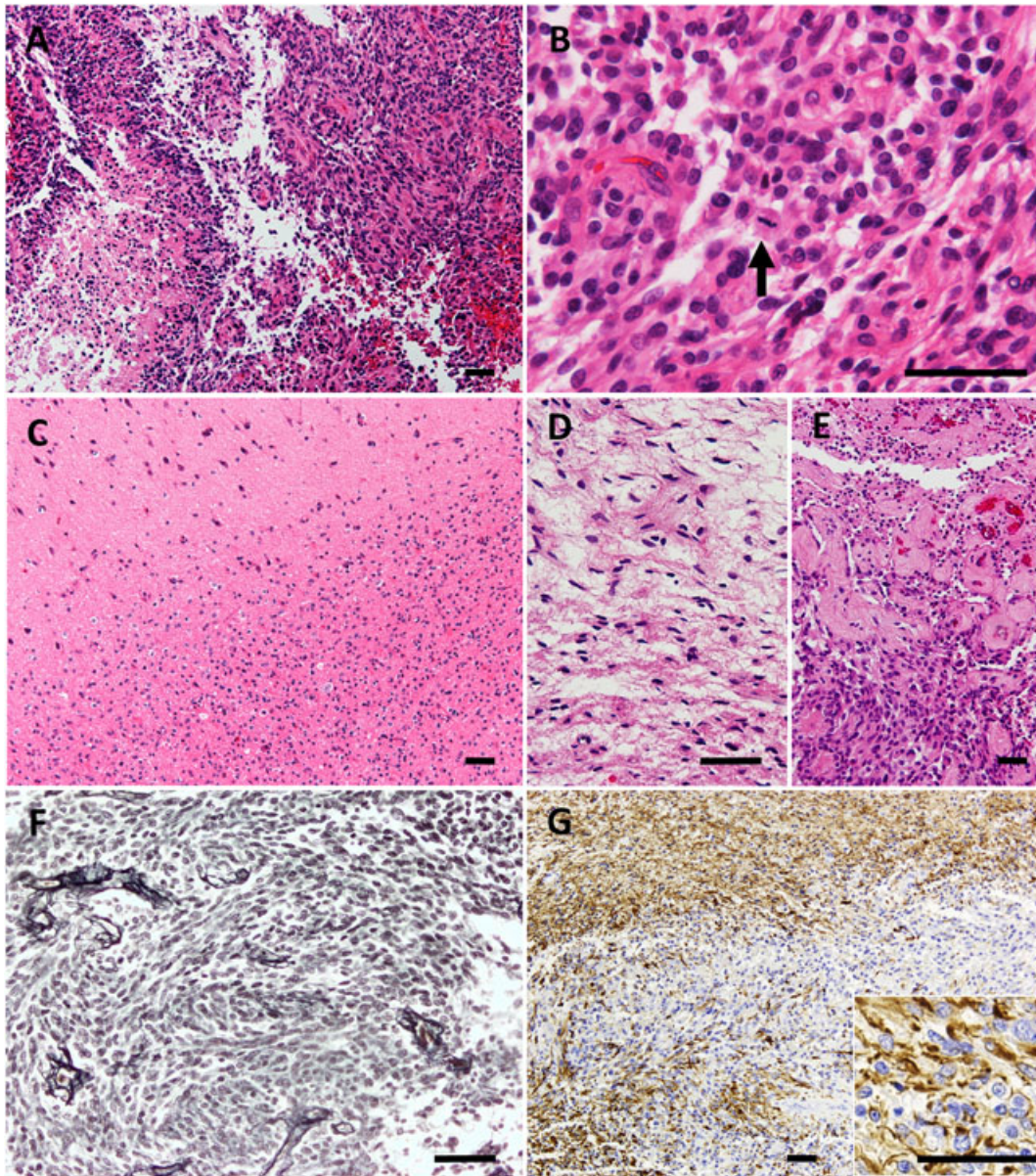


Fig. 2 Histological findings of the primary tumor. (A) The tumor is predominantly composed of spindle cells forming a compact, polynodular mass. Necrosis and palisading tumor cells are also present. (B) The dense proliferation of atypical spindle cells with frequent mitosis is shown. High mitotic activity with up to 4/10 high-power fields is observed. (C) Although tumor cells partly infiltrate into the brain parenchyma, the border is fairly clear. Subpial and perineuronal concentrations similar to those in diffuse gliomas are not present. (D) A lower-grade area with loose-textured piloid cells is shown. (E) Thick-walled hyalinized vessels are shown, which indicate a precursor lesion. (F) Reticulin fibers are limited around vessels. (G) Tumor cells are partially positive for GFAP. The boundary between the tumor (bottom) and brain parenchyma (upper) is clearly observed. Original magnification: A, $\times 100$; B, $\times 400$; C, $\times 100$; D, $\times 200$; E, $\times 100$; F, $\times 200$; G, $\times 100$, inset, $\times 400$. Bar = 50 μm .

however, normal neurons or neurites were not entrapped in the tumor mass. Immunostaining for p53, ATRX and Ki-67 could not be evaluated due to sample deterioration over time.

The recurrent tumor was similar to the primary tumor, but showed a more circumscribed pattern. Spindle cells became thicker and a hyaline-like cytoplasm was more evident than in the first tumor (Fig. 3A). A limited number of xanthic cells and eosinophilic hyaline droplets (not EGBs) was detected, whereas reticulin fibers did not increase.

Malignant features including pseudopallisading necrosis, increased mitotic activity (Fig. 3B) with up to 12/10 high-power fields, and microvascular proliferation were observed. The border between the tumor and adjacent brain parenchyma was clear (Fig. 3C). Lower-grade areas and hyalinized vessels co-existed, similar to the primary tumor (Fig. 3D). In immunohistochemistry, tumor cells were positive for glial markers. Notably, tumor cells were positive for p53 (Fig. 3E) and negative for ATRX (Fig. 3F). The Ki-67 LI was approximately 20%.

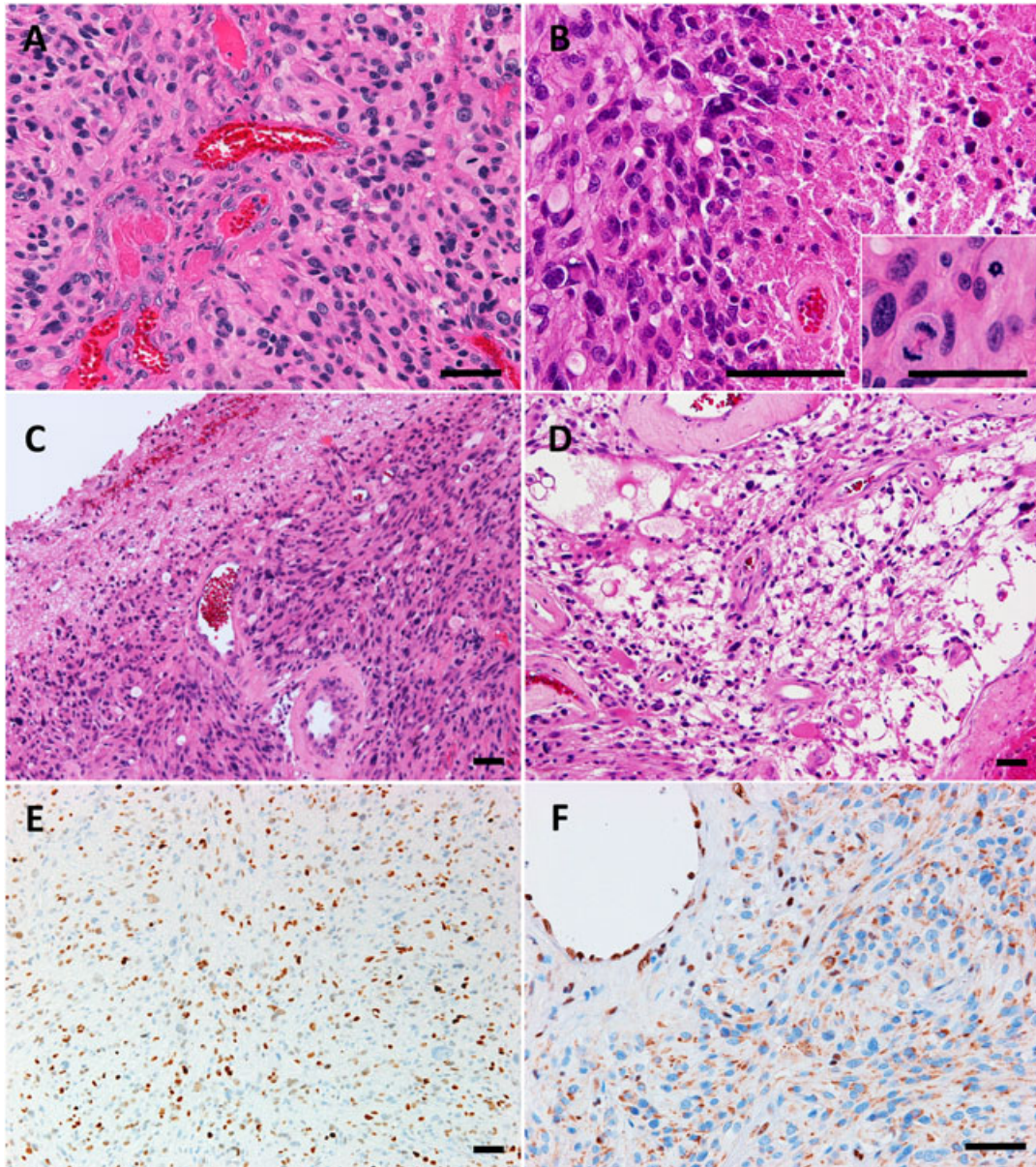


Fig. 3 Histological findings of the recurrent tumor. (A) Thick spindle cells with cellular pleomorphism form compact bundles. Microvascular proliferation is also observed. (B) Necrosis and the dense proliferation of pleomorphic tumor cells with frequent mitosis (inset) are shown. (C) The tumor (right bottom) is well-demarcated from the adjacent brain parenchyma (upper left). (D) A lower-grade area with frequent hyalinized vessels is shown. (E) Approximately 20% of tumor cells are immunopositive for p53. (F) The loss of ATRX nuclear expression is noted, whereas endothelial cells retain their expression. Original magnification: A, $\times 200$; B, $\times 400$, inset $\times 400$; C, $\times 100$; D, $\times 100$; E, $\times 100$; F, $\times 200$. Bar = 50 μm .

In DNA sequencing, the primary and recurrent tumors both harbored the mutation of a valine to glutamic acid substitution at position 600 of *BRAF* (*BRAF* V600E, Fig. 4). The *TERT* promoter and *IDH1/2* were intact.

DISCUSSION

In this case, based on the proliferation of atypical astrocytes and malignant features including pseudopallisading necrosis, brisk mitotic activity and microvascular proliferation, GBM was primarily considered for the differential diagnosis. Although GBMs are typically infiltrative, some are partially well-demarcated and their dense proliferation mimics a compact tumor mass.⁷ In the present case, the absence of intervening neurites in compact areas and the lack of the secondary structures of Scherer suggested a more circumscribed tumor.

In the current WHO classification, anaplastic PXA⁸ and PA with anaplastic features⁹ are described as localized high-grade astrocytomas; however, not all circumscribed high-grade astrocytomas clearly fit into either of these.^{2,9} In our case, PXA-like thick spindle cells with a cellular polymorphism and partly xanthic changes were detected at recurrence. However, the present case lacked some classical characteristics of PXAs, such as reticulin fibers, frequent EGBs and CD34-positive tumor cells.^{2,8} In addition, immunohistochemical results for p53 and *ATRX*, which strongly suggest both mutations,^{10–12} are common in pediatric GBM¹³ and extremely rare in PXA; p53 mutations have only been detected in 6% of PXA,⁸ and *ATRX*-mutated PXA has never been reported; one case of diffuse glioma with a combined PXA-like component was described elsewhere.¹⁴

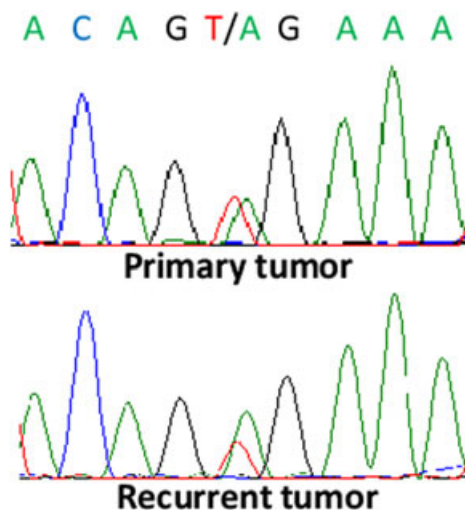


Fig. 4 Direct DNA sequencing for the encoded valine-to-glutamic acid substitution at position 600 of the serine/threonine-protein kinase *BRAF* (*BRAF* V600E). *BRAF* V600E is detected in the primary tumor (upper) and recurrent tumor (lower).

The *BRAF* V600E mutation has been reported in 60–70% of PXA,^{2,15} but in only 2–3% of conventional GBM.^{15,16} Additionally, recent studies revealed a subset of pediatric and young adult GBM showing a higher percentage of the *BRAF* V600E mutation and taking less malignant courses.^{17–19} Korshunov *et al.* reported a subgroup of pediatric GBM with PXA or PA-like genome methylation profiles, 40% of which harbored the *BRAF* V600E mutation, which followed significantly longer courses.¹⁷ Zhang *et al.* and Matthew *et al.* also reported that 16 out of 107 cases of young adult GBM and five out of 10 cases of pediatric secondary GBM exhibited the *BRAF* V600E mutation and had better prognoses.^{18,19} Although detailed histology was not provided, these cases of pediatric GBM with a PXA-like methylation pattern appear to resemble our case.¹⁷

It currently remains unknown whether concurrent *BRAF* V600E and *ATRX* mutations are associated with a specific glioma subtype or clinical course. We searched a public database (cBioPortal for Cancer Genomics: <http://www.cbioportal.org>^{20,21}) to investigate cases concurrently showing these mutations. In 812 samples of grades II to IV gliomas in The Cancer Genome Atlas (TCGA) project,²² the *BRAF* V600E and *ATRX* mutations were detected in 0.9% and 26% of samples, respectively, but were not concurrent. In other case series, one adult case of grade II diffuse glioma and one pediatric case of GBM harbored these mutations together; however, detailed histology and clinical courses were not reported.^{23,24} Our case cannot be regarded as ordinary diffuse glioma or glioblastoma due to its well-demarcated histology and excellent course.

We previously reported a case of epithelioid GBM that concurrently harbored the *TERT* promoter and *BRAF* V600E mutation.⁶ Epithelioid GBM is a rare aggressive subtype of GBM, with 50% of cases harboring the *BRAF* V600E mutation.²⁵ *TERT* promoter and *ATRX* mutations are both associated with abnormal telomere maintenance; the former is mediated by activated telomerase²⁶ and the latter by the alternative lengthening of telomeres.²⁷ These mutations are nearly mutually exclusive in gliomas and associated with certain histological subtypes.^{22,28} The combinatory features of these mutations may be connected with some histological types and clinical behaviors.

The limitation of this study is the lack of evidence of *ATRX* mutation in the primary tumor. A possibility remains that the primary tumor harbored only *BRAF* V600E mutation, and subsequent acquisition of *ATRX* mutation caused the late recurrence and progression. Further studies are needed to uncover the significance of concurrent *BRAF* V600E and *ATRX* mutations.

In conclusion, our case illustrates the excellent prognosis of localized high-grade astrocytoma. This case cannot be categorized into a specific subtype based on histological

features and molecular profiles, and further suggests the presence of unclassified variants of pediatric localized high-grade astrocytoma in addition to anaplastic PXA/PA. More of these cases need to be identified and their histological and molecular characteristics assessed, and this will ultimately contribute to a more robust diagnosis and appropriate risk stratification.

ACKNOWLEDGMENTS

We thank Ms. Machiko Yokota and Mr. Tatsuya Yamazaki (Gunma University) for their excellent technical assistance.

REFERENCES

- Louis DN, Perry A, Reifenberger G *et al.* The 2016 World Health Organization Classification of Tumors of the Central Nervous System: a summary. *Acta Neuropathol* 2016; **131**: 803–820.
- Ida CM, Rodriguez FJ, Burger PC *et al.* Pleomorphic xanthoastrocytoma: natural history and long-term follow-up. *Brain Pathol* 2015; **25**: 575–586.
- Rodriguez FJ, Scheithauer BW, Burger PC, Jenkins S, Giannini C. Anaplasia in pilocytic astrocytoma predicts aggressive behavior. *Am J Surg Pathol* 2010; **34**: 147–160.
- Cykowski MD, Allen RA, Kanaly AC *et al.* The differential diagnosis of pilocytic astrocytoma with atypical features and malignant glioma: an analysis of 16 cases with emphasis on distinguishing molecular features. *J Neurooncol* 2013; **115**: 477–486.
- Vern-Gross TZ, Schreiber JE, Broniscer A *et al.* Prospective evaluation of local control and late effects of conformal radiation therapy in children, adolescents, and young adults with high-grade glioma. *Neuro Oncol* 2014; **16**: 1652–1660.
- Matsumura N, Nakajima N, Yamazaki T *et al.* Concurrent TERT promoter and BRAF V600E mutation in epithelioid glioblastoma and concomitant low-grade astrocytoma. *Neuropathology* 2016. DOI:10.1111/neup.12318.
- Burger PC, Scheithauer BW. Glioblastoma. In: *AFIP Atlas of Tumor Pathology* Fourth Series, Fascicle 7, Tumors of the Central Nervous System. Washington DC: Armed Forces Institute of Pathology, 2007; 55–77.
- Giannini C, Paulus W, Louis DN, Liberski PP, Figarella-Branger D, Capper D. Pleomorphic xanthoastrocytoma. In: Louis DN, Ohgaki H, Otmar D *et al.*, eds. *World Health Organization classification of Tumours of the Central Nervous System*, Revised 4th edn. Lyon: IARC Press, 2016; 94–97.
- Collins VP, Tihan T, VandenBerg SR *et al.* Pilocytic astrocytoma. In: Louis DN, Ohgaki H, Otmar D *et al.*, eds. *World Health Organization classification of Tumours of the Central Nervous System*, Revised 4th edn. Lyon: IARC Press, 2016; 80–89.
- Takami H, Yoshida A, Fukushima S *et al.* Revisiting TP53 mutations and immunohistochemistry - A comparative study in 157 diffuse gliomas. *Brain Pathol* 2015; **25**: 256–265.
- Ikemura M, Shibahara J, Mukasa A *et al.* Utility of ATRX immunohistochemistry in diagnosis of adult diffuse gliomas. *Histopathology* 2016; **69**: 260–267.
- Hewer E, Vajtai I, Dettmer MS, Berezowska S, Vassella E. Combined ATRX/IDH1 immunohistochemistry predicts genotype of oligoastrocytomas. *Histopathology* 2016; **68**: 272–278.
- Wu G, Diaz AK, Paugh BS *et al.* The genomic landscape of diffuse intrinsic pontine glioma and pediatric non-brainstem high-grade glioma. *Nat Genet* 2014; **46**: 444–450.
- Yamada S, Kipp BR, Voss JS, Giannini C, Raghunathan A. Combined “infiltrating astrocytoma/pleomorphic xanthoastrocytoma” harboring IDH1 R132H and BRAF V600E mutations. *Am J Surg Pathol* 2016; **40**: 279–284.
- Schindler G, Capper D, Meyer J *et al.* Analysis of BRAF V600E mutation in 1,320 nervous system tumors reveals high mutation frequencies in pleomorphic xanthoastrocytoma, ganglioglioma and extra-cerebellar pilocytic astrocytoma. *Acta Neuropathol* 2011; **121**: 397–405.
- Knobbe CB, Reifenberger J, Reifenberger G. Mutation analysis of the Ras pathway genes NRAS, HRAS, KRAS and BRAF in glioblastomas. *Acta Neuropathol* 2004; **108**: 467–470.
- Korshunov A, Ryzhova M, Hovestadt V *et al.* Integrated analysis of pediatric glioblastoma reveals a subset of biologically favorable tumors with associated molecular prognostic markers. *Acta Neuropathol* 2015; **129**: 669–678.
- Zhang R, Shi Z, Chen H *et al.* Biomarker-based prognostic stratification of young adult glioblastoma. *Oncotarget* 2016; **7**: 5030–5041.
- Mistry M, Zhukova N, Merico D *et al.* BRAF Mutation and CDKN2A deletion define a clinically distinct subgroup of childhood secondary high-grade glioma. *J Clin Oncol* 2015; **33**: 1015–1022.
- Cerami E, Gao J, Dogrusoz U *et al.* The cBio cancer genomics portal: An open platform for exploring multidimensional cancer genomics data. *Cancer Discov* 2012; **2**: 401–404.
- Paugh BS, Qu C, Jones C *et al.* Integrated molecular genetic profiling of pediatric high-grade gliomas reveals key differences with the adult disease. *J Clin Oncol* 2010; **28**: 3061–3068.

22. Ceccarelli M, Barthel FP, Malta TM *et al*. Molecular profiling reveals biologically discrete subsets and pathways of progression in diffuse glioma. *Cell* 2016; **164**: 550–563.
23. Johnson BE, Mazar T, Hong C *et al*. Mutational analysis reveals the origin and therapy-driven evolution of recurrent glioma. *Science* 2014; **343**: 189–193.
24. Bettegowda C, Agrawal N, Jiao Y *et al*. Exomic sequencing of four rare central nervous system tumor types. *Oncotarget* 2013; **4**: 572–583.
25. Kleinschmidt-DeMasters BK, Aisner DL, Foreman NK. BRAF VE1 immunoreactivity patterns in epithelioid glioblastomas positive for BRAF V600E mutation. *Am J Surg Pathol* 2015; **39**: 528–540.
26. Horn S, Figl A, Rachakonda PS *et al*. TERT promoter mutations in familial and sporadic melanoma. *Science* 2013; **339**: 959–961.
27. Heaphy CM, de Wilde RF, Jiao Y *et al*. Altered telomeres in tumors with ATRX and DAXX mutations. *Science* 2011; **333**: 425.
28. Eckel-Passow JE, Lachance DH, Molinaro AM *et al*. Glioma groups based on 1p/19q, IDH, and TERT promoter mutations in tumors. *N Engl J Med* 2015; **372**: 2499–2508.